



RNA-MEDIATED EPIGENETIC AND TRANSCRIPTIONAL REGULATION

EDITED BY: Yicheng Long, A. Rasim Barutcu and Mo Motamedi

PUBLISHED IN: *Frontiers in Genetics* and

Frontiers in Cell and Developmental Biology



frontiers

Frontiers eBook Copyright Statement

The copyright in the text of individual articles in this eBook is the property of their respective authors or their respective institutions or funders. The copyright in graphics and images within each article may be subject to copyright of other parties. In both cases this is subject to a license granted to Frontiers.

The compilation of articles constituting this eBook is the property of Frontiers.

Each article within this eBook, and the eBook itself, are published under the most recent version of the Creative Commons CC-BY licence.

The version current at the date of publication of this eBook is CC-BY 4.0. If the CC-BY licence is updated, the licence granted by Frontiers is automatically updated to the new version.

When exercising any right under the CC-BY licence, Frontiers must be attributed as the original publisher of the article or eBook, as applicable.

Authors have the responsibility of ensuring that any graphics or other materials which are the property of others may be included in the CC-BY licence, but this should be checked before relying on the CC-BY licence to reproduce those materials. Any copyright notices relating to those materials must be complied with.

Copyright and source acknowledgement notices may not be removed and must be displayed in any copy, derivative work or partial copy which includes the elements in question.

All copyright, and all rights therein, are protected by national and international copyright laws. The above represents a summary only. For further information please read Frontiers' Conditions for Website Use and Copyright Statement, and the applicable CC-BY licence.

ISSN 1664-8714

ISBN 978-2-88976-455-6

DOI 10.3389/978-2-88976-455-6

About Frontiers

Frontiers is more than just an open-access publisher of scholarly articles: it is a pioneering approach to the world of academia, radically improving the way scholarly research is managed. The grand vision of Frontiers is a world where all people have an equal opportunity to seek, share and generate knowledge. Frontiers provides immediate and permanent online open access to all its publications, but this alone is not enough to realize our grand goals.

Frontiers Journal Series

The Frontiers Journal Series is a multi-tier and interdisciplinary set of open-access, online journals, promising a paradigm shift from the current review, selection and dissemination processes in academic publishing. All Frontiers journals are driven by researchers for researchers; therefore, they constitute a service to the scholarly community. At the same time, the Frontiers Journal Series operates on a revolutionary invention, the tiered publishing system, initially addressing specific communities of scholars, and gradually climbing up to broader public understanding, thus serving the interests of the lay society, too.

Dedication to Quality

Each Frontiers article is a landmark of the highest quality, thanks to genuinely collaborative interactions between authors and review editors, who include some of the world's best academicians. Research must be certified by peers before entering a stream of knowledge that may eventually reach the public - and shape society; therefore, Frontiers only applies the most rigorous and unbiased reviews.

Frontiers revolutionizes research publishing by freely delivering the most outstanding research, evaluated with no bias from both the academic and social point of view. By applying the most advanced information technologies, Frontiers is catapulting scholarly publishing into a new generation.

What are Frontiers Research Topics?

Frontiers Research Topics are very popular trademarks of the Frontiers Journals Series: they are collections of at least ten articles, all centered on a particular subject. With their unique mix of varied contributions from Original Research to Review Articles, Frontiers Research Topics unify the most influential researchers, the latest key findings and historical advances in a hot research area! Find out more on how to host your own Frontiers Research Topic or contribute to one as an author by contacting the Frontiers Editorial Office: frontiersin.org/about/contact

RNA-MEDIATED EPIGENETIC AND TRANSCRIPTIONAL REGULATION

Topic Editors:

Yicheng Long, Cornell University, United States

A. Rasim Barutcu, University of Toronto, Canada

Mo Motamedi, Harvard Medical School, United States

Citation: Long, Y., Barutcu, A. R., Motamedi, M., eds. (2022). RNA-Mediated Epigenetic and Transcriptional Regulation. Lausanne: Frontiers Media SA.
doi: 10.3389/978-2-88976-455-6

Table of Contents

- 04 Editorial: RNA-Mediated Epigenetic and Transcriptional Regulation**
A. Rasim Barutcu, Yicheng Long and Mo Motamedi
- 06 Profiling of MicroRNAs in Midguts of *Plutella xylostella* Provides Novel Insights Into the *Bacillus thuringiensis* Resistance**
Jie Yang, Xuejiao Xu, Sujie Lin, Shiyao Chen, Guifang Lin, Qisheng Song, Jianlin Bai, Minsheng You and Miao Xie
- 22 RNA Biological Characteristics at the Peak of Cell Death in Different Hereditary Retinal Degeneration Mutants**
Chunling Wei, Yan Li, Xiaoxiao Feng, Zhulin Hu, François Paquet-Durand and Kangwei Jiao
- 40 Identification of m6A-Related lncRNAs Associated With Prognoses and Immune Responses in Acute Myeloid Leukemia**
Ding Li, Jiaming Liang, Cheng Cheng, Wenbin Guo, Shuolei Li, Wenping Song, Zhenguo Song, Yongtao Bai, Yongna Zhang, Xuan Wu and Wenzhou Zhang
- 53 Identification of m6A Regulator-Associated Methylation Modification Clusters and Immune Profiles in Melanoma**
Fengying Du, Han Li, Yan Li, Yang Liu, Xinyu Li, Ningning Dang, Qingqing Chu, Jianjun Yan, Zhen Fang, Hao Wu, Zihao Zhang, Xingyu Zhu and Xiaokang Li
- 70 Transcriptome-Wide m6A Analysis Provides Novel Insights Into Testicular Development and Spermatogenesis in Xia-Nan Cattle**
Shen-he Liu, Xiao-ya Ma, Ting-ting Yue, Zi-chen Wang, Kun-long Qi, Ji-chao Li, Feng Lin, Hossam E. Rushdi, Yu-yang Gao, Tong Fu, Ming Li, Teng-yun Gao, Li-guo Yang, Xue-lei Han and Ting-xian Deng
- 83 Current Advances in N6-Methyladenosine Methylation Modification During Bladder Cancer**
Qiang Liu
- 94 Transcriptomic and Metabolomic Analyses Reveal Inhibition of Hepatic Adipogenesis and Fat Catabolism in Yak for Adaptation to Forage Shortage During Cold Season**
Juanshan Zheng, Mei Du, Jianbo Zhang, Zeyi Liang, Anum Ali Ahmad, Jiahao Shen, Ghasem Hosseini Salekdeh and Xuezhi Ding
- 109 Analysis of N6-Methyladenosine Methylome in Adenocarcinoma of Esophagogastric Junction**
Jia-Bin Huang, Bin-Bin Hu, Rong He, Lian He, Chen Zou, Chang-Feng Man and Yu Fan
- 127 Global Landscape of m6A Methylation of Differently Expressed Genes in Muscle Tissue of Liaoyu White Cattle and Simmental Cattle**
Yunlong Dang, Qiao Dong, Bowei Wu, Shuhua Yang, Jiaming Sun, Gengyuan Cui, Weixiang Xu, Meiling Zhao, Yunxuan Zhang, Peng Li and Lin Li



Editorial: RNA-Mediated Epigenetic and Transcriptional Regulation

A. Rasim Barutcu^{1*}, Yicheng Long^{2*} and Mo Motamedi^{3*}

¹Donnelly Centre for Cellular and Biomolecular Research, University of Toronto, Toronto, ON, Canada, ²Department of Biochemistry, Cardiovascular Research Institute, Weill Cornell Medicine, New York, NY, United States, ³Massachusetts General Hospital Center for Cancer Research and Department of Medicine, Harvard Medical School, Charlestown, MA, United States

Keywords: RNA, transcription, RNA modification, miRNA, RNA epigenetic regulation

Editorial on the Research Topic

RNA-Mediated Epigenetic and Transcriptional Regulation

RNA plays major regulatory roles in many processes beyond transcription, including protein complex formation, maintenance of genomic stability, and establishment of higher-order cellular structures *via* phase separation. Accordingly, regulation of RNA abundance, processing, and modification can have a profound impact on cellular and organismal biology. In recent years, significant progress has been made to decipher the complex molecular details and functional interplay between RNA and regulatory processes have begun to emerge. These studies have shed light on how perturbation to these mechanisms can yield aberrant biology, including formation of disease states such as cancers. In this Research Topic “RNA-Mediated Epigenetic and Transcriptional Regulation,” several articles highlight the importance of RNA-mediated regulation in different pathological contexts such as cancers and retinal degeneration, and developmental/adaptation processes such as sperm development, resistance to pathogens, and adaptation to cold. Altogether, this Research Topic further highlights the importance of RNA as an effector molecule in biology and underscores its biochemical versatility as a regulatory molecule.

N⁶-methyladenosine (m6A) is the most prevalent, conserved and abundant co-transcriptional modification observed in eukaryotic mRNAs. It plays important roles in splicing, translation, RNA stability, and higher-order RNA structures (Jiang et al., 2021) among other biological processes. There are several regulatory complexes which “write,” “erase,” and “read” this modification on RNA molecules. The delicate regulatory control of m6A has been implicated in numerous physiological and pathological conditions, especially in cancers. In this Research Topic, three research papers and a review paper evaluate, identify, and summarize the m6A landscape of several cancers, including melanoma, acute myeloid leukemia (AML), adenocarcinoma of the esophagogastric junction (AEG) and bladder cancer. Du et al. performed computational analyses on over one thousand melanoma patient samples to determine whether there is a relationship between m6A modification and melanoma immunogenicity. By performing clustering analyses and devising a specialized m6A enrichment scoring system, the authors identified distinct expression profiles of m6A machinery and m6A modification patterns that correlate with known immune phenotypes in melanoma. Li et al. used The Cancer Genome Atlas (TCGA) AML cohort and identified seven long non-coding RNAs (lncRNAs), whose expression not only correlated with at least one m6A regulator, but also could be used as prognostic markers for AML and its immunotherapy response in patients. By using matched tumor and normal tissues Huang et al., performed m6A sequencing to generate an m6A map of AEG. Their work identified several AEG-specific m6A sites on important cancer-related mRNAs, suggesting their importance in this cancer. Finally, Liu reviewed m6A modification and its

OPEN ACCESS

Edited by:

William C. Cho,
QEH, Hong Kong SAR, China

Reviewed by:

Robert Martienssen,
Cold Spring Harbor Laboratory,
United States

*Correspondence:

A. Rasim Barutcu
rasim.barutcu@utoronto.ca
Yicheng Long
yil4011@med.cornell.edu
Mo Motamedi
mmotamedi@hms.harvard.edu

Specialty section:

This article was submitted to
RNA,
a section of the journal
Frontiers in Genetics

Received: 25 April 2022

Accepted: 10 May 2022

Published: 06 June 2022

Citation:

Barutcu AR, Long Y and Motamedi M
(2022) Editorial: RNA-Mediated
Epigenetic and
Transcriptional Regulation.
Front. Genet. 13:928335.
doi: 10.3389/fgene.2022.928335

potential regulatory role in bladder cancer proliferation and infiltration. Altogether, these articles showcase m6A dynamics and its potential impact on a disease state such as cancer.

Recent studies have shown that m6A modification also plays important roles in organismal development. Dang et al., assessed the differences in the transcriptomes and m6A profiles of two distinct cattle breeds, differentiated based on their muscle composition. They identified several differentially m6A-modified mRNAs important in muscle development and related pathways. These data suggest that differential m6A modification of these mRNAs could play a role in the distinct muscle profiles found in these cattle breeds. In another report, Liu et al. investigated the role of m6A modification in bovine spermatogenesis during three developmental stages (pre-puberty, puberty, and post-puberty). Their analyses revealed important genes and developmental pathways display differential RNA expression and m6A profiles at distinct ages, correlating m6A regulation with sperm development.

RNA regulation also has a profound impact on development and tuning the metabolic state of organisms, especially in response to stress. Focusing on retinal development, Wei et al. performed RNA-seq on tissues obtained from three different mouse models for inherited retinal degeneration (RD) and identified important regulatory networks such transcription factors, lncRNAs and circular RNAs, whose expression change in RD. In another study Zheng et al., performed transcriptomic and metabolomic profiling of a yak breed during the cold season and generated an integrative transcriptome and metabolome map revealing several differentially regulated metabolic pathways which could help the animals survive long periods of malnutrition and cold temperatures.

MicroRNAs (miRNAs) constitute a highly conserved family of eukaryotic regulatory small non-coding RNAs, typically 19–24 nucleotides in length, formed by cleavage of endogenous hairpin non-coding RNAs. They mediate silencing of the complementary

transcripts by promoting degradation or inhibiting translation of the complementary transcripts. They function in a myriad of developmental and pathological processes. Further implicating the importance of RNA-mediated gene regulation, Yang et al. investigated the role of miRNAs in pesticide resistance of the diamondback moth, which is one of the deadliest and most destructive pests worldwide. By performing small RNA sequencing from the guts of drug-resistant and sensitive moths, the authors identify dozens of differentially expressed miRNAs whose predicted target genes may be involved in pesticide resistance.

Altogether, these descriptive studies further establish the link between RNA and its regulatory potential in governing a wide array of biological processes. They also underscore the importance of answering several outstanding mechanistic questions about how cells harness the unique biochemical properties of RNA to mediate mechanisms impacting many important biological activities. Indeed, such molecular insight will not only extend our understanding of the basic biology of cellular processes, but also help us develop potential therapeutics for several diseases.

AUTHOR CONTRIBUTIONS

All authors listed have made a substantial, direct, and intellectual contribution to the work and approved it for publication.

FUNDING

ARB was supported by Banting and CIHR Postdoctoral Fellowships. YL was supported by NIH K99/R00 grant (R00GM132546) and AHA Career Development Award (935361). MM was supported by R01 (GM125782) and ACS Research Scholar Grant (18-056-01-RMC).

Conflict of Interest: The authors declare that the research was conducted in the absence of any commercial or financial relationships that could be construed as a potential conflict of interest.

Publisher's Note: All claims expressed in this article are solely those of the authors and do not necessarily represent those of their affiliated organizations, or those of the publisher, the editors and the reviewers. Any product that may be evaluated in this article, or claim that may be made by its manufacturer, is not guaranteed or endorsed by the publisher.

Copyright © 2022 Barutcu, Long and Motamedi. This is an open-access article distributed under the terms of the Creative Commons Attribution License (CC BY). The use, distribution or reproduction in other forums is permitted, provided the original author(s) and the copyright owner(s) are credited and that the original publication in this journal is cited, in accordance with accepted academic practice. No use, distribution or reproduction is permitted which does not comply with these terms.

REFERENCES

- Jiang, X., Liu, B., Nie, Z., Duan, L., Xiong, Q., Jin, Z., et al. (2021). The Role of m6A Modification in the Biological Functions and Diseases. *Sig Transduct. Target Ther.* 6. doi:10.1038/s41392-020-00450-x
- Wei, C., Li, Y., Feng, X., Hu, Z., Paquet-Durand, F., and Jiao, K. (2021). RNA Biological Characteristics at the Peak of Cell Death in Different Hereditary Retinal Degeneration Mutants. *Front. Genet.* 12, 728791. doi:10.3389/fgene.2021.728791
- Zheng, J., Du, M., Zhang, J., Liang, Z., Ahmad, A. A., Shen, J., et al. (2021). Transcriptomic and Metabolomic Analyses Reveal Inhibition of Hepatic Adipogenesis and Fat Catabolism in Yak for Adaptation to Forage Shortage during Cold Season. *Front. Cell Dev. Biol.* 9, 759521. doi:10.3389/fcell.2021.759521



Profiling of MicroRNAs in Midguts of *Plutella xylostella* Provides Novel Insights Into the *Bacillus thuringiensis* Resistance

Jie Yang^{1,2,3}, Xuejiao Xu^{1,2,3}, Sujie Lin^{1,2,3}, Shiyao Chen⁴, Guifang Lin^{1,2,3}, Qisheng Song⁵, Jianlin Bai^{1,2,3}, Minsheng You^{1,2,3*} and Miao Xie^{1,2,3,4*}

¹ State Key Laboratory of Ecological Pest Control for Fujian and Taiwan Crops, Institute of Applied Ecology, Fujian Agriculture and Forestry University, Fuzhou, China, ² Joint International Research Laboratory of Ecological Pest Control, Ministry of Education, Fujian Agriculture and Forestry University, Fuzhou, China, ³ Ministerial and Provincial Joint Innovation Centre for Safety Production of Cross-Strait Crops, Fujian Agriculture and Forestry University, Fuzhou, China, ⁴ College of Life Sciences, Fujian Agriculture and Forestry University, Fuzhou, China, ⁵ Division of Plant Sciences, University of Missouri, Columbia, MO, United States

OPEN ACCESS

Edited by:

A. Rasim Barutcu,
University of Toronto, Canada

Reviewed by:

Kang He,
Zhejiang University, China
Hikmet Budak,
Montana Bioagriculture, Inc.,
United States

*Correspondence:

Minsheng You
msyou@fafu.edu.cn
Miao Xie
xmshelly@163.com

Specialty section:

This article was submitted to
RNA,
a section of the journal
Frontiers in Genetics

Received: 12 July 2021

Accepted: 20 August 2021

Published: 08 September 2021

Citation:

Yang J, Xu X, Lin S, Chen S,
Lin G, Song Q, Bai J, You M and
Xie M (2021) Profiling of MicroRNAs
in Midguts of *Plutella xylostella*
Provides Novel Insights Into
the *Bacillus thuringiensis* Resistance.
Front. Genet. 12:739849.
doi: 10.3389/fgene.2021.739849

The diamondback moth (DBM), *Plutella xylostella*, one of the most destructive lepidopteran pests worldwide, has developed field resistance to *Bacillus thuringiensis* (Bt) Cry toxins. Although miRNAs have been reported to be involved in insect resistance to multiple insecticides, our understanding of their roles in mediating Bt resistance is limited. In this study, we constructed small RNA libraries from midguts of the Cry1Ac-resistant (Cry1S1000) strain and the Cry1Ac-susceptible strain (G88) using a high-throughput sequencing analysis. A total of 437 (76 known and 361 novel miRNAs) were identified, among which 178 miRNAs were classified into 91 miRNA families. Transcripts per million analysis revealed 12 differentially expressed miRNAs between the Cry1S1000 and G88 strains. Specifically, nine miRNAs were down-regulated and three up-regulated in the Cry1S1000 strain compared to the G88 strain. Next, we predicted the potential target genes of these differentially expressed miRNAs and carried out GO and KEGG pathway analyses. We found that the cellular process, metabolism process, membrane and the catalytic activity were the most enriched GO terms and the Hippo, MAPK signaling pathway might be involved in Bt resistance of DBM. In addition, the expression patterns of these miRNAs and their target genes were determined by RT-qPCR, showing that partial miRNAs negatively while others positively correlate with their corresponding target genes. Subsequently, novel-miR-240, one of the differentially expressed miRNAs with inverse correlation with its target genes, was confirmed to interact with *Px017590* and *Px007885* using dual luciferase reporter assays. Our study highlights the characteristics of differentially expressed miRNAs in midguts of the Cry1S1000 and G88 strains, paving the way for further investigation of miRNA roles in mediating Bt resistance.

Keywords: microRNAs, *Bacillus thuringiensis*, resistance, *Plutella xylostella*, differential expression analysis

INTRODUCTION

Bacillus thuringiensis (Bt), a class of spore-forming gram-positive bacterium that can produce different insecticidal crystal proteins (Cry and Cyt toxins), has been widely used as an entomopathogen for pest control (Wu et al., 2008; Raymond et al., 2010; Palma et al., 2014). The application of Bt toxins cannot only increase crop yields and bring substantial economic benefits, but also reduce environmental pollution caused by the abuse of chemical insecticides (Bravo et al., 2011). Bt Cry toxin has specific control efficiency on lepidopteran pests, and the mode of action involves toxin solubilization, proteolytic activation, interaction with midgut proteins of insects, formation of a pre-pore oligomeric structure, facilitation of the insertion into cell membrane, and creation of an ionic pore that kills midgut cells (Bravo et al., 2011). There are several resistance strategies taken by insects to counter Bt toxins, including mutations in receptor [e.g., cadherin, aminopeptidase N (APN) or ATP-binding cassette (ABC) transporters], alteration in Cry toxin activation and binding ability to gut membrane, sequestration of toxins by glycolipid moieties or esterases, and the elevation of insects immune responses (Pardo-Lopez et al., 2013). So far, more than 22 cases of field-evolved Bt resistance in several insect species have been documented, potentially reducing the control efficacy of Bt toxins toward agricultural pests (Janmaat and Myers, 2003; Tabashnik and Carrière, 2017, 2019; Calles-Torrez et al., 2019). Therefore, to delay the resistance evolution, it is urgent to understand the mechanisms causing Bt resistance and provide novel targets for pest control.

The diamondback moth (DBM), *Plutella xylostella*, a notorious pest of cruciferous crops, has caused severe economic losses globally. One of the main challenges of DBM control is its rapid evolution of resistance against a wide range of insecticides, including Bt-based products (Furlong et al., 2013). Considering its severe insecticide-resistance, short life cycle and host range expansion (Li et al., 2016), microRNA (miRNA)-mediated efficient and environmentally friendly approaches have been proposed to combat DBM (Vaschetto and Beccacece, 2019).

MiRNAs are a class of endogenous non-coding RNAs ranged from 19 to 24 nt in length and play crucial roles in the post-transcriptional regulation (Bartel, 2004; Cullen, 2004; Asgari, 2013). MiRNAs regulate gene expression by partially or completely binding their seed sequence region with the 3' untranslated region (3'UTR) of corresponding target genes (Bartel, 2004). A large number of miRNAs have been identified from multiple insect species, participating in insect development (Liu et al., 2018, 2020b; Xu et al., 2019; Lim et al., 2020), reproduction (Lucas et al., 2015; He et al., 2016; Ling et al., 2017), behavior (Cristino et al., 2014; Chen and Rosbash, 2016; Niu et al., 2019), and host-pathogen interaction (Singh et al., 2014; Dubey et al., 2019; Wu et al., 2019). Recently, a growing body of evidence has illustrated the pivotal role of miRNAs in responses to environmental chemical and pathogen exposures, which attracts great interests in the field of insect toxicology. Insecticide resistance is predominantly caused by the rising metabolic detoxification of insecticides and declining in the target sites sensitivity of the insecticides (Liu, 2015).

MiRNAs enhance insecticide resistance by negatively regulating the expression of detoxification-related genes or altering insect susceptibility to various kinds of insecticides. In *Culex pipiens pallens*, the pyrethroid-resistance is modulated by miR-92a via suppressing *CpCPR4* expression (Ma et al., 2017), miR-278-3p and miR-932 are also involved in the pyrethroid resistance by targeting *CYP6AG11* and *CpCPR5*, respectively (Lei et al., 2014; Liu et al., 2016). In addition, it has been reported that miR-13664 could interact with *CpCYP314A1* and subsequently regulate deltamethrin resistance (Sun et al., 2019). Another study confirms the significant role of miR-2~13-71 cluster in deltamethrin resistance by regulating the expression of *CYP9J35* and *CYP325BG3* (Guo et al., 2017). In DBM, miR-7a and miR-8519 regulate chlorantraniliprole resistance via overexpressing *ryanodine receptor (RyR)* (Li X. et al., 2015). MiR-2b-3p and miR-14-5p are proposed to inhibit the detoxification pathways by suppressing the transcript levels of *CYP9F2* and *CYP307a1*, respectively (Etebari et al., 2018). MiR-189942 directly targets the *ecdysone receptor (EcR) isoform B* and increased the tolerance to fufenozide (Li X. et al., 2020). Besides, miR-998-3p is implicated in Bt resistance through targeting *ABCC2*, a putative receptor for Bt Cry1Ac toxin in three lepidopterans *P. xylostella*, *Helicoverpa armigera*, and *Spodoptera exigua* (Zhu et al., 2019). While these studies provide insight into the critical roles of miRNAs in regulating metabolic resistance to insecticides, most of them are focused on the chemical insecticide. The mechanism of miRNA-mediated Bt resistance still remains limited.

A previous study has profiled the dynamic expression patterns of miRNAs in response to Bt at different time courses using the whole body of DBM, indicating the potential role of miR-2b-3p in regulating insect immunity (Li S. et al., 2019). In the present study, we aimed to expand the numbers of identified miRNAs in specific tissues, i.e., midguts of the Bt resistant and susceptible DBM strains and explore the potential mechanisms of miRNA-mediated regulation in Bt resistance. The differentially expressed miRNAs in midguts of both strains were putatively linked to Bt resistance. One of the differentially expressed miRNAs, novel-miR-240, which showed an inverse correlation with its target genes, was then selected for dual luciferase assays to validate the interaction with its target genes. Our work is important for further understanding the potential roles of miRNAs in the evolution of Bt resistance in DBM field populations, providing novel insights for their putative applications in integrated pest management.

MATERIALS AND METHODS

Insects Rearing

The insecticide-susceptible DBM strain (Geneva 88, G88) was originally collected from the New York State Agricultural Experiment Station in 1988 and maintained on an artificial diet without exposure to insecticide. A colony of DBM, which was established from a crucifer field in Florida in 1992, was used to investigate its resistance to *B. thuringiensis* subsp. *kurstaki* spray formula. Specifically, it was challenged with the transgenic broccoli expressing Cry1Ac toxin, and the survived moths were

maintained as a Cry1Ac-R strain (Zhao et al., 2002). The Cry1Ac-R resistance strain was further selected with 1,000 µg/ml Cry1Ac protoxin in 2016 and then reared on an artificial diet without additional insecticide exposure for more than 50 generations. This strain was thereafter named as Cry1S1000 (Liu et al., 2020a). Both the G88 susceptible and Cry1S1000 resistance strains were reared with the same approach reported before (Xu et al., 2020). In brief, artificial diet and 10% honey solution were, respectively, used to feed larvae and adults at $25 \pm 1^\circ\text{C}$, with a 16:8 h light: dark cycle and $65 \pm 5\%$ relative humidity.

Sample Collection and Small RNA Library Construction

Fresh midguts dissected from 60 4th instar larvae of the Cry1S1000 and G88 strains were collected in separate tubes and the midgut contents were gently scraped off. The midgut samples were immediately immersed in liquid nitrogen and subsequently frozen in -80°C until further analysis. To generate a small RNA (sRNA) library, the miRNeasy Mini Kit (Qiagen, Germany) was used for total RNA extraction from the midgut samples. RNA concentration and purity were measured using the NanoDrop 2000 (Thermo Fisher Scientific, United States) and Agilent Bioanalyzer 2100 system (Agilent Technologies, United States), respectively. To generate sRNA libraries, 3 µg RNA per sample was used for adaptor ligation in both of 5' and 3' ends using the NEBNext Multiplex Small RNA Library Prep Kit for Illumina (NEB, United States). Then, the M-MuLV Reverse Transcriptase (RNase H⁻) was used for the first strand cDNA synthesis. The PCR amplification was performed and the fragments of 140~160 bp were recovered and sequenced using the Illumina HiSeq 2500 sequencing platform (Illumina Inc., United States).

Bioinformatic Analysis

To obtain the clean reads, low-quality reads, reads containing more than 10% unknown base N, without 3' adaptor sequence, shorter than 18 nt, or longer than 30 nt and 3' adapter reads were removed from the raw sequences, and the identical reads were collapsed in order to remove redundancy. After that, the trimmed sequences were aligned to Silva, GtRNAdb, Rfam, and Rfam databases to filter the ncRNAs including ribosomal RNA (rRNA), transfer RNA (tRNA), small nuclear RNA (snRNA), small nucleolar RNA (snoRNA), and repetitive RNAs. The remaining reads mapped to the reference genome¹ with Bowtie software were used for further miRNA identification. Known miRNAs were identified by aligning with mature sequences in miRBase (release22)² with one mismatched allowed. For novel miRNAs identification, the miRDeep2 package was utilized to obtain potential precursor sequences. Prediction of novel miRNAs was completed based on the precursor structure energy information and the distribution information of reads on precursor sequence (Friedlander et al., 2012).

Expression Patterns of miRNAs Based on Transcripts per Million

To identify the miRNAs differentially expressed in the Cry1S1000 and G88 strains, transcripts per million (TPM) was used to estimate miRNA expression levels. The normalization formula was: normalized expression = (number of mapped reads for each miRNA/total number of mapped reads) $\times 10^6$. The DESeq2 algorithm (Love et al., 2014) was performed to estimate the differences in reads frequencies comparing the Cry1S1000 to G88 strains, and *p*-value was adjusted using the Benjamini-Hochberg false discovery rate (FDR) procedure (Puolivaali et al., 2020). Only those miRNAs with a log2 fold-change > 1.58 or < -1.58 in expression and a FDR ≤ 0.01 were determined to be significantly differentially expressed between the Cry1S1000 and G88 strains.

Target Gene Prediction and Enrichment Analysis

To predict and analyze the potential target genes of differentially expressed miRNAs, miRanda (Rehmsmeier et al., 2004), and TargetScan (Lewis et al., 2005) algorithms with default parameters were employed. The DBM genome sequence (DBM-DB)³ was used as a reference and the coding sequence (CDS) was searched for predicting miRNA targets. To screen more reliable results, only those genes predicted by both algorithms were retained. The predicted miRNA targets were annotated based on NR, Swiss-Prot (Apweiler et al., 2004), Gene Ontology (GO) (Ashburner et al., 2000), COG (Tatusov et al., 2000), Kyoto Encyclopedia of Genes and Genomes (KEGG) (Kanehisa et al., 2004), KOG (Koonin et al., 2004) and Pfam databases using BLAST program with a cut-off *E*-value = 10^{-5} . To further investigate the functions of the putative target genes, the software Database for Annotation Visualization and Integrated Discovery (DAVID)⁴ was used to conduct the GO enrichment consisted of biological processes, cellular components and molecular functions. Pathway analysis was based on the KEGG database that determine the pathways associated with the target genes of the differentially expressed miRNA. The DBM genome database was used as a background to determine the most enriched GO terms with a corrected *p*-value ≤ 0.05 as the threshold. The KEGG analysis was performed and a corrected *p*-value was set as 0.05 for identifying significantly enriched pathways within the predicted differentially expressed miRNA target dataset.

Expression Patterns of miRNAs and Target Genes Based on RT-qPCR

Total RNA was extracted from midguts of 20 fourth instar larvae using a PF miRNA Isolation Kit (Omega, United States), and the concentration was measured by NanoDrop 2000 (Thermo Fisher Scientific, United States). The miRNA reverse transcription reactions were conducted using the miScript II RT kit (Qiagen, Germany), and the RevertAid First Strand cDNA Synthesis Kit (Thermo Fisher Scientific, United States) was used to synthesize the first-strand cDNA of target genes.

¹<https://www.ncbi.nlm.nih.gov/genome/?term=Plutella+xylostella>

²<http://www.mirbase.org/>

³<http://59.79.254.1/dbm/>

⁴<http://david.ncicrf.gov/>

Reverse transcriptase-quantitative PCR (RT-qPCR) reactions of miRNAs were performed using the miScript SYBR Green PCR kit (Qiagen, Germany) with miRNA-specific forward primers (**Supplementary Table 1**), and the RT-qPCR reactions of target genes were performed using the Eastep qPCR Master Mix (Promega, United States). All amplification reactions were performed on the Bio-Rad Real-time PCR system (Bio-Rad, United States) with three technical repeats and three independent biological replicates. The normalized expression levels were calculated with $2^{-\Delta\Delta C_t}$ method using the internal references U6 snRNA for miRNAs normalization and *RPL32* for target genes normalization. The significance was analyzed using Student's *t*-test with SPSS 25.0 program. All the reagents and kits used in the current study were applied according to the manufacturer's instruction unless stated specifically.

Dual Luciferase Reporter (DLR) Assay

Novel-miR-240 agomir (5'-UCCUCAUAUUAUUAUCC UCGC-3') and negative control (NC) agomir (5'-UUCUCCGAACGUGUCACGUTT-3') were synthesized by Sangon Biotech (Shanghai, China). An agomir is a sequence of double-strand RNA with special chemical modification, and it can mimic the function of miRNA and up-regulate the expression of endogenous miRNA. The luciferase reporter plasmids were constructed by cloning the wild type (WT) and the mutated (MUT) target sequences of *Px017590* and *Px007885* into the pmirGLO vector (Promega, United States). The fragments of *Px017590* and *Px007885* containing WT and MUT sequences were then confirmed by sequencing. To obtain high transfection efficiency and low background expression, HEK293T cell line was used for the DLR assay. HEK293T cells were cultured in a 24-well plate and co-transfected with the reporter plasmid and the miRNA agomir or NC agomir using the Attractene Transfection Reagent (Qiagen, Germany). Each well containing 1 μ g reporter plasmid and 50 nM miRNA agomir or NC agomir. The activities of the Firefly and Renilla luciferases were performed by using a Dual-Glo Luciferase Assay System (Promega, United States) at 48 h post-transfection. Firefly luciferase activity was normalized to Renilla luciferase activity.

RESULTS

Overview of the sRNA Libraries

To analyze the role of miRNAs in the Bt resistance of DBM, we performed the deep sequencing for identification and characterization of miRNAs in the larval midguts of the Cry1S1000 and G88 strains. Using the high-throughput sequencing, a total of 125,558,480 raw reads (≥ 17.6 million per library) were obtained. After removing low-quality reads and 3' adaptor, only the reads ranging from 18 to 30 nt were kept. Clean reads from three Cry1S1000 libraries (15,964,505, 18,860,033, and 16,118,802) and three G88 libraries (12,107,465, 13,815,968, and 18,445,775) were obtained, respectively. The clean reads were aligned with Silva, GtRNadb, Rfam, and Rfam databases and then mapped to the reference genome

using the Bowtie package. A total of 9,200,300 mapped reads were retained and used to predict mature miRNAs in subsequent analyses (**Table 1**).

Identification of Known and Novel miRNAs

Bioinformatic analysis was carried out to identify miRNAs expressed in the larval midguts of the Cry1S1000 and G88 strains. By searching against miRBase, 76 miRNAs in our libraries were identical to mature miRNA sequences and annotated as known miRNAs. Additionally, the miRDeep2 software package (Wen et al., 2012) was used to predict novel miRNAs by exploring the potential precursor sequences and estimating their randfold value. In total, 361 novel miRNAs were identified (**Table 1**). The length distribution of both known and novel miRNAs showed a peak at 22 nt, which is the standard size of animal miRNAs (**Figures 1A,B**). The first base preference of identified miRNAs was also investigated, and the result showed a dominant bias toward uracil (U). This bias was particularly evident in both known miRNAs (20 and 22 nt in length) and novel miRNAs (19 nt and 22 nt in length). Calculation of the miRNA nucleotide bias at each position demonstrated that U and A (adenine) were more common than C (cytosine) and G (guanine) in almost all positions, especially at base 14 (**Figures 1C,D**).

Next, we classified 178 known and novel miRNAs into 91 families based on the sequence conservation across different species, while the remaining 259 miRNAs could not be classified into any families. Six main families, which hold relatively more members compared with other sets, were discovered. To be specific, 12 identified miRNAs belonged to the miR-4864 family and ten miRNAs belonged to the miRNA-8517 family. It was also estimated that the miR-279 and miR-9 families, respectively, contained six miRNAs, while the other two miRNA families (miR-2 and miR-185) were each represented by five miRNAs. In comparison, the remaining families were predicted to have less than five miRNA members each (**Figure 2**). All of the 178 identified miRNAs and their miRNA families were listed in **Supplementary Table 2**.

In addition, the miRNA expression levels were assessed by TPM formula. The most abundant known miRNA was pxy-miR-279b-3p, followed by pxy-miR-750, pxy-miR-8494-5p, pxy-miR-306, and pxy-miR-8532-3p, while the five most highly expressed novel miRNAs were novel-miR-1, novel-miR-246, novel-miR-176, novel-miR-28, and novel-miR-132. Interestingly, the average expression value of the listed novel miRNAs was significantly higher than the known miRNAs. The most abundant known and novel miRNAs in the libraries were represented in **Figure 3** and the details of all the identified miRNAs were listed in **Supplementary Table 3**.

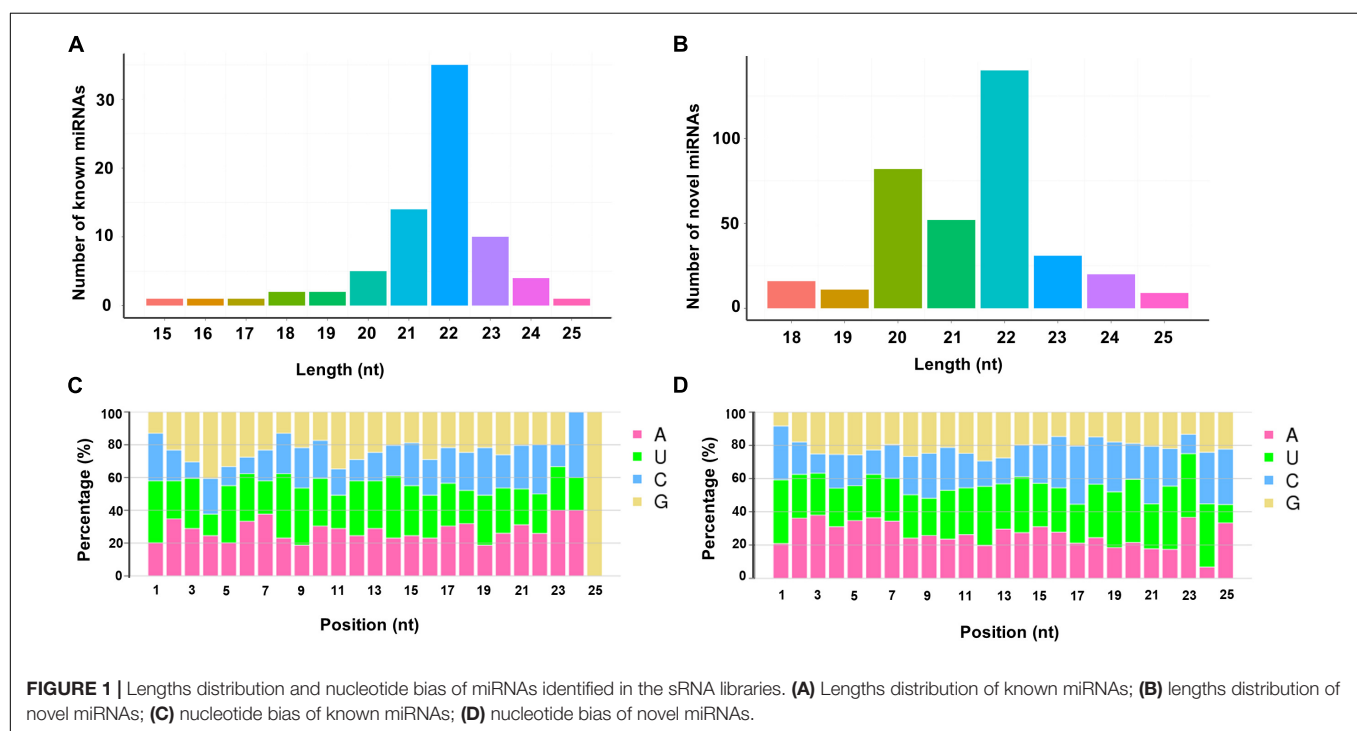
Differentially Expressed miRNAs in the Cry1S1000 and G88 Strains

The expression levels of known and novel miRNAs were compared after normalization by TPM formula described above.

TABLE 1 | sRNA libraries of the Cry1S1000 and G88 strains.

Group of reads*	Number of reads						Total reads
	Cry1S1000-1	Cry1S1000-2	Cry1S1000-3	G88-1	G88-2	G88-3	
Raw reads	21,847,848	22,213,713	20,886,851	17,688,151	19,614,812	23,307,105	125,558,480
Clean reads	15,964,505	18,860,033	16,118,802	12,107,465	13,815,968	18,445,775	95,312,548
Unannotated reads	7,404,038 (46.38%)	8,081,934 (42.86%)	6,681,832 (41.45%)	4,213,087 (34.8%)	6,724,759 (48.68%)	7,604,070 (41.22%)	40,709,720
rRNA	8,251,242 (51.68%)	10,487,087 (55.60%)	9,224,539 (57.23%)	76,575,610 (63.25%)	6,597,046 (47.75%)	10,448,645 (56.65%)	121,584,169
tRNA	307,827 (1.93%)	288,842 (1.53%)	210,446 (1.31%)	235,307 (1.94%)	492,090 (3.56%)	390,902 (2.12%)	1,925,414
snRNA	0 (0.00%)	0 (0.00%)	0 (0.00%)	0 (0.00%)	1 (0.00%)	1 (0.00%)	2
snoRNA	90 (0.00%)	183 (0.00%)	241 (0.00%)	140 (0.00%)	237 (0.00%)	211 (0.00%)	1,102
Repeat	1,308 (0.01%)	1,987 (0.01%)	1,744 (0.01%)	1,421 (0.01%)	1,835 (0.01%)	1,946 (0.01%)	10,241
Mapped reads	1,675,527 (22.63%)	1,796,235 (22.23%)	1,215,274 (18.19%)	1,058,410 (25.12%)	1,650,946 (24.55%)	1,803,908 (23.72%)	9,200,300
Known miRNA	57	59	57	53	67	60	76
Novel miRNA	289	288	264	249	327	321	361

*rRNA, ribosomal RNA; tRNA, transfer RNA; snRNA, small nuclear RNA; snoRNA, small nucleolar RNA.



Twelve differentially expressed miRNAs including nine down-regulated and three up-regulated miRNAs were found in the Cry1S1000 strain, compared to the G88 strain. In these miRNAs, novel-miR-210 and novel-miR-48 were predicted to show the strongest up-regulation and down-regulation trends, respectively (with the highest Log2-fold change value among listed miRNAs) (Table 2). Additionally, novel-miR-97 and novel-miR-237 were classified into the miR-973 and the miR-587 families, respectively, while others did not belong to any known miRNA family. Furthermore, the cluster analysis was performed to investigate the expression patterns of 12 differentially expressed miRNAs. Among all tested miRNAs, novel-miR-240, novel-miR-237, novel-miR-48, and novel-miR-97 showed significantly lower expression levels in the Cry1S1000 strain than in the G88 strain,

while novel-miR-210 displayed a relatively higher expression level in the Cry1S1000 strain (Figure 4). It was noted that novel-miR-118 and novel-miR-24 shared the same sequence with novel-miR-97, novel-miR-157 shared the same sequence with novel-miR-210, and the sequence of novel-miR-266 was the same with novel-miR-225. Thus, these miRNAs sharing the same sequences were combined and, respectively, named as novel-miR-97, novel-miR-210, and novel-miR-225 hereafter.

Target Gene Prediction of the Differentially Expressed miRNAs

A total of 7,647 target genes of the miRNAs identified in our study were predicted by miRanda and TargetScan, of which

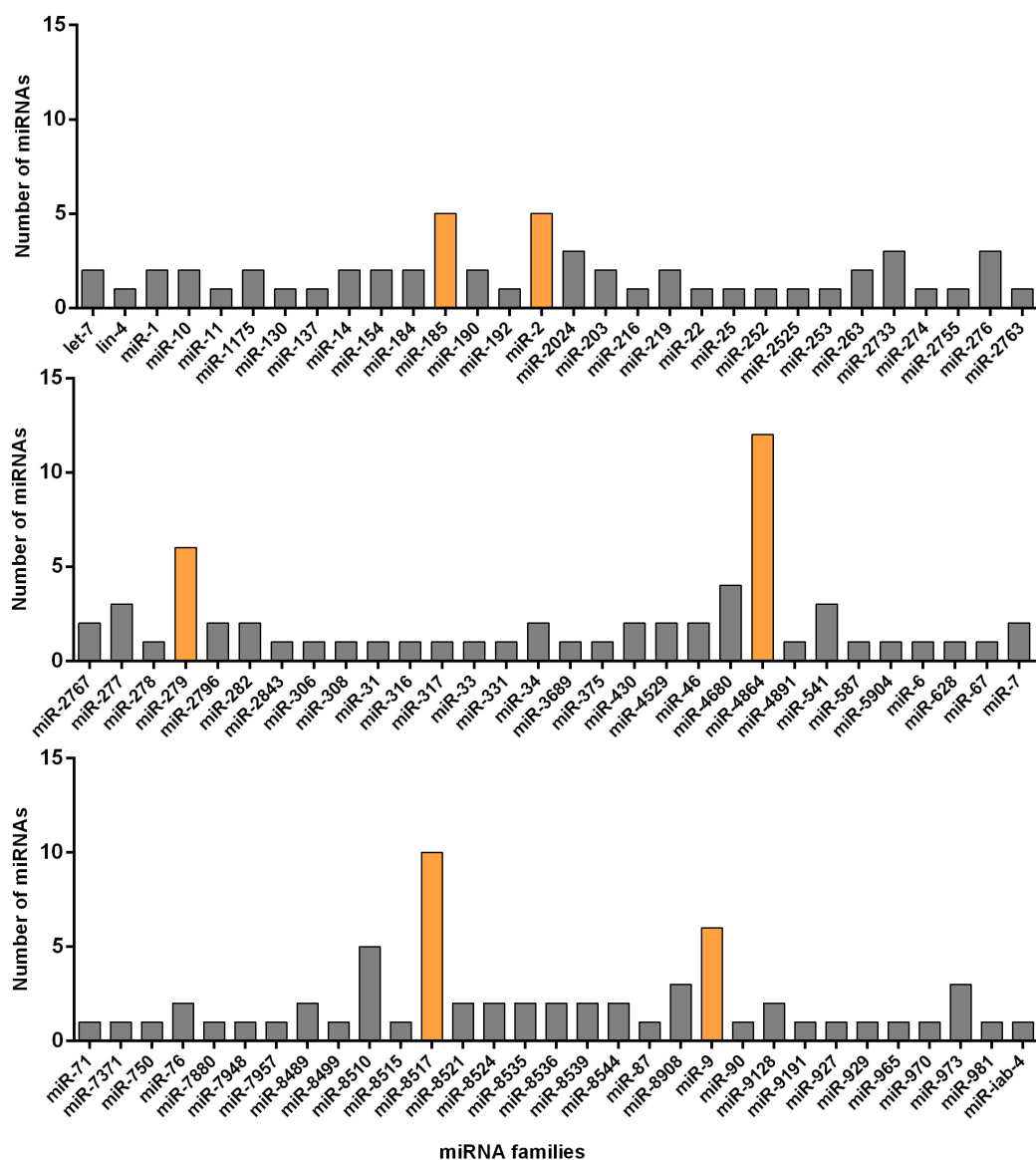


FIGURE 2 | Number of known miRNAs expressed in the resistant (Cry1S1000) and susceptible (G88) strains of DBM in each of the miRNA families. The families with relatively more members are marked with orange color while others with gray.

7,485 target genes were annotated with NR, Swiss-Prot, GO, COG, KEGG, KOG, and Pfam databases (Finn et al., 2014). To further explore the roles of the differentially expressed miRNAs, 44 genes potentially targeted by these 12 differentially expressed miRNAs were selected and represented in **Table 3**. Among them, the number of predicted target genes for each miRNA ranged from zero to 27, which implying a complex regulatory network between miRNAs and their target genes. Most miRNAs had multiple target genes. Conversely, some of the genes were also modulated by multiple miRNAs. Additionally, the annotation using the DBM-DB database showed that these putative transcripts were likely involved in multiple biological processes. Some of the differentially expressed miRNAs were predicted to regulate genes encoding chitinase A1, cuticle protein

6, transporting P-type ATPase, alyl-tRNA synthetase and cell wall protein, which might be closely related to the defense of external toxicant, energy transportation and metabolism and likely be involved in the insect immunity and insecticide resistance.

GO Enrichment and KEGG Pathway Analysis of Target Genes of Differentially Expressed miRNAs

GO annotation enrichment was performed to evaluate the presumptive functions of target genes of differentially expressed miRNAs (**Figure 5**). GO term analysis for these target genes revealed seven cellular components, five molecular processes, and seven different biological processes, among

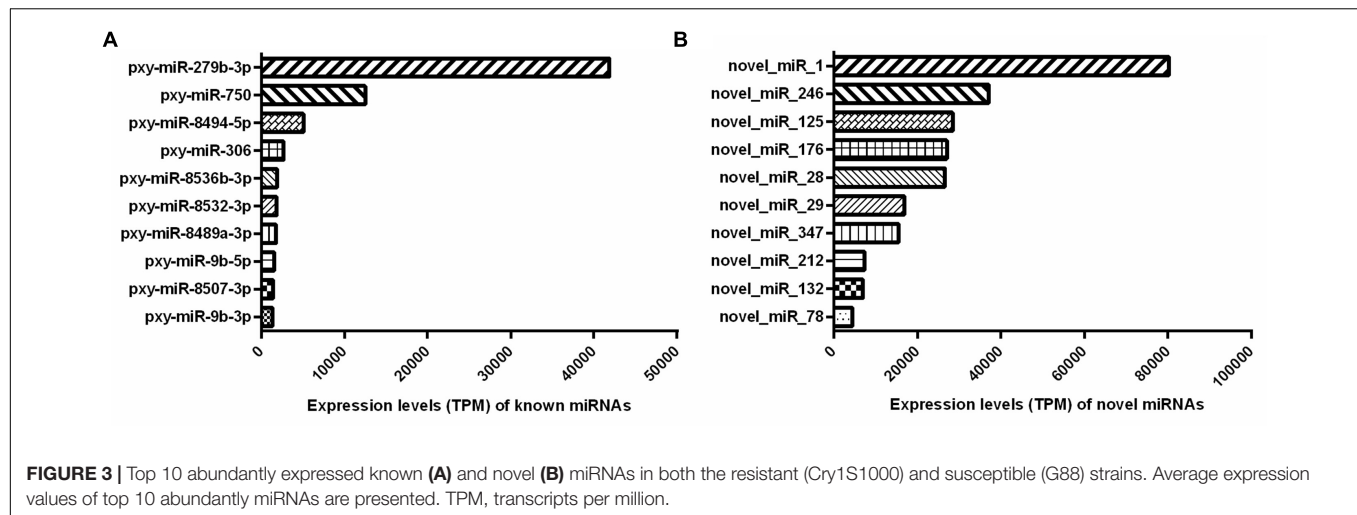


TABLE 2 | Differentially expressed miRNAs in the Cry1S000 and G88 strains.

sRNA	Sequence (5'–3')	Potential miRNA	E-value	Length	miRNA family	Log2-fold change	Regulatory trend
Novel_miR_210	uugugacguaggauugucaaua	Pma-miR-212-5p		22	–	3.970	Up
Novel-miR-274	ucagucucuguauucuccuaua	Pxy-miR-8529		23	–	2.030	Up
Novel-miR-288	cuaauccuccauagacucuaugu	Pxy-miR-8505 Gga-miR-7448-5p		24	–	1.624	Up
Novel-miR-48	uagcaccguagcauugaagu	*		20	–	–4.133	Down
Novel-miR-240	uccucaaaucauauuccucgc	*		22	–	–3.855	Down
Novel-miR-97	ccuagcuagauuuaucaucau	Prd-miR-60-3p		23	miR-973	–3.832	Down
Novel-miR-25	cagagaaaccugacccccucc	*		22	–	–2.800	Down
Pxy-miR-8522	auuugccgaagguucugauacc	*		22	–	–2.795	Down
Novel-miR-237	uuuccaccagagaugucuaug	*		22	miR-587	–2.787	Down
Novel-miR-225	uuaaaucgagauuugacacu	*		20	–	–2.750	Down
Novel-miR-270	aaacaucgaugaaacaucuga	Ame-miR-9864-5p	3.0	23	–	–2.301	Down
Novel-miR-116	uaccuaagcaggaacugauc	*		20	–	–1.957	Down

Potential miRNA, sequences of differentially expressed miRNAs were similar to those in other species but differ in some nucleotide positions. *Means miRNA sequences were not found in other species in miRbase (V22) with E-value cutoff < 3.

which cellular process (GO:0009987), metabolic process (GO:0008152), single-organism process (GO:0044699), and biological regulation (GO:0065007) were dominant. Additionally, most of the target genes were classified in membrane (GO:0016020), binding (GO:0005488), and catalytic activity (GO:0003824), implying the putative roles of these differentially expressed miRNAs in transmembrane transport and translation. A KEGG pathway analysis was also conducted to elucidate the biological interpretation of genes targeted by differentially expressed miRNAs (Figure 6). The result exhibited that *Px008940* and *Px016226* were enriched in the Hippo signaling pathway, *Px007475* and *Px008286* were enriched in aminoacyl-tRNA biosynthesis and *Px006958* was enriched in MAPK signaling pathway, which were associated with energy metabolism in insects. In addition, the remaining target genes were enriched in the metabolic pathways such as ubiquitin mediated proteolysis, ribosome biogenesis in eukaryotes, protein processing in endoplasmic reticulum and fatty acid metabolism (Supplementary Table 4).

RT-qPCR Validation of Differentially Expressed miRNAs and Their Putative Target Genes

To further analyze the actual expression patterns of miRNAs identified above, RT-qPCR was performed to estimated the relative expression patterns of the 12 differentially expressed miRNAs (one known and 11 novel) in midguts of the Cry1S1000 and G88 strains, respectively (Figure 7A). Five miRNAs (novel-miR-210, novel-miR-274, novel-miR-288, novel-miR-25, and pxy-miR-8522) represented significantly higher expression levels in the Cry1S1000 strain than in the G88 strain, while the expression levels of other seven miRNAs (novel-miR-48, novel-miR-240, novel-miR-97, novel-miR-237, novel-miR-225, novel-miR-270, and novel-miR-116) were relatively lower in the Cry1S1000 strain, whereas only novel-miR-240, novel-miR-270, and novel-miR-116 exhibited a significant difference. Additionally, novel-miR-48, novel-miR-240, novel-miR-97, and novel-miR-237 were consistent with those predicted with TPM, whereas others presented opposite trends (Figure 7B).

The potential target genes of differentially expressed miRNAs were investigated with two miRNA targets prediction algorithms, miRanda and TargetScan. A total of 34 target genes were profiled using RT-qPCR. Twelve target genes (*Px013363*, *Px014239*, *Px008286*, *Px011169*, *Px002074*, *Px009200*, *Px011234*, *Px006256*, *Px017590*, *Px007885*, *Px015953*, and *Px010315*) were significantly induced in the Cry1S1000 strain, among which *Px006256* and *Px015953* were significantly up-regulated for more than 4 times, while others were increased for 1~3 times. Moreover, only four target genes (*Px001355*, *Px002066*, *Px008303*, and *Px000596*) showed the significantly lower expression levels in the Cry1S1000 strain compared to those in the G88 strain. The expression levels of *Px017590* and *Px007885* exhibited opposite trends with their corresponding novel-miR-240. But there was no predicted target genes for the differentially expressed novel-miR-270 and novel-miR-116 (Figure 8).

DLR Validation of the Interaction Between Novel-miR-240 and Its Target Genes

DLR assay was used to assessed whether the novel-miR-240 could regulated the expression of *Px017590* and *Px007885* by acting on their predicted binding sites. The target sequences (~40 bp DNA fragments) containing the binding sites in the CDS of *Px017590* and *Px007885* were synthesized and cloned into the pmirGLO vector (pmirGLO-*Px017590*-WT and pmirGLO-*Px007885*-WT), respectively (Figures 9A,B). When novel-miR-240 agomir were co-transfected with pmirGLO-*Px017590*-WT or pmirGLO-*Px007885*-WT in HEK293T cells, the normalized firefly luciferase activity were significantly declined by 30 or 50% compared to the NC agomir control. Furthermore, we also designed the mutant fragments by altering the bases in the seed binding regions of *Px017590* and *Px007885* (pmirGLO-*Px017590*-MUT and pmirGLO-*Px007885*-MUT). As expected, the luciferase reporter activity was not affected by novel-miR-240 agomir, when it was co-transfected with pmirGLO-*Px017590*-MUT or pmirGLO-*Px007885*-MUT in HEK293T cells (Figures 9C,D). These results revealed that novel-miR-240 could regulate the expression of *Px017590* and *Px007885* by binding to their seed regions and therefore inhibiting mRNA translation.

DISCUSSION

MiRNAs, a class of endogenous non-coding RNAs, are considered to be modulators of gene expression at the post-transcriptional level (Lee et al., 2004). In recent years, with the development of the *in silico* miRNA identification platform such as mirMachine (Cagirici et al., 2021), miRanda (Rehmsmeier et al., 2004) and RNAhybrid (Mohebbi et al., 2021), many miRNAs have been characterized from multiple organisms including plants, vertebrates and invertebrates following the integration of various tools in bioinformatics, genetics, molecular biology and biochemistry. In insects, miRNAs played indispensable roles in development (Shen et al., 2020), behavior (Niu et al., 2019), immunity (Li R. et al., 2019), host-virus interaction (Singh, 2020), and resistance to multiple insecticides

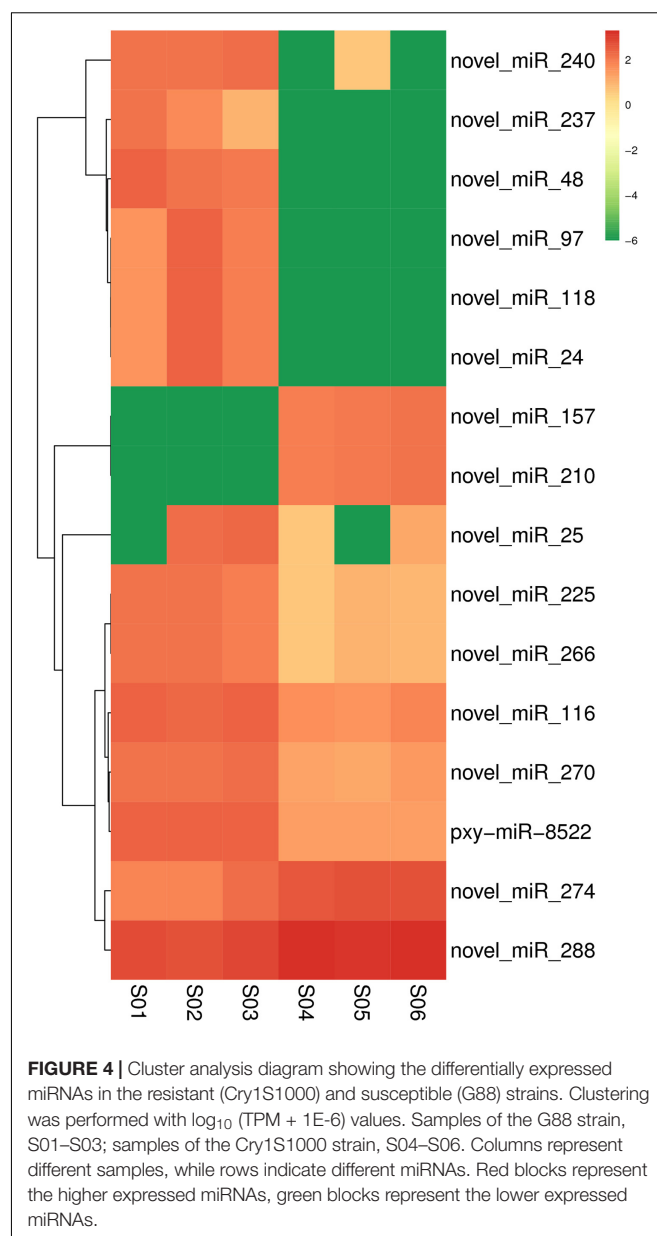


FIGURE 4 | Cluster analysis diagram showing the differentially expressed miRNAs in the resistant (Cry1S1000) and susceptible (G88) strains. Clustering was performed with $\log_{10} (\text{TPM} + 1\text{E}-6)$ values. Samples of the G88 strain, S01–S03; samples of the Cry1S1000 strain, S04–S06. Columns represent different samples, while rows indicate different miRNAs. Red blocks represent the higher expressed miRNAs, green blocks represent the lower expressed miRNAs.

(Zhu et al., 2019; Li X. et al., 2020). In addition, the high-quality genome offers the opportunity to explore the putative biological function of identified miRNAs (Robertson et al., 2018). DBM is a notorious agriculture pest, understanding the roles played by miRNAs in insecticides resistance can provide a significant theoretical basis for finding novel targets for pest control.

Here, we successfully constructed sRNA libraries from Bt resistant and susceptible strains, and identified a total of 437 miRNAs including 76 known and 361 novel miRNAs belonging to 91 miRNA families. Importantly, 12 differentially expressed miRNAs (three up and nine down) were revealed in the Cry1S1000 strain compared to the G88 strain. We also predicted the putative target genes for each of these 12 differentially expressed miRNAs, and the target genes were enriched in 43 GO

TABLE 3 | Putative target genes of differentially expressed novel miRNAs.

miRNA	Target gene	Annotation of target genes with DBM-DB
Novel-miR-210	Px006169	–
	Px000808	Nesprin-1
Novel-miR-274	Px013363	Exostosin-2
	Px012927	Exocyst complex component 1
	Px013839	Carnitine O-palmitoyltransferase 1, liver isoform
	Px007475	Valyl-tRNA synthetase
	Px014239	Mannosyl-oligosaccharide glucosidase
	Px009012	Midasin
	Px008940	Moesin/ezrin/radixin homolog 2
	Px008286	Valyl-tRNA synthetase
	Px011169	Nephrin
	Px002074	Mycosubtilin synthase subunit C
	Px002344	S phase cyclin A-associated protein in the endoplasmic reticulum
	Px001355	Putative cation-transporting P-type ATPase
	Px016226	Moesin/ezrin/radixin homolog 2
	Px006958	Importin-7
	Px002066	Protogenin
	Px008303	Spondin, N-terminal
	Px002006	Polypeptide N-acetylgalactosaminyltransferase 5
	Px001769	Ubiquitin carboxyl-terminal hydrolase calypso
	Px006107	Interleukin-1 receptor accessory protein-like 1-B
	Px016576	E3 ubiquitin-protein ligase HERC2
	Px010440	GAS2-like protein 1
	Px005898	Putative uncharacterized protein
	Px004830	GG20930
	Px002366	MAGUK p55 subfamily member 6
	Px009200	Dynein heavy chain 3, axonemal
	Px006757	Cell wall protein, putative
	Px008634	Putative uncharacterized protein
Novel-miR-288	Px016171	Prolyl endopeptidase
Novel-miR-48	Px011234	Nose resistant to fluoxetine protein 6
	Px006256	Lachesin
	Px004597	Thyrotropin-releasing hormone receptor
Novel-miR-240	Px003379	Dynein heavy chain, cytoplasmic
	Px017590	Alsin
	Px007885	Discoidin domain-containing receptor 2
Novel-miR-25	Px014091	Leucine-rich PPR motif-containing protein, mitochondrial
	Px015953	Chitinase A1
	Px002493	Carbonic anhydrase 2
	Px000596	Cuticle protein 6
	Px005729	Monocarboxylate transporter 12
Novel-miR-237	Px010315	Bromodomain adjacent to zinc finger domain protein 2B
	Px000280	Elongation of very long chain fatty acids protein 7
	Px016697	Putative L-ribulose-5-phosphate 3-epimerase sgbU

terms based on GO and KEGG pathway analyses. Furthermore, the expression patterns of these differentially expressed miRNAs and their potential target genes were investigated with RT-qPCR. Finally, the dual luciferase assay was carried out to confirm the interaction between novel-miR-240 and its target genes *Px017590* and *Px007885*.

From the identified miRNAs, a member of the miR-279 family, miR-279b-3p, was listed as the most abundant miRNA in our sRNA libraries. Previously, it has been found that miR-279, another member of the miR-279 family, was also listed as an abundantly expressed miRNA in DBM larvae after destruxin A injection and predicted to regulate the immunity-related genes (Shakeel et al., 2018). MiR-306, a common abundantly expressed miRNA identified in our study, has been shown to associated with Bt Cry1Ab resistance in *Ostrinia furnacalis* (Xu et al., 2015).

Additionally, a total of 78 known and novel miRNAs were classified into 91 miRNA families. MiRNAs sharing the same seed region were classified as a miRNA family, which likely indicated that they targeted the same genes and performed similar biological functions. In the current study, novel-miR-133 and novel-miR-250 were classified into the *let-7* family, which is functionally conserved from insects to humans and participated in multiple biological processes. In insects, modulating the abundance of *let-7* altered the tolerance of *Myzus persicae nicotianae* to nicotine (Peng et al., 2016). *Let-7* was also required in many developmental processes, such as sleep homeostasis (Goodwin et al., 2018), age-dependent behavioral changes (Behura and Whitfield, 2010), developmental transitions of egg hatching, molting, pupation, adult eclosion (Zhang et al., 2020) and the regulation of ecdysone levels (Liu et al., 2007).

Novel-miR-93 and novel-miR-125 were classified into the miR-14 family, which is conserved in insects and is closely related to olfactory and chemoreception (Shan et al., 2020). Another study showed that miR-14-3p, another member of the miR-14 family, could tightly control the ecdysone signaling pathway by regulating *EcR* and *E75* (Luo et al., 2020). A total of five miRNAs (novel-miR-142, novel-miR-214, novel-miR-219, novel-miR-222, and novel-miR-253) identified in our study belong to the miR-2 family. The conserved miR-2 family was an invertebrate-specific family of miRNAs and involved in insect metamorphosis (Lozano et al., 2015), oogenesis (Song et al., 2019) neural development (Marco et al., 2012), as well as deltamethrin resistance in *Cx. pipiens pallens* (Guo et al., 2017).

Pxy-miR-252 belonged to the miR-252 family. It has been found that miR-252 could directly repress the *mbt* expression to control the developmental growth of *Drosophila* (Lim et al., 2019) and was also involved in dengue virus replication in *Aedes albopictus* (Yan et al., 2014). Pxy-miR-274 was classified into the miR-274 family. Inhibition of miR-274-3p could facilitate *B. mori* cytoplasmic polyhedrosis virus (BmCPV) replication (Wu et al., 2017). Novel-miR-78 was classified into the miR-276 family. The miR-276 family might be involved in the spiriotetramat resistance of *Aphis gossypii* Glover (Wei et al., 2016) and the dengue virus (DENV) replication in C6/36 cells (Su et al., 2019). Pxy-miR-277 belonged to the miR-277 family, which was conserved in insects and participated in multiple physiological processes such as restoring immune homeostasis of the IMD pathway (Li R. et al., 2020), controlling metamorphosis (Shen et al., 2020), lipid metabolism and reproduction (Ling et al., 2017). MiR-277-3p was also a part of the molecular toolkit regulating reproductive diapause in *Culex pipiens* (Meuti et al., 2018) and *Helicoverpa zea* (Reynolds et al., 2019). Hence, we speculate that the pxy-miR-277 might be involved in diverse biological processes in

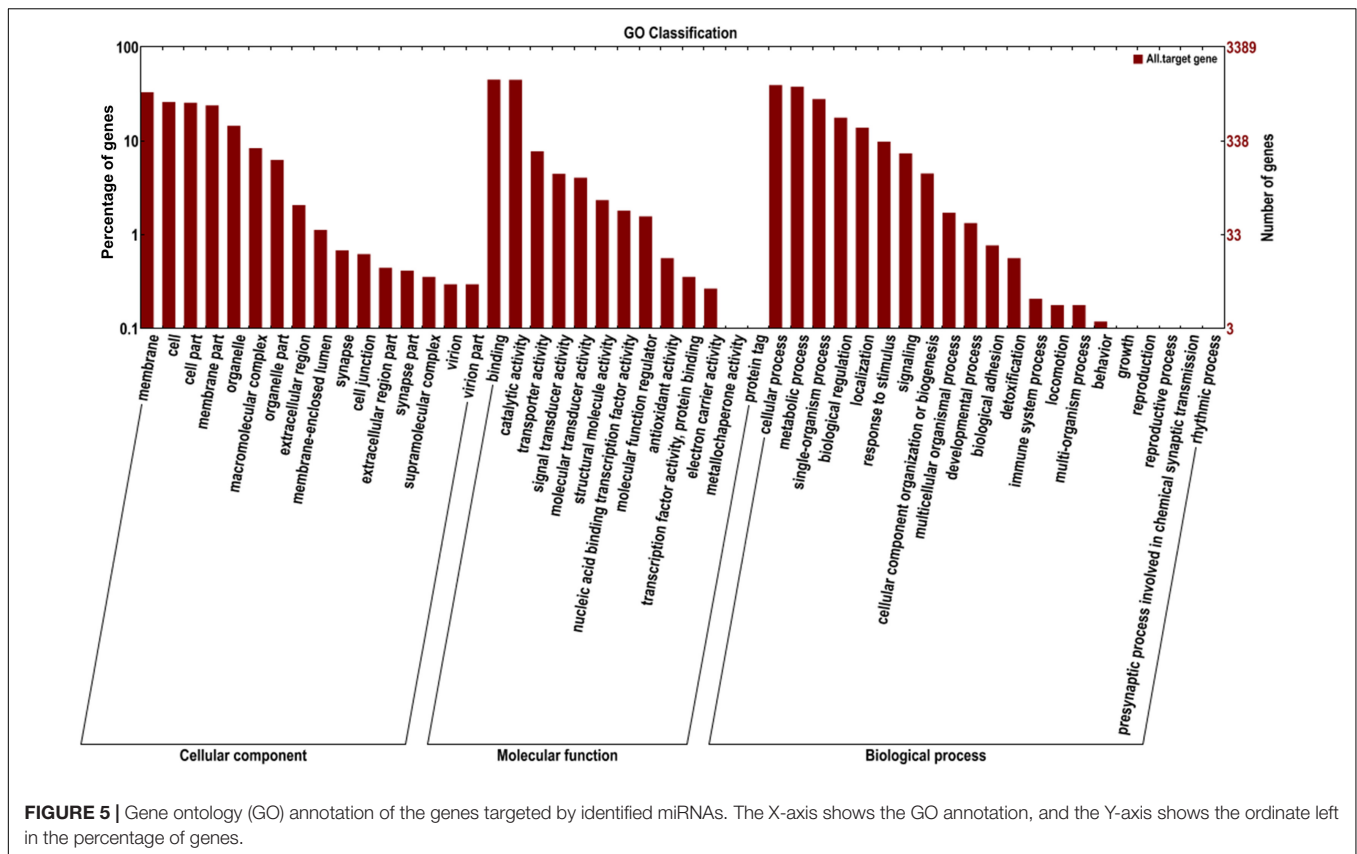


FIGURE 5 | Gene ontology (GO) annotation of the genes targeted by identified miRNAs. The X-axis shows the GO annotation, and the Y-axis shows the ordinate left in the percentage of genes.

DBM and indirectly affect detoxification of Bt Cry toxin. Pxy-miR-279a, pxy-279b-5p, and pxy-279-3p were classified to the miR-279 family. It has been reported that miR-279 was essential to maintain circadian rhythm (Sun et al., 2015) and reproductive responses by females to male sex peptide in *D. melanogaster* (Fricke et al., 2014). So, pxy-miR-279a, pxy-279b-5p, and pxy-279-3p might play the similar roles with miR-279 in insects. Pxy-miR-306 and pxy-miR-308 belonged to miR-306 and miR-308 families, respectively. MiR-279, miR-306, and miR-308 were also predicted to be involved in the Destruxin A-responsive immunity process in DBM (Shakeel et al., 2018), indicating that these miRNA families might be closely associated with Bt resistance. Novel-miR-21 was classified into the miR-317 family, and miR-317 was found to be involved in the process of pupation in *B. dorsalis* (Zhang et al., 2020). In *Drosophila*, miR-87 was an important regulator of dendrite regeneration (Kitatani et al., 2020), so we speculated that novel-miR-199 as a member of the miR-87 family, might play the similar roles in DBM. In summary, these miRNA families identified in the current study were widely involved in diverse biological processes in insects, some of the miRNA families also took part in insect immunity. Investigating the functions of these conserved miRNA families and their representative members will provide a better understanding of miRNA-mediate post-transcriptional regulation in insects.

It has been previously shown that the differentially expressed miRNAs among the susceptible and resistant strains might be related to insecticides resistance in DBM. For instance, the

expression of miR-276-5p and miR-8530-5p were 2–3 times higher in the chlorantraniliprole resistant DBM strain compared to the susceptible strain, indicating that these two miRNAs likely participated in the response of DBM to chlorantraniliprole (Zhu et al., 2017). The expression level of miR-278-3p was 4.2 fold lower in the deltamethrin-resistant strain (DR-strain), which induced the pyrethroid resistance in *Cx. pipiens pallens* (Lei et al., 2014). The other two conserved miRNAs, miR-932 and miR-285 were estimated to be 1.8- and 2.8-fold higher, respectively, in the DR-strain and were involved in pyrethroid resistance (Liu et al., 2016; Tian et al., 2016). In this study, the expression levels of novel-miR-240, novel-miR-270 and novel-miR-116 in the resistant Cry1S1000 strain were significantly lower than that in the susceptible G88 strain, other miRNAs such as novel-miR-210, novel-miR-274, novel-miR-288, novel-miR-25, and pxy-miR-8522 represented significantly higher expression levels in the resistant Cry1S1000 strain, and novel-miR-48, novel-miR-97, novel-miR-237, and novel-miR-225 exhibited no significant difference between these two strains. Moreover, the differentially expressed novel-miR-240, novel-miR-270, and novel-miR-116 did not belong to any known miRNA family, indicating that there was no miRNA shared the same seed regions or derived from the same arm of the stem-loop with these two miRNAs (Meyers et al., 2008). While novel-miR-270 had a similar sequence with ame-miR-9864-5p, suggesting that they may be the same miRNA in different species and play similar roles in insects. Our results suggested that the expression of miRNAs varies among different

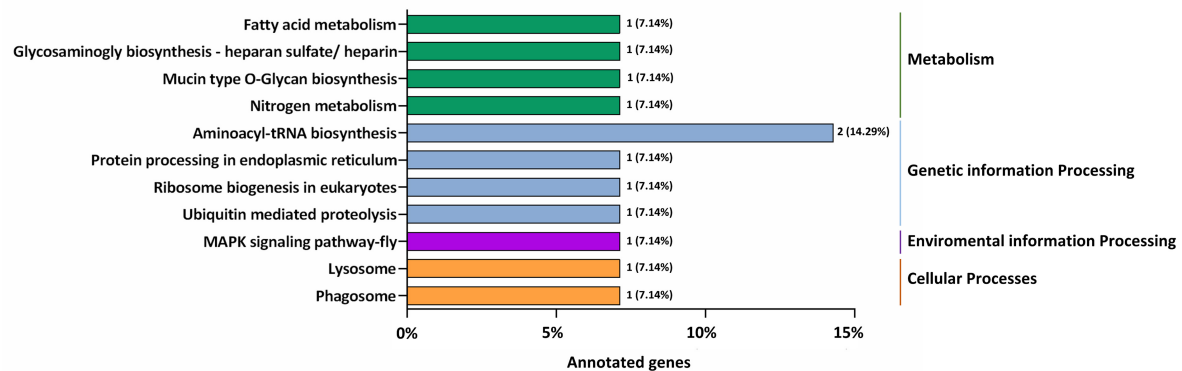


FIGURE 6 | The most enriched KEGG pathways based on the genes targeted by differentially expressed miRNAs in the resistant (Cry1S1000) and susceptible (G88) strains. The X-axis shows the number of genes annotated to the pathway and the ratio of the number of annotated genes to the total genes annotated, and the Y-axis shows the pathway names. The different color of column indicates different type of KEGG pathway.

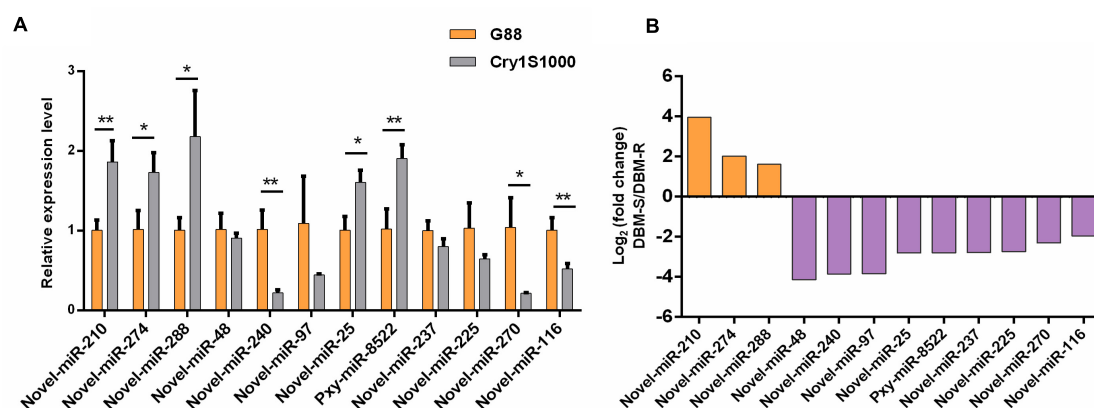


FIGURE 7 | Relative expression levels of differentially expressed miRNAs in midguts of the resistant (Cry1S1000) and susceptible (G88) strains by RT-qPCR (A), and up-/down-regulated expression of the miRNAs based on Illumina sequencing (B). The expression levels of miRNAs were normalized by U6. Statistical significance was analyzed using one-way ANOVA. The asterisks represent significance, where two asterisks indicate $p < 0.01$, and one asterisk indicates $p < 0.05$. (B) The orange column above the X-axis shows up-regulated miRNAs, while the purple column below the X-axis shows down-regulated miRNAs based on Illumina sequencing.

strains, and these differentially expressed miRNAs may regulate detoxification to Bt Cry1Ac toxin in a complicated manner by targeting detoxification-related genes.

It should be noted that novel-miR-240 represents down-regulated expression in the Cry1S1000 strain relative to the G88 strain, whereas its target genes *Px017590* and *Px007885* were up-regulated in the Cry1S1000 strain. The DLR assay results implied the involvement of novel-miR-240 in the regulation of *Px017590* and *Px007885*, indicating that this miRNA might modulate Bt resistance of DBM via negatively regulating its target genes.

Furthermore, GO annotation exhibited that most of the predicted target genes of differentially expressed miRNAs were enriched in biological process (cellular process, metabolism process, single-organism process, and biological regulation), cellular component (membrane, cell, cell part, and membrane part) and molecular function (binding and catalytic activity),

which might be related to the insect immunity and the metabolism to the Bt Cry1Ac toxin. The target genes of differentially expressed miRNAs were mostly enriched in metabolic-related pathways such as Hippo signaling pathway, aminoacyl-tRNA biosynthesis and MAPK signaling pathway. And in a previous study, MAPK signaling pathway was found to lead to Bt Cry1Ac resistance by mediating differential expression of APN and other midgut genes in DBM (Guo et al., 2020). The DBM-DB database was used for the annotation of target genes. *Px015953* and *Px000596*, the target genes of novel-miR-25, were predicted to be associated with chitinase and cuticle protein, which may be involved in the process of DBM combating the exogenous Bt Cry1Ac toxin.

Chitinase, an insect molting enzyme, is a potential biopesticide that degrades chitin to low molecular weight, soluble and insoluble oligosaccharides. Previous research has shown that

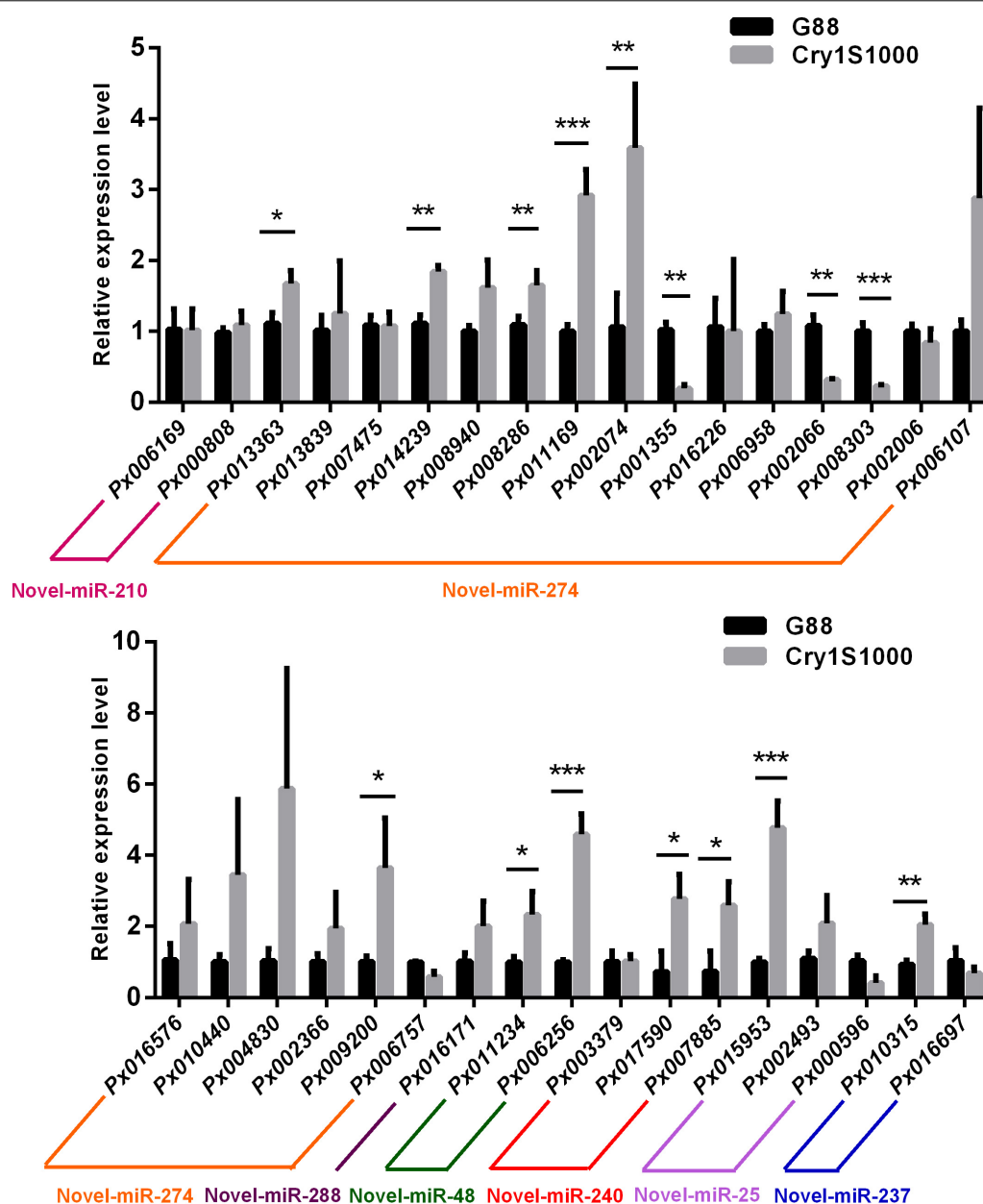


FIGURE 8 | Relative expression levels of target genes in midguts of the resistant (Cry1S1000) and susceptible (G88) strains based on RT-qPCR. The expression levels of target genes were normalized by *RPL32*. Statistical significance was analyzed using one-way ANOVA. The asterisks represent significance, where three asterisks indicate $p < 0.001$, two asterisks indicate $p < 0.01$, and one asterisk indicates $p < 0.05$.

chitinases could degrade the vital structures of insects such as their peritrophic membranes and cuticles, thus facilitating the entry of the pathogens into the tissues of susceptible insects (Brandt et al., 1978). Chitinases also facilitated the penetration of host cuticle by entomopathogenic fungi. Analysis of the top 20 differentially expressed genes showed that the chitinase *ChiA2* was up-regulated after *Beauveria bassiana* infected non-natural hosts such as *H. armigera* and *Clanis bilineata* (Liu et al., 2021). These chitinase-related genes indicated that when entomopathogenic fungi transfer to non-original hosts, the fungi

changed the metabolic response of hosts and used the novel infection strategies to break the barrier of different cuticle chitin components to better adaption to new hosts. Therefore, the chitin based bioformulation may act as an effective pesticide against Lepidopterous pests. A prior work revealed that the expression of cuticle proteins were significantly induced at 6 h post-treatment of Cry1Ac toxin (Qin et al., 2021). Genes encoding cuticle proteins were induced during *B. mori* bidensovirus (BmBDV) infection (Sun et al., 2020). The down-regulation of some *Cardinium*-responsive miRNAs enhanced the cuticle

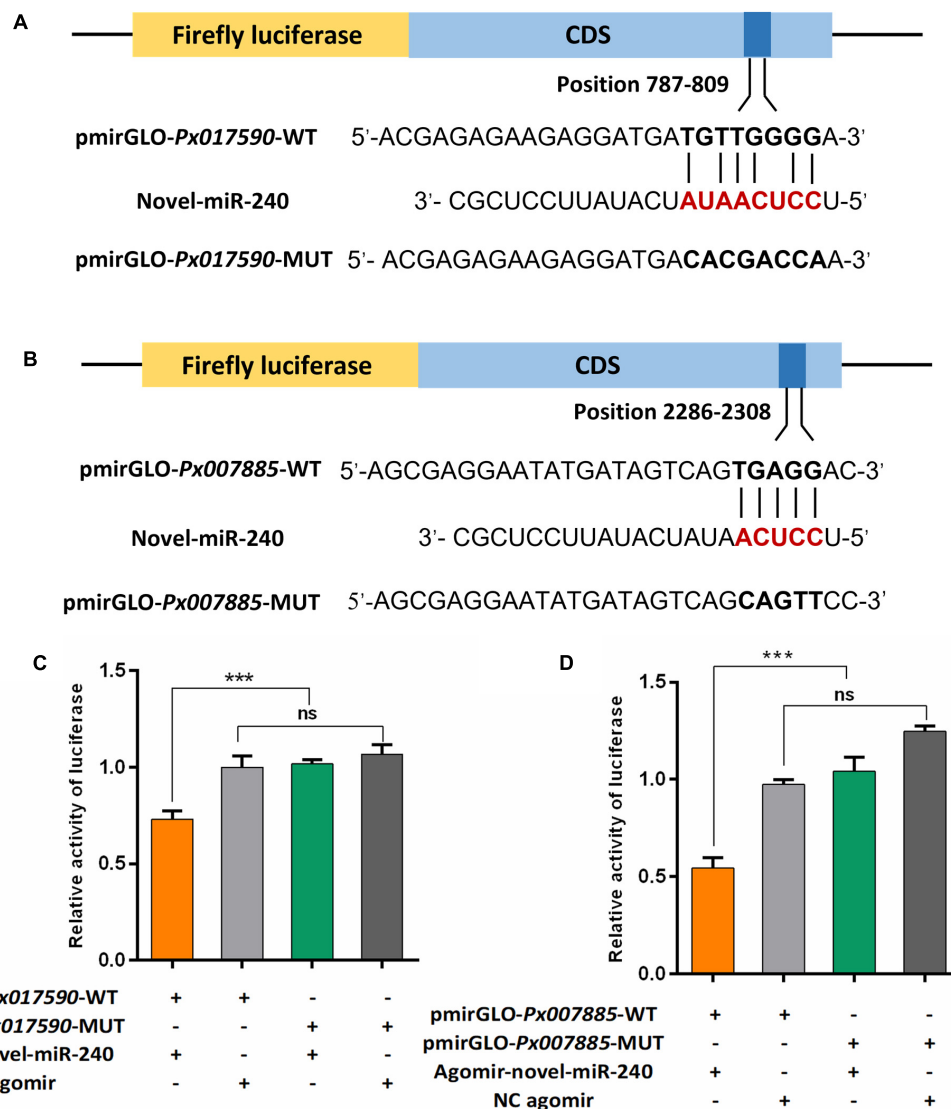


FIGURE 9 | Dual luciferase reporter assay confirmed the interaction between novel-miR-240 and its target genes in vitro. **(A)** Predicted target sites of novel-miR-240 in the CDS of *Px017590*. **(B)** Predicted target sites of novel-miR-240 in the CDS of *Px007885*. WT, wild-type sequence; MUT, mutant sequence. **(C)** The interaction between novel-miR-240 and *Px017590*. **(D)** The interaction between novel-miR-240 and *Px007885*. Statistical significance was analyzed using one-way ANOVA followed by Tukey's multiple comparisons. The three asterisks indicate $p < 0.001$ and "ns" represents no significance.

proteins in whitefly *Bemisia tabaci* (Gennadius) biotype Q and modulated insect reproduction and growth (Li et al., 2018). In addition, RNA-seq of *Cryptolestes ferrugineus* individuals from phosphine susceptible and resistant populations revealed the significantly increased expression levels of nine cuticular protein genes in the resistance population, demonstrating that the cuticular protein genes might be related to phosphine resistance (Chen et al., 2021). In the current study, the target genes of identified differentially expressed miRNAs, especially the chitinase and cuticle protein, might involved in the insects immune response and the detoxification of xenobiotics including the Bt Cry1Ac toxin. Although the RT-qPCR results showed that some of the identified differentially expressed miRNAs exhibited

positively correlate with their potential targets, the target genes of these differentially expressed miRNAs were still worthy for further investigation, where functional characterizations of the target genes will provide novel insights of insects immunity and detoxification mechanisms.

CONCLUSION

In the present study, we identified 76 known and 361 novel miRNAs from midguts of the Bt resistant and susceptible DBM strains. Among the identified miRNAs, 178 were classified into 91 miRNA families, and the potential functions of these miRNA

families have also been illustrated. Expression of 12 differentially expressed miRNAs and their potential target genes were profiled, revealing that these miRNAs may play vital roles in detoxicating Bt Cry1Ac toxins by regulating their corresponding target genes. Moreover, the interaction between novel-miR-240 and its target genes *Px017590* and *Px007885* have been confirmed by the DLR assay. However, further experiments are still required to demonstrate the functional pathways which the differentially expressed miRNAs and their target genes are involved in. Our study contributes to the field for further investigation of the miRNA-mediated gene regulation at the post-transcriptional level in insect resistance and the RNAi-based pest management.

DATA AVAILABILITY STATEMENT

The datasets presented in this study can be found in online repositories. The names of the repository/repositories and accession number(s) can be found below: NCBI SRA; PRJNA754494.

REFERENCES

- Apweiler, R., Bairoch, A., Wu, C. H., Barker, W. C., Boeckmann, B., Ferro, S., et al. (2004). UniProt: the Universal Protein knowledgebase. *Nucleic Acids Res.* 32, D115–D119. doi: 10.1093/nar/gkh131
- Asgari, S. (2013). MicroRNA functions in insects. *Insect Biochem. Mol. Biol.* 43, 388–397. doi: 10.1016/j.ibmb.2012.10.005
- Ashburner, M., Ball, C. A., Blake, J. A., Botstein, D., Butler, H., Cherry, J. M., et al. (2000). Gene ontology: tool for the unification of biology. The Gene Ontology Consortium. *Nat. Genet.* 25, 25–29. doi: 10.1038/75556
- Bartel, D. P. (2004). MicroRNAs: genomics, biogenesis, mechanism, and function. *Cell* 116, 281–297.
- Behura, S. K., and Whitfield, C. W. (2010). Correlated expression patterns of microRNA genes with age-dependent behavioural changes in honeybee. *Insect Mol. Biol.* 19, 431–439. doi: 10.1111/j.1365-2583.2010.01010.x
- Brandt, C. R., Adang, M. J., and Spence, K. D. (1978). The peritrophic membrane: ultrastructural analysis and function as a mechanical barrier to microbial infection in *Orgyia pseudotsugata*. *J. Invertebr. Pathol.* 32, 12–24. doi: 10.1016/0022-2011(78)90169-6
- Bravo, A., Likitvatanavong, S., Gill, S. S., and Soberón, M. (2011). *Bacillus thuringiensis*: a story of a successful bioinsecticide. *Insect Biochem. Mol. Biol.* 41, 423–431. doi: 10.1016/j.ibmb.2011.02.006
- Cagirici, H. B., Sen, T. Z., and Budak, H. (2021). mirMachine: a one-stop shop for plant miRNA annotation. *J. Vis. Exp.* 171:e62430. doi: 10.3791/62430
- Calles-Torrez, V., Knodel, J. J., Boetel, M. A., French, B. W., Fuller, B. W., and Ransom, J. K. (2019). Field-evolved resistance of northern and western corn rootworm (Coleoptera: Chrysomelidae) populations to corn hybrids expressing single and pyramided Cry3Bb1 and Cry34/35Ab1 Bt proteins in North Dakota. *J. Econ. Entomol.* 112, 1875–1886. doi: 10.1093/jeet/toz111
- Chen, E. H., Duan, J. Y., Song, W., Wang, D. X., and Tang, P. A. (2021). RNA-seq analysis reveals mitochondrial and cuticular protein genes are associated with phosphine resistance in the Rusty Grain Beetle (Coleoptera:Laemophloeidae). *J. Econ. Entomol.* 114, 440–453. doi: 10.1093/jeet/toaa273
- Chen, X., and Rosbash, M. (2016). Mir-276a strengthens *Drosophila* circadian rhythms by regulating timeless expression. *Proc. Natl. Acad. Sci. U.S.A.* 113, E2965–E2972. doi: 10.1073/pnas.1605837113
- Cristino, A. S., Barchuk, A. R., Freitas, F. C., Narayanan, R. K., Biergans, S. D., Zhao, Z., et al. (2014). Neuroligin-associated microRNA-932 targets actin and regulates memory in the honeybee. *Nat. Commun.* 5:5529. doi: 10.1038/ncomms6529
- Cullen, B. R. (2004). Transcription and processing of human microRNA precursors. *Mol. Cell* 16, 861–865.
- Dubey, S. K., Shrinet, J., and Sunil, S. (2019). *Aedes aegypti* microRNA, miR-2944b-5p interacts with 3'UTR of chikungunya virus and cellular target vps-13 to regulate viral replication. *PLoS Negl. Trop. Dis.* 13:e0007429. doi: 10.1371/journal.pntd.0007429
- Etebari, K., Afrad, M. H., Tang, B., Silva, R., Furlong, M. J., and Asgari, S. (2018). Involvement of microRNA miR-2b-3p in regulation of metabolic resistance to insecticides in *Plutella xylostella*. *Insect Mol. Biol.* 27, 478–491. doi: 10.1111/imb.12387
- Finn, R. D., Bateman, A., Clements, J., Coghill, P., Eberhardt, R. Y., Eddy, S. R., et al. (2014). Pfam: the protein families database. *Nucleic Acids Res.* 42, D222–D230. doi: 10.1093/nar/gkt1223
- Fricke, C., Green, D., Smith, D., Dalmay, T., and Chapman, T. (2014). MicroRNAs influence reproductive responses by females to male sex peptide in *Drosophila melanogaster*. *Genetics* 198, 1603–1619. doi: 10.1534/genetics.114.167320
- Friedlander, M. R., Mackowiak, S. D., Li, N., Chen, W., and Rajewsky, N. (2012). miRDeep2 accurately identifies known and hundreds of novel microRNA genes in seven animal clades. *Nucleic Acids Res.* 40, 37–52. doi: 10.1093/nar/gkr688
- Furlong, M. J., Wright, D. J., and Dosdall, L. M. (2013). Diamondback moth ecology and management: problems, progress, and prospects. *Annu. Rev. Entomol.* 58, 517–541. doi: 10.1146/annurev-ento-120811-153605
- Goodwin, P. R., Meng, A., Moore, J., Hobin, M., Fulga, T. A., Van Vactor, D., et al. (2018). MicroRNAs regulate sleep and sleep homeostasis in *Drosophila*. *Cell Rep.* 23, 3776–3786. doi: 10.1016/j.celrep.2018.05.078
- Guo, Q., Huang, Y., Zou, F., Liu, B., Tian, M., Ye, W., et al. (2017). The role of miR-2~13~71 cluster in resistance to deltamethrin in *Culex pipiens pallens*. *Insect Biochem. Mol. Biol.* 84, 15–22. doi: 10.1016/j.ibmb.2017.03.006
- Guo, Z., Kang, S., Sun, D., Gong, L., Zhou, J., Qin, J., et al. (2020). MAPK-dependent hormonal signaling plasticity contributes to overcoming *Bacillus thuringiensis* toxin action in an insect host. *Nat. Commun.* 11:3003. doi: 10.1038/s41467-020-16608-8
- He, J., Chen, Q., Wei, Y., Jiang, F., Yang, M., Hao, S., et al. (2016). MicroRNA-276 promotes egg-hatching synchrony by up-regulating *brm* in locusts. *Proc. Natl. Acad. Sci. U.S.A.* 113, 584–589. doi: 10.1073/pnas.1521098113
- Janmaat, A. F., and Myers, J. (2003). Rapid evolution and the cost of resistance to *Bacillus thuringiensis* in greenhouse populations of cabbage loopers, *Trichoplusia ni*. *Proc. Biol. Sci.* 270, 2263–2270. doi: 10.1098/rspb.2003.2497
- Kanehisa, M., Goto, S., Kawashima, S., Okuno, Y., and Hattori, M. (2004). The KEGG resource for deciphering the genome. *Nucleic Acids Res.* 32, D277–D280. doi: 10.1093/nar/gkh063

AUTHOR CONTRIBUTIONS

MX and MY conceived and designed the study. JY performed the experiments and analyzed the data with the help of GL, SC, and JB. JY wrote the first draft of the manuscript. XX, SL, MX, MY, and QS participated in manuscript drafted and modification. All authors reviewed and approved the final manuscript.

FUNDING

This work was supported by the National Natural Science Foundation of China (31701796) and the Natural Science Foundation of Fujian Province (2018J01618).

SUPPLEMENTARY MATERIAL

The Supplementary Material for this article can be found online at: <https://www.frontiersin.org/articles/10.3389/fgene.2021.739849/full#supplementary-material>

- Kitatani, Y., Tezuka, A., Hasegawa, E., Yanagi, S., Togashi, K., Tsuji, M., et al. (2020). *Drosophila* miR-87 promotes dendrite regeneration by targeting the transcriptional repressor Tramtrack69. *PLoS Genet.* 16:e1008942. doi: 10.1371/journal.pgen.1008942
- Koonin, E. V., Fedorova, N. D., Jackson, J. D., Jacobs, A. R., Krylov, D. M., Makarova, K. S., et al. (2004). A comprehensive evolutionary classification of proteins encoded in complete eukaryotic genomes. *Genome Biol.* 5:R7. doi: 10.1186/gb-2004-5-2-r7
- Lee, Y., Kim, M., Han, J., Yeom, K. H., Lee, S., Baek, S. H., et al. (2004). MicroRNA genes are transcribed by RNA polymerase II. *EMBO J.* 23, 4051–4060. doi: 10.1038/10.1038/
- Lei, Z., Lv, Y., Wang, W., Guo, Q., Zou, F., Hu, S., et al. (2014). MiR-278-3p regulates pyrethroid resistance in *Culex pipiens pallens*. *Parasitol. Res.* 114, 699–706. doi: 10.1007/s00436-014-4236-7
- Lewis, B. P., Burge, C. B., and Bartel, D. P. (2005). Conserved seed pairing, often flanked by adenosines, indicates that thousands of human genes are microRNA targets. *Cell* 120, 15–20. doi: 10.1016/j.cell.2004.12.035
- Li, H., Wei, X., Ding, T., and Chu, D. (2018). Genome-wide profiling of *Cardinium*-responsive microRNAs in the exotic whitefly, *Bemisia tabaci* (Gennadius) biotype Q. *Front. Physiol.* 9:1580. doi: 10.3389/fphys.2018.01580
- Li, R., Huang, Y., Zhang, Q., Zhou, H., Jin, P., and Ma, F. (2019). The miR-317 functions as a negative regulator of Toll immune response and influences *Drosophila* survival. *Dev. Comp. Immunol.* 95, 19–27. doi: 10.1016/j.dci.2019.01.012
- Li, R., Zhou, H., Jia, C., Jin, P., and Ma, F. (2020). *Drosophila* Myc restores immune homeostasis of Imd pathway via activating miR-277 to inhibit imd/Tab2. *PLoS Genet.* 16:e1008989. doi: 10.1371/journal.pgen.1008989
- Li, S., Xu, X., Zheng, Z., Zheng, J., Shakeel, M., and Jin, F. (2019). MicroRNA expression profiling of *Plutella xylostella* after challenge with *B. thuringiensis*. *Dev. Comp. Immunol.* 93, 115–124. doi: 10.1016/j.dci.2018.12.008
- Li, X., Guo, L., Zhou, X., Gao, X., and Liang, P. (2015). MiRNAs regulated overexpression of ryanodine receptor is involved in chlorantraniliprole resistance in *Plutella xylostella* (L.). *Sci. Rep.* 5:14095. doi: 10.1038/srep14095
- Li, X., Ren, X., Liu, Y., Smagghe, G., Liang, P., and Gao, X. (2020). MiR-189942 regulates fufenozide susceptibility by modulating ecdysone receptor isoform B in *Plutella xylostella* (L.). *Pestic. Biochem. Physiol.* 163, 235–240. doi: 10.1016/j.pestbp.2019.11.021
- Li, Z., Feng, X., Liu, S. S., You, M., and Furlong, M. J. (2016). Biology, ecology, and management of the diamondback moth in China. *Annu. Rev. Entomol.* 61, 277–296. doi: 10.1146/annurev-ento-010715-023622
- Lim, D. H., Lee, S., Choi, M. S., Han, J. Y., Seong, Y., Na, D., et al. (2020). The conserved microRNA miR-8-3p coordinates the expression of V-ATPase subunits to regulate ecdysone biosynthesis for *Drosophila* metamorphosis. *FASEB J.* 34, 6449–6465. doi: 10.1096/fj.201901516R
- Lim, D. H., Lee, S., Han, J. Y., Choi, M. S., Hong, J. S., and Lee, Y. S. (2019). MicroRNA miR-252 targets *mbt* to control the developmental growth of *Drosophila*. *Insect Mol. Biol.* 28, 444–454. doi: 10.1111/imb.12562
- Ling, L., Kokoza, V. A., Zhang, C., Aksoy, E., and Raikhel, A. S. (2017). MicroRNA-277 targets *insulin-like peptides 7* and *8* to control lipid metabolism and reproduction in *Aedes aegypti* mosquitoes. *Proc. Natl. Acad. Sci. U.S.A.* 114, E8017–E8024. doi: 10.1073/pnas.1710970114
- Liu, B., Tian, M., Guo, Q., Ma, L., Zhou, D., Shen, B., et al. (2016). MiR-932 regulates pyrethroid resistance in *Culex pipiens pallens* (Diptera: Culicidae). *J. Med. Entomol.* 53, 1205–1210. doi: 10.1093/jme/tjw083
- Liu, J., Ling, Z., Wang, J., Xiang, T., Xu, L., Gu, C., et al. (2021). In vitro transcriptomes analysis identifies some special genes involved in pathogenicity difference of the *Beauveria bassiana* against different insect hosts. *Microb. Pathog.* 154:104824. doi: 10.1016/j.micpath.2021.104824
- Liu, N. (2015). Insecticide resistance in mosquitoes: impact, mechanisms, and research directions. *Annu. Rev. Entomol.* 60, 537–559. doi: 10.1146/annurev-ento-010814-020828
- Liu, S., Xia, Q., Zhao, P., Cheng, T., Hong, K., and Xiang, Z. (2007). Characterization and expression patterns of let-7 microRNA in the silkworm (*Bombyx mori*). *BMC Dev. Biol.* 7:88. doi: 10.1186/1471-213X-7-88
- Liu, Z., Fu, S., Ma, X., Baxter, S. W., Vasseur, L., Xiong, L., et al. (2020a). Resistance to *Bacillus thuringiensis* Cry1Ac toxin requires mutations in two *Plutella xylostella* ATP-binding cassette transporter paralogs. *PLoS Pathog.* 16:e1008697. doi: 10.1371/journal.ppat.1008697
- Liu, Z., Ling, L., Xu, J., Zeng, B., Huang, Y., Shang, P., et al. (2018). MicroRNA-14 regulates larval development time in *Bombyx mori*. *Insect Biochem. Mol. Biol.* 93, 57–65. doi: 10.1016/j.ibmb.2017.12.009
- Liu, Z., Xu, J., Ling, L., Luo, X., Yang, D., Yang, X., et al. (2020b). miR-34 regulates larval growth and wing morphogenesis by directly modulating ecdysone signaling and cuticle protein in *Bombyx mori*. *RNA Biol.* 17, 1342–1351. doi: 10.1080/15476286.2020.1767953
- Love, M. I., Huber, W., and Anders, S. (2014). Moderated estimation of fold change and dispersion for RNA-seq data with DESeq2. *Genome Biol.* 15:550. doi: 10.1186/s13059-014-0550-8
- Lozano, J., Montañez, R., and Belles, X. (2015). MiR-2 family regulates insect metamorphosis by controlling the juvenile hormone signaling pathway. *Proc. Natl. Acad. Sci. U.S.A.* 112, 3740–3745. doi: 10.1073/pnas.1418522112
- Lucas, K. J., Roy, S., Ha, J., Gervaise, A. L., Kokoza, V. A., and Raikhel, A. S. (2015). MicroRNA-8 targets the Wingless signaling pathway in the female mosquito fat body to regulate reproductive processes. *Proc. Natl. Acad. Sci. U.S.A.* 112, 1440–1445. doi: 10.1073/pnas.1424408112
- Luo, W., Huang, L. X., Qin, S. K., Zhang, X., Feng, Q. L., Gu, J., et al. (2020). Multiple microRNAs control ecdysone signaling in the midgut of *Spodoptera litura*. *Insect Sci.* 27, 1208–1223. doi: 10.1111/1744-7917.12745
- Ma, K., Li, X., Hu, H., Zhou, D., Sun, Y., Ma, L., et al. (2017). Pyrethroid-resistance is modulated by miR-92a by targeting *CpCPR4* in *Culex pipiens pallens*. *Comp. Biochem. Phys. B.* 203, 20–24. doi: 10.1016/j.cbpb.2016.09.002
- Marco, A., Hooks, K., and Griffiths-Jones, S. (2012). Evolution and function of the extended miR-2 microRNA family. *RNA Biol.* 9, 242–248. doi: 10.4161/rna.19160
- Meuti, M. E., Bautista-Jimenez, R., and Reynolds, J. A. (2018). Evidence that microRNAs are part of the molecular toolkit regulating adult reproductive diapause in the mosquito, *Culex pipiens*. *PLoS One* 13:e0203015. doi: 10.1371/journal.pone.0203015
- Meyers, B. C., Axtell, M. J., Bartel, B., Bartel, D. P., Baulcombe, D., Bowman, J. L., et al. (2008). Criteria for annotation of plant MicroRNAs. *Plant Cell* 20, 3186–3190. doi: 10.1105/tpc.108.064311
- Mohebbi, M., Ding, L., Malmberg, R. L., and Cai, L. (2021). Human MicroRNA target prediction via multi-hypotheses learning. *J. Comput. Biol.* 28, 117–132. doi: 10.1089/cmb.2020.0227
- Niu, Y., Liu, Z., Nian, X., Xu, X., and Zhang, Y. (2019). MiR-210 controls the evening phase of circadian locomotor rhythms through repression of *Fasciclin 2*. *PLoS Genet.* 15:e1007655. doi: 10.1371/journal.pgen.1007655
- Palma, L., Munoz, D., Berry, C., Murillo, J., and Caballero, P. (2014). *Bacillus thuringiensis* toxins: an overview of their bioicidal activity. *Toxins (Basel)* 6, 3296–3325. doi: 10.3390/toxins6123296
- Pardo-Lopez, L., Soberon, M., and Bravo, A. (2013). *Bacillus thuringiensis* insecticidal three-domain Cry toxins: mode of action, insect resistance and consequences for crop protection. *FEMS Microbiol. Rev.* 37, 3–22. doi: 10.1111/j.1574-6976.2012.00341.x
- Peng, T., Pan, Y., Gao, X., Xi, J., Zhang, L., Ma, K., et al. (2016). Reduced abundance of the *CYP6CY3*-targeting let-7 and miR-100 miRNAs accounts for host adaptation of *Myzus persicae* nicotianae. *Insect Biochem. Mol. Biol.* 75, 89–97. doi: 10.1016/j.ibmb.2016.06.002
- Puolivali, T., Palva, S., and Palva, J. M. (2020). Influence of multiple hypothesis testing on reproducibility in neuroimaging research: a simulation study and Python-based software. *J. Neurosci. Methods* 337:108654. doi: 10.1016/j.jneumeth.2020.108654
- Qin, S., Zhang, S., Sun, X., Kong, Y., Hou, C., and Li, M. (2021). Transcriptome reveal the response to Cry1Ac toxin in susceptible *Bombyx mori*. *Arch Insect Biochem. Physiol.* 107:e21794. doi: 10.1002/arch.21794
- Raymond, B., Johnston, P. R., Nielsen-LeRoux, C., Lereclus, D., and Crickmore, N. (2010). *Bacillus thuringiensis*: an impotent pathogen? *Trends Microbiol.* 18, 189–194. doi: 10.1016/j.tim.2010.02.006
- Rehmsmeier, M., Steffen, P., Hochsmann, M., and Giegerich, R. (2004). Fast and effective prediction of microRNA/target duplexes. *Bioinformatics* 10, 1507–1517. doi: 10.1261/rna.5248604
- Reynolds, J. A., Nachman, R. J., and Denlinger, D. L. (2019). Distinct microRNA and mRNA responses elicited by ecdysone, diapause hormone and a diapause hormone analog at diapause termination in pupae of the corn earworm, *Helicoverpa zea*. *Gen. Comp. Endocrinol.* 278, 68–78. doi: 10.1016/j.ygcen.2018.09.013

- Robertson, H. M., Waterhouse, R. M., Walden, K. K. O., Ruzzante, L., Reijnders, M., Coates, B. S., et al. (2018). Genome sequence of the wheat stem sawfly, *Cephus cinctus*, representing an early-branching lineage of the hymenoptera, illuminates evolution of hymenopteran chemoreceptors. *Genome Biol. Evol.* 10, 2997–3011. doi: 10.1093/gbe/evy232
- Shakeel, M., Xu, X., Xu, J., Li, S., Yu, J., Zhou, X., et al. (2018). Genome-wide identification of destruxin a-responsive immunity-related microRNAs in diamondback moth, *Plutella xylostella*. *Front. Immunol.* 9:185. doi: 10.3389/fimmu.2018.00185
- Shan, S., Wang, S. N., Song, X., Khashaveh, A., Lu, Z. Y., Dhilloo, K. H., et al. (2020). Characterization and target gene analysis of microRNAs in the antennae of the parasitoid wasp *Microplitis mediator*. *Insect Sci.* 28, 1033–1048. doi: 10.1111/1744-7917.12832
- Shen, Z. J., Liu, Y. J., Zhu, F., Cai, L. M., Liu, X. M., Tian, Z. Q., et al. (2020). MicroRNA-277 regulates dopa decarboxylase to control larval-pupal and pupal-adult metamorphosis of *Helicoverpa armigera*. *Insect Biochem. Mol. Biol.* 122:103391. doi: 10.1016/j.ibmb.2020.103391
- Singh, C. P. (2020). Role of microRNAs in insect-baculovirus interactions. *Insect Biochem. Mol. Biol.* 127:103459. doi: 10.1016/j.ibmb.2020.103459
- Singh, C. P., Singh, J., and Nagaraju, J. (2014). Bmnpv-miR-3 facilitates BmNPV infection by modulating the expression of viral P6.9 and other late genes in *Bombyx mori*. *Insect Biochem. Mol. Biol.* 49, 59–69. doi: 10.1016/j.ibmb.2014.03.008
- Song, J., Li, W., Zhao, H., and Zhou, S. (2019). Clustered miR-2, miR-13a, miR-13b and miR-71 coordinately target *Notch* gene to regulate oogenesis of the migratory locust *Locusta migratoria*. *Insect Biochem. Mol. Biol.* 106, 39–46. doi: 10.1016/j.ibmb.2018.11.004
- Su, J., Wang, G., Li, C., Xing, D., Yan, T., Zhu, X., et al. (2019). Screening for differentially expressed miRNAs in *Aedes albopictus* (Diptera: Culicidae) exposed to DENV-2 and their effect on replication of DENV-2 in C6/36 cells. *Parasit Vectors* 12:44. doi: 10.1186/s13071-018-3261-2
- Sun, K., Jee, D., de Navas, L. F., Duan, H., and Lai, E. C. (2015). Multiple in vivo biological processes are mediated by functionally redundant activities of *Drosophila* mir-279 and mir-996. *PLoS Genet.* 11:e1005245. doi: 10.1371/journal.pgen.1005245
- Sun, Q., Guo, H., Xia, Q., Jiang, L., and Zhao, P. (2020). Transcriptome analysis of the immune response of silkworm at the early stage of *Bombyx mori* bidensovirus infection. *Dev. Comp. Immunol.* 106:103601. doi: 10.1016/j.dci.2019.103601
- Sun, X. H., Xu, N., Xu, Y., Zhou, D., Sun, Y., Wang, W. J., et al. (2019). A novel miRNA, miR-13664, targets *CpCYP314A1* to regulate deltamethrin resistance in *Culex pipiens pallens*. *Parasitology* 146, 197–205. doi: 10.1017/S0031182018001002
- Tabashnik, B. E., and Carrière, Y. (2017). Surge in insect resistance to transgenic crops and prospects for sustainability. *Nat. Biotechnol.* 35, 926–935. doi: 10.1038/nbt.3974
- Tabashnik, B. E., and Carrière, Y. (2019). Global patterns of resistance to Bt crops highlighting Pink Bollworm in the United States, China, and India. *J. Econ. Entomol.* 112, 2513–2523. doi: 10.1093/jeet/toz173
- Tatusov, R. L., Galperin, M. Y., Natale, D. A., and Koonin, E. V. (2000). The COG database: a tool for genome-scale analysis of protein functions and evolution. *Nucleic Acids Res.* 28, 33–36. doi: 10.1093/nar/28.1.33
- Tian, M., Liu, B., Hu, H., Li, X., Guo, Q., Zou, F., et al. (2016). MiR-285 targets P450 (*CYP6N23*) to regulate pyrethroid resistance in *Culex pipiens pallens*. *Parasitol. Res.* 115, 4511–4517. doi: 10.1007/s00436-016-5238-4
- Vaschetto, L. M., and Beccacece, H. M. (2019). The emerging importance of noncoding RNAs in the insecticide tolerance, with special emphasis on *Plutella xylostella* (Lepidoptera: Plutellidae). *WIREs RNA* 10:e1539. doi: 10.1002/wrna.1539
- Wei, X., Zheng, C., Peng, T., Pan, Y., Xi, J., Chen, X., et al. (2016). miR-276 and miR-3016-modulated expression of acetyl-CoA carboxylase accounts for spirotetramat resistance in *Aphis gossypii* Glover. *Insect Biochem. Mol. Biol.* S0965-1748, 30158–30158. doi: 10.1016/j.ibmb.2016.10.011
- Wen, M., Shen, Y., Shi, S., and Tang, T. (2012). miREvo: an integrative microRNA evolutionary analysis platform for next-generation sequencing experiments. *BMC Bioinformatics* 13:140. doi: 10.1186/1471-2105-13-140
- Wu, K. M., Lu, Y. H., Feng, H. Q., Jiang, Y. Y., and Zhao, J. Z. (2008). Suppression of cotton bollworm in multiple crops in China in areas with Bt toxin-containing cotton. *Science* 321, 1676–1678. doi: 10.1126/science.1160550
- Wu, P., Jiang, X., Sang, Q., Annan, E., Cheng, T., and Guo, X. (2017). Inhibition of miR-274-3p increases BmCPV replication by regulating the expression of BmCPV NS5 gene in *Bombyx mori*. *Virus Genes* 53, 643–649. doi: 10.1007/s11262-017-1466-7
- Wu, P., Shang, Q., Dweteh, O. A., Huang, H., Zhang, S., Zhong, J., et al. (2019). Over expression of bmo-miR-2819 suppresses BmNPV replication by regulating the BmNPV ie-1 gene in *Bombyx mori*. *Mol. Immunol.* 109, 134–139. doi: 10.1016/j.molimm.2019.03.013
- Xu, L. N., Ling, Y. H., Wang, Y. Q., Wang, Z. Y., Hu, B. J., Zhou, Z. Y., et al. (2015). Identification of differentially expressed microRNAs between *Bacillus thuringiensis* Cry1Ab-resistant and -susceptible strains of *Ostrinia furnacalis*. *Sci. Rep.* 5:15461. doi: 10.1038/srep15461
- Xu, X., Yang, J., Harvey-Samuel, T., Huang, Y., Asad, M., Chen, W., et al. (2020). Identification and characterization of the *vasa* gene in the diamondback moth, *Plutella xylostella*. *Insect Biochem. Mol. Biol.* 122:103371. doi: 10.1016/j.ibmb.2020.103371
- Xu, X., Zhu, H., Yang, F., Wu, C., Jiang, C., Yu, W., et al. (2019). Bmo-miR-79 downregulates the expression of *BmEm4* in the silkworm, *Bombyx mori*. *Gene* 690, 113–119. doi: 10.1016/j.gene.2018.12.034
- Yan, H., Zhou, Y., Liu, Y., Deng, Y., and Chen, X. (2014). miR-252 of the Asian tiger mosquito *Aedes albopictus* regulates dengue virus replication by suppressing the expression of the dengue virus envelope protein. *J. Med. Virol.* 86, 1428–1436. doi: 10.1002/jmv.23815
- Zhang, Q., Dou, W., Song, Z.-H., Jin, T.-J., Yuan, G.-R., De Schutter, K., et al. (2020). Identification and profiling of *Bactrocera dorsalis* microRNAs and their potential roles in regulating the developmental transitions of egg hatching, molting, pupation and adult eclosion. *Insect Biochem. Mol. Biol.* 127:103475. doi: 10.1016/j.ibmb.2020.103475
- Zhao, J. Z., Li, Y. X., Collins, H. L., and Shelton, A. M. (2002). Examination of the F2 screen for rare resistance alleles to *Bacillus thuringiensis* toxins in the diamondback moth (Lepidoptera: Plutellidae). *J. Econ. Entomol.* 95, 14–21. doi: 10.1603/0022-0493-95.1.14
- Zhu, B., Li, X., Liu, Y., Gao, X., and Liang, P. (2017). Global identification of microRNAs associated with chlorantraniliprole resistance in diamondback moth *Plutella xylostella* (L.). *Sci. Rep.* 7:40713. doi: 10.1038/srep40713
- Zhu, B., Sun, X., Nie, X., Liang, P., and Gao, X. (2019). MicroRNA-998-3p contributes to Cry1Ac-resistance by targeting *ABCC2* in lepidopteran insects. *Insect Biochem. Mol. Biol.* 117:103283. doi: 10.1016/j.ibmb.2019.103283

Conflict of Interest: The authors declare that the research was conducted in the absence of any commercial or financial relationships that could be construed as a potential conflict of interest.

Publisher's Note: All claims expressed in this article are solely those of the authors and do not necessarily represent those of their affiliated organizations, or those of the publisher, the editors and the reviewers. Any product that may be evaluated in this article, or claim that may be made by its manufacturer, is not guaranteed or endorsed by the publisher.

Copyright © 2021 Yang, Xu, Lin, Chen, Lin, Song, Bai, You and Xie. This is an open-access article distributed under the terms of the Creative Commons Attribution License (CC BY). The use, distribution or reproduction in other forums is permitted, provided the original author(s) and the copyright owner(s) are credited and that the original publication in this journal is cited, in accordance with accepted academic practice. No use, distribution or reproduction is permitted which does not comply with these terms.



RNA Biological Characteristics at the Peak of Cell Death in Different Hereditary Retinal Degeneration Mutants

OPEN ACCESS

Edited by:

Yicheng Long,
Cornell University, United States

Reviewed by:

Ulrike Schumann,
Australian National University,
Australia

Xueqian Zhuang,
Memorial Sloan Kettering Cancer
Center, United States

Qiao Lu,
NYU Grossman School of Medicine,
United States

Mingqiang Wang,
Stanford University, United States

*Correspondence:

Zhulin Hu
hzl77@263.net
François Paquet-Durand
francois.paquet-durand@
klinikum.uni-tuebingen.de
Kangwei Jiao
kangwei.jiao@ynu.edu.cn

[†]These authors have contributed
equally to this work and share first
authorship

Specialty section:

This article was submitted to
RNA,
a section of the journal
Frontiers in Genetics

Received: 22 June 2021

Accepted: 21 September 2021

Published: 29 October 2021

Citation:

Wei C, Li Y, Feng X, Hu Z,
Paquet-Durand F and Jiao K (2021)
RNA Biological Characteristics at the
Peak of Cell Death in Different
Hereditary Retinal
Degeneration Mutants.
Front. Genet. 12:728791.
doi: 10.3389/fgene.2021.728791

Chunling Wei^{1,2†}, Yan Li^{2,3†}, Xiaoxiao Feng^{2,3}, Zhulin Hu^{2,3*}, François Paquet-Durand^{4*} and Kangwei Jiao^{2,3*}

¹Kunming Medical University, Kunming, China, ²Department of Ophthalmology, Affiliated Hospital of Yunnan University, Yunnan University, Kunming, China, ³Key Laboratory of Yunnan Province, Yunnan Eye Institute, Kunming, China, ⁴Institute for Ophthalmic Research, Eberhard-Karls-Universität Tübingen, Tübingen, Germany

Purpose: The present work investigated changes in the gene expression, molecular mechanisms, and pathogenesis of inherited retinal degeneration (RD) in three different disease models, to identify predictive biomarkers for their varied phenotypes and to provide a better scientific basis for their diagnosis, treatment, and prevention.

Methods: Differentially expressed genes (DEGs) between retinal tissue from RD mouse models obtained during the photoreceptor cell death peak period (*Pde6b*^{rd1} at post-natal (PN) day 13, *Pde6b*^{rd10} at PN23, *Prph*^{rd2} at PN29) and retinal tissue from C3H wild-type mice were identified using Illumina high-throughput RNA-sequencing. Co-expression gene modules were identified using a combination of GO and KEGG enrichment analyses and gene co-expression network analysis. CircRNA-miRNA-mRNA network interactions were studied by genome-wide circRNA screening.

Results: *Pde6b*^{rd1}, *Pde6b*^{rd10}, and *Prph*^{rd2} mice had 1,926, 3,096, and 375 DEGs, respectively. Genes related to ion channels, stress, inflammatory processes, tumor necrosis factor (TNF) production, and microglial cell activation were up-regulated, while genes related to endoplasmic reticulum regulation, metabolism, and homeostasis were down-regulated. Differential expression of transcription factors and non-coding RNAs generally implicated in other human diseases was detected (e.g., glaucoma, diabetic retinopathy, and inherited retinal degeneration). CircRNA-miRNA-mRNA network analysis indicated that these factors may be involved in photoreceptor cell death. Moreover, excessive cGMP accumulation causes photoreceptor cell death, and cGMP-related genes were generally affected by different pathogenic gene mutations.

Conclusion: We screened genes and pathways related to photoreceptor cell death. Additionally, up-stream regulatory factors, such as transcription factors and non-coding RNA and their interaction networks were analyzed. Furthermore, RNAs involved in RD were functionally annotated. Overall, this study lays a foundation for future studies on photoreceptor cell death mechanisms.

Keywords: inherited retinal degeneration (IRD), RNA-seq, biogenic analysis, cGMP-related genes, photoreceptor cell death

INTRODUCTION

Retinitis pigmentosa (RP) is a set of heterogeneous inherited retinal degenerations (RDs), with a prevalence of approximately 1/4,000 globally (Zhang, 2016). The disease can be caused by mutations in over 65 genes and may show a variety of inheritance patterns, including x-linked inheritance (Salveti et al., 2021), autosomal dominant congenital (Sarkar et al., 2020), autosomal recessive (Owczarek-Lipska et al., 2020), and mitochondrial (Kim et al., 2018). In a few cases digenic inheritance has also been reported (Gao et al., 2017). Most mutated genes in RP are expressed in rod photoreceptor cells, leading to rod cell death, night blindness, and loss of peripheral vision in early disease stages. Secondary death of cone photoreceptor cells (Veleri et al., 2015), with complete loss of vision, occurs in late-stage RP. At present, treatment developments have included gene (Ducloyer et al., 2020) and cell (Akiba et al., 2020) therapies, as well as subretinal prosthetic device implantation (Chow, 2013). However, each of these therapeutic approaches has its limitations, and no general RP treatment exists at present. Therefore, studying photoreceptor cell death mechanisms to devise novel methods to prevent retinal degeneration progress may aid effective RP and RD treatment. Of special interest might be changes in transcriptional activity that may precede the execution of cell death.

While the genetic causes of RD have often been established, the cellular mechanisms of photoreceptor cell death triggered by those genetic defects are still poorly understood. In many cases exceedingly high intracellular cGMP levels were observed in RD photoreceptors (Wang et al., 2017; Power et al., 2020) and continuous cGMP elevation likely results in over-activation of cyclic nucleotide gated cation channels (CNGC) and protein kinase G (PKG). CNGC activation mediates Ca^{2+} influx, which in turn may lead to activation of calpain-type proteases (Arango-Gonzalez et al., 2014), ultimately leading to photoreceptor cell death. Associated with high cGMP and PKG activation are the enzymatic activities of histone deacetylases (HDAC) and poly (ADP-Ribose) polymerase (PARP) activation (Sancho-Pelluz and Paquet-Durand, 2012). The latter produces poly (ADP-Ribose) (PAR) polymers which can induce the transfer of mitochondrial apoptosis inducing factor (AIF) to the nucleus, eventually leading to cell death (Sahaboglu et al., 2010). Moreover, PAR polymer production can induce cell death through NAD^+ and ATP depletion (Ying et al., 2005).

Investigating transcriptomic changes at the peak of photoreceptor degeneration has a great significance for fully understanding RD. Here, we used RNA-Seq and bioinformatics to examine the transcriptomic differences between three RD mouse models (*Pde6b*^{rd1}, *Pde6b*^{rd10}, and *Prph*^{rd2}), at their respective peaks of photoreceptor cell death, to obtain insights into the pathogenesis of RD caused by different

gene mutations, with special attention to genes related to cGMP, PARP, and their upstream factors. Differential expression of transcription factors and non-coding RNAs may be involved in photoreceptor cell death. Moreover, as excessive cGMP accumulation causes photoreceptor cell death, cGMP-related genes were generally affected by different pathogenic gene mutations.

METHODS

Animal Procedures

RD mouse models (C3H *Pde6b*^{rd1}, C3H *Prph*^{rd2}, and C57Bl6/J *Pde6b*^{rd10}) as well as C3H mice carrying the wild-type (wt) alleles for *Pde6b* and *Prph2* were used irrespective of gender. All four animal colonies were regularly genotyped to ensure that they indeed carried (or not) the disease-causing mutations. The use of congenic C3H mice (Sanyal and Bal, 1973) facilitates comparative transcriptomic analysis between wild-type, *Pde6b*^{rd1} and *Prph*^{rd2}. While the *Pde6b*^{rd10} animals were not congenic to the C3H wt, the impact of the disease-causing mutation is so dramatic that relatively minor strain differences are unlikely to cause a large impact on gene expression patterns. All procedures were performed in compliance with the ARVO statement for the use of animals in Ophthalmic and Visual Research. Protocols were reviewed and approved by the Yunnan University ethical review board. All efforts were made to minimize the suffering and number of animals used. Retinal tissue was collected during the peak period of photoreceptor cell death (post-natal (PN) day 13 for *Pde6b*^{rd1}, PN23 for *Pde6b*^{rd10}, PN29 for *Prph*^{rd2}), wild-type retinal tissues were collected at corresponding time points.

Tissue Preparation

All mice (PN5-PN180) were sedated with CO_2 before decapitation. The eyes were removed after cleaning the heads with 70% ethanol. Subsequently, the eyes marked in the nasal part were incubated in 4% PFA for 45 min at room temperature (RT). This was followed by three washes in PBS (0.1 M; pH 7.4) (10 min each). Then, the eye was cut open along the limbus, and the cornea, lens, and vitreous were removed. The eyecups were then, at RT, treated with serially increasing concentrations of sucrose solution (10 min in 10% sucrose, 20 min in 20% sucrose, 30 min in 30% sucrose) for cryo-protection. Subsequently, the tissues were embedded in O.C.T™ compound (Fisher Healthcare™ Tissue-Plus™ O.C.T. Compound, Waltham, MA, United States) and immediately frozen in liquid nitrogen and stored at -20°C until sectioning. The thickness of sections were 10 μm , and the sections were baked at 40°C for 45 min before stored at -20°C or further staining.

TUNEL (In Situ Cell Death Detection) Assay

Fixed retinal sections dried at 37°C for 40 min were washed in PBS (RT, 15 min). For nuclease inactivation and inhibition of

nucleic acid reduction, the slices were incubated in TRIS with Proteinase K (10 µg/ml in 10 mM TRIS-HCL, pH 7.4–8.0; 37°C, 5 min) and then washed thrice with Tris (5 min each). Subsequently, the slices were placed in ethanol-acetic-acid (3:1) mix at –20°C for 5 min and then blocked with blocking solution (1% BSA, 10% NGS, 1% fish gelatin, 0.003% PBST) for 1 h, RT. Afterwards, the sections were stained with TUNEL kit (Fluorescein or TMR; Roche Diagnostics GmbH, Mannheim, Germany) at 37°C according to the manufacturer's instructions and mounted in Vectashield containing DAPI (Vector, Burlingame, CA, United states).

RNA Extraction, Library Preparation, and Sequencing

The sequencing was carried out by Shanghai Life Gene Biotechnology Co., Ltd., (Shanghai, China). Total RNA was extracted from the entire retinal tissues of different groups using TRIzol reagent (Invitrogen, South San Francisco, CA, United States) following the manufacturer's instructions. After measuring the quantity and quality of total RNA, a total amount of 3 µg RNA per sample was used for library preparation. Briefly, ribosomal RNA was removed, and sequencing libraries were generated using the rRNA-depleted RNA by NEBNext® Ultra™ Directional RNA Library Prep Kit for Illumina® (NEB, United States) following manufacturer's recommendations. After library preparation, the total RNA of different groups was then sequenced on the Illumina HiSeq 4,000 platform. The raw data and GEO accession number for this study are as follows: (GSE178928, <https://www.ncbi.nlm.nih.gov/geo/query/acc.cgi?acc=GSE178928>).

Quality Control, Alignment, and Quantification of RNA-Seq Data

Clean data were obtained from in-house Perl scripts by removing reads containing adapter, reads containing poly-N, and low-quality reads from FASTQ raw data. At the same time, Q20, Q30, and GC content of the clean data were calculated to evaluate the quality of sequencing. Subsequently, we aligned the clean reads to the mouse reference genome GRCm38. After that, HTSeq v0.11.2 was used to count the read numbers mapped to each gene, and then Fragments Per Kilobase of transcript sequence per Millions (FPKM) of each gene was calculated.

Identification of Differentially Expressed Genes

DEGs between two groups (C3H vs. *Pde6b*^{rd1}, C3H vs. *Prph*^{rd2} and C3H vs. *C57Bl6/J Pde6b*^{rd10}) were identified using DESeq2 R package (1.28.0). *p*-value < 0.05 and fold change ≥ 1.5 were set as the thresholds for DEGs. Then, these identified DEGs were submitted for Gene Ontology (GO) and Kyoto Encyclopedia of Genes and Genomes (KEGG) pathway enrichment analyses. A *p*-value < 0.05 was recognized as indicating significant enrichment.

Functional Enrichment Analysis

Gene Ontology (GO) and Kyoto Encyclopedia of Genes and Genomes (KEGG) pathway enrichment analyses for DEGs were performed using the DAVID (v6.8) and KOBAS (v3.0) software, respectively. *p* value < 0.05 was recognized as indicating significant enrichment.

CircRNA Annotation and Identification of Differentially Expressed CircRNAs

The obtained clean reads were aligned to the mouse genome (mm10) using TopHat2 (v2.1.1). The CIRCexplorer program (v2.2.3) was used with the fusion junctions obtained from TopHat2 to identify both the circularizing junction and the spliced sequence of circRNAs. All candidate circRNAs with junction reads less than two were discarded. CircRNA expression level was determined by transcripts per million (TPM). DE-circRNAs between two groups (C3H vs. *Pde6b*^{rd1}, C3H vs. *Prph*^{rd2} and C3H vs. *C57Bl6/J Pde6b*^{rd10}) were screened using the limma R package (3.40.6), and changes were considered as significant with *p*-value < 0.05 and fold change ≥ 2.

CeRNA Network Construction

The candidate miRNAs were predicted based on miRBase (www.mirbase.org). Targetscan (v7.1) was used to predict the downstream target genes of these miRNAs. The circRNA-miRNA interactions and circRNA-mRNA interactions were selected for ceRNA construction using the Cytoscape v3.7.1 software. The genes in the ceRNA networks were then submitted for GO and KEGG enrichment analyses.

Weighted Correlation Network Analysis

WGCNA (Langfelder and Horvath, 2008) was used for scale-free network topology analysis. Standard WGCNA parameters were used for analysis, with the exceptions of soft-thresholding power and the deep split. Using WGCNA, a co-expression module was quickly extracted for subsequent analysis. In brief, genes with expression correlation were clustered into a module. First, the correlation matrix between two genes was constructed using the main connecting rod and the Pearson correlation matrix. Second, hierarchical clustering analysis was performed using the hclust R function, and the soft thresholding power was determined by analysis of network topology. The adjacency was transformed into a topological overlap matrix. Subsequently, network construction and module detection were performed. Modules with a size less than 30 were merged into one module. The calculation process was performed using the blockwiseConsensusModules function of the WGCNA package.

Real-Time Quantitative PCR

We chose seven differentially expressed genes obtained by sequencing for further validation. The total RNA was reversely transcribed into cDNA using PrimeScript™ II 1st Strand cDNA synthesis Kit (Takara Biomedical Technology Co., Ltd.). The sequences of all primers are shown in **Supplementary Table S4**. The total volume of RT-qPCR was 20 µL, including 10 µL SYBR Premix EX Taq, 1 µL forward primer (10 µM), 1 µL reverse

primer (10 μ M), 2 μ L cDNA and 6 μ L RNase free water. The RT-qPCR reaction were initiated at 95°C for 10 min, followed by a total of 40 cycles of 95°C for 15 s and 60°C for 30 s. GAPDH served as a housekeeping gene, and the levels of *Xist*, *Foxg1*, *H2K2*, *Maff*, *Klf6*, *mmu-cicr0000135*, and *mmu-cicr0008206* were calculated using the $2^{-\Delta\Delta Ct}$ method.

Immunofluorescence Assay

The cryosections were washed in PBS for 15 mins, and then used for antigen retrieval, after that, sections were incubated with anti-PITX2 antibody, (1:200, GB112180, Servicebio, Wuhan, China) anti AIF (1:200, GB11314, Servicebio, Wuhan, China), at 4°C overnight. On the next day, the sections were incubated with the secondary antibody (FITC-labeled 488 goat anti rabbit IgG, 1:300 Servicebio) in the dark at RT for 50 mins. After washing with PBS, the sections were stained with DAPI (Servicebio) in the dark for 10 mins, and then spontaneous fluorescence quencher (Servicebio) was added for 5 mins. After rinsing under running water for 10 min, the sections were sealed with an anti-fluorescence quencher (Servicebio), and then were observed under a fluorescence microscope and confocal Microscope (LSM 900 Airyscan 2, Zeiss, Oberkochen, Germany).

Microscopy, Cell Counting, and Statistical Analysis

Light and fluorescence microscopy was performed with a Zeiss Imager M2 Microscope and LSM 900 Airyscan two equipped with a Zeiss Axiocam digital camera (Zeiss, Oberkochen, Germany). Images were captured using the Zeiss Axiovision 4.7 software, and representative pictures were obtained from central areas of the retina. Adobe Illustrator CC 2019 (Adobe Systems Incorporated, San Jose, CA) was used for primary image processing. For cell quantification, whole radial slice pictures were captured using the Mosaic mode of Axiovision 4.7. Labelled cells were counted manually. The total number of cells was determined by dividing the outer nuclear layer (ONL) area by the average cell size. The total number of ONL cells was determined by dividing the percentage of positive cells by the number of positive cells. Three sections each from at least three different animals were tested for each genotype and experimental condition. Statistical comparisons between experimental groups were made using one-way ANOVA and Bonferroni's correction using Prism eight for Mac OS (Graph Pad Software, La Jolla, CA). Values are presented as mean \pm standard deviation (SD) or standard error of means (SEM). Levels of significance were as follows: n.s. > 0.05; *, p < 0.05; **, p < 0.01; and ***, p < 0.001.

RESULTS

The Peak of Photoreceptor Cell Death in Different RD Mutants *in vivo*

Apoptosis relates to the orderly process of changes in cell morphology and biochemistry that finally results in cell death (Kerr and Thompson, 1972). Aside from apoptosis a variety of programmed cell death mechanisms are known, including

programmed necrosis, necroptosis, and PARthanatos (Leist and Jaattela, 2001). TUNEL (Terminal deoxynucleotidyl transference dUTP nick end labeling) is a common method to detect DNA fragmentation as end result of apoptosis but also of other forms of cell death, for instance in necrosis (Grasl-Kraupp et al., 1995; Loo, 2002). We used the TUNEL cell death assay to identify photoreceptor cell death in these three genetically distinct RD models to assess to what extent universal gene expression changes might underlie photoreceptor degeneration.

The first animal model was the *Pde6b^{rd1}* mouse, one of the most studied animal models for early onset and rapid rod photoreceptor degeneration (Keeler, 1924). The *Pde6b^{rd1}* mouse carries a retroviral insertion in the rod *Pde6b* gene that leads to non-sense mediated mRNA decay and hence no functional PDE6B protein is made (Pittler and Baehr, 1991). As the second animal model, we employed the *Prph^{rd2}* mouse, also referred to as *rd* or "retinal degeneration slow", which harbors a mutation in the *Prph2* gene that leads to an absence of photoreceptor outer segments (Goldberg, 2006). The third model used was the *Pde6b^{rd10}* mouse (Chang et al., 2007). As opposed to the *rd1* mutation, the *rd10* mutation is a point mutation that affects the catalytic site of the PDE6B enzyme. While this does not abolish protein expression, it dramatically reduces PDE6 activity.

Our own TUNEL analysis largely confirmed the previous data from the literature. In the *Pde6b^{rd1}* mouse, we found that cell death started at post-natal 9 (PN9), while it began at PN16 in *Pde6b^{rd10}*, and at PN11 in *Prph^{rd2}*. In all of these RD models, individual dying cells and photoreceptor cells rows were detectable as late as PN31 in *Pde6b^{rd1}*, PN38 in *Pde6b^{rd10}* (Figures 1B5,C5), and PN180 in *Prph^{rd2}* (Figure 1D5).

In wild-type (wt) controls, TUNEL positive cells were seen only occasionally in the ONL (Figures 1A1–A5). Compared to wt retinae, *Pde6b^{rd1}* retinae showed a significant elevation of photoreceptor cell death at PN13 (Figures 1B1–B5), and the photoreceptor degeneration was the earliest compared to other two RD mutants. The TUNEL positive cells peaked at PN23 in *Pde6b^{rd10}* while in *Prph^{rd2}* the TUNEL peak was at PN29 (Figures 1C1–C5,D1–D5). All three RD mutants showed significantly higher numbers of TUNEL positive cells than wt (Figures 1E1–E4).

Quantification of photoreceptor rows in *Pde6b^{rd1}* showed the highest number at PN9 (13 ONL cell rows remaining), declining thereafter, with only one ONL cell row remaining at PN21 (Figure 1F2). A slower cell loss was observed for *Pde6b^{rd10}* retinae, which declined from 12 ONL cell rows at PN9 to one ONL cell row at PN38 (Figure 1F3). The *Prph^{rd2}* mutant had 13 photoreceptor rows at PN13, declining to four rows at PN180 (Figure 1F4). In the wt animals photoreceptor row counts remained nearly constant at 11–13 from P9–P38 (Figure 1F1).

Transcriptomic Characterization of the Three RD Mouse Models

Through sequencing, a total of 522, 228, 400 raw reads were obtained from the 12 samples (triplicates in each group) using the Illumina HiSeq 4,000 platform. After trimming the low-quality paired-end sequences and adapter sequences, we obtained a total

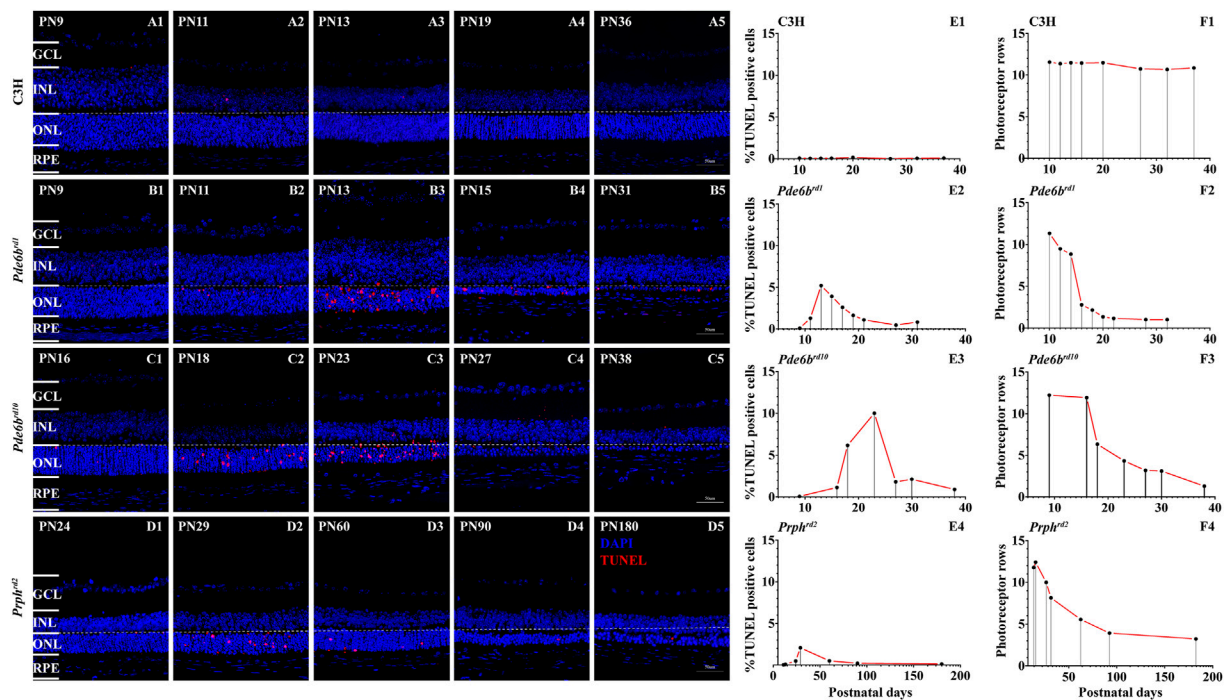


FIGURE 1 | TUNEL assay and cell death in RD mutants. The number of TUNEL positive cells in the three different RD mutants ONL was strongly increased when compared with wt (**A1–D5**). Quantification of photoreceptor cell death and photoreceptor rows during the first 40 postnatal days in C3H wild-type, *Pde6b^{rd1}*, *Pde6b^{rd10}* mutants and 180 days in *Prph^{rd2}* (**A–F**). Increased numbers of TUNEL positive cells, showing a peak at PN13 in *Pde6b^{rd1}*, PN23 in *Pde6b^{rd10}*, PN29 in *Prph^{rd2}* was observed (**B1–D5**). Quantification of photoreceptor rows during the first 40 postnatal days in *Pde6b^{rd1}*, *Pde6b^{rd10}*, C3H and 180 days in *Prph^{rd2}*. In *Pde6b^{rd1}*, photoreceptor rows showed the highest number at PN9 (13 ONL cell rows remaining), declining thereafter. In the other two mutants the photoreceptor rows showed the highest number at PN9 in *Pde6b^{rd10}* (12 ONL cell rows remaining) and PN13 in *Prph^{rd2}*, declining thereafter. In the RD models, dying cells and photoreceptor cells rows were detectable as late as PN40 in *Pde6b^{rd1}* and *Pde6b^{rd10}* (**B5, C5**), at PN180 in *Prph^{rd2}* (**D5**). The values shown originate from three RD mutants from at least three different specimens. Scale bar represents 50 μ m.

of 496, 619, 835 clean reads. At more than 95%, the % of clean reads was very high, with over 10G clean bases in each sample; the single base sequencing error rate was $<0.01\%$. For all twelve sequencing libraries, the lowest Q20 and Q30 were 97.20 and 92.54%, respectively. No GC bias was found (**Supplementary Table S1**). Subsequently, we aligned the clean reads to the mouse reference genome GRCm38. We found that, in each sample, more than 93% of reads could be aligned to the reference genome, with 87.84–91.02% unique mapping. The clean read percentage and the mapping percentage suggested good sequence quality (**Supplementary Table S2**). Therefore, all libraries proved to be suitable for further study.

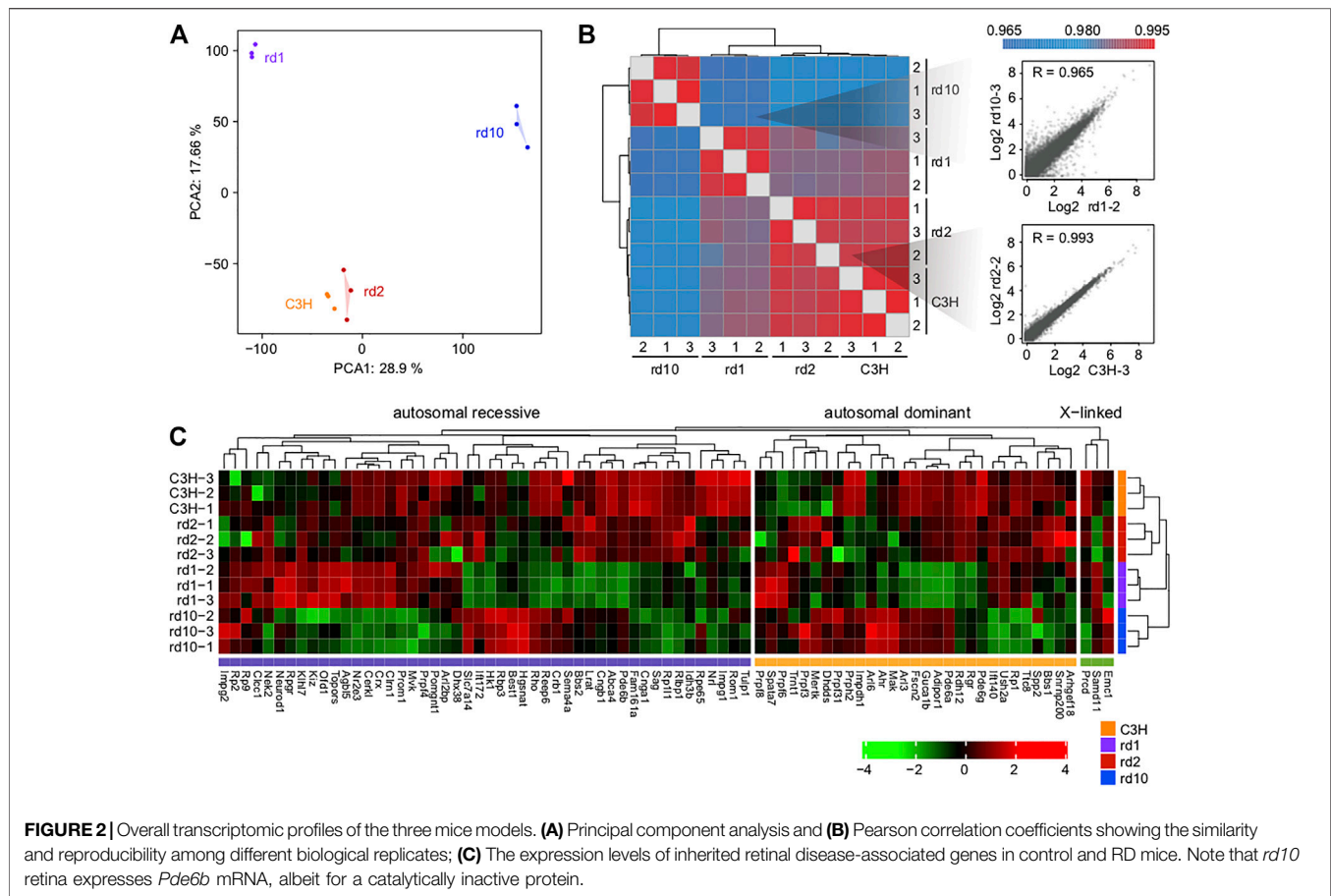
Principal component analysis (PCA) of gene expression profiles showed significant cell type differences (**Figure 2A**). Pearson correlation analysis revealed that the correlations within each group were stronger than the correlations between groups (**Figure 2B**). Notably, the wt and *Prph^{rd2}* groups had a high correlation and largest degree of similarity, indicating that the gene expression patterns between two groups were more similar. This may correlate with the rather slow progression of *Prph^{rd2}* degeneration which results in relatively few gene expression changes compared to wt.

We searched for genes implicated in RD through RetNet (<https://sph.uth.edu/RETNET/>) and investigated whether their

expression levels were affected in RD mice (**Supplementary Table S3**). Although disease gene mutations are the leading cause of functional defects in photoreceptors, gene expression imbalance further contributes to photoreceptor degradation. Interestingly, especially in *Pde6b^{rd1}* and *Pde6b^{rd10}* mice, quite a few genes showed a decrease in expression (**Figure 2C**). This phenomenon suggested that single gene mutations (as in *Pde6b* in the present study) may affect the function of several important genes in various ways.

Analysis of Photoreceptor Cell Death-Related Genes and Pathways

To examine the potential mechanism underlying photoreceptor cell degeneration, we analyzed the DEGs between C3H and RD mice (**Figure 3A**; **Supplementary Figure S1A**). Totally, 1,926 DEGs (1,169 upregulated, 756 downregulated) existed between *Pde6b^{rd1}* and C3H. Despite being derived from the same mutant gene *Pde6b*, *Pde6b^{rd10}* showed 3,096 (1,950 upregulated, 1,144 downregulated) DEGs. However, between *Prph^{rd2}* and wt only 375 (202 upregulated, 173 downregulated) DEGs were identified, indicating the presence of different molecular regulatory mechanisms in the *Prph^{rd2}* model. Unsupervised hierarchical clustering of all DEGs showed clear boundaries among groups



with clustering of genes with similar expression behaviors (**Supplementary Figures S1B,C**).

Among these DEGs, many were known critical regulators of RD. Typically, PDE6 loss-of-function mutations lead to extremely high cGMP levels and death of the affected photoreceptor cell type (Power et al., 2020). Thus, we examined the photoreceptor cGMP-related RD gene expression. Genes involved in cGMP synthesis and hydrolysis were generally differentially expressed, especially in the PDE6 mutant *Pde6b^{rd1}* and *Pde6b^{rd10}* mice (**Figure 3B**). Obviously, insufficient expression of various PDE6 subunits (*Pde6a*, *Pde6b*, and *Pde6g*) reflected a strong link between gene mutations and transcriptional defects.

Since many dysregulated genes were detected in RD mice, we combined GO and KEGG analyses to further understand the functional defects caused by gene mutations (**Figure 3C**). Highly consistent with the mouse RD phenotype, the activation of apoptosis-related functions and the degeneration of the photoreceptors were observed. However, only a few DEGs were identified in *Prph^{rd2}* mice (**Figures 3A,C**). Therefore, we focused on general functional associations determined through the study of *Pde6b^{rd1}* and *Pde6b^{rd10}* mice. In summary, the GO terms mainly enriched among upregulated genes were ion channels, stress, inflammatory processes, TNF production, and microglia. The GO terms mainly enriched among downregulated genes were related to the regulation of endoplasmic reticulum,

metabolism, and intracellular homeostasis. As one of its roles, in the presence of a high cGMP concentration, PDE6 may activate Ca^{2+} ion channels to trigger Ca^{2+} ion influx; the increased intracellular Ca^{2+} may be a major factor leading to photoreceptor degeneration (Dean et al., 2002). In addition to genetic defects, research indicates that oxidative stress, neuroinflammation, and intracellular toxicity may contribute to retinal degeneration progression (Martinez-Fernandez de la Camara et al., 2013; Yoshida et al., 2013). Insufficient energy production and intracellular environment disorders are both hallmark events of cell death (Hassa et al., 2006). Thus, these dysregulated functions are key to explaining RD pathogenesis. Notably, while the above-mentioned functions were more activated in *Pde6b^{rd10}*, they were extensively inhibited in *Pde6b^{rd1}* mice, suggesting that mutations at different locations in a single gene could affect the phenotype in different ways. Another interpretation would be that genes regulated in opposing ways between *Pde6b^{rd1}* and *Pde6b^{rd10}* are, in fact, not relevant for the degeneration and were instead due to different post-natal age and developmental stage (i.e., PN13 vs. PN23).

Roles of Transcription Factors in Regulating RD

To investigate the transcription factor (TF) mechanisms responsible for retina formation and visual nerve development,

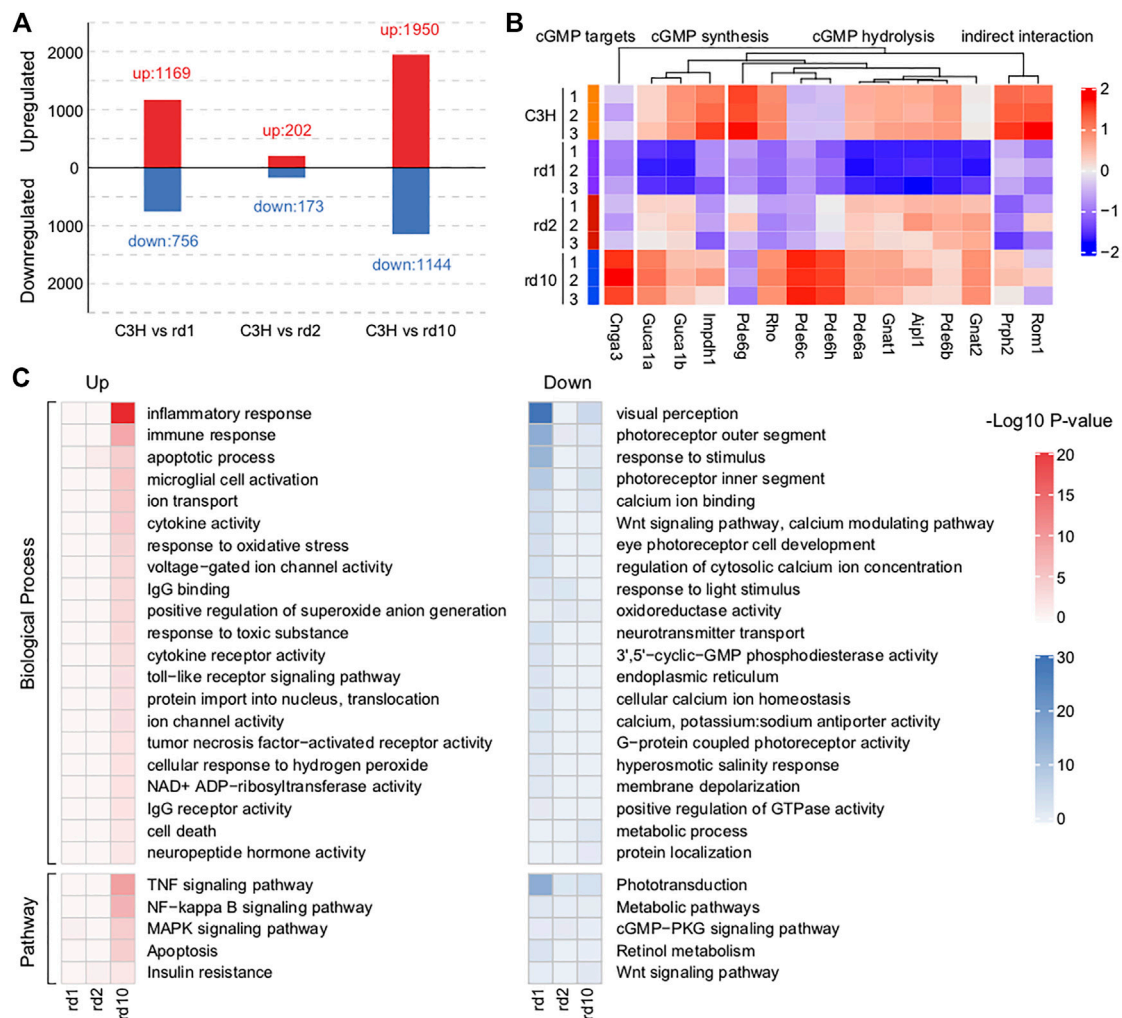


FIGURE 3 | Impaired functions related to phototransduction found in RD mice retina. **(A)** The numbers of differentially expressed genes (DEGs) between C3H mice and each RD model. A total of 1,925 DEGs (1,169 up-regulated and 756 down-regulated), 375 DEGs (202 up-regulated and 173 down-regulated), and 3,094 DEGs (1,950 up-regulated and 1,144 down-regulated) were respectively identified between *Pde6b^{rd1}* and C3H mice, between *Prph^{rd2}* and C3H mice, and between *Pde6b^{rd10}* and C3H mice. **(B)** Changes in the expression of key genes related to cGMP synthesis, hydrolysis, and targets in RD mice versus that in C3H mice. Genes involved in cGMP synthesis and hydrolysis were generally differentially expressed, especially in the PDE6 mutant *Pde6b^{rd1}* and *Pde6b^{rd10}* mice. **(C)** Functional enrichment analysis of the identified DEGs based on $p < 0.05$. These up-regulated DEGs mainly were enriched ion channel activity, inflammatory process, immune response, TNF signaling pathway, MAPK signaling pathway, and microglial cell activation. The down-regulated DEGs were related to visual perception, Wnt signaling pathway, calcium modulating pathway, positive regulation of GTPase activity, cGMP-PKG signaling pathway and retinal metabolism.

we extracted genes with significantly altered transcriptional relationships in the three RD mouse models (**Figures 4A,C,E**). In *Pde6b^{rd1}* and *Pde6b^{rd10}* mice, more TFs were activated, whereas a large area with high TF suppression existed in *Prph^{rd2}* mice. TF enrichment by mutated genes was highly consistent with the TF expression pattern, confirming that the continuous activation or inhibition of upstream signals caused a series of downstream functional changes (**Figures 4B,D,F**). Notably, *Pitx2* was downregulated in all three RD models, showing the lowest fold change in *Prph^{rd2}* mice, which could be due to its later developmental age at PN29. *Pitx2* in particular has been related to neural crest cell (NCC) survival and migration, as well as optic stalk development, and is critical for eye morphogenesis (Evans

and Gage, 2005; Chawla et al., 2016; Hendee et al., 2018). Considering that the functional defect caused by *Pitx2* mutation often induces ocular cell death (Semina et al., 1996), we speculated that the inhibition of *Pitx2* transcriptional activity was also related to the increased risk of neurodegenerative diseases. Compared with *Pitx2*, *Dlx1*, and *Foxg1* had a more significant reduction in expression in *Pde6b^{rd1}* mice. *Dlx1* participates in neurotransmitter transmission and is essential for neuron proliferation, differentiation, and migration; and may regulate cell cycle progression through Wnt signaling (Maira et al., 2010; Wright et al., 2020). *Foxg1* is important for embryonic primitive streak development and reprogramming; its “transcriptional switch” function has received widespread

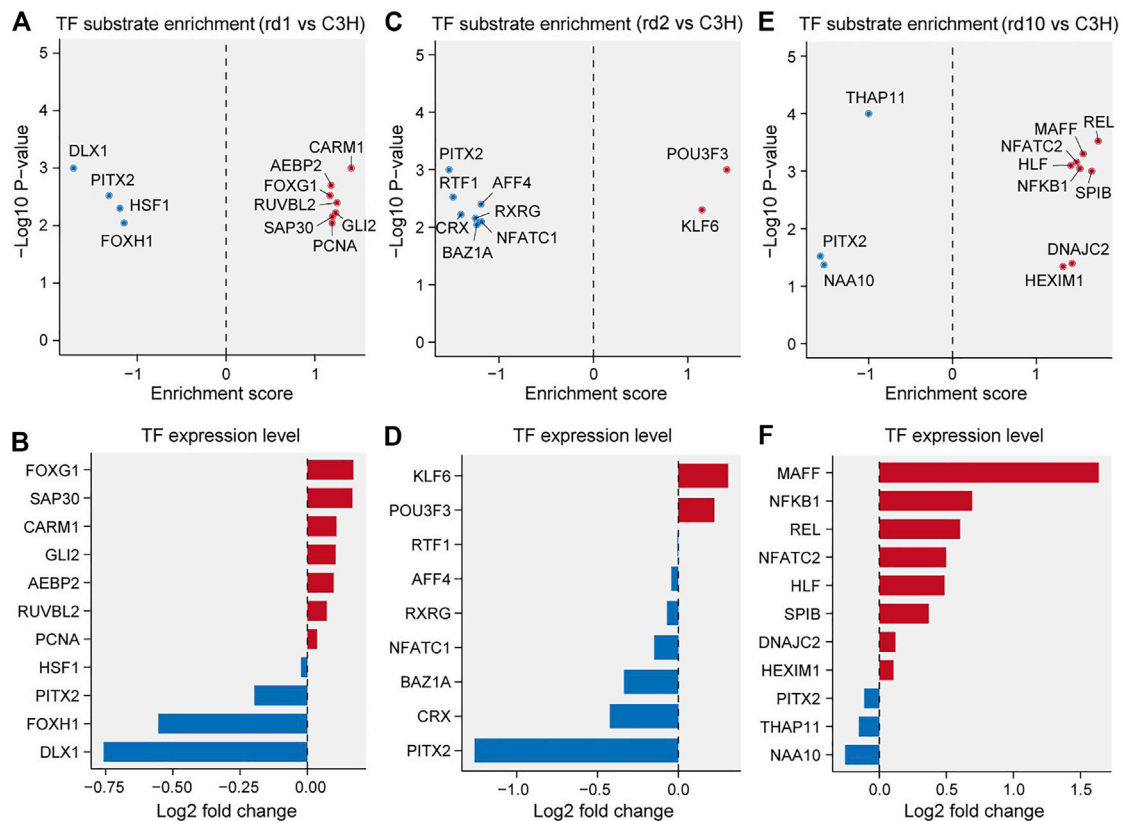


FIGURE 4 | Transcriptional factor (TF) substrate enrichment analysis in the three RD models versus C3H mice. **(A, C, E)** TF substrate enrichment score and significance in *Pde6b^{rd1}* **(B)**, *Prph^{rd2}* **(D)**, and *Pde6b^{rd10}* **(F)** mice; PITX2 were all down-regulated in RD mice compared with the C3H mice. **(B, D, F)** Log2 fold changes of the indicated TF expression levels in *Pde6b^{rd1}* **(B)**, *Prph^{rd2}* **(D)**, and *Pde6b^{rd10}* **(F)** mice. FOXG1, KLF6, and MAFF were up-regulated in RD mice; while DLX1 and NAA10 were down-regulated in RD mice.

attention in embryonic development (Reid et al., 2016; Wang et al., 2019). The lack of TFs for genes encoding these important proteins would impede optic nerve development. In *Pde6b^{rd10}* mice, *Maff* was highly upregulated. The MAFF protein can regulate photoreceptor gene expression and is closely associated with inflammatory responses in neuronal diseases (Katsuoka et al., 2003; Chevillard et al., 2007; Saliba et al., 2019). We speculate that constant MAFF activation may contribute to inflammatory processes in the microenvironment through pro-inflammatory cytokines or chemokines, thereby mediating photoreceptor cell death. Thus, our data suggests that functional abnormalities of key TFs may accelerate RD pathogenesis.

Functional Analysis of Differentially Expressed lncRNAs

Long non-coding RNAs (lncRNAs) are involved in gene activation and silencing. lncRNAs have emerged as important regulators of photoreceptor development, as well as of ocular physiology, and their dysregulation is associated with numerous eye-related diseases (Wawrzyniak et al., 2018). Therefore, we extracted molecules annotated as lncRNAs among the identified

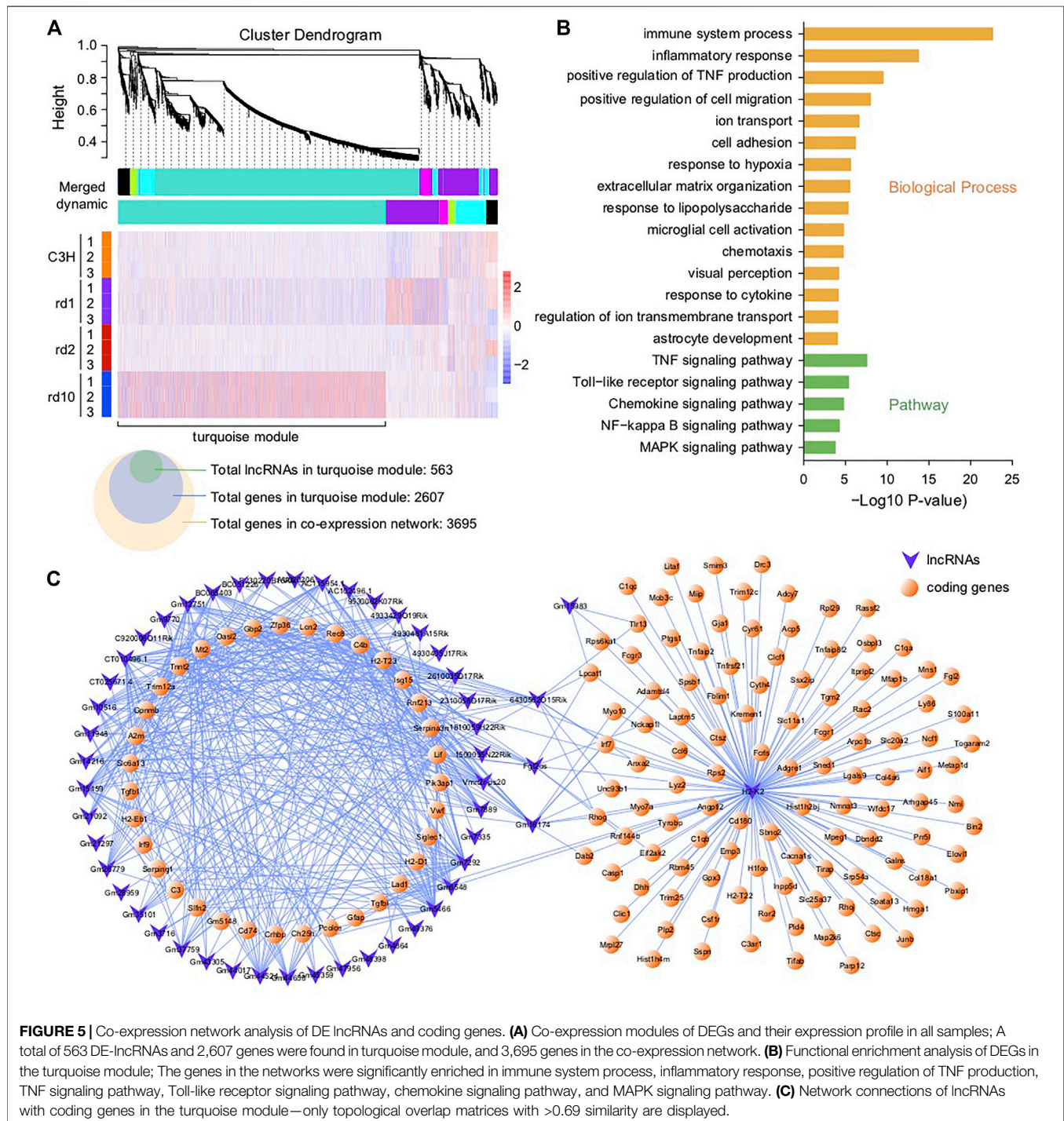
DEGs, described their expression profile characteristics, and explored the role of important lncRNAs in RD.

In total, 482 differentially expressed lncRNAs (DE lncRNAs) were detected in *Pde6b^{rd1}* mice (312 upregulated and 170 downregulated). *Pde6b^{rd10}* mice showed 728 DE lncRNAs (367 upregulated and 361 downregulated). In *Prph^{rd2}* mice, 101 DE lncRNAs were detected (55 upregulated and 46 downregulated) (**Supplementary Figures S2A–C**). Similar to the number of DEGs (**Figure 3A**), *Prph^{rd2}* mice had the lowest number of DE lncRNAs. Unsupervised cluster analysis of DE lncRNAs also showed an evident expression pattern among the three groups (**Supplementary Figures S2D,E**). In particular, we observed that the gene encoding for X inactive-specific transcript (*Xist*) had the highest degree of upregulation among all three RD mouse models. *Xist* is an X-chromosomal non-coding transcript essential for the initiation and spread of X-inactivation. *Xist* abnormal expression is related to malignancy progression (Xing et al., 2018; Yang et al., 2018; Liu et al., 2019). In retinoblastoma, *Xist* expression dysregulation has been reported to affect cell proliferation and apoptosis (Wang et al., 2018). Overexpressed *Xist* protects human retinal pigment epithelial cells against hyperglycemia-related damage by reducing apoptosis and restoring migration (Dong et al., 2020). Therefore,

we speculate that *Xist* overexpression in defense against cell injury may cause apoptotic signaling in RD mouse photoreceptor cells.

To further understand the regulatory relationship between lncRNAs and coding genes in RD, we performed a weighted gene co-expression network analysis (WGCNA) of all DEGs, including DE lncRNAs. A total of five co-expression modules were observed (Figure 5A, excluding black module). Among these, the module with the largest number of correlated genes (*i.e.*, the turquoise

module in Figure 5) was the largest and comprised more than 70% of DEGs in the co-expression network, 20% of which were lncRNAs (Figure 5A). This module therefore formed the focus of our subsequent analysis. GO and KEGG analyses showed that functions related to stress response, immunity, inflammation, TNF production, cell migration, chemotaxis, visual perception, and ion transport were extensively enriched in the turquoise module (Figure 5B). Thus, the above biological processes seem to



be important in RD, indicating that, in the RD murine gene co-expression network, lncRNAs may generally participate in the regulation of degenerative pathways (Figure 3C). Similarly, several lncRNAs were hub nodes (Figure 5C), likely deserving more attention. For instance, based on the report that lncRNA H2K2 promoted diabetic nephropathy progression via the miR-449a/b/Trim11/Mek signaling pathway (Chen et al., 2019), we inferred that dysregulated H2K2 in RD mice may partially mediate retinal disease progression via the competitive endogenous RNA (ceRNA) mechanism, in which lncRNAs may compete with protein-coding mRNAs for binding to miRNAs. However, the functional roles and regulatory mechanisms of lncRNAs acting as ceRNAs in RD are still unclear.

Characterization of circRNAs and Construction of ceRNA Network

Previous reports indicate that circRNAs can regulate synaptic activity and are essential for the normal function of the central nervous system (Rybak-Wolf et al., 2015). The retina is a key component of the visual phototransduction system. While circRNAs participate in retinal development, abnormally expressed circRNAs may cause various neurological disorders and diabetic retinopathy (Lukiw, 2013; Shan et al., 2017). However, the circRNA-regulation of retinal degeneration is still unclear. Here, we tried to characterize the circRNA expression profile and the functional relationship of circRNAs with coding DNA in RD mice.

A total of the 12,510 unique circRNAs were identified in our 12 samples (Supplementary Figure S3A). Most circRNAs (7,866, 64.74%) were novel when compared with those in circBase. Notably, the proportion of novel circRNAs in each sample was always less than half (Supplementary Figure S3B), implying that more novel circRNAs have a spatiotemporal pattern in different retinal diseases. Likewise, less than 1/4 circRNAs were shared among the three RD mice models and control mice. Most circRNAs were <1,000 nt long (Supplementary Figure S3C). The distribution of circRNA genomic origins showed that about half of the host genes (1,714, 43.12%) produced only one circRNA, whereas a few host genes (559, 14.06%) produced more than six circRNAs (Supplementary Figure S3D). In general, circRNAs originated from coding exons (Supplementary Figure S3E) and were encoded by less than seven exons (usually two to four) (Supplementary Figure S3F). Additionally, nearly 20% retinal circRNAs in each RD mouse model were conserved in human genome sequences (Supplementary Figure S3G).

Analysis of differentially expressed circRNAs (DE circRNAs) revealed 314 DE circRNAs in *Pde6b^{rd1}* mice (26 upregulated and 228 downregulated), 515 DE circRNAs in *Pde6b^{rd10}* mice (355 upregulated and 160 circRNAs downregulated), and 183 DE circRNAs in *Prph^{rd2}* mice (124 upregulated and 59 downregulated) (Figure 6A). Interestingly, although the expression levels of most DE circRNAs were specific for different retinal pathological states, almost all the shared DE circRNAs were consistently suppressed (Supplementary Figures S3H,I).

The interaction of circRNAs and miRNAs may indirectly regulate gene expression. Thus, we constructed a ceRNA network using the circRNAs and DEGs of all RD mouse models to explore the circRNA-miRNA-mRNA regulatory axis that may be related to retinal degeneration. The constructed network had 25 genes, 6 circRNAs as decoys, and 6 predicted miRNAs in total (Figure 6B), suggesting that circRNAs can competitively bind to miRNAs through binding sites, thereby indirectly regulating miRNA target genes. Notably, many targets were key genes or genes encoding transcription factors associated with neuronal synapses, ion channels, and inflammation, which may be important in retinopathy pathogenesis. This network provided useful clues indicating that circRNAs play a role in the pathogenesis of retinal degeneration by indirectly targeting certain important genes.

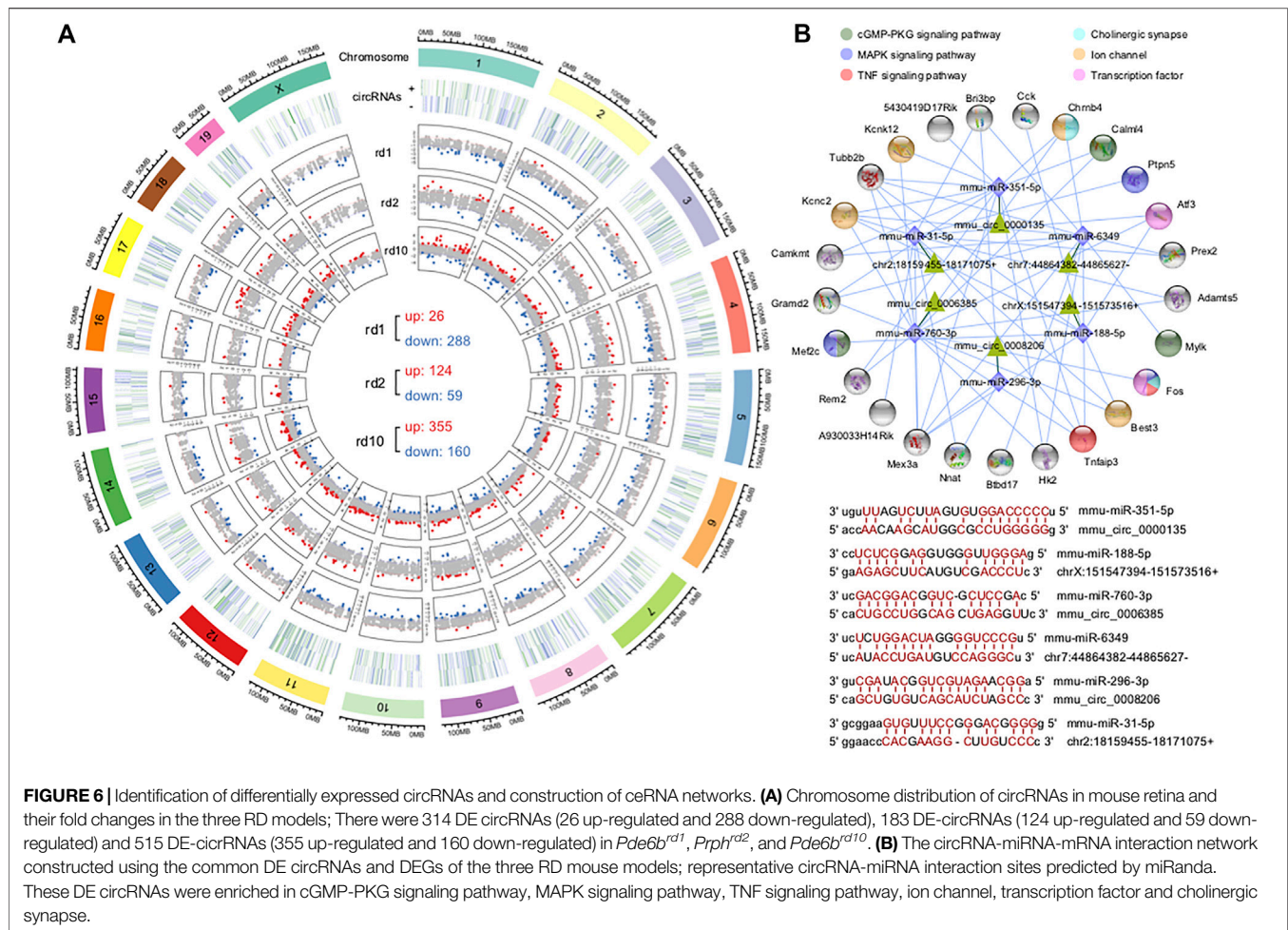
Validation of Gene Expression Analysis

To further validate the gene expression data, we performed RT-qPCR and immunofluorescence staining on retinal sections. While the expression of *Xist* was significantly up-regulated in the *Pde6b^{rd1}* mice at PN13 compared with C3H control ($p < 0.05$), no significant differences were observed in *Xist* expression between C3H control and *Pde6b^{rd10}* mice at PN23, as well as between C3H control and *Pde6b^{rd2}* mice at PN29 ($p > 0.05$, Figure 7A). For H2K2, its expression was evidently up-regulated in all three RD mutant mice when compared to C3H ($p < 0.05$, Figure 7A). *Klf6* was markedly up-regulated in both *Pde6b^{rd1}* and *Pde6b^{rd2}* mice compared with the C3H mice ($p < 0.05$), yet, there was no significant difference in *Klf6* expression between C3H control and *Pde6b^{rd10}* ($p > 0.05$; Figure 7A). Compared with the C3H control, the level of circ0000135 was significantly lower in the *Pde6b^{rd1}* and *Pde6b^{rd10}* mice ($p < 0.05$), while no significant difference was found between C3H and *Pde6b^{rd2}* mice ($p > 0.05$, Figure 7A). The trend of *Maff* gene expression in different groups was similar to that of *Xist* expression, with a significant increase only in the *Pde6b^{rd1}* mouse (Figure 7A). For circ0008206 a significant down-regulation was observed only in *Pde6b^{rd2}* mice ($p > 0.05$, Figure 7A).

In addition, PITX2 protein expression was assessed by immunofluorescence. Remarkably, PITX2 expression was significantly increased in the photoreceptor layer of all three RD mutant mice ($p < 0.05$, Figure 7B). The latter indicated that PITX2 may indeed play an important role in RD pathogenesis.

DISCUSSION

RNA-Seq, a new-generation sequencing method with a higher accuracy than microarrays, promises a more comprehensive understanding of the changes in gene regulation in RD (Cai and Lyu, 2012). Here, we screened genes and pathways related to photoreceptor cell death in different RD models. Additionally, up-stream regulatory factors, such as transcription factors and non-coding RNA, and their interaction networks were analyzed. Furthermore, RNAs involved in RD were functionally annotated. Overall, this study lays a foundation for future studies on the



transcriptional changes leading up to photoreceptor cell death and the discovery of potential targets in the treatment of RD.

RNA-Seq Transcriptome Profiling of RD Models

During the period of photoreceptor cell death, a previous RNA-Seq study on *Pde6b^{rd10}* mutant retinal tissue showed a lack of gene expression specificity in rod cells and an increased gene transcription in Muller cells and indicated the importance of gliosis in innate immune activation in RD (Uren et al., 2014). In their retinal degeneration study, Xu et al. showed that, in *Pde6b^{rd1}* mice, intravitreal metformin injection delayed visual impairment and inhibited photoreceptor cell death (A et al., 2019). Moreover, metformin treatment altered the gene expression profile of *Pde6b^{rd1}* mice. Furthermore, GO and KEGG enrichment analyses showed that immunity and inflammation played a relatively important role in this change (A et al., 2019). Here, since the number of DEGs observed was low and pathway modifications of significance were absent in *Prph^{rd2}* mice (Figures 3A,C), we focused mainly on *Pde6b^{rd1}* and *Pde6b^{rd10}* mice and summarized the PDE6 gene mutations inducing RD pathogenesis.

Wnt/ β -Catenin Signaling Protects Photoreceptors From Degradation

Loss of function PDE6 mutation resulted in decreased PDE6 α/β activity and a high cytoplasmic cGMP concentration (Tsang et al., 1996). Photoreceptor cell physiology relies on the regulation and interplay of the second messenger signaling molecule cGMP and Ca²⁺ levels (Vighi et al., 2018; Das et al., 2021). Classic opsin signaling involves cGMP-gated ion channels; high intracellular cGMP concentrations perpetually open cGMP-gated ion channels, leading to increased Ca²⁺ influx and, ultimately, photoreceptor degeneration (Dean et al., 2002). We found ion channel activity and ion transport to be activated, while cellular Ca²⁺ homeostasis and Ca²⁺-binding mechanisms were impaired, probably leading to excessive intracellular Ca²⁺ accumulation (Figure 3C). Notably, the cGMP-PKG signaling pathway was enriched in downregulated genes.

In addition to causing toxicity and increasing osmotic pressure, high intracellular Ca²⁺ concentrations promote Ca²⁺-dependent calpain-type protease activation, which in turn activates both caspase-dependent and -independent apoptotic pathways (Susin et al., 1999; Mizukoshi et al., 2010). Moreover, mitochondrial calpains can activate AIF, a cell death executioner,

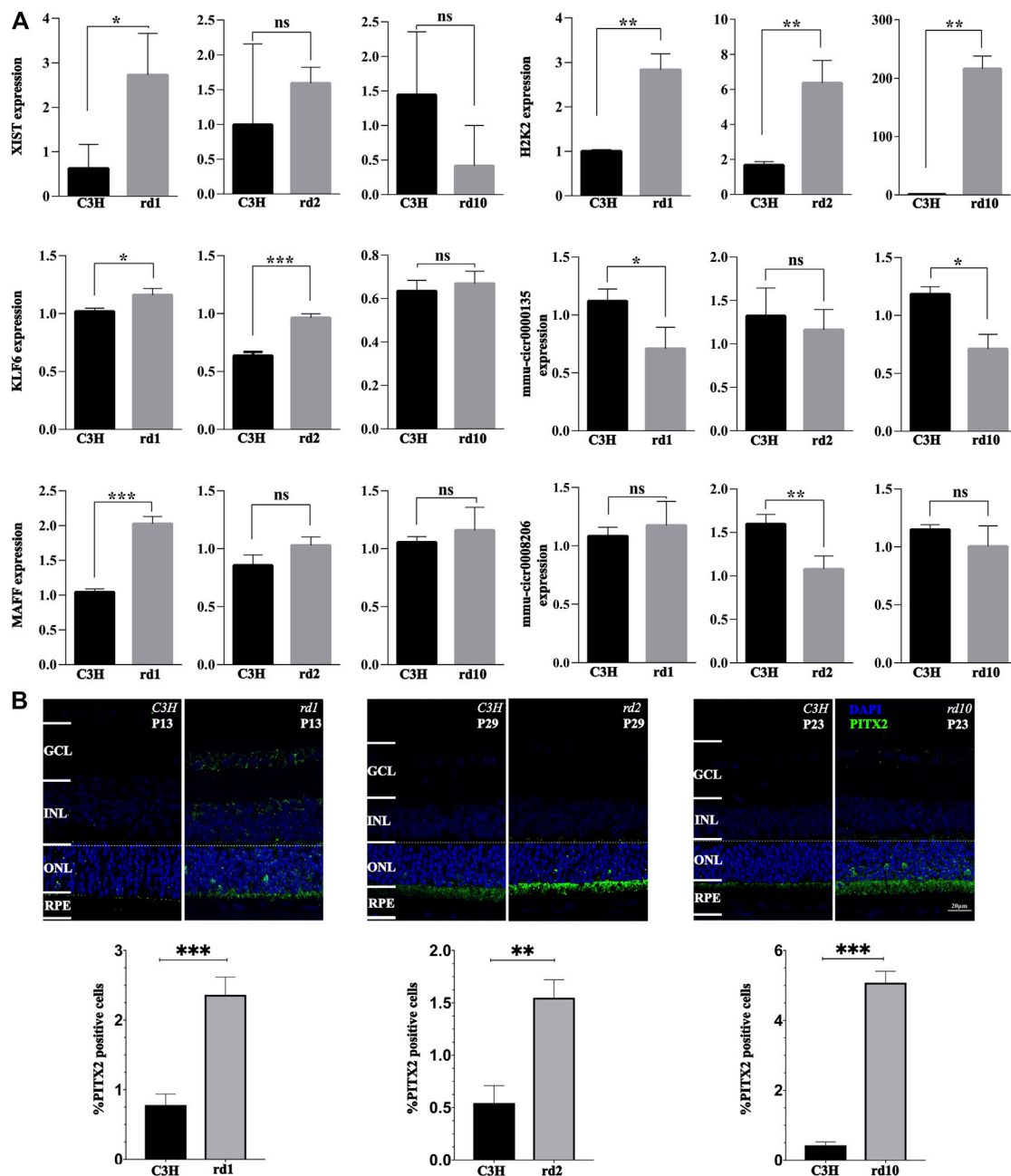


FIGURE 7 | Validation of gene expression changes via qPCR and immunofluorescence. **(A)** The relative levels of XIST, H2K2, MAFF, KLF6, mmu-circ0000135, and mmu-circ0008206 in different groups at different times determined by real-time quantitative PCR. **(B)** PITX2 expression in C3H wild-type, *rd1*, *rd2*, and *rd10* retina at time-points corresponding to the peak of retinal degeneration as assessed by immunofluorescence. Quantification in bar graphs displays the percentage of PITX2 positive cells in the outer nuclear layer (ONL). Significance levels indicated by asterisks: * = $p < 0.05$, ** = $p < 0.01$, *** = $p < 0.001$.

which, upon translocation from mitochondria to the nucleus promotes chromatin fragmentation (Polster et al., 2005; Mizukoshi et al., 2010). Curiously, our transcriptomic analysis did not indicate changes in calpain related genes. This may be due to the fact that the rapid metabolic activation by high levels of Ca^{2+} does not affect the transcriptome, most likely because when calpains become activated the cell is already undergoing the final stages of cell death, at which point the transcriptional machinery no longer works.

Activated insulin receptors are likely to play a neuroprotective effect by closing cGMP-gated ion channels and reducing Ca^{2+} entry into cells (Rajala et al., 2008; Gupta et al., 2012). Moreover, wnt/ β -catenin signaling protects photoreceptors from degradation (Patel et al., 2015). Our data showed that insulin resistance pathways were activated, whereas the wnt signaling pathway was inhibited in RD (Figure 3C). Thus, targeting molecules related to these pathways may rescue photoreceptor cell degeneration.

X Inactive-Specific Transcript

Xist mRNA, as a potential non-coding transcript encoded by the X chromosome and essential for the initiation and spread of X-inactivation, plays an important role in epigenetic processes due to its widespread transcriptional activity. In our RNAseq data *Xist* had the highest degree of up regulation among all three RD models, a finding that was partly confirmed by qPCR. *Xist* abnormal expression is related to malignancy progression (Xing et al., 2018; Yang et al., 2018; Liu et al., 2019). In retinoblastoma, *Xist* expression dysregulation has been reported to affect cell proliferation and apoptosis (Wang et al., 2018). Overexpressed *Xist* protects human retinal pigment epithelial cells against hyperglycemia-related damage by reducing apoptosis and restoring migration (Dong et al., 2020). On the other hand, deletion of the *Xist* gene results in skewed inactivation of the wt X chromosome, indicating that this locus is essential for gene silencing. Our qPCR results showed that *Xist* was up-regulated in the *rd1* and *rd2* mice, indicating that *Xist* may be closely associated with RD pathogenesis. Taken together, we speculate that *Xist* overexpression in defense against cell injury may cause apoptotic signaling in RD mouse photoreceptor cells.

Pitx2 Related to RD Pathogenesis

Paired-like homeodomain transcription factor 2 (*Pitx2*), one of the homeobox transcription factors that play key roles during embryogenesis, has been reported to be crucial in the asymmetric development of the internal organs and the symmetric development of eye tissues (Okubo et al., 2020). *Pitx2* participates in the development of keratocytes, scleral cells, corneal endothelial cells, ciliary muscles, trabecular mesenchymal cells, and peripheral connective tissues connected to the extraocular muscles (Gage et al., 2005; Kimura et al., 2014). Mutations in *PITX2* or *FOXC1* cause Axenfeld-Rieger syndrome, which is characterized by hypoplasia of the anterior segment and mild dental and craniofacial malformations (Seifi et al., 2016). A previous study indicated that *SLC13A3* is a direct downstream target of *Pitx2* transcriptional regulation, and the levels of *PITX2* and *SLC13A3* regulate responses to oxidative stress in ocular cells (Strungaru et al., 2011). Another report showed that deficiency of *Pitx2* could lead to abnormal ocular and craniofacial development in zebrafish (Ji et al., 2016). Our study found that *Pitx2* mRNA was significantly down-regulated in all three RD models. However, immunostaining for *PITX2* revealed a strong increase in individual photoreceptor cells in all three RD models. This may indicate an increased translation or stabilization of the *Pitx2* mRNA. Alternatively, the *PITX2* protein may be less degraded during the degeneration. In either case the association with the RD models suggests that *Pitx2* play important roles in RD pathogenesis, and further *in vivo* and *in vitro* experiments need to be performed to validate this conclusion.

Apoptosis-Inducing Factor Activated in Photoreceptor of RD Models

Based on our analysis of cell death progression presented above, we chose to study the peak of photoreceptor cell death for all our

studies (Figure 1). AIF is a mitochondrial protein usually located in the inner segment of cells containing mitochondria and endoplasmic reticulum (ER) and in the cytoplasm of other retinal cells (Sanges et al., 2006). When stimulated by apoptosis signals, the mature AIF protein translocate into the nucleus, causing DNA breaks and inducing apoptosis. During the hydrolysis of AIF, Calpains (I/II) play a key role in its maturation and release process. When homeostasis of Ca^{2+} is unbalanced in the cells that will cause the number of intracellular Ca^{2+} to rise, calpain activates the hydrolysis and release of AIF (Polster et al., 2005; Badugu et al., 2008). Although, calpain activity may not be reflected at the transcriptional level, we have performed immunofluorescence of AIF to verify if the reallocation of AIF to the nucleus as a result of calpain activity is a confirmed phenomenon. In the stage of peak of photoreceptor cell death, a large nuclear translocation of AIF is found within the RDs photoreceptor segments, areas which are known to host large numbers of mitochondria. However, AIF was not observed in wild type (wt), as determined by confocal analyses (Figures 8A–F), suggesting that AIF plays a primary role in RD cell death event. These data confirm that, before the induction of apoptosis mitochondria stain for AIF, and after the induction of apoptosis, AIF gets redistributed from mitochondria to the nucleus. Because some AIF will be distributed in the cytoplasm, further affecting mitochondrial functions, the increase of mitochondrial membrane permeability leads to an increase in Ca^{2+} . So, the translocation of AIF is related to initial cell death changes in the nucleus. The process follows Calpain activation and triggers downstream cell death events (e.g., PARPs) (Plesnila et al., 2004), eventually leading to late cell death as well.

Identification of PARP Regulated Transcriptomic Signatures

The role of poly (ADP-ribose) polymerase-1 (PARP-1) in responding to DNA damage and genomic stability (Durkacz et al., 1980), maintenance of telomeres (Beneke et al., 2008), and the stability of the replication fork (Bryant et al., 2009) is well known. However, the transcriptional functions of PARP-1 that may relate to chromatin remodeling as a means to regulate DNA repair are unknown (Ikejima et al., 1990). There is evidence that the enzyme and transcription functions of PARP-1 increase as the disease progresses, and are unrelated with DNA repair in cancer (Schiewer et al., 2018). In neurodegenerative diseases, the effects of PARP-mediated photoreceptor degeneration were multifaceted. NAD^+ is a PARP cofactor. Therefore, sustained PARP activity may reduce NAD^+ levels, inhibit glycolysis and the TCA cycle, and ultimately decrease ATP production (Goodwin et al., 1978; Bernofsky, 1980), which could lead to an energetic collapse and, subsequently, photoreceptor cell death (Hassa et al., 2006). Moreover, PARP generates PAR polymers, which may mediate AIF nuclear translocation and accelerate DNA defragmentation (Fatokun et al., 2014). Toxicity caused by excessive accumulation of PAR in photoreceptor cells may be

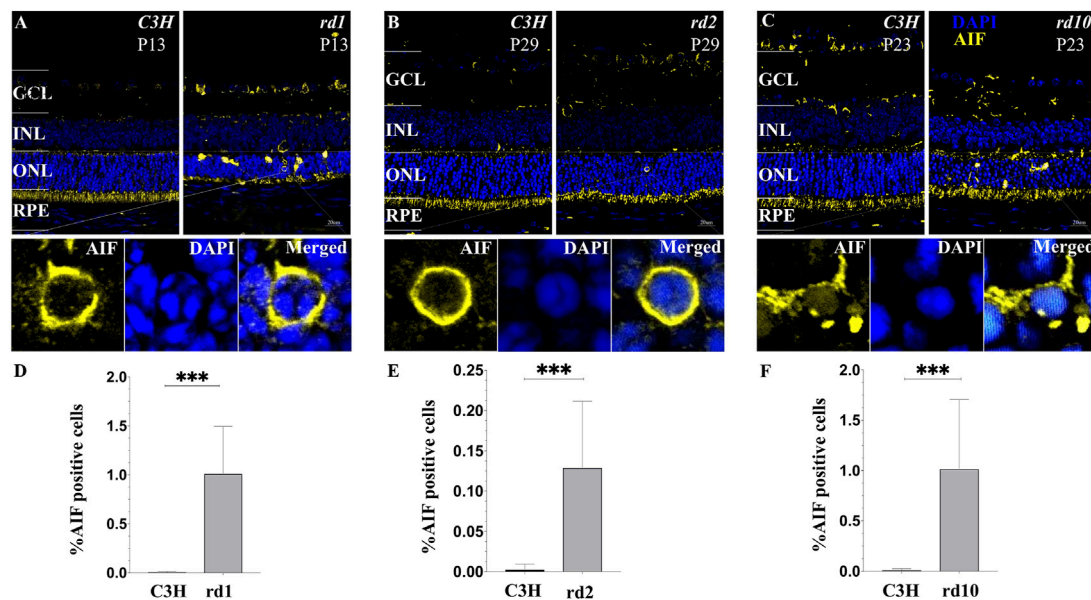


FIGURE 8 | Translocation of AIF in various models of RD photoreceptors. **(A–C)** Confocal microscopy of RD retinal sections stained with AIF (yellow fluorescence) and the nuclear dye DAPI (blue). Cells that demonstrate a clear AIF staining of the nucleus were regarded as positive for AIF translocation. **(D–F)** Note that C3H wild-type control lack any detectable AIF redistribution to the nucleus. The values shown originate from three RD mutants from at least three different specimens. Quantification in bar graphs displays the percentage of AIF positive cells in the outer nuclear layer (ONL). Significance levels indicated by asterisks: * = $p < 0.05$, ** = $p < 0.01$, *** = $p < 0.001$.

another cause of cell death. Consistent with these points, our data indicate increased NAD⁺ ADP-ribosyltransferase activity, nuclear translocation, and cytotoxicity and down regulation of pathways related to metabolism (**Figure 3C**). Oxidative stress in cells was observed, probably due to the increase in reactive oxygen species (ROS) levels caused by mitochondrial respiration impairment. Oxidative stress plays a pivotal role in retinal degeneration pathogenesis (Lee et al., 2011; Oveson et al., 2011). Interestingly, elevated cGMP levels were found to correlate with increased PARP activity in dying photoreceptor cells (Paquet-Durand et al., 2007; Sahaboglu et al., 2010), implying that the cGMP-mediated cell death process might, to some extent, be related to PARP levels.

Considering the potential impact of PARP mediated function in the process of RD and the need for biomarkers of PARP response, it is particularly important to understand the molecular mechanisms of PARP in different RD models and different ages, and determine the contribution of PARP mediated transcription events to the death of photoreceptor cells. Our study shows that, compared with *wt* mice, the expression of *Parp-1*, *Tank1*, *Parp-6*, *Parp-8*, *Parp-11*, and *Tiparp* was elevated in *Pde6b*^{rd1} retina, while the expression of *Parp-3*, *Parp-4*, *Parp-9*, *Parp-12*, *Parp-14*, and *Parp-16* was elevated in the *Pde6b*^{rd10} situation. However, there was no significant differential expression of PARP genes in *Prph*^{rd2} mice (**Supplementary Figure S1D**). The latter may be due to the fact that the numbers of dying cells are relatively low in *Prph*^{rd2}, even at the peak of cell death. Further investigation of the PARP regulated transcriptome would bring new

understanding of PARP and transcriptional functions that are related to the function of RD progression.

PARP cytotoxic levels, stress response, and inflammation are closely linked to a myriad pathological conditions, including in neuroinflammation (Martinez-Fernandez de la Camara et al., 2013; Yoshida et al., 2013). Accordingly, we found that biological processes involved in inflammatory or immune response were dysregulated (**Figure 3C**). Remarkably, TNF signaling, associated with ocular inflammatory diseases and retinal degeneration (Valentincic et al., 2011; Yoshida et al., 2013), is highly activated in RD mice. TNF is considered both an apoptotic and a necroptotic inducer; it can trigger downstream NF- κ B, MAPKs, and apoptotic pathways (Vandenabeele et al., 2010). These pathways were activated in our RD mice (**Figure 3C**). Inhibition of TNF signaling reduces photoreceptor cell death (Martinez-Fernandez de la Camara et al., 2015). Thus, its inhibition may prove useful in reducing neurodegeneration caused by inflammation and could therefore be an important target in future RD treatments. TNF is secreted in the retina, most likely by activated macrophages or microglia. Genes involved in the positive regulation of leukocyte migration and inflammatory responses were upregulated, which is reflected in increased cellular stress and accelerated TNF release. Furthermore, microglial activation, a neuropathology hallmark and an early event in retinal degeneration and photoreceptor cell death, was observed (Gupta et al., 2003). Therefore, various microglial activation inhibitors and TNF inhibitors have been suggested for RD treatment. For instance, minocycline delayed photoreceptor cell death in an RD mice model (Peng et al., 2014). Furthermore, by specifically blocking the interaction

between transmembrane TNF and its receptor, adalimumab protects the neuroretina by reducing microglial cell activation and inhibiting downstream cell apoptosis signaling (Mirshahi et al., 2012; Fernandez-Bueno et al., 2013). Therefore, it can be inferred that PARP regulated transcriptome may play essential roles in RD pathogenesis.

Nevertheless, there are some limitations in this study. Firstly, the specific roles of the identified DEGs in RD pathogenesis need to be further investigated *in vitro* and *in vivo*, and the related mechanisms of PITX2 in RD also should be further explored. Given the potential involvement of *Xist*, experiments it may be of interest to also study the effects of gender in RD.

In conclusion, the photoreceptor cell death mechanism is complex and requires further comprehensive studies. In addition to studying alterations in important genes and pathways involved in RD, we focused on the possible roles of upstream regulators. TFs are essential for initiating gene expression, cell proliferation, differentiation, and cell fate determination. Furthermore, many non-coding RNAs play key roles in the regulation of cell homeostasis (Amaral et al., 2013). In the retina, non-coding RNAs can regulate the expression of genes involved in oxidative stress, ion channels, retinal layer connections, basement membrane integrity, and receptor clusters (Donato et al., 2018), which are all related to RD pathogenesis (Giblin et al., 2016). Accordingly, our results showed that dysregulated TFs or non-coding RNAs, including lncRNAs and circRNAs, may be of importance for photoreceptor cell death and participate in RD pathogenesis by mediating the stress response, apoptotic factor production, ion channel activity, optic nerve signal transduction, metabolism, and homeostasis regulation. Additionally, many TFs and non-coding RNAs (e.g., *Xist*, *Pitx2*, PARPs) were identified as key regulatory molecules associated with RD. In this way, our work lays a foundation to discover and develop novel potential therapeutic targets for treating RD.

DATA AVAILABILITY STATEMENT

The series entry (GSE178928, <https://www.ncbi.nlm.nih.gov/geo/query/acc.cgi?acc=GSE178928>) provides access to all of our data and is the accession that can be quoted in any article discussing the data.

REFERENCES

- A, L., Zou, T., He, J., Chen, X., Sun, D., Fan, X., et al. (2019). Rescue of Retinal Degeneration in Rd1 Mice by Intravitreally Injected Metformin. *Front. Mol. Neurosci.* 12, 102. doi:10.3389/fnmol.2019.00102
- Akiba, R., Matsuyama, T., Takahashi, M., and Mandai, M. (2020). Toward Establishment of Regenerative Cell Therapy for Retinitis Pigmentosa Using iPS Cell Derived Retinal Sheet. *Folia Pharmacol. Jpn.* 155, 93–98. doi:10.1254/fpj.19124
- Amaral, P. P., Dinger, M. E., and Mattick, J. S. (2013). Non-coding RNAs in Homeostasis, Disease and Stress Responses: an Evolutionary Perspective. *Brief. Funct. Genomics* 12, 254–278. doi:10.1093/bfpg/elt016

ETHICS STATEMENT

The animal study was reviewed and approved by the Ethics Review Committee of Yunnan University (No. YNUCARE20210024) and the Ethical Review Committee of the Affiliated Hospital of Yunnan University (No. 2021045).

AUTHOR CONTRIBUTIONS

CW carried out the animal preparation, participated in the bioinformatic analysis; YL participated in the TUNEL and carried out parts of the analysis, and drafted the article; XF participated in the analysis and interpretation; FP-D, ZH, KJ conceived and participated in the design of the study, and helped to write the article. All authors read and approved the final article.

FUNDING

This study was supported by grants from the National Natural Science Foundation of China (No. 81960180), Charlotte and Tistou Kerstan Foundation, the European Union (transMed; H2020-MSCA-765441, Partly from the Yunnan Applied Basic Research Projects (Nos. 2018FB123, 2019FB093), Joint key project of Yunnan Provincial Department of Science and Technology and Kunming Medical University on Applied Basic Research (No. 2018FE001-008).

ACKNOWLEDGMENTS

We thank the cell death mechanism group, Institute for Ophthalmic Research, Eberhard-Karls-Universität Tübingen for sharing the RD models used in this study. We thank Prof. Bernd Wissinger for his very helpful review of the manuscript.

SUPPLEMENTARY MATERIAL

The Supplementary Material for this article can be found online at: <https://www.frontiersin.org/articles/10.3389/fgene.2021.728791/full#supplementary-material>

- Arango-Gonzalez, B., Trifunović, D., Sahaboglu, A., Kranz, K., Michalakakis, S., Farinelli, P., et al. (2014). Identification of a Common Non-apoptotic Cell Death Mechanism in Hereditary Retinal Degeneration. *PLoS One* 9, e112142. doi:10.1371/journal.pone.0112142
- Badugu, R., Garcia, M., Bondada, V., Joshi, A., and Geddes, J. W. (2008). N Terminus of Calpain 1 Is a Mitochondrial Targeting Sequence. *J. Biol. Chem.* 283, 3409–3417. doi:10.1074/jbc.m706851200
- Beneke, S., Cohausz, O., Malanga, M., Boukamp, P., Althaus, F., and Bürkle, A. (2008). Rapid Regulation of Telomere Length Is Mediated by poly(ADP-Ribose) Polymerase-1. *Nucleic Acids Res.* 36, 6309–6317. doi:10.1093/nar/gkn615
- Bernofsky, C. (1980). Physiology Aspects of Pyridine Nucleotide Regulation in Mammals. *Mol. Cel. Biochem.* 33, 135–143. doi:10.1007/BF00225285

- Bryant, H. E., Petermann, E., Schultz, N., Jemth, A.-S., Loseva, O., Issaeva, N., et al. (2009). PARP Is Activated at Stalled forks to Mediate Mre11-dependent Replication Restart and Recombination. *EMBO J.* 28, 2601–2615. doi:10.1038/emboj.2009.206
- Cai, L., and Lyu, Y. L. (2012). Analysis of Retinal Development and Diseases Using RNA-Seq. *Cell Dev. Biol.* 1. doi:10.4172/2168-9296.1000e113
- Chang, B., Hawes, N. L., Pardue, M. T., German, A. M., Hurd, R. E., Davisson, M. T., et al. (2007). Two Mouse Retinal Degenerations Caused by Missense Mutations in the β -subunit of Rod cGMP Phosphodiesterase Gene. *Vis. Res.* 47, 624–633. doi:10.1016/j.visres.2006.11.020
- Chawla, B., Schley, E., Williams, A. L., and Bohnsack, B. L. (2016). Retinoic Acid and Pitx2 Regulate Early Neural Crest Survival and Migration in Craniofacial and Ocular Development. *Birth Defects Res. B.* 107, 126–135. doi:10.1002/bdrb.21177
- Chen, W., Peng, R., Sun, Y., Liu, H., Zhang, L., Peng, H., et al. (2019). The Topological Key lncRNA H2k2 from the ceRNA Network Promotes Mesangial Cell Proliferation in Diabetic Nephropathy via the miR-449a/b/Trim11/Mek Signaling Pathway. *FASEB J.* 33, 11492–11506. doi:10.1096/fj.201900522r
- Chevillard, G., Derjuga, A., Devost, D., Zingg, H. H., and Blank, V. (2007). Identification of Interleukin-1 β Regulated Genes in Uterine Smooth Muscle Cells. *Reproduction* 134, 811–822. doi:10.1530/rep-07-0289
- Chow, A. Y. (2013). Retinal Prostheses Development in Retinitis Pigmentosa Patients-Progress and Comparison. *Asia-Pacific J. Ophthalmol.* 2, 253–268. doi:10.1097/apo.0b013e3182a0b4fe
- Das, S., Chen, Y., Yan, J., Christensen, G., Belhadj, S., Tolone, A., et al. (2021). The Role of cGMP-Signalling and Calcium-Signalling in Photoreceptor Cell Death: Perspectives for Therapy Development. *Pflugers Arch. - Eur. J. Physiol.* 473, 1411–1421. doi:10.1007/s00424-021-02556-9
- Dean, D. M., Nguitragool, W., Miri, A., McCabe, S. L., and Zimmerman, A. L. (2002). All-trans-retinal Shuts Down Rod Cyclic Nucleotide-Gated Ion Channels: a Novel Role for Photoreceptor Retinoids in the Response to Bright Light? *Proc. Natl. Acad. Sci.* 99, 8372–8377. doi:10.1073/pnas.122681899
- Donato, L., Scimone, C., Rinaldi, C., D'Angelo, R., and Sidoti, A. (2018). RETRACTED ARTICLE: Non-coding RNAome of RPE Cells under Oxidative Stress Suggests Unknown Regulatory Aspects of Retinitis Pigmentosa Etiopathogenesis. *Sci. Rep.* 8, 16638. doi:10.1038/s41598-018-35086-z
- Dong, Y., Wan, G., Peng, G., Yan, P., Qian, C., and Li, F. (2020). Long Non-coding RNA XIST Regulates Hyperglycemia-Associated Apoptosis and Migration in Human Retinal Pigment Epithelial Cells. *Biomed. Pharmacother.* 125, 109959. doi:10.1016/j.biopha.2020.109959
- Ducloyer, J.-B., Le Meur, G., Cronin, T., Adjali, O., and Weber, M. (2020). La thérapie génique des rétinites pigmentaires héréditaires. *Med. Sci. (Paris)* 36, 607–615. doi:10.1051/medsci/2020095
- Durkacz, B. W., Omidiji, O., Gray, D. A., and Shall, S. (1980). (ADP-ribose) n Participates in DNA Excision Repair. *Nature* 283, 593–596. doi:10.1038/283593a0
- Evans, A. L., and Gage, P. J. (2005). Expression of the Homeobox Gene Pitx2 in Neural Crest Is Required for Optic Stalk and Ocular Anterior Segment Development. *Hum. Mol. Genet.* 14, 3347–3359. doi:10.1093/hmg/ddi365
- Fatokun, A. A., Dawson, V. L., and Dawson, T. M. (2014). Parthanatos: Mitochondrial-Linked Mechanisms and Therapeutic Opportunities. *Br. J. Pharmacol.* 171, 2000–2016. doi:10.1111/bph.12416
- Fernandez-Bueno, I., Garcia-Gutierrez, M. T., Srivastava, G. K., Gayoso, M. J., Gonzalo-Orden, J. M., and Pastor, J. C. (2013). Adalimumab (Tumor Necrosis Factor-Blocker) Reduces the Expression of Glial Fibrillary Acidic Protein Immunoreactivity Increased by Exogenous Tumor Necrosis Factor Alpha in an Organotypic Culture of Porcine Neuroretina. *Mol. Vis.* 19, 894–903.
- Gage, P. J., Rhoades, W., Prucka, S. K., and Hjalt, T. (2005). Fate Maps of Neural Crest and Mesoderm in the Mammalian Eye. *Invest. Ophthalmol. Vis. Sci.* 46, 4200–4208. doi:10.1167/iovs.05-0691
- Gao, F. J., Zhang, S. H., Chen, J. Y., Xu, G. Z., and Wu, J. H. (2017). Digenic Heterozygous Mutations in EYS/LRP5 in a Chinese Family with Retinitis Pigmentosa. *Int. J. Ophthalmol.* 10, 325–328. doi:10.18240/ijo.2017.02.25
- Giblin, J. P., Comes, N., Strauss, O., and Gasull, X. (2016). Ion Channels in the Eye. *Adv. Protein Chem. Struct. Biol.* 104, 157–231. doi:10.1016/bbsapcsb.2015.11.006
- Goldberg, A. F. X. (2006). Role of Peripherin/rds in Vertebrate Photoreceptor Architecture and Inherited Retinal Degenerations. *Int. Rev. Cytol.* 253, 131–175. doi:10.1016/s0074-7696(06)53004-9
- Goodwin, P. M., Lewis, P. J., Davies, M. I., Skidmore, C. J., and Shall, S. (1978). The Effect of Gamma Radiation and Neocarzinostatin of NAD and ATP Levels in Mouse Leukaemia Cells. *Biochim. Biophys. Acta (Bba) - Gen. Subjects* 543, 576–582. doi:10.1016/0304-4165(78)90312-4
- Gupta, N., Brown, K. E., and Milam, A. H. (2003). Activated Microglia in Human Retinitis Pigmentosa, Late-Onset Retinal Degeneration, and Age-Related Macular Degeneration. *Exp. Eye Res.* 76, 463–471. doi:10.1016/s0014-4835(02)00332-9
- Gupta, V. K., Rajala, A., and Rajala, R. V. S. (2012). Insulin Receptor Regulates Photoreceptor CNG Channel Activity. *Am. J. Physiology-Endocrinology Metab.* 303, E1363–E1372. doi:10.1152/ajpendo.00199.2012
- Hassa, P. O., Haenni, S. S., Elser, M., and Hottiger, M. O. (2006). Nuclear ADP-Ribosylation Reactions in Mammalian Cells: where Are We Today and where Are We Going?. *Microbiol. Mol. Biol. Rev.* 70, 789–829. doi:10.1128/mmbr.00040-05
- Hendee, K. E., Sorokina, E. A., Muheisen, S. S., Reis, L. M., Tyler, R. C., Markovic, V., et al. (2018). PITX2 Deficiency and Associated Human Disease: Insights from the Zebrafish Model. *Hum. Mol. Genet.* 27, 1675–1695. doi:10.1093/hmg/ddy074
- Ikejima, M., Noguchi, S., Yamashita, R., Ogura, T., Sugimura, T., Gill, D. M., et al. (1990). The Zinc Fingers of Human poly(ADP-Ribose) Polymerase Are Differentially Required for the Recognition of DNA Breaks and Nicks and the Consequent Enzyme Activation. Other Structures Recognize Intact DNA. *J. Biol. Chem.* 265, 21907–21913. doi:10.1016/s0021-9258(18)45824-3
- Ji, Y., Buel, S. M., and Amack, J. D. (2016). Mutations in Zebrafish Pitx2 Model Congenital Malformations in Axenfeld-Rieger Syndrome but Do Not Disrupt Left-Right Placement of Visceral Organs. *Dev. Biol.* 416, 69–81. doi:10.1016/j.ydbio.2016.06.010
- Katsuoka, F., Motohashi, H., Tamagawa, Y., Kure, S., Igarashi, K., Engel, J. D., et al. (2003). Small Maf Compound Mutants Display central Nervous System Neuronal Degeneration, Aberrant Transcription, and Bach Protein Mislocalization Coincident with Myoclonus and Abnormal Startle Response. *Mol. Cell. Biol.* 23, 1163–1174. doi:10.1128/mcb.23.4.1163-1174.2003
- Keeler, C. E. (1924). The Inheritance of a Retinal Abnormality in White Mice. *Proc. Natl. Acad. Sci.* 10, 329–333. doi:10.1073/pnas.10.7.329
- Kerr, W. G., and Thompson, M. A. (1972). Acceptance of Disability of Sudden Onset in Paraplegia. *Spinal Cord* 10, 94–102. doi:10.1038/sc.1972.16
- Kimura, M., Tokita, Y., Machida, J., Shibata, A., Tatematsu, T., Tsurusaki, Y., et al. (2014). A Novel PITX2 Mutation Causing Iris Hypoplasia. *Hum. Genome Var.* 1, 14005. doi:10.1038/hgv.2014.5
- Kim, S., Han, J., Kim, H. A., Lim, B. C., Seo, J. E., Choi, M., et al. (2018). Neuropathy, Ataxia, Retinitis Pigmentosa-like Phenotype Associated with a Mitochondrial G8363A Mutation in a Family. *Ann. Clin. Lab. Sci.* 48, 546–548.
- Kraupp, B. G., Ruttikay-Nedecky, B., Koudelka, H., Bukowska, K., Bursch, W., and Schulte-Hermann, R. (1995). *In Situ* detection of Fragmented DNA (TUNEL Assay) Fails to Discriminate Among Apoptosis, Necrosis, and Autolytic Cell Death: a Cautionary Note. *Hepatology* 21, 1465–1468. doi:10.1002/hep.1840210534
- Langfelder, P., and Horvath, S. (2008). WGCNA: an R Package for Weighted Correlation Network Analysis. *BMC Bioinformatics* 9, 559. doi:10.1186/1471-2105-9-559
- Lee, S. Y., Usui, S., Zafar, A.-b., Oveson, B. C., Jo, Y.-J., Lu, L., et al. (2011). N-acetylcysteine Promotes Long-Term Survival of Cones in a Model of Retinitis Pigmentosa. *J. Cell. Physiol.* 226, 1843–1849. doi:10.1002/jcp.22508
- Leist, M., and Jäätelä, M. (2001). Four Deaths and a Funeral: from Caspases to Alternative Mechanisms. *Nat. Rev. Mol. Cell. Biol.* 2, 589–598. doi:10.1038/35085008
- Liu, A., Liu, L., and Lu, H. (2019). lncRNA XIST Facilitates Proliferation and Epithelial-Mesenchymal Transition of Colorectal Cancer Cells through Targeting miR-486-5p and Promoting Neuropilin-2. *J. Cell Physiol* 234, 13747–13761. doi:10.1002/jcp.28054
- Loo, D. T. (2002). TUNEL Assay: An Overview of Techniques. *Methods Mol. Biol.* 203, 21–30. doi:10.1385/1-59259-179-5:21
- Lukiw, W. J. (2013). Circular RNA (circRNA) in Alzheimer's Disease (AD). *Front. Genet.* 4, 307. doi:10.3389/fgene.2013.00307

- Maira, M., Long, J. E., Lee, A. Y., Rubenstein, J. L. R., and Stifani, S. (2010). Role for TGF- β Superfamily Signaling in Telencephalic GABAergic Neuron Development. *J. Neurodevelop. Disord.* 2, 48–60. doi:10.1007/s11689-009-9035-6
- Martínez-Fernández de la Cámara, C., Hernández-Pinto, A. M., Olivares-González, L., Cuevas-Martín, C., Sánchez-Aragó, M., Hervás, D., et al. (2015). Adalimumab Reduces Photoreceptor Cell Death in A Mouse Model of Retinal Degeneration. *Sci. Rep.* 5, 11764. doi:10.1038/srep11764
- Martínez-Fernández de la Cámara, C., Salom, D., Sequedo, M. D., Hervás, D., Marín-Lambies, C., Aller, E., et al. (2013). Altered Antioxidant-Oxidant Status in the Aqueous Humor and Peripheral Blood of Patients with Retinitis Pigmentosa. *PLoS One* 8, e74223. doi:10.1371/journal.pone.0074223
- Mrshahi, A., Hoehn, R., Lorenz, K., Kramann, C., and Baatz, H. (2012). Anti-tumor Necrosis Factor Alpha for Retinal Diseases: Current Knowledge and Future Concepts. *J. Ophthalmic Vis. Res.* 7, 39–44.
- Mizukoshi, S., Nakazawa, M., Sato, K., Ozaki, T., Metoki, T., and Ishiguro, S.-i. (2010). Activation of Mitochondrial Calpain and Release of Apoptosis-Inducing Factor from Mitochondria in RCS Rat Retinal Degeneration. *Exp. Eye Res.* 91, 353–361. doi:10.1016/j.exer.2010.06.004
- Okubo, T., Hayashi, R., Shibata, Y., Kudo, Y., Ishikawa, S., Inoue, Y., et al. (2020). Generation and Validation of a PITX2-EGFP Reporter Line of Human Induced Pluripotent Stem Cells Enables Isolation of Periocular Mesenchymal Cells. *J. Biol. Chem.* 295, 3456–3465. doi:10.1074/jbc.RA119.010713
- Oveson, B. C., Iwase, T., Hackett, S. F., Lee, S. Y., Usui, S., Sedlak, T. W., et al. (2011). Constituents of Bile, Bilirubin and TUDCA, Protect against Oxidative Stress-Induced Retinal Degeneration. *J. Neurochem.* 116, 144–153. doi:10.1111/j.1471-4159.2010.07092.x
- Owczarek-Lipska, M., Song, F., Jakšić, V., and Neidhardt, J. (2020). Compound Heterozygous RPE65 Mutations Associated with an Early Onset Autosomal Recessive Retinitis Pigmentosa. *J. Gene Med.* 22, e3211. doi:10.1002/jgm.3211
- Paquet-Durand, F., Silva, J., Talukdar, T., Johnson, L. E., Azadi, S., Van Veen, T., et al. (2007). Excessive Activation of poly(ADP-Ribose) Polymerase Contributes to Inherited Photoreceptor Degeneration in the Retinal Degeneration 1 Mouse. *J. Neurosci.* 27, 10311–10319. doi:10.1523/jneurosci.1514-07.2007
- Patel, A. K., Surapaneni, K., Yi, H., Nakamura, R. E. I., Karli, S. Z., Syeda, S., et al. (2015). Activation of Wnt/ β -Catenin Signaling in Muller Glia Protects Photoreceptors in a Mouse Model of Inherited Retinal Degeneration. *Neuropharmacology* 91, 1–12. doi:10.1016/j.neuropharm.2014.11.015
- Peng, B., Xiao, J., Wang, K., So, K.-F., Tipoe, G. L., and Lin, B. (2014). Suppression of Microglial Activation Is Neuroprotective in a Mouse Model of Human Retinitis Pigmentosa. *J. Neurosci.* 34, 8139–8150. doi:10.1523/jneurosci.5200-13.2014
- Pittler, S. J., and Baehr, W. (1991). Identification of a Nonsense Mutation in the Rod Photoreceptor cGMP Phosphodiesterase Beta-Subunit Gene of the Rd Mouse. *Proc. Natl. Acad. Sci.* 88, 8322–8326. doi:10.1073/pnas.88.19.8322
- Plesnila, N., Zhu, C., Culmsee, C., Gröger, M., Moskowitz, M. A., and Blomgren, K. (2004). Nuclear Translocation of Apoptosis-Inducing Factor after Focal Cerebral Ischemia. *J. Cereb. Blood Flow Metab.* 24, 458–466. doi:10.1097/00004647-200404000-00011
- Polster, B. M., Basañez, G., Etzebarria, A., Hardwick, J. M., and Nicholls, D. G. (2005). Calpain I Induces Cleavage and Release of Apoptosis-Inducing Factor from Isolated Mitochondria. *J. Biol. Chem.* 280, 6447–6454. doi:10.1074/jbc.M413269200
- Power, M., Das, S., Schütze, K., Marigo, V., Ekström, P., and Paquet-Durand, F. (2020). Cellular Mechanisms of Hereditary Photoreceptor Degeneration - Focus on cGMP. *Prog. Retin. Eye Res.* 74, 100772. doi:10.1016/j.preteyeres.2019.07.005
- Rajala, A., Tanito, M., Le, Y. Z., Kahn, C. R., and Rajala, R. V. S. (2008). Loss of Neuroprotective Survival Signal in Mice Lacking Insulin Receptor Gene in Rod Photoreceptor Cells. *J. Biol. Chem.* 283, 19781–19792. doi:10.1074/jbc.M802374200
- Reid, C. D., Steiner, A. B., Yaklichkin, S., Lu, Q., Wang, S., Hennessy, M., et al. (2016). FoxH1 Mediates a Grg4 and Smad2 Dependent Transcriptional Switch in Nodal Signaling during Xenopus Mesoderm Development. *Dev. Biol.* 414, 34–44. doi:10.1016/j.ydbio.2016.04.006
- Rybak-Wolf, A., Stottmeister, C., Glažar, P., Jens, M., Pino, N., Giusti, S., et al. (2015). Circular RNAs in the Mammalian Brain Are Highly Abundant, Conserved, and Dynamically Expressed. *Mol. Cell.* 58, 870–885. doi:10.1016/j.molcel.2015.03.027
- Sahaboglu, A., Tanimoto, N., Kaur, J., Sancho-Pelluz, J., Huber, G., Fahl, E., et al. (2010). PARP1 Gene Knock-Out Increases Resistance to Retinal Degeneration without Affecting Retinal Function. *PLoS One* 5, e15495. doi:10.1371/journal.pone.0015495
- Saliba, J., Coutaud, B., Solovieva, V., Lu, F., and Blank, V. (2019). Regulation of CXCL 1 Chemokine and CSF 3 Cytokine Levels in Myometrial Cells by the MAFF Transcription Factor. *J. Cel. Mol. Med.* 23, 2517–2525. doi:10.1111/jcmm.14136
- Salveti, A. P., Nanda, A., and Maclaren, R. E. (2021). RPGR-related X-Linked Retinitis Pigmentosa Carriers with a Severe "Male Pattern". *Ophthalmologica* 244, 60–67. doi:10.1159/000503687
- Sancho-Pelluz, J., and Paquet-Durand, F. (2012). HDAC Inhibition Prevents Rd1 Mouse Photoreceptor Degeneration. *Adv. Exp. Med. Biol.* 723, 107–113. doi:10.1007/978-1-4614-0631-0_15
- Sanges, D., Comitato, A., Tammara, R., and Marigo, V. (2006). Apoptosis in Retinal Degeneration Involves Cross-Talk between Apoptosis-Inducing Factor (AIF) and Caspase-12 and Is Blocked by Calpain Inhibitors. *Proc. Natl. Acad. Sci.* 103, 17366–17371. doi:10.1073/pnas.0606276103
- Sanyal, S., and Bal, A. K. (1973). Comparative Light and Electron Microscopic Study of Retinal Histogenesis in normal and Rd Mutant Mice. *Z. Anat. Entwickl. Gesch.* 142, 219–238. doi:10.1007/bf00519723
- Sarkar, H., Dubis, A. M., Downes, S., and Moosajee, M. (2020). Novel Heterozygous Deletion in Retinol Dehydrogenase 12 (RDH12) Causes Familial Autosomal Dominant Retinitis Pigmentosa. *Front. Genet.* 11, 335. doi:10.3389/fgene.2020.00335
- Schiewer, M. J., Mandigo, A. C., Gordon, N., Huang, F., Gaur, S., De Leeuw, R., et al. (2018). PARP-1 Regulates DNA Repair Factor Availability. *EMBO Mol. Med.* 10, 1. doi:10.15252/emmm.201708816
- Seifi, M., Footz, T., Taylor, S. A. M., Elhady, G. M., Abdalla, E. M., and Walter, M. A. (2016). Novel PITX2 Gene Mutations in Patients with Axenfeld-Rieger Syndrome. *Acta Ophthalmol.* 94, e571–e579. doi:10.1111/aos.13030
- Semina, E. V., Reiter, R., Leysens, N. J., Alward, W. L. M., Small, K. W., Datson, N. A., et al. (1996). Cloning and Characterization of a Novel Bicoid-Related Homeobox Transcription Factor Gene, RIEG, Involved in Rieger Syndrome. *Nat. Genet.* 14, 392–399. doi:10.1038/ng1296-392
- Shan, K., Liu, C., Liu, B.-H., Chen, X., Dong, R., Liu, X., et al. (2017). Circular Noncoding RNA HIPK3 Mediates Retinal Vascular Dysfunction in Diabetes Mellitus. *Circulation* 136, 1629–1642. doi:10.1161/circulationaha.117.029004
- Strungaru, M. H., Footz, T., Liu, Y., Berry, F. B., Belleau, P., Semina, E. V., et al. (2011). PITX2 is Involved in Stress Response in Cultured Human Trabecular Meshwork Cells Through Regulation of SLC13A3. *Invest. Ophthalmol. Vis. Sci.* 52, 7625–7633. doi:10.1167/iovs.10-6967
- Susin, S. A., Lorenzo, H. K., Zamzami, N., Marzo, I., Snow, B. E., Brothers, G. M., et al. (1999). Molecular Characterization of Mitochondrial Apoptosis-Inducing Factor. *Nature* 397, 441–446. doi:10.1038/17135
- Tsang, S. H., Gouras, P., Yamashita, C. K., Kjeldbye, H., Fisher, J., Farber, D. B., et al. (1996). Retinal Degeneration in Mice Lacking the Gamma Subunit of the Rod cGMP Phosphodiesterase. *Science* 272, 1026–1029. doi:10.1126/science.272.5264.1026
- Uren, P. J., Lee, J. T., Doroudchi, M. M., Smith, A. D., and Horsager, A. (2014). A Profile of Transcriptomic Changes in the Rd10 Mouse Model of Retinitis Pigmentosa. *Mol. Vis.* 20, 1612–1628.
- Valentincic, N. V., De Groot-Mijnes, J. D., Kraut, A., Korosec, P., Hawlina, M., and Rothova, A. (2011). Intraocular and Serum Cytokine Profiles in Patients with Intermediate Uveitis. *Mol. Vis.* 17, 2003–2010.
- Vandenabeele, P., Galluzzi, L., Vanden Berghe, T., and Kroemer, G. (2010). Molecular Mechanisms of Necroptosis: An Ordered Cellular Explosion. *Nat. Rev. Mol. Cell Biol.* 11, 700–714. doi:10.1038/nrm2970
- Veleri, S., Lazar, C. H., Chang, B., Sieving, P. A., Banin, E., and Swaroop, A. (2015). Biology and Therapy of Inherited Retinal Degenerative Disease: Insights from Mouse Models. *Dis. Model. Mech.* 8, 109–129. doi:10.1242/dmm.017913
- Vighi, E., Trifunović, D., Veiga-Crespo, P., Rentsch, A., Hoffmann, D., Sahaboglu, A., et al. (2018). Combination of cGMP Analogue and Drug Delivery System

- Provides Functional protection in Hereditary Retinal Degeneration. *Proc. Natl. Acad. Sci. USA* 115, E2997–E3006. doi:10.1073/pnas.1718792115
- Wang, L., Hu, K., and Chao, Y. (2018). MicroRNA-1301 Inhibits Migration and Invasion of Osteosarcoma Cells by Targeting BCL9. *Gene* 679, 100–107. doi:10.1016/j.gene.2018.08.078
- Wang, L., Su, Y., Huang, C., Yin, Y., Zhu, J., Knupp, A., et al. (2019). FOXH1 Is Regulated by NANOG and LIN28 for Early-Stage Reprogramming. *Sci. Rep.* 9, 16443. doi:10.1038/s41598-019-52861-8
- Wang, T., Tsang, S. H., and Chen, J. (2017). Two Pathways of Rod Photoreceptor Cell Death Induced by Elevated cGMP. *Hum. Mol. Genet.* 26, 2299–2306. doi:10.1093/hmg/ddx121
- Wawrzyniak, O., Zarębska, Ż., Rolle, K., and Gotz-Więckowska, A. (2018). Circular and Long Non-coding RNAs and Their Role in Ophthalmologic Diseases. *Acta Biochim. Pol.* 65, 497–508. doi:10.18388/abp.2018_2639
- Wright, C. M., Garifallou, J. P., Schneider, S., Mentch, H. L., Kothakapa, D. R., Maguire, B. A., et al. (2020). Dlx1/2 Mice Have Abnormal Enteric Nervous System Function. *JCI Insight* 5. doi:10.1172/jci.insight.131494
- Xing, F., Liu, Y., Wu, S.-Y., Wu, K., Sharma, S., Mo, Y.-Y., et al. (2018). Loss of XIST in Breast Cancer Activates MSN-C-Met and Reprograms Microglia via Exosomal miRNA to Promote Brain Metastasis. *Cancer Res.* 78, 4316–4330. doi:10.1158/0008-5472.can-18-1102
- Yang, Y., Zhang, J., Chen, X., Xu, X., Cao, G., Li, H., et al. (2018). LncRNA FTX Sponges miR-215 and Inhibits Phosphorylation of Vimentin for Promoting Colorectal Cancer Progression. *Gene Ther.* 25, 321–330. doi:10.1038/s41434-018-0026-7
- Ying, W., Alano, C. C., Garnier, P., and Swanson, R. A. (2005). NAD⁺ as a Metabolic Link between DNA Damage and Cell Death. *J. Neurosci. Res.* 79, 216–223. doi:10.1002/jnr.20289
- Yoshida, N., Ikeda, Y., Notomi, S., Ishikawa, K., Murakami, Y., Hisatomi, T., et al. (2013). Laboratory Evidence of Sustained Chronic Inflammatory Reaction in Retinitis Pigmentosa. *Ophthalmology* 120, e5–e12. doi:10.1016/j.ophtha.2012.07.008
- Zhang, Q. (2016). Retinitis Pigmentosa. *Asia-Pacific J. Ophthalmol.* 5, 265–271. doi:10.1097/apo.0000000000000227

Conflict of Interest: The authors declare that the research was conducted in the absence of any commercial or financial relationships that could be construed as a potential conflict of interest.

Publisher's Note: All claims expressed in this article are solely those of the authors and do not necessarily represent those of their affiliated organizations, or those of the publisher, the editors and the reviewers. Any product that may be evaluated in this article, or claim that may be made by its manufacturer, is not guaranteed or endorsed by the publisher.

Copyright © 2021 Wei, Li, Feng, Hu, Paquet-Durand and Jiao. This is an open-access article distributed under the terms of the Creative Commons Attribution License (CC BY). The use, distribution or reproduction in other forums is permitted, provided the original author(s) and the copyright owner(s) are credited and that the original publication in this journal is cited, in accordance with accepted academic practice. No use, distribution or reproduction is permitted which does not comply with these terms.



Identification of m6A-Related lncRNAs Associated With Prognoses and Immune Responses in Acute Myeloid Leukemia

OPEN ACCESS

Edited by:

Yicheng Long,
Cornell University, United States

Reviewed by:

Weinan Zhou,
University of Illinois at Urbana-
Champaign, United States

Xin Zhou,
University of North Carolina at Chapel
Hill, United States

*Correspondence:

Ding Li
ld_sunshinev@163.com
Xuan Wu
843240113@qq.com
Wenzhou Zhang
hnzzwzx@sina.com

[†]These authors have contributed
equally to this work

Specialty section:

This article was submitted to
Epigenomics and Epigenetics,
a section of the journal
Frontiers in Cell and Developmental
Biology

Received: 03 September 2021

Accepted: 01 November 2021

Published: 16 November 2021

Citation:

Li D, Liang J, Cheng C, Guo W, Li S,
Song W, Song Z, Bai Y, Zhang Y, Wu X
and Zhang W (2021) Identification of
m6A-Related lncRNAs Associated
With Prognoses and Immune
Responses in Acute
Myeloid Leukemia.
Front. Cell Dev. Biol. 9:770451.
doi: 10.3389/fcell.2021.770451

Ding Li^{1*†}, Jiaming Liang^{2†}, Cheng Cheng^{3†}, Wenbin Guo⁴, Shuolei Li¹, Wenping Song¹,
Zhenguo Song¹, Yongtao Bai¹, Yongna Zhang¹, Xuan Wu^{5*} and Wenzhou Zhang^{1*}

¹Department of Pharmacy, Affiliated Cancer Hospital of Zhengzhou University, Henan Cancer Hospital, Zhengzhou, China, ²State Key Laboratory of Respiratory Disease, National Clinical Research Center for Respiratory Disease, The First Affiliated Hospital of Guangzhou Medical University, Guangzhou, China, ³Department of Hematology, Affiliated Cancer Hospital of Zhengzhou University, Henan Cancer Hospital, Zhengzhou, China, ⁴Department of Pathology, Pingtan Comprehensive Experimental Area Hospital, Fuzhou, China, ⁵Department of Internal Medicine, Affiliated Cancer Hospital of Zhengzhou University, Henan Cancer Hospital, Zhengzhou, China

Background: Acute myeloid leukemia (AML) remains the most common type of hematopoietic malignancy in adults and has an unfavorable outcome. Herein, we aimed to construct an N6-methyladenosine (m6A)-related long noncoding RNAs (lncRNAs) signature to accurately predict the prognosis of patients with AML using the data downloaded from The Cancer Genome Atlas (TCGA) database.

Methods: The RNA-seq and clinical data were obtained from the TCGA AML cohort. First, Pearson correlation analysis was performed to identify the m6A-related lncRNAs. Next, univariate Cox regression analysis was used to determine the candidate lncRNAs with prognostic value. Then, feature selection was carried out by Least absolute shrinkage and selection operator (LASSO) analysis, and seven eligible m6A-related lncRNAs were included to construct the prognostic risk signature. Kaplan–Meier and receiver operating characteristic (ROC) curve analyses were performed to evaluate the predictive capacity of the risk signature both in the training and testing datasets. A nomogram was used to predict 1-year, 2-year, and 3-year overall survival (OS) of AML patients. Next, the expression levels of lncRNAs in the signature were validated in AML samples by qRT-PCR. Functional enrichment analyses were carried out to identify probable biological processes and cellular pathways. The ceRNA network was developed to explore the downstream targets and mechanisms of m6A-related lncRNAs in AML.

Results: Seven m6A-related lncRNAs were identified as a prognostic signature. The low-risk group hold significantly prolonged OS. The nomogram showed excellent accuracy of the signature for predicting 1-year, 2-year and 3-year OS (AUC = 0.769, 0.820, and 0.800, respectively). Moreover, the risk scores were significantly correlated with enrichment in cancer hallmark- and malignancy-related pathways and immunotherapy response in AML patients.

Conclusion: We developed and validated a novel risk signature with m6A-related lncRNAs which could predict prognosis accurately and reflect the immunotherapy response in AML patients.

Keywords: M6A, long noncoding RNA, prognostic signature, immunotherapy response, acute myeloid leukemia

INTRODUCTION

Acute myeloid leukemia (AML) is one of the most aggressive hematological malignancies, with the highest incidence in adults (Short et al., 2018). Despite advancements in the biological understanding of AML, the standard treatment has not significantly improved over 40 years (Choi et al., 2020). The prognosis remains dismal, and most patients encounter disease recurrence or die of the disease several months after their initial remission. The long-term overall survival (OS) rate of young patients (<60 years) is less than 40%, and that of elderly patients (≥60 years) is only 15% (Koenig and Mims, 2020). Therefore, it is essential to identify novel molecules to accurately predict the prognosis and guide treatment in AML.

RNA methylation remains the frontier and focus of current epigenetic research, and N6-methyladenosine (m6A) is the main internal epigenetic modification in eukaryotic messenger RNAs (mRNAs) and noncoding RNAs (ncRNAs) (Deng et al., 2018). m6A affects the stability, alternative splicing, nuclear exit and translation efficiency of mRNA, and therefore plays important roles in various disease processes, including cancer (Cao et al., 2016; Wei et al., 2017; Dai et al., 2018). Recent research has revealed that the inactivation of m6A RNA methylases and demethylases in AML suppresses malignant cells through multiple m6A-dependent mechanisms. m6A RNA methylases METTL3/14 (Vu et al., 2017; Weng et al., 2018) and demethylases FTO/ALKBH5 (Huang et al., 2019; Shen et al., 2020), which are aberrantly expressed in specific leukemia subtypes, play a critical role in leukemogenesis by regulating specific gene targets and signaling pathways. Likewise, the m6A reader YTHDF2, which is highly expressed across AML subgroups, has been found to promote leukemogenesis by inhibiting gene targets through a YTHDF2-mediated mRNA decay mechanism (Paris et al., 2019). Therefore, m6A mRNA modification has promising therapeutic and prognostic potential in AML.

Long noncoding RNAs (lncRNAs), which possess no protein-coding capacity, are defined as transcripts longer than 200 nt and regarded as “noise” in genome transcription (Gibb et al., 2011). Previous studies have revealed that lncRNAs play essential roles in many important regulatory processes, such as transcription regulation, genome imprinting, chromatin modification, and nuclear transport, which have attracted widespread attention (Groff et al., 2016; Long et al., 2017). Some lncRNAs, including CASC15 (Fernando et al., 2017), UCA1 (Li et al., 2020), H19 (Zhang et al., 2018), HOTAIRM1 (Chen et al., 2020), LINC00152 (Cui et al.,

2021), have been identified to be associated with the recurring mutations, clinical features and prognosis of AML. Accumulating studies have indicated that aberrant expression of certain specific lncRNAs in tumor cells can be used as a diagnostic marker or a potential drug target. Additionally, lncRNAs can easily be detected in serum and saliva, urine, blood, or tissue biopsy, which makes them attractive for clinical diagnosis and prognostic prediction (Chandra Gupta and Nandan Tripathi, 2017).

Extensive studies have showed that some m6A modifications could be directly or indirectly regulated by lncRNAs. The interaction of m6A modification and lncRNAs plays crucial roles in tumor progression, metastasis, response to immune, drug resistance, and offers new insights for early diagnosis and new treatment strategies of cancer (Chen et al., 2020). However, specific roles of the m6A-related lncRNAs in AML remains to be elucidated. Therefore, understanding how m6A-related lncRNAs work may enable to identify potential molecules as therapeutic targets. In this study, we first constructed a prognostic risk signature with seven m6A-related lncRNAs and further validated the reliability and sensitivity of the signature. Moreover, we also explored the correlation of the risk score and tumor microenvironment. Finally, we built a ceRNA and PPI networks in order to further study the potential mechanisms of m6A-related lncRNAs in AML.

MATERIALS AND METHODS

Data Collection

We obtained the RNA-seq data and relevant clinical profiles of AML patients from The Cancer Genome Atlas (TCGA) database. After screening, cases with missing clinical data and/or OS ≤ 30 days were excluded from the study, and a total of 144 AML cases were included in the analysis. We subsequently transformed the probe IDs of each AML cohort into gene symbols based on the annotation files. The clinical characteristics for AML cases were summarized in **Supplementary Table S1**.

Correlation Analysis

We retrieved 21 m6A gene expression matrixes from the TCGA AML cohort, including expression data on methyltransferases, binding proteins, and demethylases. The 21 m6A genes included erasers (ALKBH5 and FTO), writers (ZC3H13, KIA1429, RBM15, RBM15B, METTL3, METTL14, METTL16 and WTAP), and readers (RBMX, HNRNPA2B1, HNRNPC, IGF2BP1, IGF2BP2, IGF2BP3, YTHDC1, YTHDC2, YTHDF1, YTHDF2 and YTHDF3). 11,904 lncRNA expression data were extracted from the TCGA AML cohort. Subsequently, Pearson correlation analysis was applied to investigate the relationship

between m6A genes and lncRNA expression to determine the m6A-related lncRNAs with a correlation coefficient >0.3 and $p < 0.05$.

Generation of a Prognostic Signature Using LASSO Regularization

To establish a reliable signature, the 144 cases were randomly divided into training (100 cases) and testing datasets (44 cases). The log-rank test was performed to extract the m6A-related lncRNAs that were closely associated with survival time for development of the prognostic signature. Subsequently, least absolute shrinkage and selection operator (LASSO) was performed to exclude the candidate lncRNAs significantly associated with each other to restrict overfitting with the R package “glmnet.” Then, we identified seven m6A-related lncRNAs to build the signature through multivariate Cox proportional hazards regression analysis. The risk scores were calculated using the following formula based on the included m6A-related lncRNAs. Based on the median risk score, the samples were classified to high- and low-risk groups.

$$\begin{aligned} \text{Risk Score} = & 0.1906265 * \text{USP30} - \text{AS1} + 0.10995083 * \text{AC114271.2} \\ & + 0.0704641 * \text{AF064858.8} + 0.02511635 * \text{RP11} - 22\text{L13.1} \\ & + (-0.129286) * \text{MIR181A1HG} + (-0.0512868) * \text{RP11} \\ & - 544\text{A12.4} + (-0.0383528) * \text{MIR133A1HG} \end{aligned}$$

Survival Analysis

Kaplan–Meier curves analysis and log-rank tests were used to compare the discrepancy of OS between the predicted high-risk and low-risk groups. $p \leq 0.05$ was defined as statistical difference. All survival analyses and log-rank tests were carried out using the R package survival, while the R package “survminer” was used to plot the Kaplan–Meier curve.

Construction and Evaluation of the Nomogram

R package “rms” was performed to construct a nomogram based on clinical stage, T stage and the risk score using the TCGA AML cohort. To evaluate the utility of the nomogram, the R package “ROC survival” was used to construct ROCs for the prediction of the 1-, 2- and 3-year OS by the nomogram. The R package “ggDCA” was used to construct a decision analysis curve to evaluate the clinical utility. Finally, package “rms” was used to establish a calibration curve to assess the precision for prediction of 1-, 2- and 3-year OS.

Functional Enrichment Analysis

Gene Ontology (GO) and Kyoto Encyclopedia of Genes and Genomes (KEGG) enrichment analyses of the differentially expressed genes (DEGs) in the two risk groups were performed by “cluster Pofolier” package. (Yu et al., 2012). Further, Gene Set Enrichment Analysis (GSEA) was used to analyze the biological functions and pathways associated with

the high and low-risk groups. FDR <0.05 and $p < 0.05$ were regarded statistically significant.

CeRNA Network

MiRcode was used to predict the miRNAs that interact with m6A-related lncRNAs. A total of 25 pairs of interactions between 9 lncRNAs and 10 miRNAs were identified by the miRcode database. A total of 271 mRNAs interacting with the miRNAs were identified to construct a PPI network through TargetScan, miRDB, and miR TarBase. The ceRNA network was visualized using Cytoscape software. The Cyto Hubba plugin was performed to obtain hub genes from the PPI network. GO and KEGG enrichment analyses were conducted to identify biological processes and potential signaling pathways.

Sample Collection

We totally collected 21 bone marrow samples, including 14 AML samples (derived from 7 AML patients at the time of first diagnosis and at first relapse) and 7 healthy controls in the Hematological Department of The Affiliated Cancer Hospital of Zhengzhou University. This research was approved by the Medical Ethics Committee of The Affiliated Cancer Hospital of Zhengzhou University (approval no. 2020239). Informed consent and approval were provided by all participants.

qRT-PCR Analysis

Total RNA was isolated from 21 patients' samples. cDNA synthesis was conducted with a reverse transcription kit (TransGen Biotech, #AU311-02). Then, real-time PCR was performed on the ABI 7500 Fast System (Applied Biosystems, United States) with TB Green Premix Ex Taq (Takara Bio, #RR420A). Relative expression of lncRNAs were normalized to GAPDH and calculated by $2^{-\Delta\Delta C_t}$ method. Primers sequences are listed in **Supplementary Table S2**.

Statistical Analysis

All statistical data were analyzed using R version 4.0.2. Pearson's correlation analyses were applied to evaluate the correlation between the risk score and specific gene expression. Kaplan–Meier curves and log-rank tests were conducted for survival analysis. Univariate and multivariate Cox regression were applied to assess the prognostic independence. The reliability and sensitivity of the signature were evaluated using ROC curve analysis. Student's *t*-test was used to determine significance between two groups. $p < 0.05$ was defined as statistical significance.

RESULTS

Construction of the m6A-Related lncRNAs Prognostic Signature for AML Patients

The flowchart summarized the construction and subsequent analysis of the risk signature (**Figure 1**). The expression profiles of 21 well known m6A genes and 11,904 lncRNAs

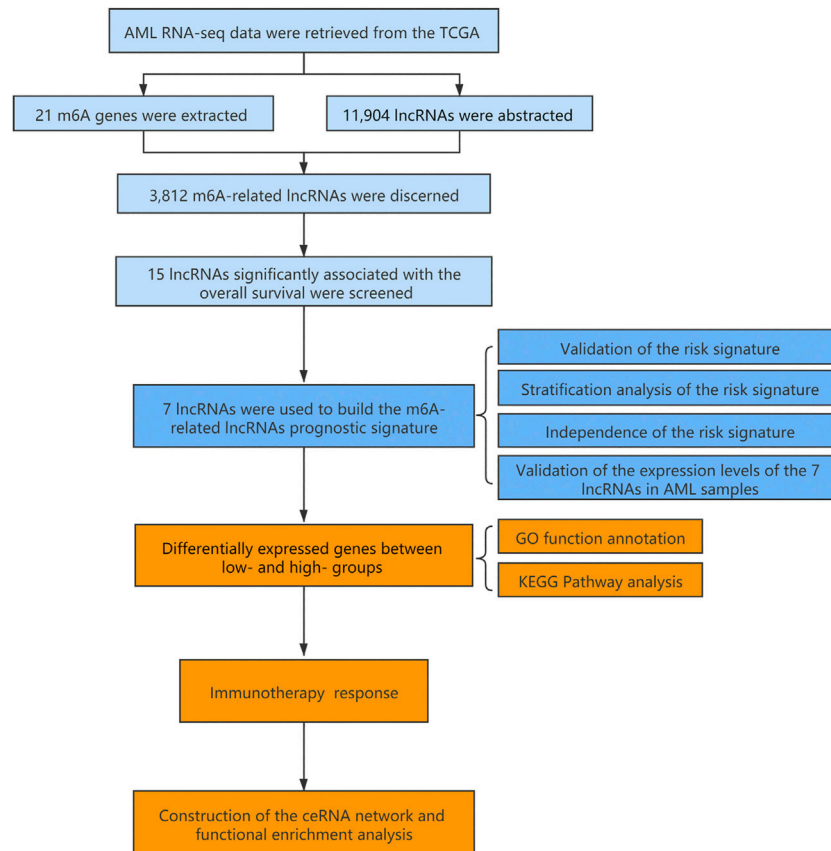


FIGURE 1 | Flow chart of the design in the study.

were extracted from TCGA AML cohort. The m6A-related lncRNAs were defined as ones which were associated with one or more of these m6A genes ($|\text{Pearson } R| > 0.3$ and $p < 0.05$), and a total of 3,812 lncRNAs were included (**Figure 2A**). Next, 15 m6A-related lncRNAs significantly related to the OS of AML patients were screened out through univariate Cox regression analysis ($p < 0.001$). Then, feature selection was performed using LASSO analysis, and 7 m6A-related lncRNAs were ultimately identified to develop the prognostic risk signature (**Figures 2B–D**). Among them, USP30-AS1, AC114271.2, AF064858.8 and RP11-22L13.1 are detrimental factors with a hazard ratio (HR) > 1 , whereas MIR181A1HG, RP11-544A12.4 and MIR133A1HG are protective factors with a HR < 1 (**Figure 2E**). Sankey diagram shows the relationship between the lncRNAs and m6A genes and the risk types (**Figure 2F**).

Validation of the Signature Performance in the TCGA Dataset

Based on the median risk score, the samples were classified to high- and low-risk groups. The scatter plot showed that

mortality increased with a higher risk score (**Figure 3A**). Furthermore, the heatmap showed that the expression level of AF064858.8, RP11-22L13.1, USP30-AS1 and AC114271.2 were higher in the high-risk group, whereas MIR181A1HG, RP11-544A12.4 and MIR133A1HG were at lower expressed levels (**Figure 3B**). Moreover, Kaplan–Meier curve analyses indicated that the low-risk group had prolonged OS (**Figure 3C**). In addition, the AUC values for the 1-year, 2-year, and 3-year OS were 0.74, 0.765 and 0.702, respectively (**Figure 3D**), suggesting the high predictive capacity of the signature in the training dataset.

To further validate the predictive capacity of the signature, we used the same algorithm to calculate the risk scores both in the testing dataset and the overall dataset. The risk score distribution plot, scatter plot, and heatmaps were consistent with those in the training dataset. Furthermore, Kaplan–Meier curve analyses showed the consistent results in the testing dataset and overall dataset ($p < 0.001$). In addition, the time-ROC curves and their AUC values also displayed good performance for predicting prognosis. The AUCs for 1-year, 2-year and 3-year OS in the testing dataset were 0.798, 0.813 and 0.784, and in the overall dataset, the AUCs were 0.748, 0.778 and 0.719, respectively.

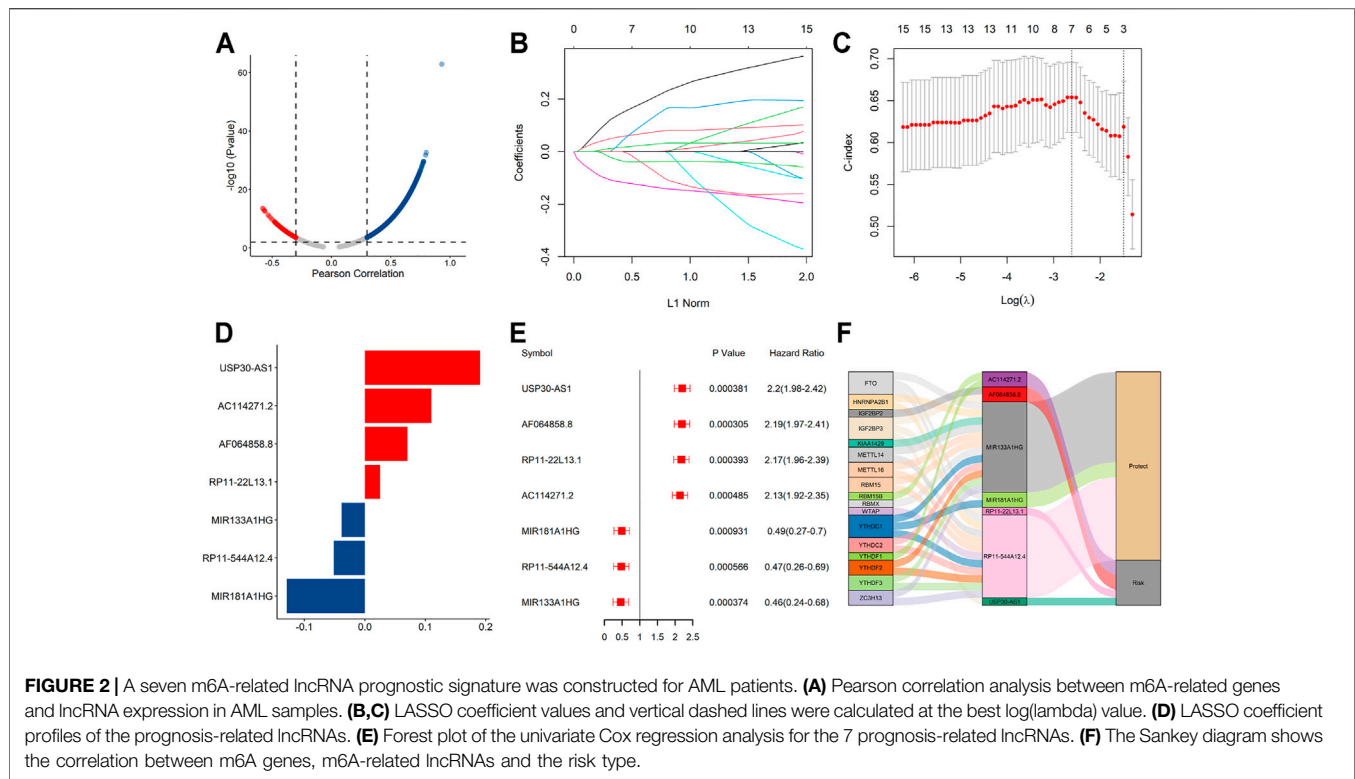


(Figure 4). In summary, the high-risk score based on the signature could indicate a poor prognosis, accurately.

Stratification Analyses of the Signature With Clinicopathological Characteristics

A stratified analysis was carried out according to the clinicopathological characteristics, including age (<60/ ≥ 60 years, **Figures 5A,B**), sex (female/male, **Figures 5C,D**), abnormalities (normal/abnormal, **Figures 5E,F**), chromosomal FLT3 mutations (no/yes, **Figures 5G,H**), IDH1 mutations (no/yes, **Figures 5I,J**), NPM1 mutations (no/yes, **Figure 5K,L**), and RAS mutations (no/yes, **Figures 5M,N**). Kaplan–Meier curve analyses revealed that high-risk group had worse survival outcome than low-risk group when stratified by the different clinical features, except for IDH1, NPM1 or RAS mutations.

Independent Prognostic and Clinicopathological Correlation Analyses

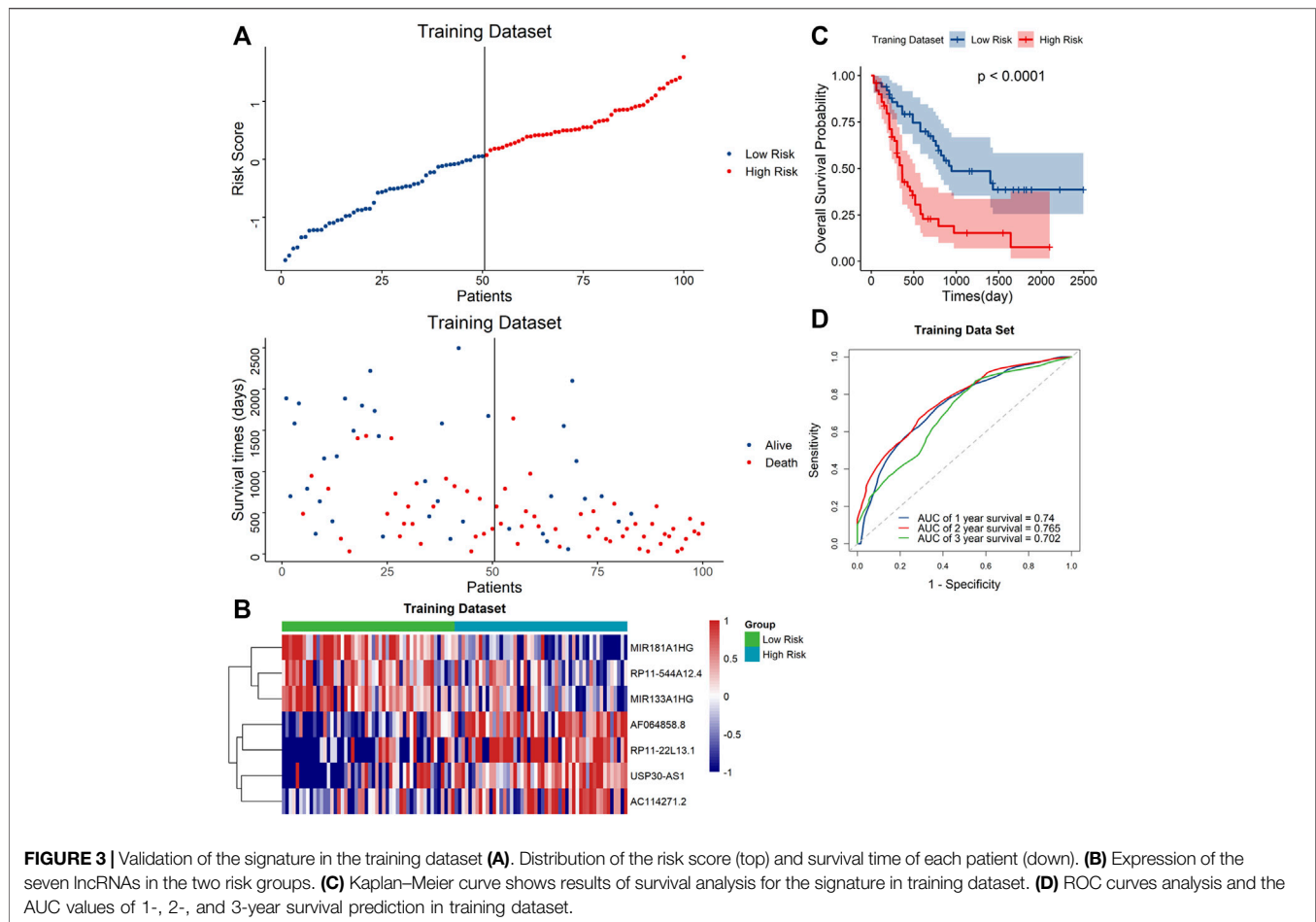
Univariate and stepwise multivariate Cox regression analyses were applied to explore whether the m6A-related lncRNAs signature and clinical characteristics, such as age, sex, cytogenic abnormalities, FLT3 mutation, IDH1 mutation, NPM1 mutation and RAS mutation, may serve as independent prognostic factors. Finally, age and risk score were selected as independent prognostic factors for the survival prediction (**Figures 6A,B**). Next, to quantitatively predict the survival probability of each case, a prognostic nomogram incorporating the clinical features and the signature was plotted (**Figure 6C**).

Furthermore, calibration curves of 1-year, 2-year, and 3-year OS were plotted to confirm the predictive probability of the nomogram. The results showed that the predicted survival probability by the nomogram was consistent to the actual one (**Figures 6D–F**). Moreover, time-dependent ROC curves revealed that the nomogram showed remarkable accuracy to predict 1-, 2- and 3-year OS (AUC = 0.769, 0.82, and 0.8, respectively) (**Figure 6G**). In addition, the decision curve analysis of the LNM nomogram showed that even if the threshold probability of the patient is very small, the use of the LNM nomogram in predicting LNM brings more benefit than treating either all or no patients (**Figure 6H**). Above all, this signature displayed good performance in predicting the survival of AML.

Validation of the Expression Levels of Seven m6A-Related lncRNAs in AML Samples

Besides, Kaplan–Meier curve analyses were used to evaluate the prognostic role of each gene from the signature, and the results showed that higher expression levels of USP30-AS1, AC114271.2, AF064858.8 and RP11-22L13.1, and lower expression levels of MIR181A1HG, RP11-544A12.4 and MIR133A1HG were associated with poorer survival outcomes (**Supplementary Figure S1**).

To further demonstrate the feasibility of the prognostic signature and measure the potential in clinical practice, we performed qRT-PCR assays in our collected bone marrow samples. Our results showed that seven of the m6A-related lncRNAs could be easily detected both in AML patients and healthy controls. And, the expression levels of these lncRNAs



were relatively higher in AML patients than healthy controls. It is worthy of note, compared with samples at first diagnosis, the detrimental factors of USP30-AS1, AC114271.2, AF064858.8 and RP11-22L13.1 were upregulated, and the protective factors of MIR181A1HG, RP11-544A12.4 and MIR133A1HG exhibited a decreased tendency in first relapsed AML patients (Figure 7). Generally speaking, the relapsed AML patients always encounter therapy resistance, resulting in poor survival outcomes, which consistent with our experimental validation in AML samples.

Cellular Biological Effects Related to the Signature

t-distributed stochastic neighborhood embedding (t-SNE) was used to investigate the differences between the low-risk and high-risk groups. The results obtained based on entire genes, 21 m6A genes and 7 m6A-related lncRNAs showed that the distributions were relatively scattered (Figures 8A–C). However, the result obtained based on the signature showed that the two risk groups have different distributions, which suggested that the prognostic signature can easily distinguish the low-risk and high-risk groups (Figure 8D).

In view of the excellent predictive capacity of this signature, we further investigated the biological effect related to the molecular

heterogeneity. We first identified 1,186 DEGs between the two risk groups. And the DEGs were primarily enriched in the following terms, including cellular defense response, mononuclear cell differentiation, chemokine-mediated signaling pathway and positive regulation of T cell activation (GO Biological Processes) (Figure 8E). Antigen processing and presentation, cytokine-cytokine receptor interaction, intestinal immune network for IgA production as well as Th1 and Th2 cell differentiation (KEGG Pathway) (Figure 8F). GSEA showed several tumor hallmarks were enriched in the high-risk group, such as interferon γ response, HEME metabolism, allograft rejection, interferon α response, complement, myogenesis, inflammatory response, KRAS signaling up, TNF α signaling via NF- κ B and so on (Supplementary Figure S2). Above all, these evidences indicated that the signature is correlated with immune cell-related biological pathways and may be associated with the immune microenvironment in AML.

Correlation of the Signature and Immunotherapy Response

We subsequently evaluated the immunotherapy response in patients with different risk scores. The analysis indicated that the low-risk group had a higher response rate than the high-risk

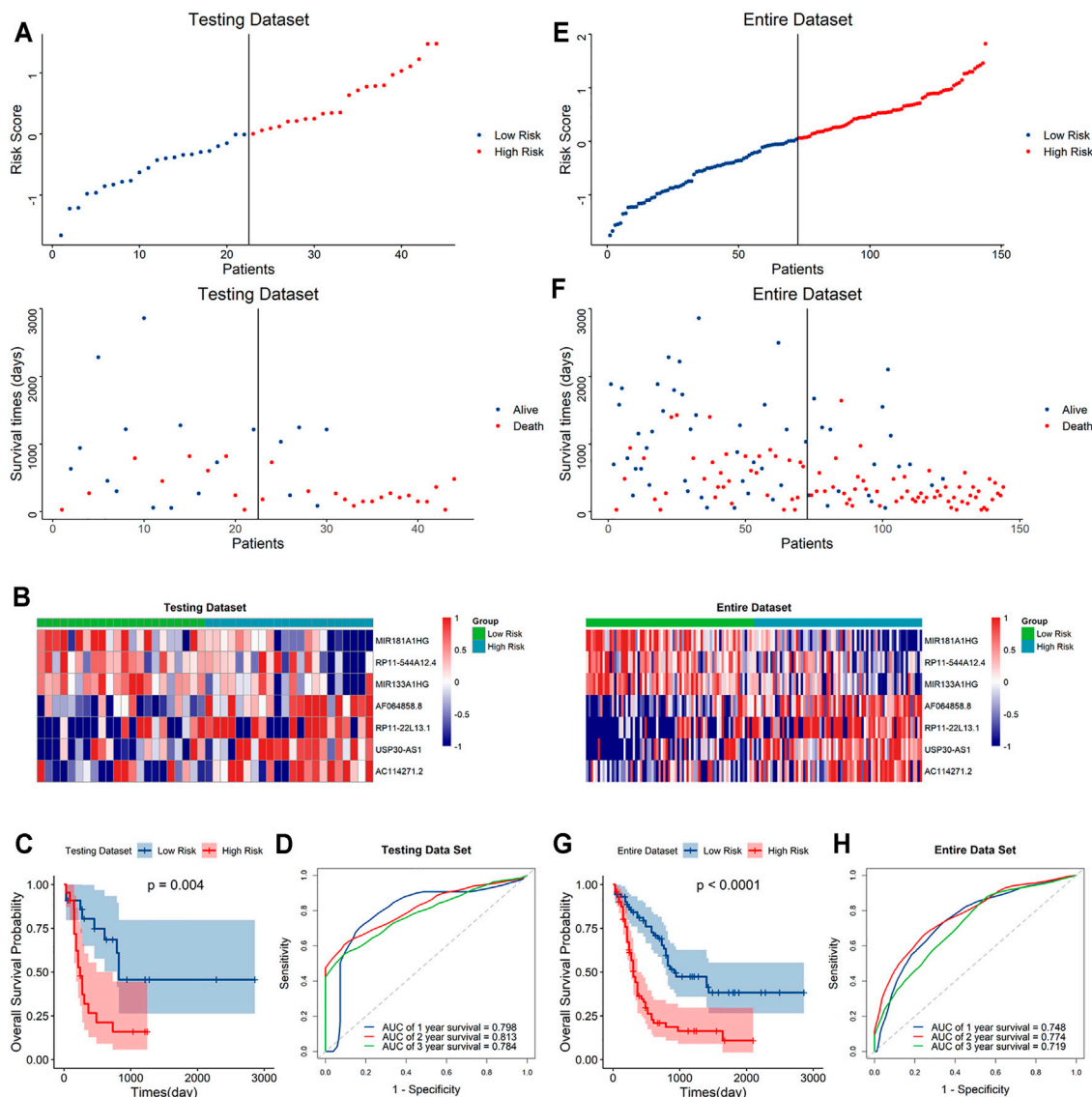


FIGURE 4 | Evaluation of the signature in the testing and whole datasets (A,E). Distribution of the risk score (top) and survival time of each patient (bottom) in the testing dataset (A) and whole dataset (E). (B,F) Expression of the seven lncRNAs in the high- and low-risk groups in the testing dataset (B) and whole dataset (F). (C,G) Kaplan-Meier curve analysis of the signature in the testing dataset (C) and whole datasets (G). (D,H) ROC curves and their AUC values showed 1-, 2-, and 3-year predictions in the testing set (D) and whole dataset (H).

group ($p < 0.05$) (Figure 9A), and the risk scores in the no-response group were higher than those in the response group (Figure 9B). These results suggested that the signature might serve as a good tool to evaluate the immunotherapy response in AML.

Construction of the ceRNA Network and Functional Enrichment Analysis

lncRNAs can regulate the expression of downstream mRNAs by combining shared miRNAs as ceRNAs (Tay et al., 2014). Therefore, a ceRNA network was constructed to view the potential roles of the m6A-related lncRNAs in AML. A total

of 9 lncRNAs, 10 microRNAs and 271 mRNAs were used to construct the network (Figure 10A). Two significant modules, dominated by FOS and NOTCH1 nodes, were identified from the PPI network, and 10 hub genes were extracted (Figure 10B). Moreover, the functional enrichment analysis with 271 target mRNAs showed that the target genes were enriched in regulation of protein serine/threonine kinase activity, protein autophosphorylation, positive regulation of catabolic process, response to transforming growth factor β and epithelial cell proliferation and migration (GO Biological Processes, Figure 10C). MAPK, PI3K-Akt, Rap1, Ras, TGF- β , Estrogen, FoxO signaling pathway, and microRNA in cancer (KEGG Pathway, Figure 10D). The results showed other m6A-related

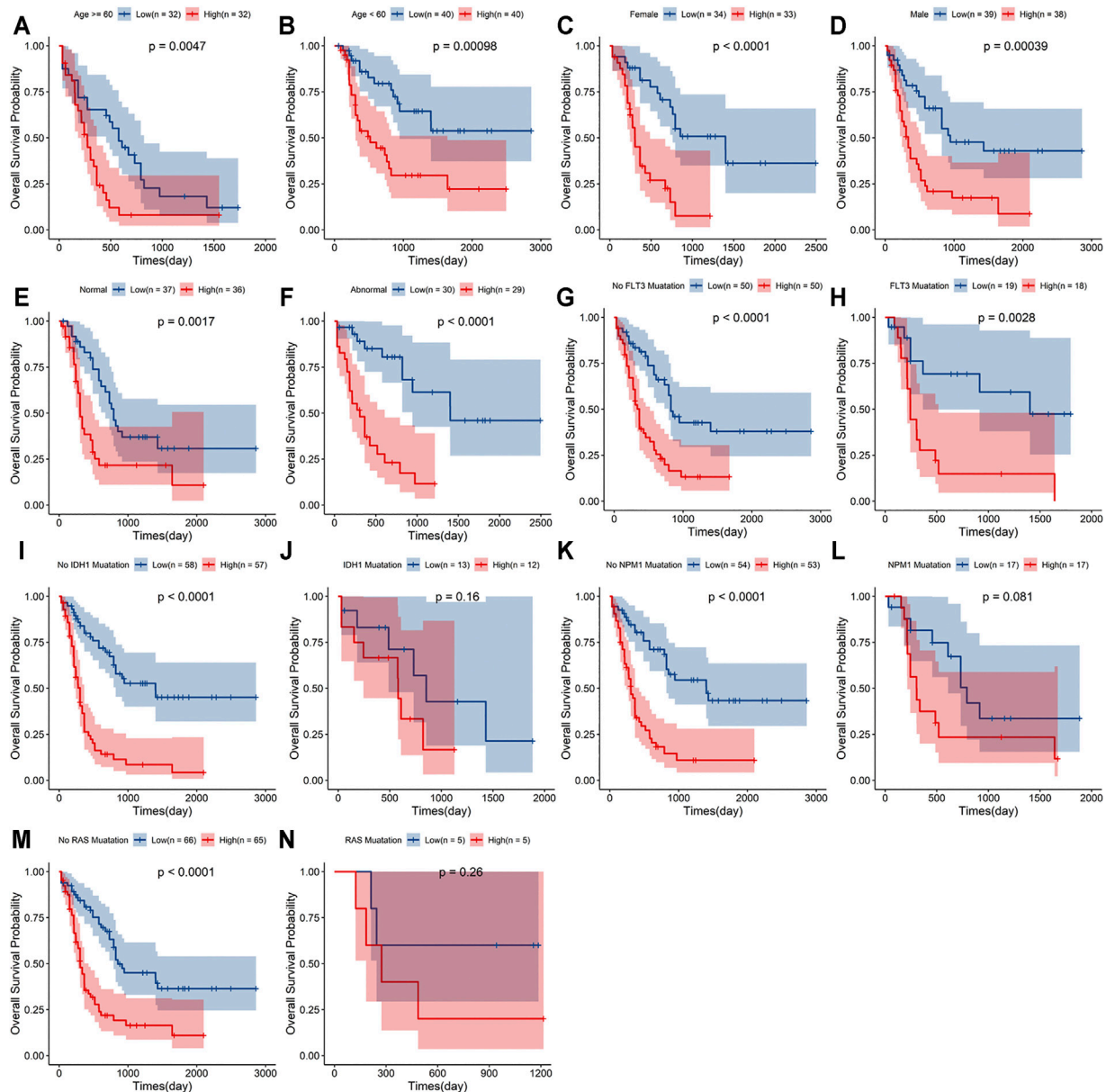


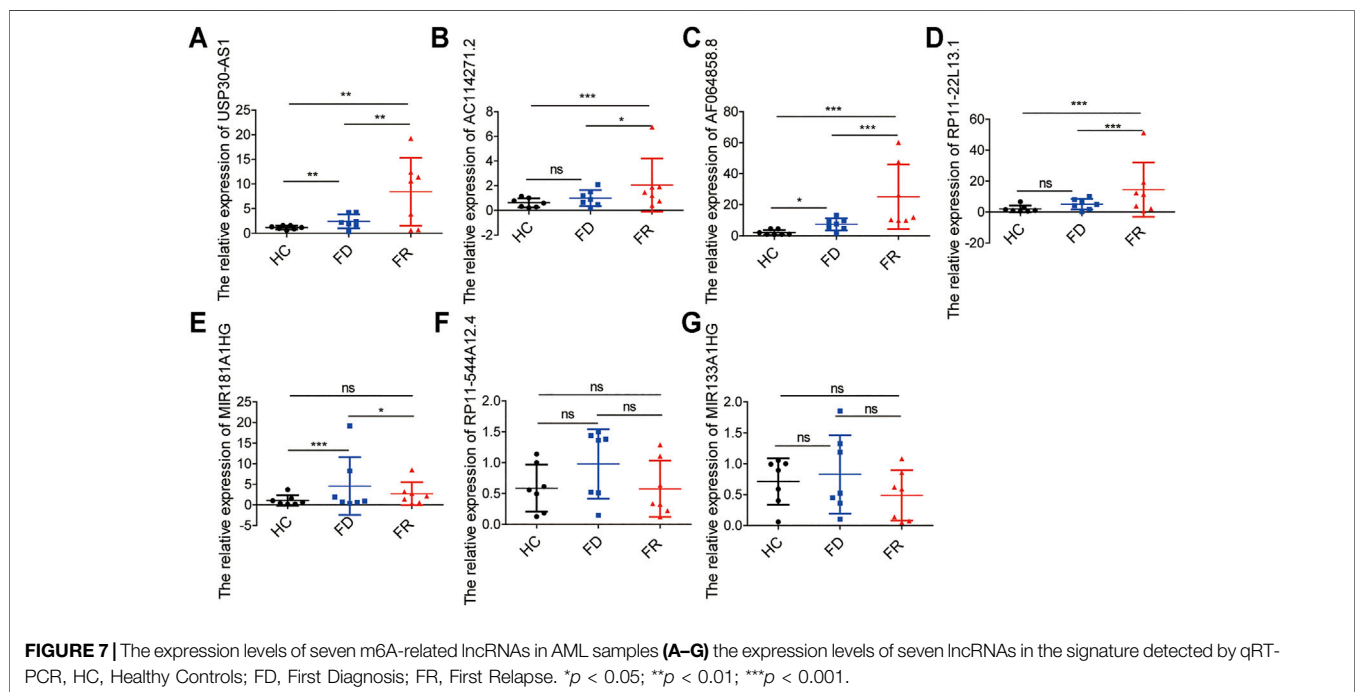
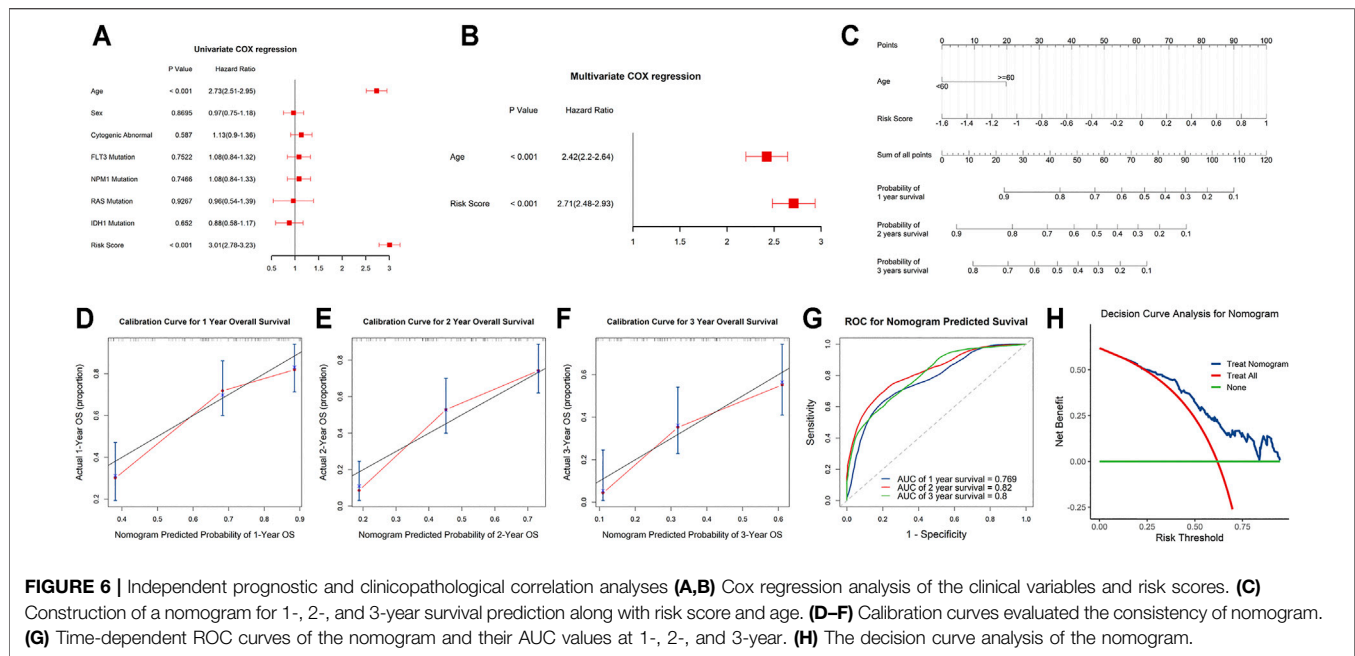
FIGURE 5 | Stratification analyses of the signature based on prognosis-related clinicopathological characteristics. The survival outcomes of the patients stratified according to age (A,B), sex (C,D), chromosomal abnormalities (E,F), FLT3 mutations (G,H), IDH1 mutations (I,J), NPM1 mutations (K,L) and RAS mutations (M,N) in the two risk groups.

lncRNAs also play critical roles during tumor progression, and provide new insights to study the potential roles and mechanism of m6A-related lncRNAs in AML.

DISCUSSION

To the best of our knowledge, AML is a deadly disease associated with poor outcomes despite advancements in targeted molecular and immunotherapy (Short et al., 2018). The m6A is the most abundant epigenetic modification of mRNA and lncRNAs and

plays important roles in many biological processes (Wei et al., 2017). The lncRNAs do not possess protein coding ability but participate in a plethora of cellular functions (Ponting et al., 2009; Morlando and Fatica, 2018). The m6A modifications of lncRNAs are associated with the development, occurrence, and prognosis of a variety of tumors and other diseases, including AML (Coker et al., 2019), lncRNAs can also affect tumor invasive progression by targeting m6A regulators as competitive endogenous RNAs (ceRNAs) (Tu et al., 2020). Both m6A and lncRNAs are important regulators of AML (Zimta et al., 2019; Zheng and Gong, 2021). However, the potential roles of m6A-related

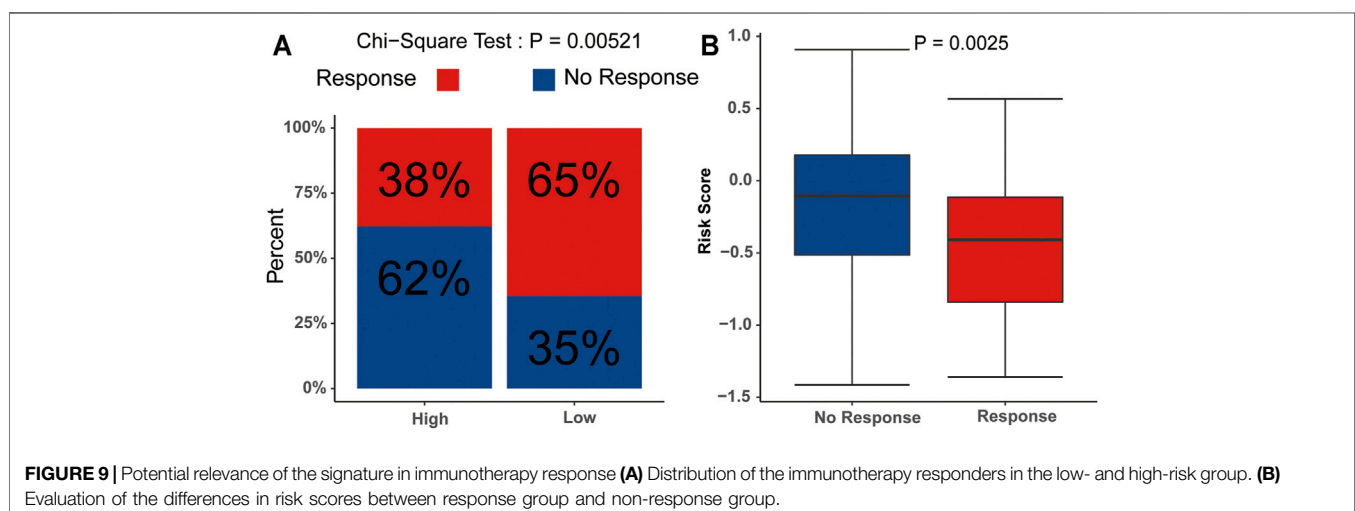
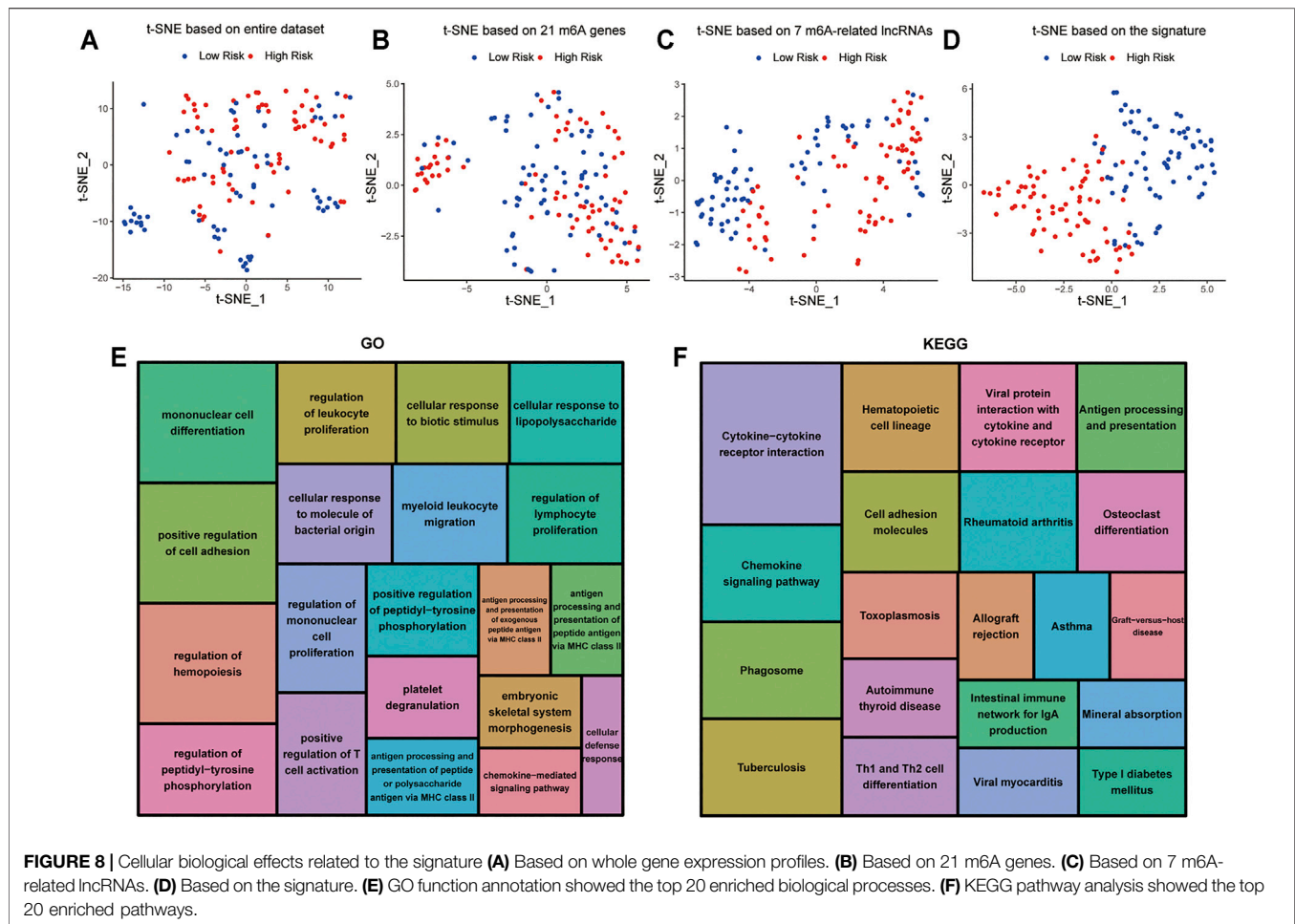


lncRNAs in AML remains unclear. Thus, based on the data from the TCGA dataset, we developed a novel m6A-related lncRNAs signature to accurately predict the prognoses in AML.

A total of 144 AML samples were included to explore the prognostic value of m6A-related lncRNAs. Seven of 15 m6A-related lncRNAs with prognostic value were used to establish a signature to predict the OS of AML patients. The high-risk group was significantly associated with a poor prognosis. Furthermore,

multivariate Cox regression analysis illustrated that the signature acts as an independent prognostic factor in AML, which was consistent with the results of ROC curve analysis.

Among the lncRNAs in the prognostic signature, USP30-AS1 has been reported to be related to autophagy and immunity in bladder cancer (Wan et al., 2021), cervical cancer (Chen et al., 2020) and melanoma (Ding et al., 2021). MIR133A1HG was also reported to be one of the lncRNAs in the autophagy-related



signature for AML (Zhao et al., 2021). However, the underlying molecular biological mechanism has not been elucidated. Notably, AC114271.2, AF064858.8, RP11-22L13.1, RP11-544A12.4 and MIR181A1HG were revealed for the first time.

The correlation analysis revealed that two of seven lncRNAs, MIR133A1HG and RP11-544A12.4, have significant correlation with the expression of almost all m6A regulators, and that MIR181A1HG, AC114271.2 and USP30-AS1 were related to

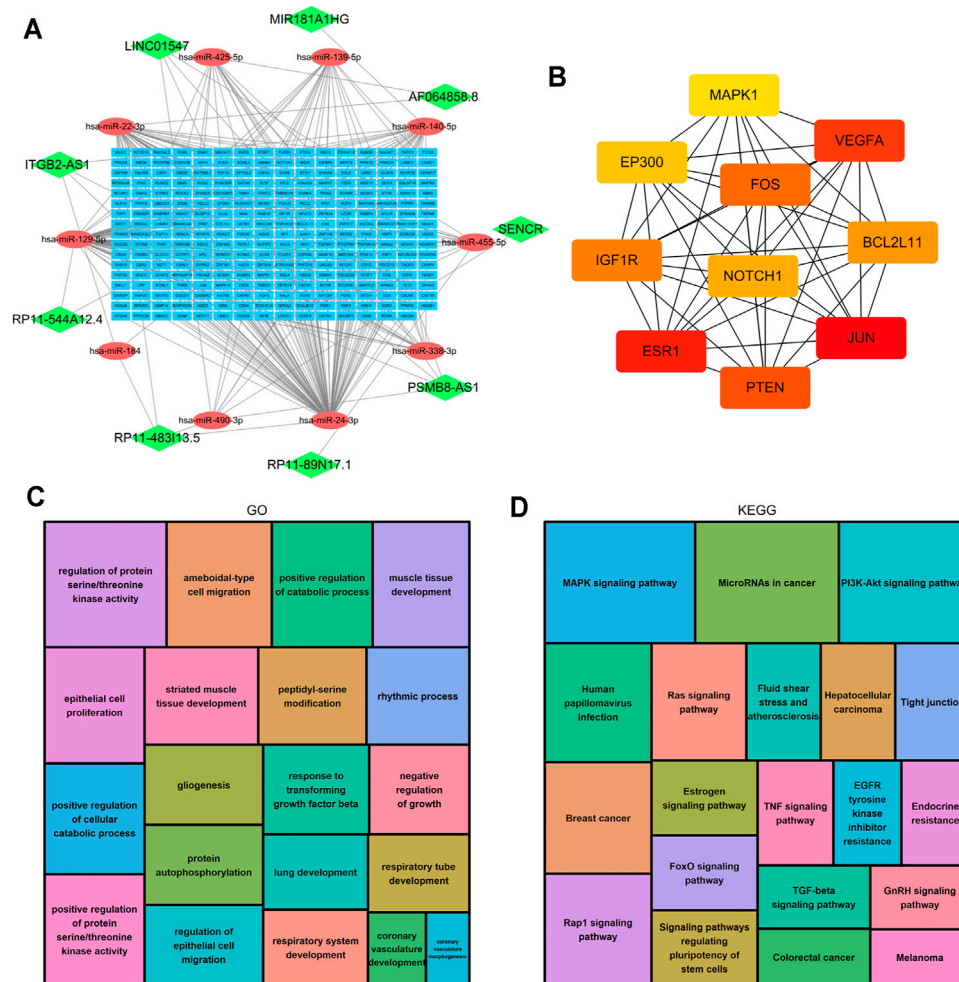


FIGURE 10 | Construction of the ceRNA network and functional enrichment analysis. **(A)** The ceRNA network of lncRNAs (green diamonds), target miRNAs (red circles) and mRNAs (blue rectangles). **(B)** 10 hub genes were extracted from the PPI network. **(C)** GO functional annotation showed the top 20 enriched biological processes. **(D)** KEGG pathway analysis showed the top 20 enriched pathways.

some m6A regulators, including m6A writers, erasers, and readers. Furthermore, AF064858.8 is related to some m6A RNA writers and readers, while RP11-22L13.1 is related to m6A RNA readers IGF2BP2 and IGF2BP3. However, the specific mechanism on how lncRNA regulates m6A remains to be further studied (**Supplementary Figure S3**). The results of the pan-cancer analysis showed that USP30-AS1, AF064858.8, MIR133A1HG, RP11-544A12.4 and MIR181A1HG were specifically expressed in AML, which indicated that these lncRNAs play a crucial role in its carcinogenesis (**Supplementary Figures S4, S5**).

GO and KEGG revealed that cancer hallmark-related and malignancy-related pathways were more enriched in the high-risk group. In addition, we found that T cell activation was also enriched, indicating that m6A-related lncRNAs may affect the prognosis of patients through immune mechanisms, which is consistent with the results of the previous studies (Xu et al., 2021; Zhang et al., 2021). The infiltrating immune cells in the

tumor microenvironment (TME), particularly T cells, are key mediators of tumor destruction and play important roles in immunotherapy (Lei et al., 2020). m6A has been reported to regulate the maturation and neoantigen presentation involved in the immunotherapeutic response (Li et al., 2021). Nevertheless, the potential function and prognostic value of m6A-related lncRNAs in mediating immunotherapeutic response and prognosis in AML remain to be characterized. The TIDE prediction score is a successfully validated computational framework for immunotherapy prediction (Jiang et al., 2018). Correspondingly, the TIDE algorithm was also performed to predict the correlation between the risk score and the immunotherapeutic response, the results indicated that risk scores of the no-response group were higher than those of the response group. Obviously, this signature was significantly correlated with immunity and a potential biomarker for predicting the response to immunotherapy in AML.

Seven of the 15 m6A-related lncRNAs with prognostic value were used to construct the prognostic signature. This does not necessarily mean that these 7 lncRNAs are more important than other m6A-related lncRNAs; rather, it indicates that the combination of these 7 m6A-related lncRNAs can adequately predict AML prognosis. The results of the ceRNA network and functional enrichment analysis showed that other m6A-related lncRNAs (SENCR, PSMB8-AS1, ITGB2-AS1, RP11-89N17.1, RP11-483I13.5 and LINC01547) also play critical roles during tumor progression by regulating the expression of important genes such as PTEN, VEGFA, MAPK1, IGF1, etc. These genes may provide us with new therapeutic targets for AML patients.

In conclusion, we first constructed a 7 m6A-related lncRNA risk signature to predict the prognosis of AML and verified the predictive reliability and sensitivity of the signature. We also explored the distinct molecular landscape classified by the signature, including biological processes, pathways, correlation with immune therapies, potential targets, and provided new insights into the potential roles and mechanisms of m6A-related lncRNAs in AML.

However, our study has several limitations. First, we used the data from the public dataset TCGA to construct and validate the signature. There was no suitable external database on AML to assess the reliability of the signature. Additionally, functional analyses and mechanistic studies of the signature were not carried out.

DATA AVAILABILITY STATEMENT

The datasets presented in this study can be found in online repositories. The names of the repository/repositories and accession number(s) can be found in the article/Supplementary Material.

ETHICS STATEMENT

The studies involving human participants were reviewed and approved by the Medical Ethics Committee of The Affiliated Cancer Hospital of Zhengzhou University. The patients/participants provided their written informed consent to participate in this study. Written informed consent was

obtained from the individual(s) for the publication of any potentially identifiable images or data included in this article.

AUTHOR CONTRIBUTIONS

WZ, XW, and DL conceived and designed the study. DL, JL, CC, WG, SL, WS, ZS, YB, and YZ participated in the coordination of data acquisition and data analysis and reviewed the manuscript.

FUNDING

This study was supported by the Henan Provincial Science and Technology Research Project (202102310157), Medical Science and Technology Research Plan (Joint Construction) Project of Henan Province (LHGJ20190676).

ACKNOWLEDGMENTS

We are grateful to the contributors to the public databases used in this study.

SUPPLEMENTARY MATERIAL

The Supplementary Material for this article can be found online at: <https://www.frontiersin.org/articles/10.3389/fcell.2021.770451/full#supplementary-material>

Supplementary Figure S1 | Kaplan–Meier survival curves for the 7 signature lncRNAs in AML.

Supplementary Figure S2 | The most pronounced differential biological processes between the high- and low-risk groups explored by GSEA.

Supplementary Figure S3 | The correlation analysis between seven lncRNAs and 21 m6A genes.

Supplementary Figure S4 | The expressions of 7 signature lncRNAs in pan-cancer from TCGA.

Supplementary Figure S5 | The expressions of 7 signature lncRNAs in AML and normal tissues analyzed by GEPIA.

Supplementary Table S1 | The clinical characteristics for AML cases.

Supplementary Table S2 | Primer sequences for qRT-PCR.

REFERENCES

- Cao, G., Li, H.-B., Yin, Z., and Flavell, R. A. (2016). Recent Advances in Dynamic m6A RNA Modification. *Open Biol.* 6 (4), 160003. doi:10.1098/rsob.160003
- Chandra Gupta, S., and Nandan Tripathi, Y. (2017). Potential of Long Non-coding RNAs in Cancer Patients: From Biomarkers to Therapeutic Targets. *Int. J. Cancer* 140 (9), 1955–1967. doi:10.1002/ijc.30546
- Chen, L., Hu, N., Wang, C., and Zhao, H. (2020a). HOTAIRM1 Knockdown Enhances Cytarabine-Induced Cytotoxicity by Suppression of Glycolysis through the Wnt/ β -Catenin/PFKF Pathway in Acute Myeloid Leukemia Cells. *Arch. Biochem. Biophys.* 680, 108244. doi:10.1016/j.abb.2019.108244
- Chen, P., Gao, Y., Ouyang, S., Wei, L., Zhou, M., You, H., et al. (2020b). A Prognostic Model Based on Immune-Related Long Non-coding RNAs for

- Patients with Cervical Cancer. *Front. Pharmacol.* 11, 585255. doi:10.3389/fphar.2020.585255
- Chen, Y., Lin, Y., Shu, Y., He, J., and Gao, W. (2020c). Interaction between N6-Methyladenosine (m6A) Modification and Noncoding RNAs in Cancer. *Mol. Cancer* 19 (1), 94. doi:10.1186/s12943-020-01207-4
- Choi, W., Heo, M. Y., Kim, S. Y., Wee, J.-H., Kim, Y.-H., and Min, J. (2020). Encapsulation of Daunorubicin into *Saccharomyces Cerevisiae*-Derived Lysosome as Drug Delivery Vehicles for Acute Myeloid Leukemia (AML) Treatment. *J. Biotechnol.* 308, 118–123. doi:10.1016/j.jbiotec.2019.12.008
- Coker, H., Wei, G., and Brockdorff, N. (2019). m6A Modification of Non-coding RNA and the Control of Mammalian Gene Expression. *Biochim. Biophys. Acta (Bba) - Gene Regul. Mech.* 1862 (3), 310–318. doi:10.1016/j.bbagr.2018.12.002
- Cui, C., Wang, Y., Gong, W., He, H., Zhang, H., Shi, W., et al. (2021). Long Non-coding RNA LINC00152 Regulates Self-Renewal of Leukemia Stem Cells and

- Induces Chemo-Resistance in Acute Myeloid Leukemia. *Front. Oncol.* 11, 694021. doi:10.3389/fonc.2021.694021
- Dai, D., Wang, H., Zhu, L., Jin, H., and Wang, X. (2018). N6-methyladenosine Links RNA Metabolism to Cancer Progression. *Cell Death Dis.* 9 (2), 124. doi:10.1038/s41419-017-0129-x
- Deng, X., Su, R., Weng, H., Huang, H., Li, Z., and Chen, J. (2018). RNA N6-Methyladenosine Modification in Cancers: Current Status and Perspectives. *Cell Res.* 28 (5), 507–517. doi:10.1038/s41422-018-0034-6
- Ding, Y., Li, T., Li, M., Tayier, T., Zhang, M., Chen, L., et al. (2021). A Novel Autophagy-Related lncRNA Gene Signature to Improve the Prognosis of Patients with Melanoma. *Biomed. Res. Int.* 2021, 1–12. doi:10.1155/2021/8848227
- Fernando, T. R., Contreras, J. R., Zampini, M., Rodriguez-Malave, N. I., Alberti, M. O., Anguiano, J., et al. (2017). The lncRNA CASC15 Regulates SOX4 Expression in RUNX1-Rearranged Acute Leukemia. *Mol. Cancer* 16 (1), 126. doi:10.1186/s12943-017-0692-x
- Gibb, E. A., Brown, C. J., and Lam, W. L. (2011). The Functional Role of Long Non-coding RNA in Human Carcinomas. *Mol. Cancer* 10, 38. doi:10.1186/1476-4598-10-38
- Groff, A. F., Sanchez-Gomez, D. B., Sorucu, M. M. L., Gerhardinger, C., Barutcu, A. R., Li, E., et al. (2016). *In Vivo* Characterization of Linc-P21 Reveals Functional Cis -Regulatory DNA Elements. *Cel Rep.* 16 (8), 2178–2186. doi:10.1016/j.celrep.2016.07.050
- Huang, Y., Su, R., Sheng, Y., Dong, L., Dong, Z., Xu, H., et al. (2019). Small-Molecule Targeting of Oncogenic FTO Demethylase in Acute Myeloid Leukemia. *Cancer Cell* 35 (4), 677–691. e610. doi:10.1016/j.ccell.2019.03.006
- Jiang, P., Gu, S., Pan, D., Fu, J., Sahu, A., Hu, X., et al. (2018). Signatures of T Cell Dysfunction and Exclusion Predict Cancer Immunotherapy Response. *Nat. Med.* 24 (10), 1550–1558. doi:10.1038/s41591-018-0136-1
- Koenig, K., and Mims, A. (2020). Relapsed or Primary Refractory AML. *Curr. Opin. Hematol.* 27 (2), 108–114. doi:10.1097/MOH.0000000000000561
- Lei, X., Lei, Y., Li, J.-K., Du, W.-X., Li, R.-G., Yang, J., et al. (2020). Immune Cells within the Tumor Microenvironment: Biological Functions and Roles in Cancer Immunotherapy. *Cancer Lett.* 470, 126–133. doi:10.1016/j.canlet.2019.11.009
- Li, J., Wang, M., and Chen, X. (2020). Long Non-coding RNA UCA1 Modulates Cell Proliferation and Apoptosis by Regulating miR-296-3p/Myc axis in Acute Myeloid Leukemia. *Cell Cycle* 19 (12), 1454–1465. doi:10.1080/15384101.2020.1750814
- Li, M., Zha, X., and Wang, S. (2021). The Role of N6-Methyladenosine mRNA in the Tumor Microenvironment. *Biochim. Biophys. Acta (Bba) - Rev. Cancer* 1875 (2), 188522. doi:10.1016/j.bbcan.2021.188522
- Long, Y., Wang, X., Youmans, D. T., and Cech, T. R. (2017). How Do lncRNAs Regulate Transcription? *Sci. Adv.* 3 (9), eaao2110. doi:10.1126/sciadv.aao2110
- Morlando, M., and Fatica, A. (2018). Alteration of Epigenetic Regulation by Long Noncoding RNAs in Cancer. *Ijms* 19 (2), 570. doi:10.3390/ijms19020570
- Paris, J., Morgan, M., Campos, J., Spencer, G. J., Shmakova, A., Ivanova, I., et al. (2019). Targeting the RNA m6A Reader YTHDF2 Selectively Compromises Cancer Stem Cells in Acute Myeloid Leukemia. *Cell Stem Cell* 25 (1), 137–148. e136. doi:10.1016/j.stem.2019.03.021
- Ponting, C. P., Oliver, P. L., and Reik, W. (2009). Evolution and Functions of Long Noncoding RNAs. *Cell* 136 (4), 629–641. doi:10.1016/j.cell.2009.02.006
- Shen, C., Sheng, Y., Zhu, A. C., Robinson, S., Jiang, X., Dong, L., et al. (2020). RNA Demethylase ALKBH5 Selectively Promotes Tumorigenesis and Cancer Stem Cell Self-Renewal in Acute Myeloid Leukemia. *Cell Stem Cell* 27 (1), 64–80. e69. doi:10.1016/j.stem.2020.04.009
- Short, N. J., Rytting, M. E., and Cortes, J. E. (2018). Acute Myeloid Leukaemia. *The Lancet* 392 (10147), 593–606. doi:10.1016/S0140-6736(18)31041-9
- Tay, Y., Rinn, J., and Pandolfi, P. P. (2014). The Multilayered Complexity of ceRNA Crosstalk and Competition. *Nature* 505 (7483), 344–352. doi:10.1038/nature12986
- Tu, Z., Wu, L., Wang, P., Hu, Q., Tao, C., Li, K., et al. (2020). N6-Methyladenosine-Related lncRNAs Are Potential Biomarkers for Predicting the Overall Survival of Lower-Grade Glioma Patients. *Front. Cel Dev. Biol.* 8, 642. doi:10.3389/fcell.2020.00642
- Vu, L. P., Pickering, B. F., Cheng, Y., Zaccara, S., Nguyen, D., Minuesa, G., et al. (2017). The N6-Methyladenosine (m6A)-Forming Enzyme METTL3 Controls Myeloid Differentiation of normal Hematopoietic and Leukemia Cells. *Nat. Med.* 23 (11), 1369–1376. doi:10.1038/nm.4416
- Wan, J., Guo, C., Fang, H., Xu, Z., Hu, Y., and Luo, Y. (2021). Autophagy-Related Long Non-coding RNA Is a Prognostic Indicator for Bladder Cancer. *Front. Oncol.* 11, 647236. doi:10.3389/fonc.2021.647236
- Wei, W., Ji, X., Guo, X., and Ji, S. (2017). Regulatory Role of N6-Methyladenosine (m6A) Methylation in RNA Processing and Human Diseases. *J. Cel. Biochem.* 118 (9), 2534–2543. doi:10.1002/jcb.25967
- Weng, H., Huang, H., Wu, H., Qin, X., Zhao, B. S., Dong, L., et al. (2018). METTL14 Inhibits Hematopoietic Stem/Progenitor Differentiation and Promotes Leukemogenesis via mRNA m6A Modification. *Cell Stem Cell* 22 (2), 191–205. e199. doi:10.1016/j.stem.2017.11.016
- Xu, F., Huang, X., Li, Y., Chen, Y., and Lin, L. (2021). m6A-related lncRNAs Are Potential Biomarkers for Predicting Prognoses and Immune Responses in Patients with LUAD. *Mol. Ther. - Nucleic Acids* 24, 780–791. doi:10.1016/j.omtn.2021.04.003
- Yu, G., Wang, L.-G., Han, Y., and He, Q.-Y. (2012). clusterProfiler: an R Package for Comparing Biological Themes Among Gene Clusters. *OMICS: A J. Integr. Biol.* 16 (5), 284–287. doi:10.1089/omi.2011.0118
- Zhang, P., Liu, G., and Lu, L. (2021). N6-Methyladenosine-Related lncRNA Signature Is a Novel Biomarkers of Prognosis and Immune Response in Colon Adenocarcinoma Patients. *Front. Cel Dev. Biol.* 9, 703629. doi:10.3389/fcell.2021.703629
- Zhang, T.-j., Zhou, J.-d., Zhang, W., Lin, J., Ma, J.-c., Wen, X.-m., et al. (2018). H19 Overexpression Promotes Leukemogenesis and Predicts Unfavorable Prognosis in Acute Myeloid Leukemia. *Clin. Epigenet* 10, 47. doi:10.1186/s13148-018-0486-z
- Zhao, C., Wang, Y., Tu, F., Zhao, S., Ye, X., Liu, J., et al. (2021). A Prognostic Autophagy-Related Long Non-coding RNA (ARlncRNA) Signature in Acute Myeloid Leukemia (AML). *Front. Genet.* 12, 681867. doi:10.3389/fgene.2021.681867
- Zheng, X., and Gong, Y. (2021). Functions of RNA N6-Methyladenosine Modification in Acute Myeloid Leukemia. *Biomark Res.* 9 (1), 36. doi:10.1186/s40364-021-00293-w
- Zimta, A.-A., Tomuleasa, C., Sahnoune, I., Calin, G. A., and Berindan-Neagoe, I. (2019). Long Non-coding RNAs in Myeloid Malignancies. *Front. Oncol.* 9, 1048. doi:10.3389/fonc.2019.01048

Conflict of Interest: The authors declare that the research was conducted in the absence of any commercial or financial relationships that could be construed as a potential conflict of interest.

Publisher's Note: All claims expressed in this article are solely those of the authors and do not necessarily represent those of their affiliated organizations, or those of the publisher, the editors and the reviewers. Any product that may be evaluated in this article, or claim that may be made by its manufacturer, is not guaranteed or endorsed by the publisher.

Copyright © 2021 Li, Liang, Cheng, Guo, Li, Song, Song, Bai, Zhang, Wu and Zhang. This is an open-access article distributed under the terms of the Creative Commons Attribution License (CC BY). The use, distribution or reproduction in other forums is permitted, provided the original author(s) and the copyright owner(s) are credited and that the original publication in this journal is cited, in accordance with accepted academic practice. No use, distribution or reproduction is permitted which does not comply with these terms.



Identification of m⁶A Regulator-Associated Methylation Modification Clusters and Immune Profiles in Melanoma

Fengying Du^{1,2,3†}, Han Li^{4†}, Yan Li^{5†}, Yang Liu^{2,3†}, Xinyu Li⁶, Ningning Dang⁷, Qingqing Chu⁸, Jianjun Yan⁹, Zhen Fang¹⁰, Hao Wu^{2,3}, Zihao Zhang^{2,3}, Xingyu Zhu³ and Xiaokang Li^{1*}

¹Department of Dermatology, Central Hospital Affiliated to Shandong First Medical University, Jinan, China, ²Department of Gastroenterological Surgery, Shandong Provincial Hospital, Cheeloo College of Medicine, Shandong University, Jinan, China, ³Medical Science and Technology Innovation Center, Shandong First Medical University and Shandong Academy of Medical Sciences, Jinan, China, ⁴Department of Gastroenterological Surgery, The First Affiliated Hospital of Shandong First Medical University, Jinan, China, ⁵Department of Respiratory and Critical care, Shandong public health clinical center, Jinan, China, ⁶Department of Oncology, Shandong Provincial Hospital Affiliated to Shandong First Medical University, Jinan, China, ⁷Department of Dermatology, Shandong Provincial Hospital Affiliated to Shandong First Medical University, Jinan, China, ⁸Outpatient of Podiatric Rehabilitation, Maternity and Child Health Care of Zaozhuang, Zaozhuang, China, ⁹Department of Dermatology, Qilu Hospital, Shandong University, Jinan, China, ¹⁰Department of General Surgery, Xuanwu Hospital, Capital Medical University, Beijing, China

OPEN ACCESS

Edited by:

Yicheng Long,
Cornell University, United States

Reviewed by:

Cai Chen,
Merck (United States), United States
Xueqian Zhuang,
Memorial Sloan Kettering Cancer
Center, United States
Mingqiang Wang,
Stanford University, United States

*Correspondence:

Xiaokang Li
silukangkang@163.com

[†]These authors have contributed
equally to this work

Specialty section:

This article was submitted to
Epigenomics and Epigenetics,
a section of the journal
Frontiers in Cell and Developmental
Biology

Received: 19 August 2021

Accepted: 25 October 2021

Published: 21 December 2021

Citation:

Du F, Li H, Li Y, Liu Y, Li X, Dang N,
Chu Q, Yan J, Fang Z, Wu H, Zhang Z,
Zhu X and Li X (2021) Identification of
m⁶A Regulator-Associated
Methylation Modification Clusters and
Immune Profiles in Melanoma.
Front. Cell Dev. Biol. 9:761134.
doi: 10.3389/fcell.2021.761134

RNA N6-methyladenosine (m⁶A) modification in tumorigenesis and progression has been highlighted and discovered in recent years. However, the molecular and clinical implications of m⁶A modification in melanoma tumor microenvironment (TME) and immune infiltration remain largely unknown. Here, we utilized consensus molecular clustering with nonnegative matrix factorization based on the melanoma transcriptomic profiles of 23 m⁶A regulators to determine the m⁶A modification clusters and m⁶A-related gene signature. Three distinct m⁶A modification patterns (m⁶A-C1, C2, and C3), which are characterized by specific m⁶A regulator expression, survival outcomes, and biological pathways, were identified in more than 1,000 melanoma samples. The immune profile analyses showed that these three m⁶A modification subtypes were highly consistent with the three known immune phenotypes: immune-desert (C1), immune-excluded (C2), and immune-inflamed (C3). Tumor digital cytometry (CIBERSORT, ssGSEA) algorithm revealed an upregulated infiltration of CD8⁺ T cell and NK cell in m⁶A-C3 subtype. An m⁶A scoring scheme calculated by principal component of m⁶A signatures stratified melanoma patients into high- and low-m⁶sig score subgroups; a high score was significantly associated with prolonged survival and enhanced immune infiltration. Furthermore, fewer somatic copy number alternations (SCNA) and PD-L1 expression were found in patients with high m⁶sig score. In addition, patients with high m⁶sig score demonstrated marked immune responses and durable clinical benefits in two independent immunotherapy cohorts. Overall, this study indicated that m⁶A modification is involved in melanoma tumor microenvironment immune regulation and contributes to formation of tumor immunogenicity. Comprehensive evaluation of the m⁶A modification pattern of individual tumors will provide more insights into molecular mechanisms of TME characterization and promote more effective personalized biotherapy strategies.

Keywords: skin cutaneous melanoma, methylation of N6 adenosine modification, tumor microenvironment, immune profiles, immunotherapy

INTRODUCTION

Methylation of N6 adenosine (m⁶A) is a revisable RNA modification process that is widely present in various types of common RNAs, such as mRNAs, lncRNAs, and miRNAs, and essential for a variety of physiological processes and disease progression (Zhao et al., 2017; Zaccara et al., 2019). The m⁶A modification is manipulated by three regulatory proteins, methyltransferases (“writers”), demethylases (“erasers”), and binding proteins (“reader”), and this modification process is dynamic and reversible (He et al., 2019). Increasing evidence has identified the important roles m6A modifications play in various cellular processes and in cancer progression through regulating RNA stability, mRNA splicing and translation, and microRNA processing (Li et al., 2019; Chen et al., 2020a). Meanwhile, a large number of studies have shown that the process of tumor development and abnormal immune regulation of the body are associated with abnormal expression of m⁶A-modified regulatory proteins (Chen et al., 2019a; Shulman and Stern-Ginossar, 2020; Wang et al., 2020). Therefore, systematic and comprehensive explanation of tumor heterogeneity brought about by genetic variation and epigenetic regulation will facilitate the development and advancement of new therapeutic technologies based on RNA methylation (Martínez-Riaño et al., 2019).

Malignant melanoma is a highly metastatic cancer caused by abnormal transformation of pigment cells and melanocytes resulting from prolonged exposure to ultraviolet radiation (Mazurkiewicz et al., 2021). Since melanoma is curable in its initial stages, early diagnosis of this disease is crucial (Eddy and Chen, 2020). Global data show that patients with melanoma who develop metastases have a 5-years survival rate of only 25% due to the difficulty of treatment (Eddy and Chen, 2020). Multiple novel targeted therapies targeting melanoma-specific markers have been developed in recent years; however, most patients often show lower effectiveness or shorter duration to these treatments (Mazurkiewicz et al., 2021). Among the multiple factors that influence treatment outcome, the tumor microenvironment might account for a major cause in the melanoma progression. The composition of the microenvironment in melanoma is relatively complex, which includes adventitial cells (keratin-forming cells, cancer-associated fibroblasts CAF, adipocytes and infiltrating immune cells), extracellular matrix components, and tumor-specific physicochemical properties (Mazurkiewicz et al., 2021). With the increased understanding of the tumor microenvironment, the key immune cell subsets in tumorigenesis and metastasis were also gradually recognized. The evaluation of immune infiltration based on the characteristics of TME was supposed as a key technique to infer the pre-existing antitumor immunity and predict patient response to immune checkpoint inhibitor therapy (Binnewies et al., 2018; Galon and Bruni, 2019; Li et al., 2020a). Recently, the new concept of “immune context” on tumor, which classifies the TME characteristics of melanoma into three categories, i.e., hot, excluded, and cold, also implies three

different types of effective treatment options (Hegde et al., 2016; Chen and Mellman, 2017). In summary, systematic and comprehensive dissection of the components of the tumor microenvironment of melanoma and thus identification of the corresponding tumor immune phenotype is a feasible and reliable means to guide immunotherapy and predict the effectiveness of immunotherapy (Mariathasan et al., 2018; Pagès et al., 2018).

Recent studies suggest an association between TME immune cell infiltration and m⁶A modification; however, this does not appear to be fully explained by RNA degradation mechanisms (Zhao et al., 2017; Chen et al., 2019a; He et al., 2019). It has been reported that YTHDF1 can promote lysozyme in dendritic cells to regulate the degradation of tumor neoantigens, and the key to this process is that YTHDF1 can accurately recognize the m⁶A modification process of tumor neoantigens and enhance their translation level (Han et al., 2019). When YTHDF1 is absent in dendritic cells, this leads to enhanced cross-presentation of antigens and enhanced cross-stimulation of CD8⁺ T cells. FTO has been reported to be associated with cytotoxic effects in colon cells by inhibiting YTHDF2-mediated RNA decay, which in turn promotes PD-1, CXCR4, and SOX10, and suppresses interferon-gamma (IFN- γ) expression (Yang et al., 2019). This result was confirmed in an *in vitro* experiment. When FTO is knocked down exogenously, IFN- γ is substantially upregulated, which in turn makes colon cancer mice sensitive to anti-PD-1 drug treatment. METTL3, which also regulates mRNA m⁶A modifications, regulates the dynamic balance of CD40, CD80, and Snail (Lewinska et al., 2017; Wang et al., 2019). Unfortunately, due to the unsophisticated nature of the current technology, the studies mentioned are all on one or two m⁶A regulatory molecules, and the antitumor effects produced by these regulatory molecules are not the contribution of one or several molecules, but rather they work together to regulate the m⁶A modification process in the body and thus affect cancer development and metastasis. Fortunately, the explosive growth on transcriptomics and genomics sequencing database provides a rich resource for a comprehensive and integrated analysis of the role of m⁶A-related molecules in cancer and immune regulation (Finotello and Trajanoski, 2018; Chen et al., 2020b). Thus, deepening our understanding of cancer immunity and developing new targets for cancer immunotherapy requires a systematic and comprehensive dissection of the TME immune cell infiltration profile regulated by m⁶A-related molecules.

In this study, we integrated the transcriptome and genome sequencing data from 1,020 melanoma samples across TCGA and GEO databases, and systematically analyzed and discovered the direct and specific association between m⁶A modification patterns and TME immune cell infiltration features in melanoma. Using non-negative matrix factorization (NMF) clustering analysis, we identified three novel m⁶A modification patterns with TME features highly consistent with three previously reported immune phenotypes: immune inflammatory, immune rejection, and immune desert

phenotypes (Chen and Mellman, 2017). Not only that, we quantified the m⁶A modification clusters of individualized tumors in the form of scores, which can be used to predict the effectiveness of patients to ICI therapy. Our findings suggest that m⁶A modifications play a crucial role in tumor immune microenvironment signature formation and melanoma treatment planning.

MATERIALS AND METHODS

Collect and Preprocess of Publicly Attainable Expression Datasets

Gene expression data and clinical information for melanoma patient samples were obtained from the GEO database (<https://www.ncbi.nlm.nih.gov/geo/>) and TCGA database (<https://portal.gdc.cancer.gov/>), which are publicly and freely available. We screened the melanoma dataset and eventually included a total of 1,020 patients in the study for subsequent analysis, including the GSE19234, GSE22154, GSE50509, GSE59455, GSE65904, GSE22153, GSE54437, and TCGA-SCKM datasets. For data pre-processing, we downloaded the “CEL” files from the GEO database, relying on the “affy” and “simpleaffy” R packages for background correction and normalization, while the RNA sequencing data from the TCGA database is downloaded in normalized FPKM format and then converted to transcripts per kilobase million (TPM) format. With reference to previous experience, the “ComBat” method of the “sva” R package was used to reduce the batch effect between different datasets, which was mainly a problem for datasets from the GEO database (Dai et al., 2018). Both somatic mutation data and copy number variation data of TCGA-SCKM were curated from the UCSC Xena database and Davoli et al. (Davoli et al., 2017). The copy number variation of 23 m⁶A regulators in human chromosomes was mapped by the “RCircos” R package. For non-synonymous mutations such as frameshift mutations, inflammatory mutations, missense mutations, nonsense mutations, and splice site mutations, numbers represent the tumor mutational load (TML). **Supplementary Table S1** presents the clinical information of the samples from the *meta*-GEO and TCGA-SKCM databases.

Nonnegative Matrix Factorization Clustering Analysis of 23 m⁶A Regulators

A literature review of m⁶A methylation modifications revealed that there are now 23 recognized m⁶A regulators, which constitute the modification pattern of m⁶A methylation (Zhao et al., 2017; Chen et al., 2019a; He et al., 2019; Zaccara et al., 2019). Specifically, eight writers include CBLL1, KIAA1429, METTL14, METTL3, RBM15, RBM15B, WTAP, and ZC3H13; two erasers include ALKBH5 and FTO; 13 readers include ELAVL1, FMR1, HNRNPA2B1, HNRNPC, IGF2BP1, IGF2BP2, IGF2BP3, LRPPRC, YTHDC1, YTHDC2, YTHDF1, YTHDF2, and YTHDF3; and 23 of them shared the key task of m⁶A methylation modification. Using non-negative matrix decomposition (NMF), we performed a clustering analysis of the 23 m⁶A regulators based on their expression, which could identify different types of m⁶A modification patterns. The expression

matrix *A* of the 23 m⁶A regulators was first split into non-negative matrices *W* and *H*, as $A \approx WH$, and then the matrix *A* was subjected to repeated factorization, and finally the output data was summarized, which gave the clustering results of the melanoma samples. It is crucial to consider factors such as covariance, dispersion, and silhouette coefficient to determine the optimal number of clustering groups. The “NMF” R package to perform the clustering analysis used the “brunet” and “200 nruns” algorithms.

Functional Analysis and Annotation

The Hallmarker gene set (Subramanian et al., 2005) and Mariathasan et al. (Mariathasan et al., 2018) constructed gene set were used as well-defined biometric backgrounds for gene set variation analysis (GSVA) with “GSVA” R package (Hänzelmann et al., 2013), which was designed to explore the variation in biological processes across different m⁶A modification patterns. In the gene ontology (GO) analysis, we annotated the functions of 23 m⁶A regulators under three entries of cellular component (CC), molecular function (MF), and biological process (BP), which was done using the “clusterProfiler” R package. For GSVA and GO analysis, the cut-off value was set to a false discovery rate (FDR) < 0.01.

Estimation of Immune Cell Infiltration

In quantifying the relative abundance of 28 immune cell types curated by Charoentong et al. in the tumor microenvironment, we refer to recent studies using the single sample gene enrichment analysis (ssGSEA) method, which well marks the specific functional gene panels of each immune cell type (Charoentong et al., 2017; Jia et al., 2018). As in the previous study (Chen et al., 2020a), we expressed the relative abundance of various immune cell types in the form of enrichment scores, and they were normalized to a uniform distribution from 0 to 1. In terms of biosimilarity, infiltrating immune cells were evaluated and acted upon using multidimensional scaling (MDS) and Gaussian fitting models, and moreover, the deconvolution approach CIBERSORT (Newman et al., 2019) (<http://cibersort.stanford.edu/>) was then used to estimate the abundance of 22 different subpopulations of leukocytes, which have melanoma gene expression profiles.

Quantification of Immune Response Predictor

T cell-inflamed gene expression profile (GEP) is a superior predictor of response to anti-PD-1 regimens, which contained IFN- γ -responsive genes related to antigen presentation, cytotoxic activity, and adaptive immune resistance (Ayers et al., 2017). The T cell-inflamed scores were calculated and weighted by averaging of the included genes for the IFN- γ (6-gene) and expanded immune (18-gene) signatures. In modeling different types of tumor immune evasion mechanisms, we drew on the Tumor Immune Dysfunction and Exclusion (TIDE) algorithm proposed by Jiang et al. (Jiang et al., 2018). This algorithm integrates the dysfunction of tumor-infiltrating toxic T lymphocytes (CTLs) and rejection of CTLs by immunosuppressive factors. The higher TIDE score implies greater chance of immune escape of tumor cells and represents a possible poor outcome of treatment with ICIs. The method of Estimation of Stromal and Immune cells in Malignant Tumor tissues using

Expression data (ESTIMATE) (Yoshihara et al., 2013) was adopted to calculate the immune score of tumors, and this algorithm can be better based on transcriptional profiles to estimate the cellularity of the tumor and the purity of the tumor. The level of infiltrating immune and stromal cells is the basis for tumor purity, which is predicted by the immune score of the tumor. In detail, a high immune score of a tumor is an indication of a high infiltration of immune cells in the tumor tissue, or a low tumor purity.

Capture of Significantly Mutated Genes and Tumor Mutation Features

The MutSigCV algorithm was used to identify significantly mutated genes (SMGs) (Lawrence et al., 2013; Chen et al., 2019b), which takes into account the specific background mutation rate in the mutation context before evaluating the significant enrichment of non-resting somatic mutations in a gene. We considered $q < 0.1$ as statistically significant, and these genes needed to be certified in the Cancer Cell Line Encyclopedia of Humans (CCLE) (Ghandi et al., 2019) to be defined as SMGs (Chen et al., 2020c) (**Supplementary Table S2**). The “maftools” R package (Mayakonda et al., 2018) was used to characterize genes in the TCGA-SKCM cohort that underwent m⁶A modification, the mutation details of SMGs, and the capture of mutational features in the genomic data. The ExtractSignatures function based on Bayesian variation non-negative matrix decomposition was used for model construction; specifically, using this function, we split the mutation portrait matrix into two non-negative matrices and noted as “signature” and “contribution,” where “signature” represents the mutation process and “contribution” represents the corresponding mutation activities (Chong et al., 2021a). Better still, the SignatureEnrichment function allows determining the optimal number of extracted mutation features and assigning them appropriately to each sample. For comparison and annotation, using the Catalogue of Somatic Mutations in Cancer (COSMIC) (Kandoth et al., 2013) as a reference, we performed a cosine similarity analysis on the extracted melanoma mutation portraits.

Identify Differentially Expressed Genes Between Different m⁶A Modification Phenotypes

Patients were classified into three clusters of m⁶A modification patterns using a consensus clustering algorithm, and then the “limma” R package (Ritchie et al., 2015) was used to find differentially expressed genes between groups. Voom normalized data were then subjected to “lmFit” and “eBayes” function algorithms, which in turn allowed the calculation of specific data for differential expression. In this process, we set adjusted p -values < 0.001 as statistically significant differences.

Construct the m⁶Sig Score System

Based on principal component analysis (PCA), we constructed an m⁶A score system to quantify the level of m⁶A modifications in specific patients. According to DEGs, they are the intersecting parts of different m⁶A clusters, and we analyzed the prognostic impact of

each gene on melanoma patients with the help of univariate Cox regression models. Deeper feature selection was performed for genes that significantly affect the prognosis of melanoma patients, and this process was computed by the recursive feature elimination (RFE) method of random forest and the 10-fold cross-validation method included in the “caret” R package. Further, we obtained the gene expression profiles based on the above steps, and the principal components 1 and 2 obtained from PCA analysis were the basis of our feature score. The specific formula for this score system is referred to a previous study (Zhang et al., 2020; Chong et al., 2021b), m⁶Sig score = $\sum(\text{PC1i} + \text{PC2i})$.

Collect Genomic and Clinical Information for the ICI Cohort

The gene expression profiles of patients treated with ICI were retrieved in publicly available databases, focusing on matching with clinical information. Ultimately, we included metastatic melanoma treated with PD-1 (nivolumab or pembrolizumab) or PD-1 combined with CTLA-4 (ipilimumab) (Liu et al., 2019), and metastatic urothelial carcinoma (mUC) treated with atezolizumab (anti-PD-L1 mAb) (Mariathasan et al., 2018) in this study. The gene expression profiles of the samples were converted in TPM format.

Statistical Analyses

All statistical analyses in the study were performed with R 3.6.1. Student’s t -test was performed for quantitative data conforming to a normal distribution, and Wilcoxon rank sum test was performed for non-normally distributed data. When more than two sets of analyses were performed, the nonparametric test was the Kruskal-Wallis test, while the parametric test was the analysis of variance (Hazra and Gogtay, 2016). The Fisher exact test was used for the calculation of contingency rates. Kaplan-Meier survival analysis and Cox regression analysis were performed using the “Survminer” package, and the m⁶Sig score subgroup stratum was “survival” package with the surv-cutpoint function completed. “timeROC” package completed the evaluation of the m⁶Sig score model, which plotted the corresponding subject operating characteristic curve (ROC) and calculated the area under the curve (AUC). In analyzing the relationship between patient’s clinical characteristics and the m⁶Sig score system, multivariate regression models were used to adjust for confounding factors in this. $p < 0.05$ was considered as statistical significance, and the Benjamini-Hochberg method was used to perform multiple hypothesis testing for false discovery rate (FDR) (Love et al., 2014).

RESULTS

Mapping Genetic Variants of m⁶A Regulators in Melanoma

In our study, we explored the possible physiological roles of 23 m⁶A methylation-regulated genes in melanoma, including the “writers” CBLL1, KIAA1429, METTL14, METTL3, RBM15, RBM15B, WTAP, and ZC3H13; the “readers” ELAVL1, FMR1, HNRNPA2B1, HNRNPC, IGF2BP1, IGF2BP2, IGF2BP3,

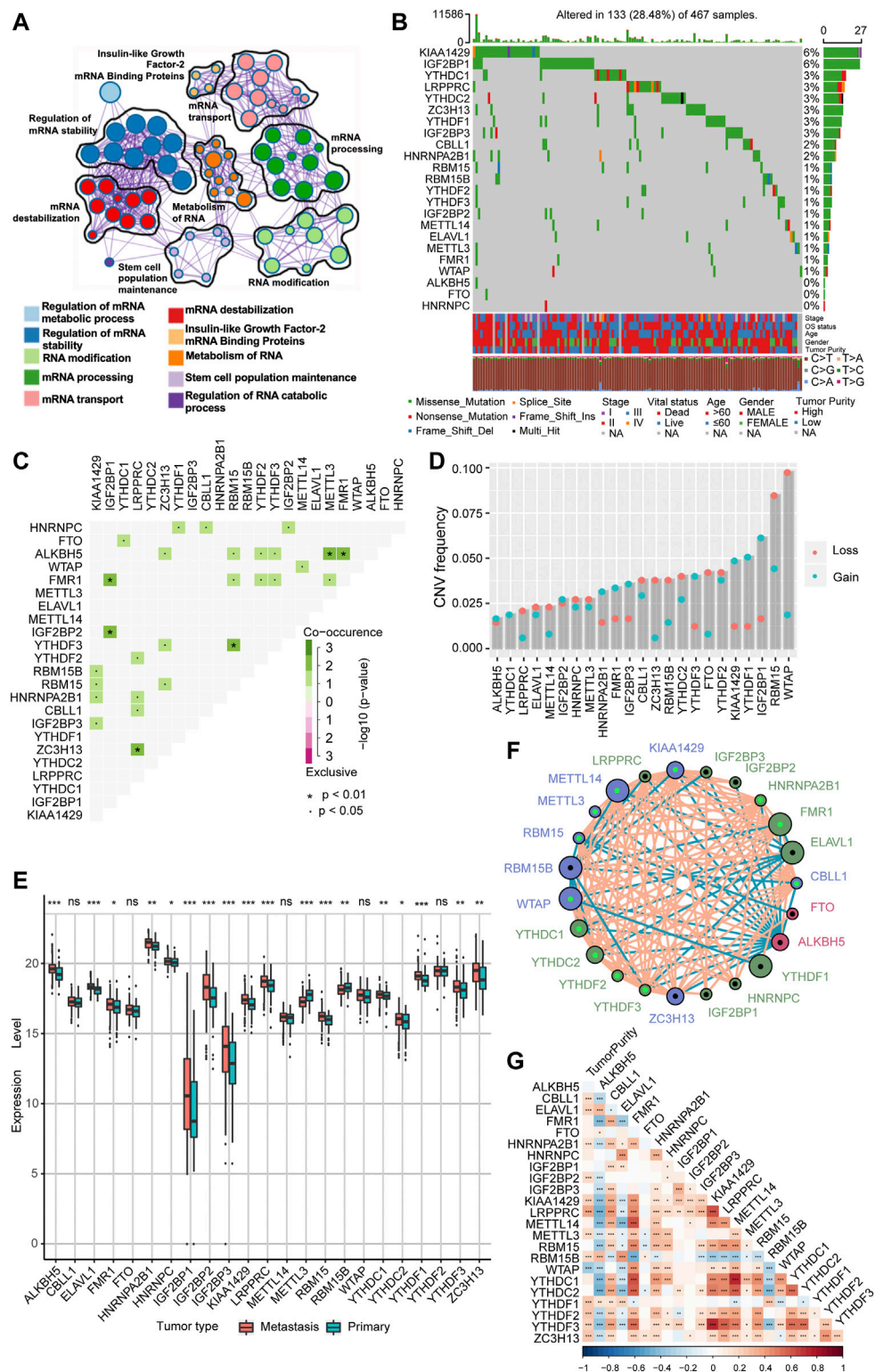


FIGURE 1 | The landscape of genetic alterations of m⁶A regulators in melanoma. **(A)** Visualization of the Metascape enrichment network presenting similarities within and between clusters of terms. The same colors represent the same clustering terms. **(B)** Mutations in 23 m⁶A regulators were present in 133 of 467 melanoma patients (28.48%), with the most prevalent missense mutations, nonsense mutations, and frame shift deletion mutations. The numbers on the right side are representative of the mutation frequency of each regulator. Each column is one patient. **(C)** Visualization of co-occurrence and exclusion of 23 m⁶A regulator mutations. Green color represents co-occurrence, and purple color represents exclusion. **(D)** CNV mutations are present in all 23 m⁶A regulators. Column heights

(Continued)

FIGURE 1 | represent mutation frequencies. Pink dots represent loss mutations, and blue dots represent gain mutations. **(E)** Differential expression of mRNA of 23 m⁶A regulators in metastatic melanoma and primary melanoma. * represents *p*-values in statistics (**p* < 0.05; ***p* < 0.01; ****p* < 0.001). **(F)** Interaction network of the three m⁶A regulators in melanoma. Different colors represent different types of m⁶A regulators; green is a reader, blue is a writer, and red is an eraser. The connecting lines represent the correlation matrix; pink is positive correlation, while blue is negative correlation. Larger circles represent smaller *p*-values for prognostic analysis, and the shiny green dot in the center of the circle represents protective factors, while the black dot represents risk factors. **(G)** Visualization of tumor purity and 23 m⁶A regulator. Red color represents co-occurrence, and blue color represents exclusion.

LRPPRC, YTHDC1, YTHDC2, YTHDF1, YTHDF2, and YTHDF3; and the “erasers” ALKBH5 and FTO. These m⁶A regulators not only recognize, remove, and add m⁶A modification sites but also, as revealed by GO enrichment analysis and Metascape analysis, can actually alter biological processes, such as regulating mRNA stability, RNA modifications, and RNA metabolism (**Figure 1A**). Among 467 melanoma patient samples with genomic sequencing, 133 (28.48%) had somatic mutations in m⁶A regulators, which mainly included missense mutations, nonsense mutations, and code-shifting mutations (**Figure 1B**). KIAA1429 had the highest mutation frequency, followed closely by IGF2BP1, and the next in the gradient were YTHDC1, LRPPRC, YTHDC2, ZC3H13, YTHDF1, and IGF2BP3. Interestingly, IGF2BP1, ZC3H13, and YTHDF1 had only missense mutations in the relatively high mutation frequencies. Analysis of the co-mutation profiles of the 23 m⁶A regulators revealed significant co-mutations between FMR1 and IGF2BP1, IGF2BP2 and IGF2BP1, ZC3H13 and LRPPRC, YTHDF3 and RBM15, ALKBH5 and METTL3, and ALKBH5 and FMR1 (**Figure 1C**). When performing CNV mutation analysis, we concluded that there was widespread CNV amplification in IGF2BP1, YTHDF1, and KIAA1429, while CNV deletion was more widespread in WTAP and RBM15 (**Figure 1D**). Comparing primary melanoma and metastases, we found that ALKBH5, ELAVL1, FMR1, HNRNPA2B1, HNRNPC, IGF2BP1/2/3, KIAA1429, LRPPRC, RBM15, YTHDC1/2, YTHDF1/3, and ZC3H13 were significantly upregulated in metastases, while RBM15B and METTL3 were significantly upregulated in primary melanoma (**Figure 1E**). The expression of m⁶A regulators with aberrant CNV amplification was also upregulated in metastases compared to primary melanoma (ALKBH5, FMR1, HNRNPA2B1, IGF2BP1/2/3, KIAA1429, YTHDC1, YTHDF1/3), and conversely, m⁶A regulators with aberrant CNV deletion were also downregulated (METTL3, RBM15B, YTHDC2), which are obtained by combining **Figure 1D**. The m⁶A regulator network mapped in **Figure 1F** showed the interaction relationships between 23 molecules that are interconnected and influence each other, which further modulates the prognosis of melanoma patients. This implies that there is a complex and well-organized crossover network between the regulators of writers, readers, and erasers, and this network allows the m⁶A modification pattern to further refine and take effect, influencing the development and metastasis of melanoma. Using the Spearman correlation test, we found that there is a mutual regulatory relationship between these m⁶A regulators. Interestingly, ALKBH5 was negatively correlated with most of the m⁶A regulators, while FMR1 and HNRNPA2B1 were positively correlated with most of them (**Supplementary Figure S1A**). We

further analyzed the association between tumor purity and 23 m⁶A modification regulators (**Figure 1G**) and found that most of the m⁶A regulators were positively correlated with tumor cell purity, whereas WTAP has a negative association, suggesting that WTAP was enriched in non-tumor cell components. Forest plots with Cox regression model were employed to speculate the relationship between m⁶A regulators and the prognosis of melanoma patients. We found that samples with high expression of WTAP, FMR1, and METTL14 were associated with improved overall survival, while an opposite tendency was observed in RBM15B and ELAVL1 (**Supplementary Figure S1B**). Taken together, we integrated the genomic and transcriptomic landscapes of m⁶A regulators in melanoma, and noticed the changes in the expression levels and genetic variation of m⁶A regulators driving the development and progression of melanoma.

The m⁶A Methylation Modification Pattern Consisting of 23 m⁶A Regulators Is Associated with Prognosis in Melanoma Patients.

Further, we stratified melanoma samples into three m⁶A modification patterns according to the expression of m⁶A regulators, a process based on consensus clustering analysis of the NMF algorithm (**Supplementary Figure S2A,C**). We named the three clusters as m⁶A-C1, m⁶A-C2, and m⁶A-C3, respectively (**Figure 2A**). The samples of m⁶A-C2 cluster had significantly different from the other two groups with regard to ELAVL1, RBM15B, YTHDF1/2/3, IGF2BP1/2/3, WTAP, METTL3, ZC3H13, RBM15, HNRNPA2B1, CBLL1, and LRPPRC. Besides, YTHDF1, IGF2BP3, METTL3, ZC3H13, and LRPPRC were significantly upregulated in the m⁶A-C1 subtype, WTAP and RBM15 were significantly upregulated in the m⁶A-C3 subtype, while ELAVL1, IGF2BP3, ZC3H13, and LRPPRC were significantly decreased in the m⁶A-C3 subtype. This conclusion was validated in the *meta*-GEO cohort consisting of five datasets, which include GSE19234, GSE22154, GSE50509, GSE59455, and GSE65904 (**Supplementary Figure S2B**). Patients in the m⁶A-C3 cluster have a significant survival advantage than other clusters in both TCGA and *meta*-GEO cohort (log-rank test, TCGA: *p* < 0.0001, **Figure 2B**; *meta*-GEO: *p* = 0.0015, **Figure 2D**). This model remained significant after multivariate Cox proportional risk regression analysis adjusted for clinicopathological factors of age, gender, and stage (TCGA: HR = 0.34 (0.21–0.51), *p* < 0.001; *meta*-GEO: HR = 0.51 (0.35–0.76), *p* < 0.001; **Figures 2C,E**).

Characterization of the Immune Landscape With Three m⁶A Modification Clusters

We performed GSVA analysis against on Hallmarker gene set in an attempt to discover differences in the biological behavior of the

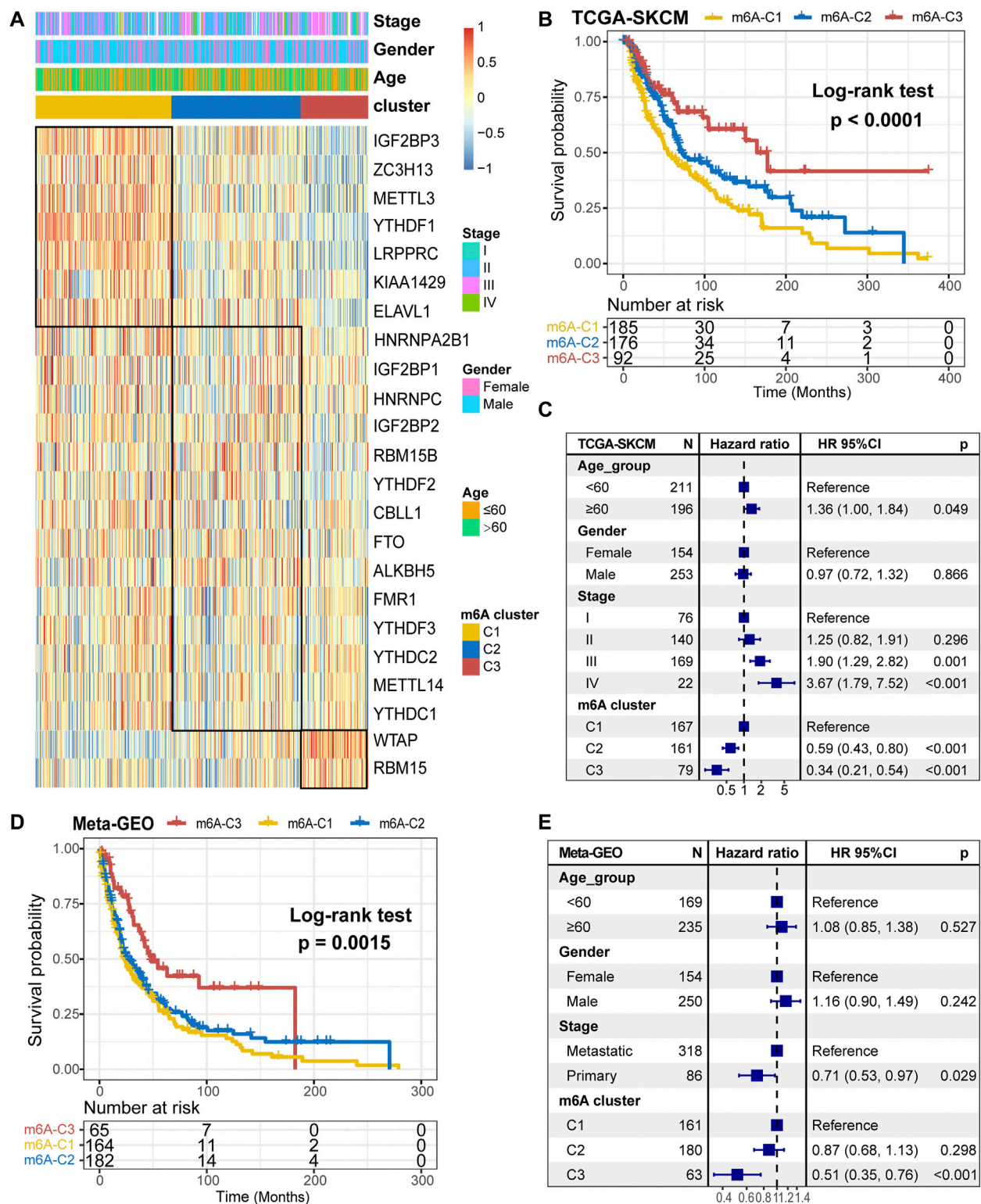


FIGURE 2 | m⁶A methylation modification cluster and unsupervised clustering. **(A)** Results of unsupervised clustering of gene expression of 23 m⁶A moderators in the TCGA-SKCM cohort. **(B)** Kaplan-Meier curves of overall survival (OS) for different m⁶A clusters in the TCGA cohort. **(C)** Subgroup analysis for estimating clinical prognostic value of m⁶A modification subtype after adjusting for age, gender, and stage in the TCGA cohort. **(D)** Kaplan-Meier curves of overall survival (OS) for different m⁶A clusters in the meta-GEO cohort. **(E)** Subgroup analysis for estimating clinical prognostic value of m⁶A modification subtype after adjusting for age, gender, and stage in the meta-GEO cohort.

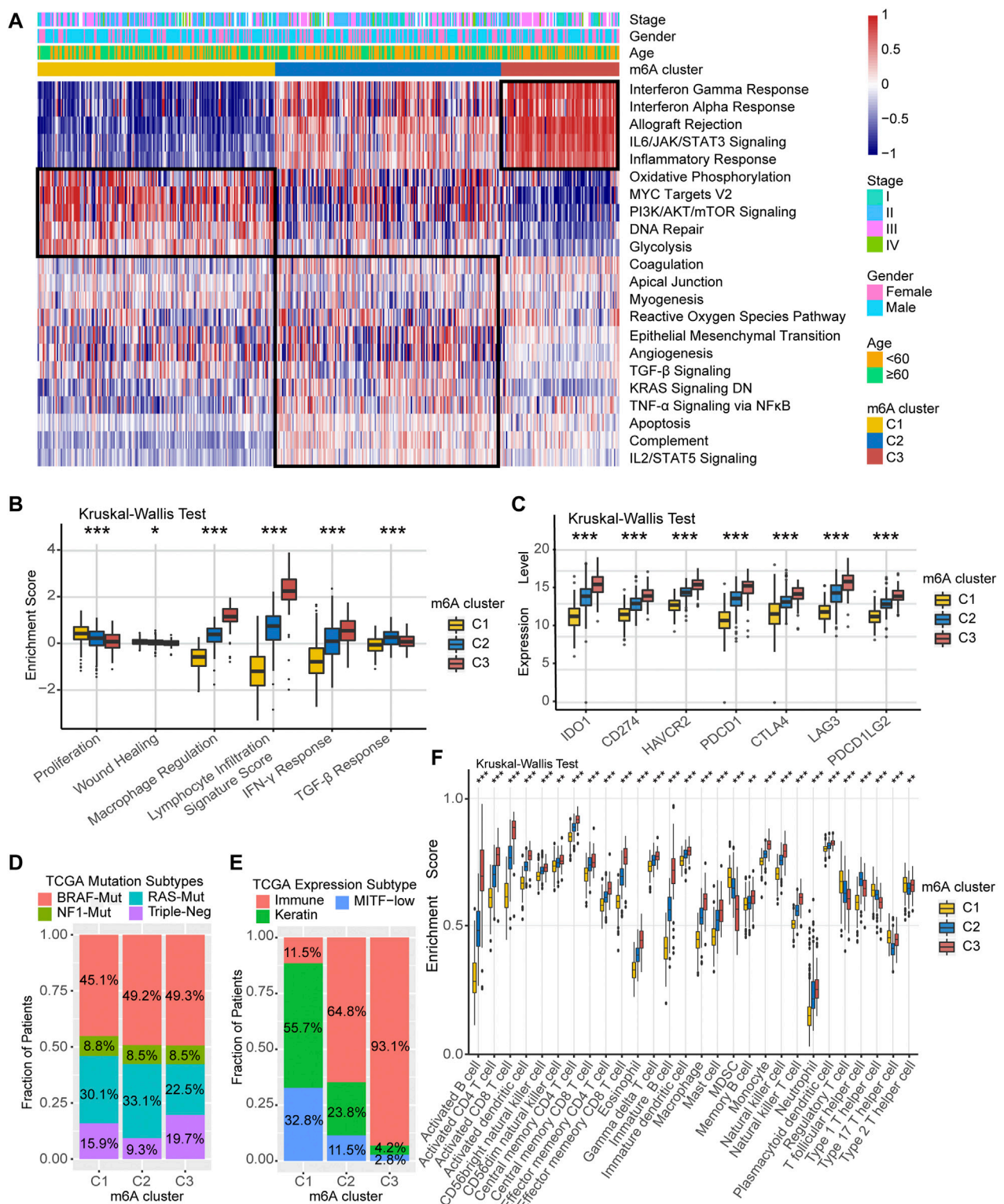


FIGURE 3 | TME characteristics in distinct m⁶A modification clusters. **(A)** Heatmap of enriched pathways based on Hallmark gene set corresponding to different m⁶A modification clusters. **(B)** Relative distribution of six immune subtype in three different m⁶A clusters. **(C)** Expression level of immune checkpoint-related key genes among the three m⁶A clusters. **(D)** Association between TCGA genomic molecular typing and m⁶A clusters. **(E)** Association between TCGA transcriptome molecular typing and m⁶A clusters. **(F)** Relative infiltration level of 28 immune cell subsets among three distinct m⁶A modification clusters.

three m⁶A modification clusters. As shown in **Figure 3A**, m⁶A-C1 cluster was associated with cell proliferation and differentiation and glucose transport, including oxidative phosphorylation, PI3K/AKT/mTOR signaling, DNA repair, and glycolysis. m⁶A-C2 cluster is distinguished by cancer and immune surveillance, involving epithelial mesenchymal transition, TGF- β signal, TNF- α signaling via NF- κ B, and IL2/STAT5 signaling. As for m⁶A-C3, it was significantly enriched in signaling pathways related to inflammation and innate immune response, such as interferon- γ response, interferon- α response, allograft rejection, IL6/JAK/STAT3 signaling, and inflammatory response. The GSVA results further corroborate that these three m⁶A methylation modification clusters are directly related to different molecular mechanism, and m⁶A-C3 was strongly associated with antitumor immunity. In addition, we further evaluated the immune enrichment level of m⁶A methylation modification clusters using the ImmuneScore model constructed by ESTIMATE algorithm. The results showed significant differences in different clusters in both TCGA-SKCM cohort and the *meta*-GEO cohort (**Supplementary Figure S3A,B**). There is a coherence between the immune activation and survival time, which cluster with higher ImmuneScore having greater survival benefit for patients, like m⁶A-C3 in the TCGA-SKCM cohort and *meta*-GEO cohort. Thorsson et al. (Thorsson et al., 2018) divided the tumor immune landscape into six immune subtypes, represented with immune infiltration and stromal activation. Consistent with our findings, the m⁶A-C1 cluster is more inclined to the “Proliferation” and “Wound Healing” subtypes, m⁶A-C2 is highly expressed in “TGF- β Response,” and m⁶A-C3 is mainly dominated by “Lymphocyte Infiltration Signature Score,” “Macrophage Regulation,” and “IFN- γ Response” subtypes (**Figure 3B**). In addition, we performed a comparative analysis of immune checkpoint-related key genes (IDO1, CD274, TIM-3, PDCD1, CTLA-4, LAG3, and PDCD1LG2) among the three clusters. The results indicated the expression levels of seven key genes differ significantly between the three clusters, and the highest expression was all observed in the m⁶A-C3 cluster. TCGA-SKCM has established molecular typing based on the genomic landscape and transcriptomic profile. Although the proportion of m⁶A modification clusters among different mutational-based molecular subtype (BRAF-Mut, RAS-Mut, NF1-Mut, and Triple Negative) were not significant (**Figure 3D**), an obvious difference was found in transcriptomic-based subtype across three m⁶A modification clusters (**Figure 3E**). Samples with TCGA-Immune subtype account for 93.1% of the m⁶A-C3 cluster, followed by 64.8% in m⁶A-C2 subtype. However, the m⁶A-C1 were dominated by TCGA-Keratin (55.7%) and TCGA-MIFT-low (32.8%) subtype, which demonstrated the desert-related immune phenotype in m⁶A-C1. It is feasible to determine immune cell type abundance and expression from bulk tissues with digital cytometry (Newman et al., 2019). We also compared the immune cell infiltration level among the three m⁶A modification clusters in **Figure 3F**. The m⁶A-C1 cluster showed more myeloid-derived suppressor cell (MDSC), regulatory T cells, and T helper cell infiltration, while the m⁶A-C3 cluster exhibited infiltration of most types of T cells, natural killer cells, and dendritic cells. This suggested that the lower survival risk of melanoma patients with m⁶A-C3 clusters

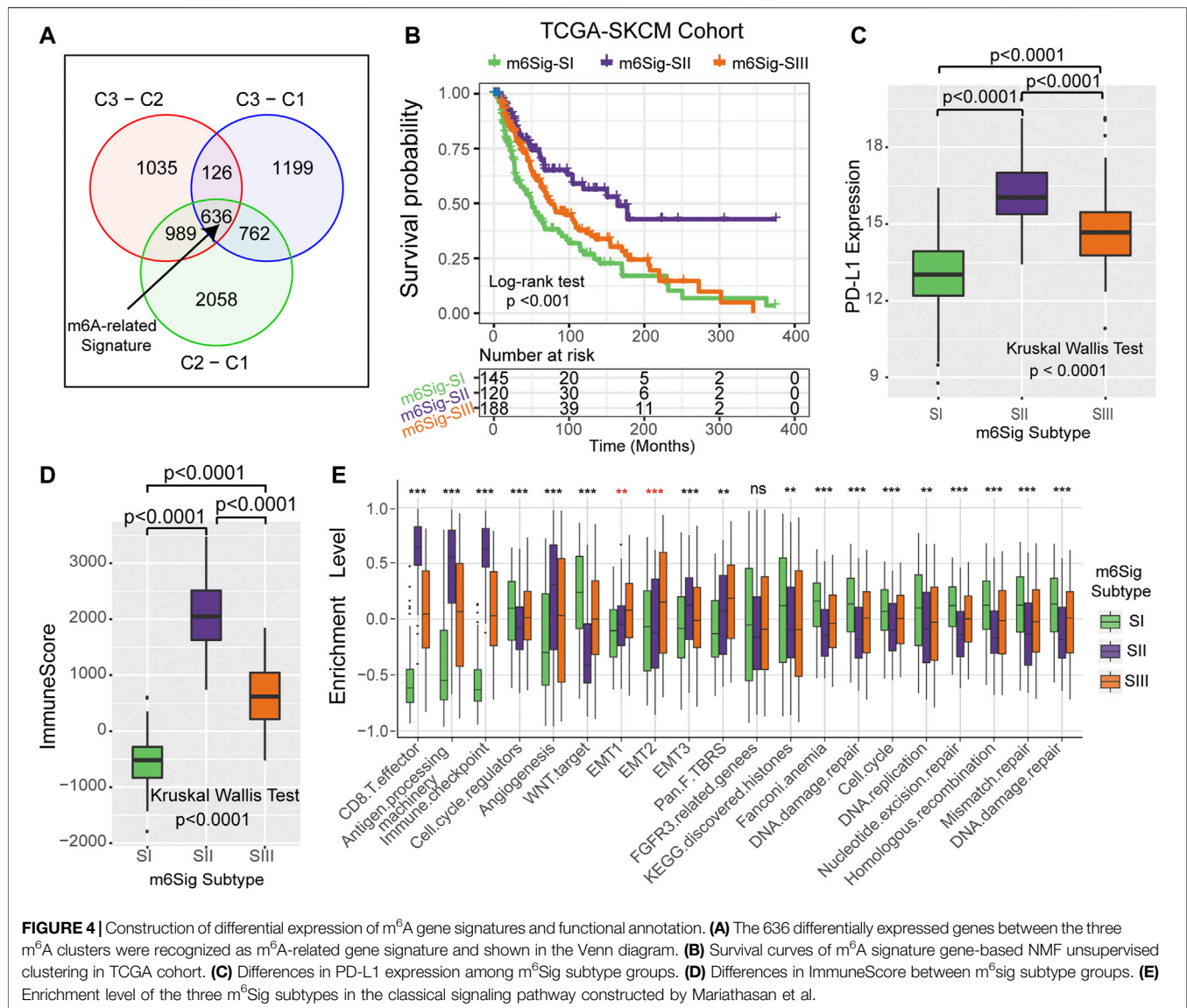
may be due to effective activation of the pre-existing immunity to inhibit tumor growth and malignant progression. Likewise, evaluation on immune cell abundance by CIBERSORT algorithm also corroborate our conclusions (**Supplementary Figure S3C**). In addition, the association between each m⁶A regulator and immune cell infiltration was also explored. As expressed in **Supplementary Figure S3D**, upregulation of WTAP and ALKBH5 was positively correlated with enhanced immune infiltration, while high expression of LRPPRC, METTL3, YTHDF1/3, and ZC3H13 was mostly associated with immunosuppression.

Differentially Expressed Genes Associated With m⁶A Methylation Modifications in Melanoma

Since RNA N⁶-methyladenosine (m⁶A) modification plays an important role in post-transcriptional regulation, we further examine the potential impact on gene expression change of each m⁶A modification cluster in melanoma. To clarify these queries, we employed the Bayesian-based method to identify differentially expressed genes (DEGs) that are differentially regulated across the three m⁶A methylation modification clusters. As illustrated in the Venn diagram of **Figure 4A**, there are a total of 636 DEGs which may play the crucial role in distinguishing the three m⁶A modification clusters (**Supplementary Table S3**). Based on these 636 representative DEGs of m⁶A signature, we further stratified the melanoma samples into three well typed transcriptomic phenotypes (denoted as m⁶Sig-SI, m⁶Sig-SII, and m⁶Sig-SIII) by unsupervised consensus clustering analysis (**Supplementary Figure S4A**). We also compared the m⁶A clusters and m⁶A signature-derived subtype, and found a significant association among these two-stratification method (**Supplementary Table S4**, adjusted χ^2 test, $p < 0.0001$). Patients in m⁶Sig-SII were proved to be associated to better prognosis, while m⁶Sig-SI had a worse outcome ($p < 0.001$, log-rank test; **Figure 4B**). PD-L1 and ImmuneScore were also highly expressed in m⁶Sig-SII subtype than the other subtypes ($p < 0.0001$, Kruskal Wallis test; **Figures 4C,D**). Mariathasan et al. (Mariathasan et al., 2018) summarized and formed a suit of gene set for assessing the activation of immune and stroma signaling pathway, whereby we adopted to evaluate the m⁶Sig signature. The m⁶Sig-SI subgroup was enriched in cell proliferation and DNA damage repair related pathways, m⁶Sig-SIII was characterized by CD8 T effector and antigen processing related pathway, whereas m⁶Sig-SII was focused in epithelial mesenchymal transition (EMT) related signaling pathway (**Figure 4E**). The expression level of 23 m⁶A regulators in three gene subgroups was also compared and shown in **Supplementary Figure S4B**. We observed significant differences of m⁶A regulator expression in the three m⁶A gene-signature subgroups, which was consistent with the expected results of the m⁶A methylation modification clusters.

The m⁶Sig Score System and Its Clinical Relevance

The results of the previous parts of the study can be concluded that m⁶A methylation modification has a strong association with



prognosis and immune regulation in melanoma patients. In order to be able to accurately predict the m⁶A methylation modification cluster of tumors in individual melanoma patients, we developed the m⁶Sig score system to quantify the m⁶A modification cluster based on the identified m⁶A-related signature genes. In **Figure 5A**, the Sankey diagram uncovered the workflow of the m⁶Sig score system in melanoma. It can be found that m⁶A-C3 was linked to a higher m⁶Sig score, and lower for keratin and MITF-low subtypes. We sought to evaluate the significance of the m⁶Sig score system in predicting the prognosis of patients with melanoma through survival analysis. As shown in **Figures 5B,C**, the m⁶Sig score system clearly distinguished patient with different prognosis in both the TCGA-SKCM cohort and *meta*-GEO cohort (patients with high m⁶Sig scores had a better prognosis). We performed the Kruskal Wallis test and showed that the m⁶Sig score could be clearly distinguished in the immune and keratin subtypes (**Figure 5D**). Encouragingly, the m⁶Sig score

system can be extremely well distinguished among the previous m⁶A clusters and m⁶Sig clusters (**Supplementary Figure S5A,B**), which are clusters constructed based on m⁶A methylation modification clusters and DEGs, respectively. Compared with clinicopathological staging, the m⁶Sig score system can better evaluate the prognosis of melanoma patients (AUCs for stage and m⁶Sig score are 0.613 and 0.681, respectively; **Supplementary Figure S5C**). In detail, multivariable cox regression model revealed that melanoma patients with low m⁶Sig scores had a worse survival outcome in TCGA (**Supplementary Figure S5D**) and *meta*-GEO cohort (**Supplementary Figure S5E**). This score system was also explored by ImmuneScore, and patients with high m⁶Sig scores had a higher ImmuneScore ($p < 0.0001$, **Supplementary Figure S5F,G**). Among the six immune subtypes, the m⁶Sig score was also differentially distributed. Samples with high scores were mostly clustered in the “Macrophage Regulation,” “Lymphocyte Infiltration Signature

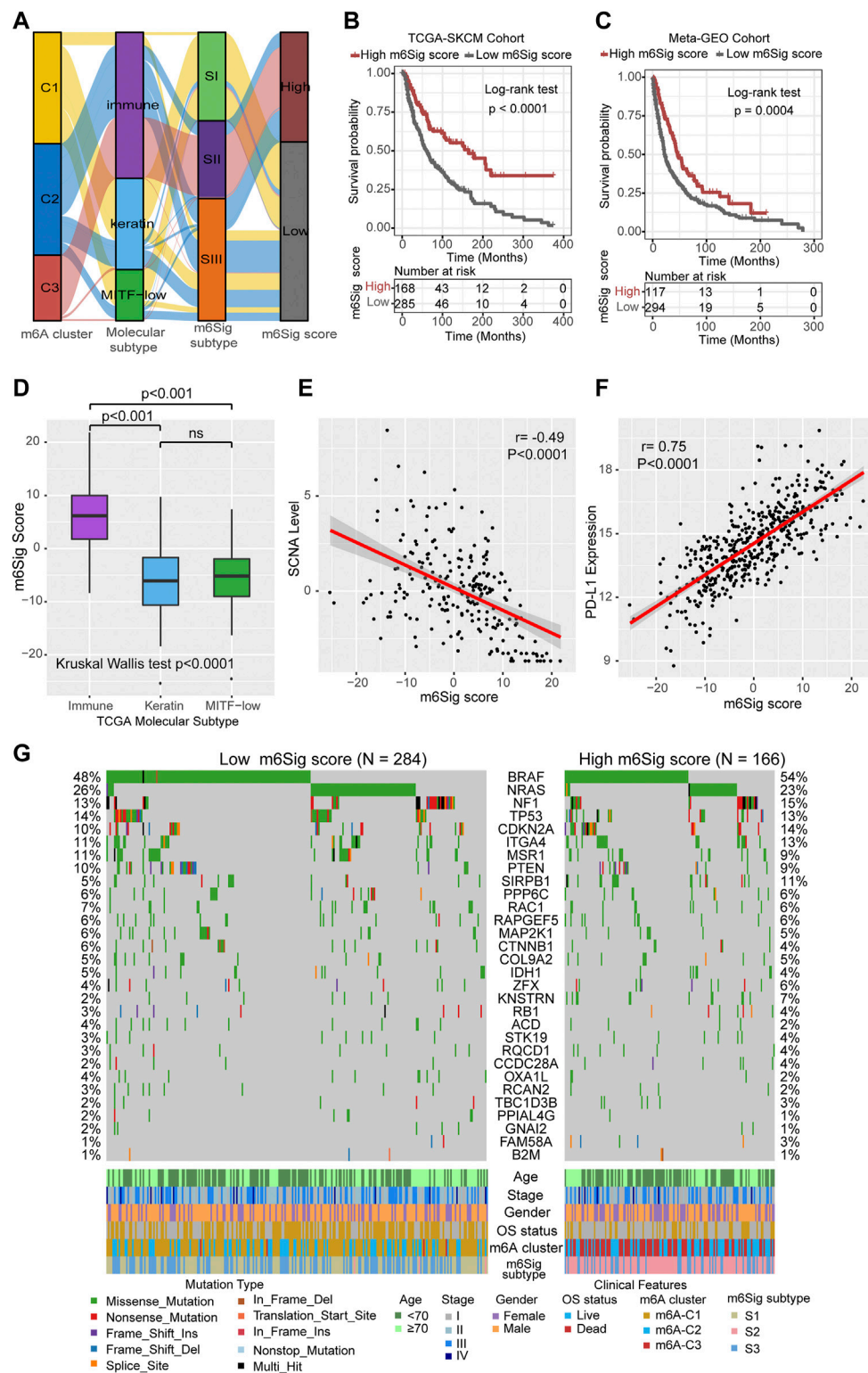


FIGURE 5 | Construction of m⁶Sig score and explore the relevance of clinical features. **(A)** Alluvial diagram of m⁶A clusters in groups with different molecular subtypes (immune, keratin, and MITF-low), m⁶A-gene cluster, and m⁶Sig score. **(B)** Kaplan-Meier curves for high and low m⁶Sig score patient groups in TCGA cohort. **(C)** Kaplan-Meier curves for high and low m⁶Sig score patient groups in meta-GEO cohort. **(D)** The m⁶Sig score differed between the three TCGA molecular types. **(E)** The m⁶A score was negatively correlated with the SCNA mutational level. **(F)** The m⁶A score was positively correlated with PD-L1 expression level. **(G)** Mutation status of significantly mutated genes (SMGs) in the TCGA cohort, stratified by subgroups with low (left) versus high m⁶Sig scores (right). Each column represents one patient. Mutation types and clinical characteristics were annotated in different colors.

Score,” and “IFN- γ Response” subtypes (**Supplementary Figure S5H**), which was similar to the m⁶A-C3 cluster. Heatmap of correlation matrix demonstrated that the m⁶Sig score was markedly positively correlated with the immune activation process and negatively correlated with cell cycle and DNA damage repair (**Supplementary Figure S5I**). To better evaluate the effectiveness of our m⁶Sig score system in predicting the prognosis of melanoma patients, we introduced two independent cohorts (GSE22153 and GSE54437) to perform a survival analysis, and the results showed that patients with high m⁶Sig score had a better prognosis (**Supplementary Figure S6A,B**). Furthermore, a survival analysis after combining all patients involved in this study revealed that a high m⁶Sig score continued to indicate a survival benefit in melanoma patients ($p < 0.0001$, **Supplementary Figure S6C**). The TCGA-SKCM cohort also demonstrated that melanoma patients with high m⁶Sig score had prolonged disease-free survival (DFS, $p = 0.0064$, **Supplementary Figure S6D**). In addition, m⁶Sig score also negatively correlated with somatic copy number alternation (SCNA) level ($r = -0.49$, $p < 0.0001$, **Figure 5E**), which is a significant predictor of immunotherapy resistance in melanoma. The PD-L1 expression levels were also positively correlated with the m⁶Sig score ($r = 0.75$, $p < 0.0001$, **Figure 5F**), suggesting that melanoma patients may also benefit from the m⁶Sig score system for PD1/PD-L1 treatment regimens. More deeply, we performed significant mutation gene (SMG) analysis of melanoma samples based on m⁶Sig score, and the waterfall plot of mutation landscape noted that BRAF (54%/48%), SIRPB1 (11%/5%), and KNSTRN (7%/2%) had higher somatic mutation rates in the high-score group, although BRAF was not statistically significant (**Figure 5G**). These data assist us to more comprehensively understand the m⁶Sig score system mapping to genomic variants, predicting that m⁶A methylation modification is closely linked to somatic mutations in melanoma patients.

The m⁶Sig Score System Can Be a Better Predictor of the Effectiveness of Immunotherapy in Cancer

Cancer treatment regimens based on immune checkpoint inhibitors have provided a landmark innovation in the treatment of malignancies, mostly in melanoma. In addition to TML and PD-L1, TIDE and T cell-inflamed GEP have been recommended to predict immune response in recent years (Chen et al., 2019c; Chen et al., 2019d). We compared the established m⁶Sig score system with the T-cell inflamed gene expression profile (GEP) score and found that melanoma patients with high m⁶Sig score had elevated T-cell inflamed GEP score in both the TCGA-SKCM cohort and the Meta-GEO cohort ($p < 0.0001$, **Figures 6A,B**). In contrast, TIDE showed increased levels in patients with low m⁶Sig scores, implying that greater chance of tumor immune escape and resistance in low m⁶Sig scores subgroup ($p < 0.0001$, **Figures 6C,D**). These results further demonstrate that m⁶A modification clusters play a critical role in the immune response of tumors, thereby affecting the immune microenvironment of tumors.

Aforementioned data point to a strong association between m⁶A modification and immune response, we next investigated whether the m⁶Sig score could predict patients' response to ICI treatment in independent immunotherapy cohorts. Patients with

high m⁶Sig score exhibited significantly longer survival time (log-rank test, $p = 0.0082$, **Figure 6E**) and markedly clinical response to PD-1/CTLA-4 treatment in melanoma (response rate, high vs low m⁶Sig score subgroup, 52.3 vs 31.2%, **Figure 6F**). This result was also identified in an anti-PD-L1 metastatic uroepithelial cancer cohort (Mariathasan et al., 2018), in which patients with high m⁶Sig scores significantly benefited from PD-L1 immunotherapy (log-rank test, $p = 0.0005$, **Figure 6G**; response rate: high vs low m⁶Sig score subgroup, 32.7 vs 17.8%, **Figure 6H**). Furthermore, we found that patients with PD-1 immune response also had a higher m⁶Sig score ($p = 0.0012$, **Figure 6I**). Metastatic uroepithelial carcinoma patients with immune inflamed phenotype had a higher m⁶Sig score than immune excluded and desert phenotype (**Figure 6J**). A significant elevation of PD-L1 was identified in high m⁶Sig score subgroup ($p < 0.0001$, **Figure 6K**). Therefore, we divided the overall population into four subgroups according to the TMEsig-score and PD-L1 distribution, including TMEsig-score-H + PD-L1-H, TMEsig-score-H + PD-L1-L, TMEsig-score-L + PD-L1-H, and TMEsig-score-L + PD-L1-L. The TMEsig-score-H + PD-L1-H subgroup exhibited the best prognostic outcome compared with the other three subgroups (log-rank test, $p < 0.0001$, **Figure 6L**). Based on the results of the above analysis, our established m⁶Sig score system enables the prediction of responsiveness and prognosis to cancer immunotherapy.

DISCUSSION

Recently, the dynamic and reversible process of m⁶A modification has been reported in participation of the innate immune, inflammatory response, and anti-tumor processes (Chen et al., 2019a; Shulman and Stern-Ginossar, 2020). Although numerous studies have recently revealed how m⁶A regulators are epigenetically regulated in the tumor immunogenicity, the association between m⁶A regulators and the overall tumor microenvironment has not yet been elucidated in melanoma. Thus, identifying distinct m⁶A modification clusters in the TME infiltration will contribute to advancing our understanding of anti-tumor immune response and facilitating more effective precision immunotherapy strategies.

In this study, we identified three different immunophenotypic m⁶A methylation modification clusters, which are characterized by different anticancer immune effects. The m⁶A-C1 phenotype is distinguished by promotion of cell proliferation and activation of PI3K/AKT/mTOR signaling pathway, and we prefer it to be the immune-desert phenotype. The m⁶A-C2 phenotype is more characteristic of cancer and immune surveillance, and it is associated with EMT, TGF- β , and TNF- α pathway activation and is an immune-excluded phenotype. The m⁶A-C3 phenotype, on the other hand, is associated with activation of pathways related to inflammatory response, innate immune response, and is an immune-inflamed phenotype. It has been shown that the tumor microenvironment plays a central role in tumorigenesis development and progression, and the levels of tumor-infiltrating CD4⁺/CD8⁺ T cells, M1 macrophages, NK cells, and

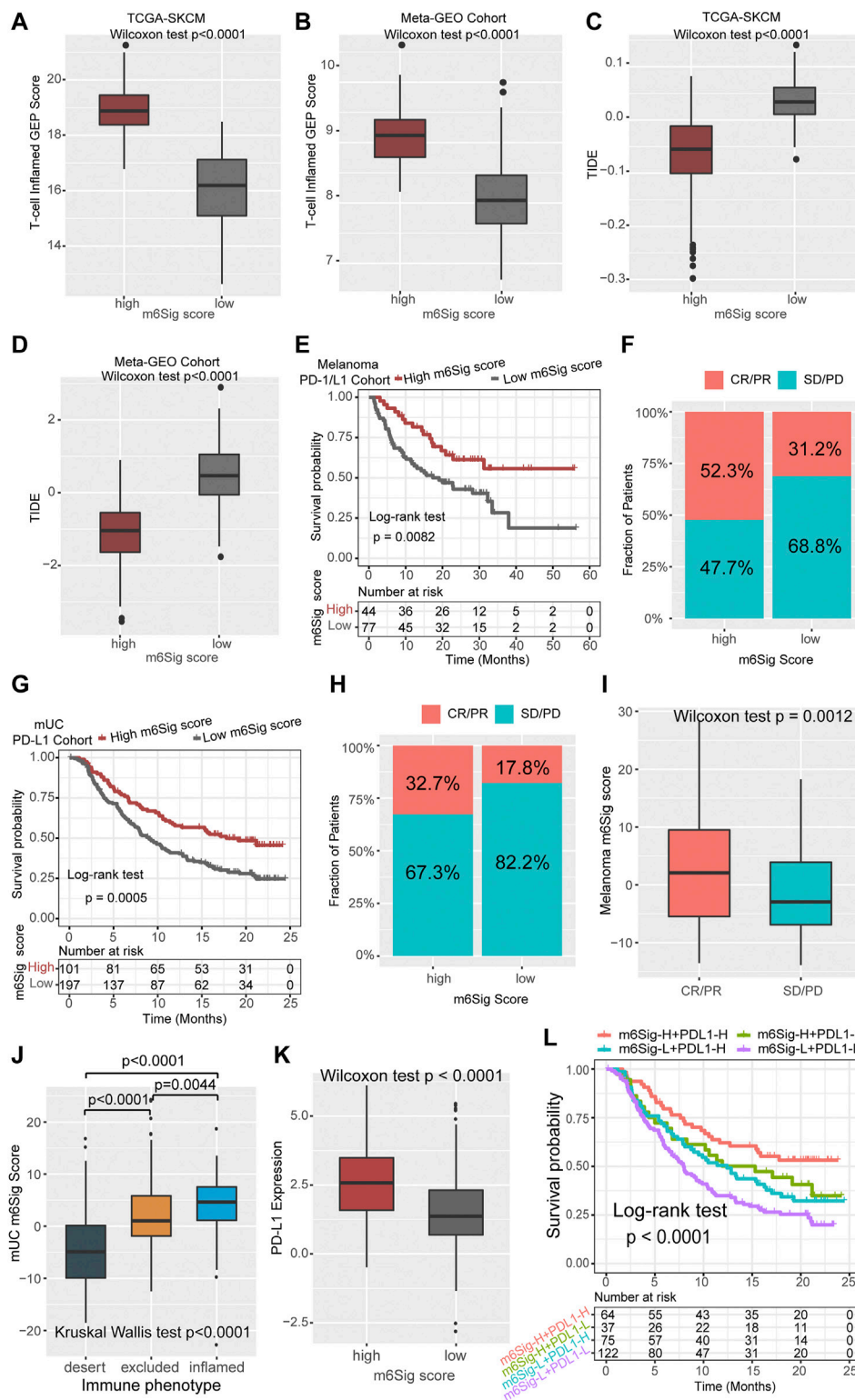


FIGURE 6 | The m^6 Sig score predicts immunotherapeutic benefits. **(A)** Comparison of the relative distribution of T-cell inflamed GEP scores between the high and low m^6 Sig score groups in the TCGA cohort. **(B)** Comparison of the relative distribution of T-cell inflamed GEP scores between the high and low m^6 Sig score groups in the meta-GEO cohort. **(C)** Comparison of the relative distribution of TIDE between the high and low m^6 Sig score groups in the TCGA cohort. **(D)** Comparison of the relative distribution of TIDE between the high and low m^6 Sig score groups in the meta-GEO cohort. **(E)** Kaplan-Meier curves for high and low m^6 Sig score patient groups in the melanoma PD-1/CTLA-4 cohort. **(F)** The fraction of patients with clinical response to anti-PD-1/CTLA-4 immunotherapy in low or high m^6 Sig score groups. (Continued)

FIGURE 6 | (G) Kaplan-Meier curves for high and low m⁶Sig score patient groups in the metastatic urothelial carcinoma (mUC) PD-L1 cohort. (H) The fraction of patients with clinical response to anti-PD-L1 immunotherapy in low or high m⁶Sig score groups of mUC cohort. (I) Distribution of m⁶Sig scores between immunotherapy response and non-response in melanoma PD-1/CTLA-4 cohort. (J) Distribution of mUC m⁶Sig scores among the three immune phenotypes. (K) The relationship between m⁶Sig score and PD-L1 expression level. (L) The m⁶Sig score combined with PD-L1 expression levels better predicted patient prognosis. CR, complete response; PR, partial response; SD, stable disease; PD, progressive disease.

inflammatory cytokines directly influence the onset of immune priming and adaptive immunity (Topalian et al., 2016; Galon and Bruni, 2019; Zeng et al., 2020). Interestingly, the m⁶A-C2 phenotype is associated with activation of the TGF- β signaling pathway and intermediate immune cell infiltration, and thus, we hypothesized that melanoma patients with m⁶A-C2 phenotype would benefit from the combination of immune checkpoint inhibitors and TGF- β blockers. There is evidence pointing out that activation of the TGF- β pathway hinders lymphocyte attack on “tumor barriers” (Tauriello et al., 2018). Moreover, inhibitors targeting TGF- β can effectively remodel the tumor microenvironment in the form of reprogrammed peritumor stromal fibroblasts, which can restore the body’s anti-tumor immunity (Mariathasan et al., 2018; Panagi et al., 2020). We found that the m⁶A-C3 phenotype was associated with enrichment of activated tumor-infiltrating lymphocytes, making this phenotype more likely responsive to ICI immunotherapy.

The m⁶A signature genes were derived from genes differentially expressed in three m⁶A modification subtypes. These m⁶A-related signature genes were further utilized to identify transcriptomic subtypes and tumor microenvironment landscapes in melanoma. Patients with m⁶Sig-SII subtype have higher PD-L1 expression levels and higher immuneScores, implying that patients with this subtype are better treated with immune checkpoint inhibitors for better therapeutic outcomes. For the sake of precision clinical practice, we optimized the m⁶Sig signatures into the m⁶Sig score scheme, a system that could be used to quantify the m⁶A modification level of individual tumors. The m⁶A modification clusters characterized by an immune-inflamed phenotype showed a higher m⁶Sig score, whereas the modification cluster characterized by an immune-desert phenotype had a lower score. The results based on survival analysis highlight that the m⁶Sig score system can effectively predict the prognosis of melanoma patients, and that this score system is strongly associated with TCGA molecular subtypes, genomic alternations, and PD-L1 expression levels. We also observed that m⁶Sig score was closely correlated with T-cell inflamed GEP score and TIDE, which are effective tools for prediction of immunotherapy benefit, further demonstrating that m⁶A RNA methylation modification can modulate the effect of immune response in melanoma. To identify the predictive value of m⁶Sig score system in immune response, we performed a series of analyses in two additional independent immunotherapy cohorts and validated the effect of this score system. In a nutshell, the m⁶A RNA methylation modification cluster can be used to determine the immune phenotype of melanoma patients, further guiding clinical treatment planning and effectively predicting the prognosis of patients.

We also noticed that certain m⁶A regulators play different roles in regulating tumorigenesis and tumor immunogenicity. Recent studies have confirmed that the mRNA stability and translation processes of the oncofetal IGF2 mRNA binding proteins (IGF2BPs) are regulated by RNA N⁶-methyladenosine (Huang et al., 2018). IGF2BP1, a member of the IGF2BPs family, was then identified as an oncogene that promotes cancer development by antagonizing cancer-suppressive miRNAs (Müller et al., 2018; Müller et al., 2019). In contrast, our results showed that IGF2BPs genes have higher expression level in patients with metastatic melanoma and m⁶A-C1 subtype. It has been demonstrated that IGF2BP2 promotes cancer progression by regulating the m⁶A-dependent glycolytic process and promotes cancer metastasis in the form of an RNA-protein ternary complex (Chen et al., 2019e). KIAA1429 is also well known as an m⁶A methyltransferase. In hepatocellular carcinoma, KIAA1429 promotes cancer metastasis and leads to poor patient prognosis by regulating post-transcriptional modifications (Lan et al., 2019). Our results also suggest this function of KIAA1429 to promote metastasis and highly expressed in m⁶A-C1 desert phenotype, but its prediction of patient survival may require the combination of RBM15, RBM15B, IGF2BP3, and HNRNPA2B1, with co-occurrence between them. YTHDCs and YTHDFs containing YTH domain act as “readers” in post-translational RNA methylation modification, and YTHDFs enhance aerobic glycolysis by degrading mRNA to further promote tumor formation (Wang et al., 2021; Xia et al., 2021). Our study confirms that both YTHDF1/3 and YTHDC1/2 are highly expressed in metastatic melanoma, and of interest, the high expression of YTHDF1 in patients with metastatic melanoma is accompanied by an indication of a poorer prognosis, which suggests a new direction for deeper studies of molecules containing YTH domain. In our study, we found that ELAVL1 was not only associated with metastasis of melanoma, but also reflected a poorer prognosis of patients, which may be related to the fact that ELAVL1 can stabilize oncogenic transcripts (Li et al., 2020b). In summary, the results of our analysis demonstrate the importance of a systematic and comprehensive consideration of m⁶A modification clusters, which are diverse in cancer across physiological processes.

Identification of significantly mutated genes underlying human cancers is a critical foundation for cancer diagnostics, therapeutics, and selection of rational therapies. In our study, we found a higher proportion of SMGs of BRAF, SIRPB1, and KNSTRN in the high m⁶Sig score subgroup, although BRAF was of marginal significance. In a pan-cancer study, it was noted that BRAF has a higher rate of specific driver mutations in leukocytes of cancer patients, a phenomenon associated with tumor-immune cell interactions (Thorsson et al., 2018). There is

new evidence that BRAFi induces the occurrence of anti-tumor cell scorching immune responses, which may be a new strategy for the treatment of melanoma (Erkes et al., 2020). Signal regulatory protein beta 1 (SIRPB1) is a member of the signal regulatory protein (SIRP) family, which also belongs to the immunoglobulin superfamily, and is a negatively regulated receptor-type transmembrane glycoprotein involved in receptor tyrosine kinase-coupled signaling processes. SIRPB1 is associated with neutrophil migration across the epithelium, which provides a new target for drug design in immunotherapy (Ribeiro et al., 2019). It has been reported that KNSTRN mutations rarely occurred in other solid tumors and leukemias, which are relatively specific for skin-related cancers (Lee et al., 2016; Schmitz et al., 2019). These tumor driver mutations in different m⁶Sig scores not only are associated with malignant progression, metastasis, and recurrence of cancer but also play a role in the regulation of immune activity, demonstrating a complex and consequently clear interaction between m⁶A RNA methylation modifications and tumor immunogenomic.

The literature review helped us to integrate the well-known 23 m⁶A RNA methylation regulators for meta-analysis, but this still requires newly discovered regulators to be included to enhance the accuracy of the established m⁶A modification clusters. There is a relative lack of PD-L1-based regimens for melanoma patients, so we introduced a dataset of uroepithelial carcinoma treated with atezolizumab, but we still hope that the m⁶Sig score system can be analyzed and validated in melanoma immunotherapy with different immune checkpoint inhibitors. Moreover, all the data in this study were obtained from retrospective cohort, which would introduce some bias. Therefore, our next study focused on establishing a prospective cohort of melanoma patients with immune checkpoint inhibitors to validate and optimize the m⁶Sig score system. In addition, the current m⁶Sig score system does not yet incorporate the clinicopathological characteristics of the patients, which also lead to the drawbacks of the system.

In our study, we systematically assessed the m⁶A modification clusters of 1,020 melanoma patients and comprehensively analyzed the impact of m⁶A modification clusters generated by 23 m⁶A regulators on the cellular infiltration characteristics of the tumor microenvironment. The results of this integrative analysis confirm that RNA methylation is essential for the regulation of tumor immune response, and assessing the m⁶A modification clusters of patient tumors will help us better understand the immune microenvironment infiltration characteristics and provide new ideas for indications and protocol modifications for immunotherapy.

REFERENCES

Ayers, M., Lunceford, J., Nebozhyn, M., Murphy, E., Loboda, A., Kaufman, D. R., et al. (2017). IFN- γ -related mRNA Profile Predicts Clinical Response to PD-1 Blockade. *J. Clin. Invest.* 127 (8), 2930–2940. doi:10.1172/JCI11190

DATA AVAILABILITY STATEMENT

Publicly available datasets were analyzed in this study. This data can be found here: Gene expression data and clinical information for melanoma patient samples were obtained from the GEO database (<https://www.ncbi.nlm.nih.gov/geo/>) and TCGA database (<https://portal.gdc.cancer.gov/>), which are publicly and freely available, including the GSE19234, GSE22154, GSE50509, GSE59455, GSE65904, GSE22153, GSE54437 and TCGA-SCKM datasets.

AUTHOR CONTRIBUTIONS

Conception and design: XKL, FD, HL; Development of methodology: FD, HL, YLi, YLiu; Acquisition of data (provided data, acquired and managed patients, provided facilities, etc.): XYL, ND, QC, ZF, HW, XZ, JY; Analysis and interpretation of data (e.g., statistical analysis, biostatistics, computational analysis): FD, HL, YLi, YLiu, XKL; Writing, review, and/or revision of the manuscript: FD, HL, XKL; Administrative, technical, or material support (i.e., reporting or organizing data, constructing databases): FD, HL, YLi, YLiu; Study supervision: XKL.

FUNDING

This study was supported by grant from Key Research and Development Program of Shandong Province (No.2019JZZY010104; No.2019GSF108146), Academic promotion programme of Shandong First Medical University (2019QL021), Special Foundation for Taishan Scholars Program of Shandong Province (No.ts20190978), The Research Incubation Funding of Shandong Provincial Hospital, and Youth Training Program for High-level Projects of Jinan Central Hospital.

ACKNOWLEDGMENTS

We sincerely thank YY from Tianjin tumor hospital for analysis advice and CA for language editing.

SUPPLEMENTARY MATERIAL

The Supplementary Material for this article can be found online at: <https://www.frontiersin.org/articles/10.3389/fcell.2021.761134/full#supplementary-material>

Binnewies, M., Roberts, E. W., Kersten, K., Chan, V., Fearon, D. F., Merad, M., et al. (2018). Understanding the Tumor Immune Microenvironment (TIME) for Effective Therapy. *Nat. Med.* 24 (5), 541–550. doi:10.1038/s41591-018-0014-x

Charoentong, P., Finotello, F., Angelova, M., Mayer, C., Efremova, M., Rieder, D., et al. (2017). Pan-cancer Immunogenomic Analyses Reveal Genotype-Immunophenotype Relationships and Predictors of Response to Checkpoint Blockade. *Cel. Rep.* 18 (1), 248–262. doi:10.1016/j.celrep.2016.12.019

- Chen, D. S., and Mellman, I. (2017). Elements of Cancer Immunity and the Cancer-Immune Set point. *Nature* 541 (7637), 321–330. doi:10.1038/nature21349
- Chen, H., Chong, W., Wu, Q., Yao, Y., Mao, M., and Wang, X. (2019). Association of LRP1B Mutation with Tumor Mutation Burden and Outcomes in Melanoma and Non-small Cell Lung Cancer Patients Treated with Immune Check-Point Blockades. *Front. Immunol.* 10, 1113. doi:10.3389/fimmu.2019.01113
- Chen, H., Chong, W., Teng, C., Yao, Y., Wang, X., and Li, X. (2019). The Immune Response-related Mutational Signatures and Driver Genes in Non-small-cell Lung Cancer. *Cancer Sci.* 110 (8), 2348–2356. doi:10.1111/cas.14113
- Chen, H., Chong, W., Yang, X., Zhang, Y., Sang, S., Li, X., et al. (2020). Age-related Mutational Signature Negatively Associated with Immune Activity and Survival Outcome in Triple-Negative Breast Cancer. *Oncoimmunology* 9 (1), 1788252. doi:10.1080/2162402X.2020.1788252
- Chen, H., Yang, M., Wang, Q., Song, F., Li, X., and Chen, K. (2019). The New Identified Biomarkers Determine Sensitivity to Immune Check-point Blockade Therapies in Melanoma. *Oncoimmunology* 8 (8), 1608132. doi:10.1080/2162402x.2019.1608132
- Chen, R. X., Chen, X., Xia, L. P., Zhang, J. X., Pan, Z. Z., Ma, X. D., et al. (2019). N6-methyladenosine Modification of circNSUN2 Facilitates Cytoplasmic export and Stabilizes HMGA2 to Promote Colorectal Liver Metastasis. *Nat. Commun.* 10, 4695. doi:10.1038/s41467-019-12651-2
- Chen, X.-Y., Zhang, J., and Zhu, J.-S. (2019). The Role of m6A RNA Methylation in Human Cancer. *Mol. Cancer* 18 (1), 103. doi:10.1186/s12943-019-1033-z
- Chen, Y.-T., Shen, J.-Y., Chen, D.-P., Wu, C.-F., Guo, R., Zhang, P.-P., et al. (2020). Identification of Cross-Talk between m6A and 5mC Regulators Associated with Onco-Immunogenic Features and Prognosis across 33 Cancer Types. *J. Hematol. Oncol.* 13 (1), 22. doi:10.1186/s13045-020-00854-w
- Chen, Z., Wu, L., Zhou, J., Lin, X., Peng, Y., Ge, L., et al. (2020). N6-methyladenosine-induced ERR γ Triggers Chemoresistance of Cancer Cells through Upregulation of ABCB1 and Metabolic Reprogramming. *Theranostics* 10 (8), 3382–3396. doi:10.7150/thno.40144
- Chong, W., Shang, L., Liu, J., Fang, Z., Du, F., Wu, H., et al. (2021). m6A Regulator-Based Methylation Modification Patterns Characterized by Distinct Tumor Microenvironment Immune Profiles in colon cancer A Regulator-Based Methylation Modification Patterns Characterized by Distinct Tumor Microenvironment Immune Profiles in colon Cancer. *Theranostics* 11 (5), 2201–2217. doi:10.7150/thno.52717
- Chong, W., Wang, Z., Shang, L., Jia, S., Liu, J., Fang, Z., et al. (2021). Association of Clock-like Mutational Signature with Immune Checkpoint Inhibitor Outcome in Patients with Melanoma and NSCLC. *Mol. Ther. - Nucleic Acids* 23, 89–100. doi:10.1016/j.omtn.2020.10.033
- Dai, W., Li, Y., Mo, S., Feng, Y., Zhang, L., Xu, Y., et al. (2018). A Robust Gene Signature for the Prediction of Early Relapse in Stage I-III colon Cancer. *Mol. Oncol.* 12 (4), 463–475. doi:10.1002/1878-0261.12175
- Davoli, T., Uno, H., Wooten, E. C., and Elledge, S. J. (2017). Tumor Aneuploidy Correlates with Markers of Immune Evasion and with Reduced Response to Immunotherapy. *Science* 355 (6322). doi:10.1126/science.aaf8399
- Eddy, K., and Chen, S. (2020). Overcoming Immune Evasion in Melanoma. *Ijms* 21 (23), 8984. doi:10.3390/ijms21238984
- Erkes, D. A., Cai, W., Sanchez, I. M., Purwin, T. J., Rogers, C., Field, C. O., et al. (2020). Mutant BRAF and MEK Inhibitors Regulate the Tumor Immune Microenvironment via Pyroptosis. *Cancer Discov.* 10 (2), 254–269. doi:10.1158/2159-8290.Cd-19-0672
- Finotello, F., and Trajanoski, Z. (2018). Quantifying Tumor-Infiltrating Immune Cells from Transcriptomics Data. *Cancer Immunol. Immunother.* 67 (7), 1031–1040. doi:10.1007/s00262-018-2150-z
- Galon, J., and Bruni, D. (2019). Approaches to Treat Immune Hot, Altered and Cold Tumours with Combination Immunotherapies. *Nat. Rev. Drug Discov.* 18 (3), 197–218. doi:10.1038/s41573-018-0007-y
- Ghandi, M., Huang, F. W., Jané-Valbuena, J., Kryukov, G. V., Lo, C. C., McDonald, E. R., 3rd, et al. (2019). Next-generation Characterization of the Cancer Cell Line Encyclopedia. *Nature* 569 (7757), 503–508. doi:10.1038/s41586-019-1186-3
- Han, D., Liu, J., Chen, C., Dong, L., Liu, Y., Chang, R., et al. (2019). Anti-tumour Immunity Controlled through mRNA m6A Methylation and YTHDF1 in Dendritic Cells. *Nature* 566 (7743), 270–274. doi:10.1038/s41586-019-0916-x
- Hänzelmann, S., Castelo, R., and Guinney, J. (2013). GSVA: Gene Set Variation Analysis for Microarray and RNA-Seq Data. *BMC Bioinformatics* 14, 7. doi:10.1186/1471-2105-14-7
- Hazra, A., and Gogtay, N. (2016). Biostatistics Series Module 3: Comparing Groups: Numerical Variables. *Indian J. Dermatol.* 61 (3), 251–260. doi:10.4103/0019-5154.182416
- He, L., Li, H., Wu, A., Peng, Y., Shu, G., and Yin, G. (2019). Functions of N6-Methyladenosine and its Role in Cancer. *Mol. Cancer* 18 (1), 176. doi:10.1186/s12943-019-1109-9
- Hegde, P. S., Karanikas, V., and Evers, S. (2016). The where, the when, and the How of Immune Monitoring for Cancer Immunotherapies in the Era of Checkpoint Inhibition. *Clin. Cancer Res.* 22 (8), 1865–1874. doi:10.1158/1078-0432.Ccr-15-1507
- Huang, X., Zhang, H., Guo, X., Zhu, Z., Cai, H., and Kong, X. (2018). Insulin-like Growth Factor 2 mRNA-Binding Protein 1 (IGF2BP1) in Cancer. *J. Hematol. Oncol.* 11, 88. doi:10.1186/s13045-018-0628-y
- Jia, Q., Wu, W., Wang, Y., Alexander, P. B., Sun, C., Gong, Z., et al. (2018). Local Mutational Diversity Drives Intratumoral Immune Heterogeneity in Non-small Cell Lung Cancer. *Nat. Commun.* 9 (1), 5361. doi:10.1038/s41467-018-07767-w
- Jiang, P., Gu, S., Pan, D., Fu, J., Sahu, A., Hu, X., et al. (2018). Signatures of T Cell Dysfunction and Exclusion Predict Cancer Immunotherapy Response. *Nat. Med.* 24 (10), 1550–1558. doi:10.1038/s41591-018-0136-1
- Kandoth, C., McLellan, M. D., Vandin, F., Ye, K., Niu, B., Lu, C., et al. (2013). Mutational Landscape and Significance across 12 Major Cancer Types. *Nature* 502 (7471), 333–339. doi:10.1038/nature12634
- Lan, T., Li, H., Zhang, D., Xu, L., Liu, H., Hao, X., et al. (2019). KIAA1429 Contributes to Liver Cancer Progression through N6-methyladenosine-dependent post-transcriptional Modification of GATA3. *Mol. Cancer* 18 (1), 186. doi:10.1186/s12943-019-1106-z
- Lawrence, M. S., Stojanov, P., Polak, P., Kryukov, G. V., Cibulskis, K., Sivachenko, A., et al. (2013). Mutational Heterogeneity in Cancer and the Search for New Cancer-Associated Genes. *Nature* 499 (7457), 214–218. doi:10.1038/nature12213
- Lee, J. H., Kim, M. S., Yoo, N. J., and Lee, S. H. (2016). Absence of KNSTRN Mutation, a Cutaneous Squamous Carcinoma-specific Mutation, in Other Solid Tumors and Leukemias. *Pathol. Oncol. Res.* 22 (1), 227–228. doi:10.1007/s12253-015-9993-9
- Lewinska, A., Adamczyk-Grochala, J., Deregoska, A., and Wnuk, M. (2017). Sulforaphane-Induced Cell Cycle Arrest and Senescence Are Accompanied by DNA Hypomethylation and Changes in microRNA Profile in Breast Cancer Cells. *Theranostics* 7 (14), 3461–3477. doi:10.7150/thno.20657
- Li, K., Huang, F., Li, Y., Li, D., Lin, H., Ni, R., et al. (2020). Stabilization of Oncogenic Transcripts by the IGF2BP3/ELAVL1 Complex Promotes Tumorigenicity in Colorectal Cancer. *Am. J. Cancer Res.* 10 (8), 2480–2494.
- Li, X.-C., Jin, F., Wang, B.-Y., Yin, X.-J., Hong, W., and Tian, F.-J. (2019). The m6A Demethylase ALKBH5 Controls Trophoblast Invasion at the Maternal-Fetal Interface by Regulating the Stability of CYR61 mRNA. *Theranostics* 9 (13), 3853–3865. doi:10.7150/thno.31868
- Li, X., Wen, D., Li, X., Yao, C., Chong, W., and Chen, H. (2020). Identification of an Immune Signature Predicting Prognosis Risk and Lymphocyte Infiltration in Colon Cancer. *Front. Immunol.* 11, 1678. doi:10.3389/fimmu.2020.01678
- Liu, D., Schilling, B., Liu, D., Sucker, A., Livingstone, E., Jerby-Arnon, L., et al. (2019). Integrative Molecular and Clinical Modeling of Clinical Outcomes to PD1 Blockade in Patients with Metastatic Melanoma. *Nat. Med.* 25 (12), 1916–1927. doi:10.1038/s41591-019-0654-5
- Love, M. I., Huber, W., and Anders, S. (2014). Moderated Estimation of Fold Change and Dispersion for RNA-Seq Data with DESeq2. *Genome Biol.* 15 (12), 550. doi:10.1186/s13059-014-0550-8
- Mariathasan, S., Turley, S. J., Nickles, D., Castiglioni, A., Yuen, K., Wang, Y., et al. (2018). TGF β Attenuates Tumour Response to PD-L1 Blockade by Contributing to Exclusion of T Cells. *Nature* 554 (7693), 544–548. doi:10.1038/nature25501
- Martínez-Riño, A., Bovolenta, E. R., Boccasavia, V. L., Ponomarenko, J., Abia, D., Oeste, C. L., et al. (2019). RRAS2 Shapes the TCR Repertoire by Setting the Threshold for Negative Selection. *J. Exp. Med.* 216 (10), 2427–2447. doi:10.1084/jem.20181959

- Mayakonda, A., Lin, D.-C., Assenov, Y., Plass, C., and Koeffler, H. P. (2018). Maftools: Efficient and Comprehensive Analysis of Somatic Variants in Cancer. *Genome Res.* 28 (11), 1747–1756. doi:10.1101/gr.239244.118
- Mazurkiewicz, J., Simiczjyew, A., Dratkiewicz, E., Ziętek, M., Matkowski, R., and Nowak, D. (2021). Stromal Cells Present in the Melanoma Niche Affect Tumor Invasiveness and its Resistance to Therapy. *Ijms* 22 (2), 529. doi:10.3390/ijms22020529
- Müller, S., Bley, N., Glass, M., Busch, B., Rousseau, V., Misiak, D., et al. (2018). IGF2BP1 Enhances an Aggressive Tumor Cell Phenotype by Impairing miRNA-Directed Downregulation of Oncogenic Factors. *Nucleic Acids Res.* 46 (12), 6285–6303. doi:10.1093/nar/gky229
- Müller, S., Glaß, M., Singh, A. K., Haase, J., Bley, N., Fuchs, T., et al. (2019). IGF2BP1 Promotes SRF-dependent Transcription in Cancer in a m6A- and miRNA-dependent Manner. *Nucleic Acids Res.* 47 (1), 375–390. doi:10.1093/nar/gky1012
- Newman, A. M., Steen, C. B., Liu, C. L., Gentles, A. J., Chaudhuri, A. A., Scherer, F., et al. (2019). Determining Cell Type Abundance and Expression from Bulk Tissues with Digital Cytometry. *Nat. Biotechnol.* 37 (7), 773–782. doi:10.1038/s41587-019-0114-2
- Pagès, F., Mlecnik, B., Marliot, F., Bindea, G., Ou, F. S., Bifulco, C., et al. (2018). International Validation of the Consensus Immunoscore for the Classification of colon Cancer: a Prognostic and Accuracy Study. *Lancet* 391 (10135), 2128–2139. doi:10.1016/S0140-6736(18)30789-X
- Panagi, M., Voutouri, C., Mpekris, F., Papageorgis, P., Martin, M. R., Martin, J. D., et al. (2020). TGF- β Inhibition Combined with Cytotoxic Nanomedicine Normalizes Triple Negative Breast Cancer Microenvironment towards Anti-tumor Immunity. *Theranostics* 10 (4), 1910–1922. doi:10.7150/thno.36936
- Ribeiro, G. E., Leon, L. E., Perez, R., Cuiza, A., Vial, P. A., Ferres, M., et al. (2019). Deletions in Genes Participating in Innate Immune Response Modify the Clinical Course of Andes Orthohantavirus Infection. *Viruses* 11 (8), 680. doi:10.3390/v11080680
- Ritchie, M. E., Phipson, B., Wu, D., Hu, Y., Law, C. W., Shi, W., et al. (2015). Limma powers Differential Expression Analyses for RNA-Sequencing and Microarray Studies. *Nucleic Acids Res.* 43 (7), e47. doi:10.1093/nar/gkv007
- Schmitz, L., Grinblat, B., Novak, B., Hoeh, A. K., Händschke, K., von Döbeler, C., et al. (2019). Somatic Mutations in Kinetochore Gene KNSTRN Are Associated with Basal Proliferating Actinic Keratoses and Cutaneous Squamous Cell Carcinoma. *J. Eur. Acad. Dermatol. Venereol.* 33 (8), 1535–1540. doi:10.1111/jdv.15615
- Shulman, Z., and Stern-Ginossar, N. (2020). The RNA Modification N6-Methyladenosine as a Novel Regulator of the Immune System. *Nat. Immunol.* 21 (5), 501–512. doi:10.1038/s41590-020-0650-4
- Subramanian, A., Tamayo, P., Mootha, V. K., Mukherjee, S., Ebert, B. L., Gillette, M. A., et al. (2005). Gene Set Enrichment Analysis: a Knowledge-Based Approach for Interpreting Genome-wide Expression Profiles. *Proc. Natl. Acad. Sci.* 102 (43), 15545–15550. doi:10.1073/pnas.0506580102
- Tauriello, D. V. F., Palomo-Ponce, S., Stork, D., Berenguer-Llgero, A., Badia-Ramentol, J., Iglesias, M., et al. (2018). TGF β Drives Immune Evasion in Genetically Reconstituted colon Cancer Metastasis. *Nature* 554 (7693), 538–543. doi:10.1038/nature25492
- Thorsson, V., Gibbs, D. L., Brown, S. D., Wolf, D., Bortone, D. S., Ou Yang, T. H., et al. (2018). The Immune Landscape of Cancer. *Immunity* 48 (4), 812–e14. doi:10.1016/j.immuni.2018.03.023
- Topalian, S. L., Taube, J. M., Anders, R. A., and Pardoll, D. M. (2016). Mechanism-driven Biomarkers to Guide Immune Checkpoint Blockade in Cancer Therapy. *Nat. Rev. Cancer* 16 (5), 275–287. doi:10.1038/nrc.2016.36
- Wang, H., Hu, X., Huang, M., Liu, J., Gu, Y., Ma, L., et al. (2019). Mettl3-mediated mRNA m6A Methylation Promotes Dendritic Cell Activation. *Nat. Commun.* 10 (1), 1898. doi:10.1038/s41467-019-09903-6
- Wang, W., Shao, F., Yang, X., Wang, J., Zhu, R., Yang, Y., et al. (2021). METTL3 Promotes Tumour Development by Decreasing APC Expression Mediated by APC mRNA N6-methyladenosine-dependent YTHDF Binding. *Nat. Commun.* 12 (1), 3803. doi:10.1038/s41467-021-23501-5
- Wang, Y., Wang, Y., Luo, W., Song, X., Huang, L., Xiao, J., et al. (2020). Roles of Long Non-coding RNAs and Emerging RNA-Binding Proteins in Innate Antiviral Responses. *Theranostics* 10 (20), 9407–9424. doi:10.7150/thno.48520
- Xia, Z., Tang, M., Ma, J., Zhang, H., Gimple, R. C., Prager, B. C., et al. (2021). Epitranscriptomic Editing of the RNA N6-Methyladenosine Modification by dCasRx Conjugated Methyltransferase and Demethylase. *Nucleic Acids Res.* 49, 7361–7374. doi:10.1093/nar/gkab517
- Yang, S., Wei, J., Cui, Y.-H., Park, G., Shah, P., Deng, Y., et al. (2019). m6A mRNA Demethylase FTO Regulates Melanoma Tumorigenicity and Response to Anti-PD-1 blockade. *mRNA Demethylase FTO Regulates Melanoma Tumorigenicity and Response to Anti-PD-1 Blockade. Nat. Commun.* 10 (1), 2782. doi:10.1038/s41467-019-10669-0
- Yoshihara, K., Shahmoradgoli, M., Martínez, E., Vegesna, R., Kim, H., Torres-García, W., et al. (2013). Inferring Tumour Purity and Stromal and Immune Cell Admixture from Expression Data. *Nat. Commun.* 4, 2612. doi:10.1038/ncomms3612
- Zaccara, S., Ries, R. J., and Jaffrey, S. R. (2019). Reading, Writing and Erasing mRNA Methylation. *Nat. Rev. Mol. Cell Biol.* 20 (10), 608–624. doi:10.1038/s41580-019-0168-5
- Zeng, D., Ye, Z., Wu, J., Zhou, R., Fan, X., Wang, G., et al. (2020). Macrophage Correlates with Immunophenotype and Predicts Anti-PD-L1 Response of Urothelial Cancer. *Theranostics* 10 (15), 7002–7014. doi:10.7150/thno.46176
- Zhang, B., Wu, Q., Li, B., Wang, D., Wang, L., and Zhou, Y. L. (2020). m6A Regulator-Mediated Methylation Modification Patterns and Tumor Microenvironment Infiltration Characterization in Gastric cancer. *Mol. Cancer* 19 (1), 53. doi:10.1186/s12943-020-01170-0
- Zhao, B. S., Roundtree, I. A., and He, C. (2017). Post-transcriptional Gene Regulation by mRNA Modifications. *Nat. Rev. Mol. Cell Biol.* 18 (1), 31–42. doi:10.1038/nrm.2016.132

Conflict of Interest: The authors declare that the research was conducted in the absence of any commercial or financial relationships that could be construed as a potential conflict of interest.

Publisher's Note: All claims expressed in this article are solely those of the authors and do not necessarily represent those of their affiliated organizations, or those of the publisher, the editors and the reviewers. Any product that may be evaluated in this article, or claim that may be made by its manufacturer, is not guaranteed or endorsed by the publisher.

Copyright © 2021 Du, Li, Li, Liu, Li, Dang, Chu, Yan, Fang, Wu, Zhang, Zhu and Li. This is an open-access article distributed under the terms of the Creative Commons Attribution License (CC BY). The use, distribution or reproduction in other forums is permitted, provided the original author(s) and the copyright owner(s) are credited and that the original publication in this journal is cited, in accordance with accepted academic practice. No use, distribution or reproduction is permitted which does not comply with these terms.



Transcriptome-Wide m6A Analysis Provides Novel Insights Into Testicular Development and Spermatogenesis in Xia-Nan Cattle

Shen-he Liu¹, Xiao-ya Ma², Ting-ting Yue³, Zi-chen Wang¹, Kun-long Qi¹, Ji-chao Li¹, Feng Lin¹, Hossam E. Rushdi⁴, Yu-yang Gao⁵, Tong Fu¹, Ming Li¹, Teng-yun Gao¹, Li-guo Yang⁶, Xue-lei Han^{1*} and Ting-xian Deng^{2*}

OPEN ACCESS

Edited by:

A. Rasim Barutcu,
University of Toronto, Canada

Reviewed by:

Jiangbo Wei,
University of Chicago, United States
Faizul Hassan,
University of Agriculture, Pakistan
Borhan Shokrollahi,
Islamic Azad University, Iran

*Correspondence:

Ting-xian Deng
dtx282000@163.com
Xue-lei Han
hxl014@126.com

Specialty section:

This article was submitted to
Epigenomics and Epigenetics,
a section of the journal
Frontiers in Cell and Developmental
Biology

Received: 08 October 2021

Accepted: 26 November 2021

Published: 22 December 2021

Citation:

Liu S-h, Ma X-y, Yue T-t, Wang Z-c,
Qi K-l, Li J-c, Lin F, Rushdi HE,
Gao Y-y, Fu T, Li M, Gao T-y, Yang L-g,
Han X-l and Deng T-x (2021)
Transcriptome-Wide m6A Analysis
Provides Novel Insights Into Testicular
Development and Spermatogenesis in
Xia-Nan Cattle.
Front. Cell Dev. Biol. 9:791221.
doi: 10.3389/fcell.2021.791221

¹College of Animal Science and Technology, Henan Agricultural University, Zhengzhou, China, ²Guangxi Provincial Key Laboratory of Buffalo Genetics, Breeding and Reproduction Technology, Buffalo Research Institute, Chinese Academy of Agricultural Sciences, Nanning, China, ³Henan Dairy Herd Improvement Co., Ltd, Zhengzhou, China, ⁴Department of Animal Production, Faculty of Agriculture, Cairo University, Giza, Egypt, ⁵Henan Dingyuan Cattle Breeding Co., Ltd., Wuhan, China, ⁶China Ministry of Education, Key Laboratory of Agricultural Animal Genetics, Breeding and Reproduction, College of Animal Science and Technology, Huazhong Agricultural University, Wuhan, China

Testis is the primary organ of the male reproductive tract in mammals that plays a substantial role in spermatogenesis. Improvement of our knowledge regarding the molecular mechanisms in testicular development and spermatogenesis will be reflected in producing spermatozoa of superior fertility. Evidence showed that N6-Methyladenosine (m6A) plays a dynamic role in post-transcription gene expression regulation and is strongly associated with production traits. However, the role of m6A in bovine testis has not been investigated yet. In this study, we conducted MeRIP-Seq analysis to explore the expression profiles of the m6A and its potential mechanism underlying spermatogenesis in nine bovine testes at three developmental stages (prepuberty, puberty and postpuberty). The experimental animals with triplicate in each stage were chosen based on their semen volume and sperm motility except for the prepuberty bulls and used for testes collection. By applying MeRIP-Seq analysis, a total of 8,774 m6A peaks and 6,206 m6A genes among the studied groups were identified. All the detected peaks were found to be mainly enriched in the coding region and 3' - untranslated regions. The cross-analysis of m6A and mRNA expression exhibited 502 genes with concomitant changes in the mRNA expression and m6A modification. Notably, 30 candidate genes were located in the largest network of protein-protein interactions. Interestingly, four key node genes (*PLK4*, *PTEN*, *EGR1*, and *PSME4*) were associated with the regulation of mammal testis development and spermatogenesis. This study is the first to present a map of RNA m6A modification in bovine testes at distinct ages, and provides new insights into m6A topology and related molecular mechanisms underlying bovine spermatogenesis, and establishes a basis for further studies on spermatogenesis in mammals.

Keywords: cattle, testis, m6A modification, spermatogenesis, semen quality, sequencing

INTRODUCTION

Xia-Nan (XN) cattle, the first specialized beef breed produced by the crossbreeding of French Charolais (male) and Nanyang cattle (female) in China, has important features including fast growth rate and high meat production performance. Enhancing the reproductive performance of XN cattle is an important breeding objective to increase the efficiency and sustainability of this breed as a major beef producer in the Chinese meat market. Testis, as a basic male reproductive organ, plays a critical role in spermatogenesis and steroidogenesis. Bull's fertility has been always considered a key issue for both cattle breeders and scientists. Different methods and common practices are traditionally used to check male reproductive performance, including a physical assessment of the bull (e.g., volume of the testicles) and semen evaluation (e.g., sperm morphology, concentration, and motility). Although these procedures offered a considerable background on testicular and epididymal function and quantitative production of sperms, infertility due to major reasons was not well recognized. Nowadays, molecular genetics techniques can efficiently target semen quality providing a powerful approach to evaluate the fertility potential of mammalian males (Puglisi et al., 2016; Vendelbo et al., 2021). Establishing an association between spermatogenesis and gene expression profile may enhance a better understanding of the causes of infertility. Improving the testicular function for acceptable production yield of high-quality semen (e.g., healthy spermatozoa) is still the basis for increasing the opportunity for the success rate of obtaining healthy offspring. Spermatogenesis can be divided into three major functional stages including the proliferative stage, meiosis, and maturation stage (Griswold, 2016). Notably, spermatogenesis is strictly regulated by the expression of stage-specific genes at both transcription and post-transcription levels (Ding et al., 2020). Thus, the testes at different developmental stages in XN cattle were taken as the experimental object in the present study, taking into consideration that identifying key regulators and signaling pathways related to testis development and spermatogenesis will provide valuable insights into improving semen quality.

N⁶-methyladenosine (m6A) is the most abundant internal RNA modification that has been recently suggested as a critical post-transcriptional mRNA regulator in most organisms, and is strongly associated with production traits (Shi et al., 2019; Zhang et al., 2020b; Xiong et al., 2021). In mammals, the RNA m6A modification is installed by a methyltransferase complex that mainly includes methyltransferase-like 3 (*METTL3*) and *METTL14*, which are responsible for catalyzing m6A modification (Liu et al., 2014). Wilms' tumor 1-associated protein (*WTAP*) is another essential member of the core component that interacts with *METTL3* and is required for its localization in the nucleus (Schwartz et al., 2014). RNA m6A modification can be removed by two known demethylases: AlkB homolog 5 (*ALKBH5*) (Zheng et al., 2013) and fat mass and obesity-associated factor (*FTO*) (Jia et al., 2011). RNA m6A modification affects almost all stages of RNA metabolism, like alternative splicing, RNA degradation, nuclear RNA export, and translation (Niu et al., 2013), and these influences can be

recognized by a category of proteins primarily composed of the YTH domain family (*YTHDF1-3*) and IGF2BPs (*IGF2BP1-3*) (Dominissini et al., 2012; Fu et al., 2014; Wang et al., 2014). Also, m6A modification can influence the spermatogenic function, for example, the combined deletion of *METTL3* and *METTL14* leads to impaired murine spermiogenesis (Lin et al., 2017). Moreover, m6A demethylase *ALKBH5* deficiency causes compromised spermatogenesis and apoptosis in mouse testis (Zheng et al., 2013). The *YTHDC2* is an m6A-binding protein gene and its knockout is related to infertile in mice (Hsu et al., 2017). Considering the various functions of m6A modification mentioned above in different species, it would seem logical to assume that m6A modification may also affect bovine testis development. During the last few years, continuously incremented works were carried out to investigate the mechanisms of spermatogenesis of cattle by comparative analysis of the gene expression associated with reproductive traits on the molecular level. However, little is known until now about the potential impacts of m6A modification on spermatogenesis in ruminants, in general, and there are no reports that document the association of m6A modification and bovine testis development in XN cattle, in specific.

Therefore, to identify the functional m6A and explore the spermatogenesis mechanism of the testes caused by the m6A RNA modification, we detected the m6A methylomes of bovine testes from birth to adulthood. This enabled us to obtain the transcriptome-wide m6A profiles in bovine testes at different stages and to provide reasonable insights into the roles of m6A modification in the mechanisms underlying spermatogenesis during post-natal testicular development.

MATERIALS AND METHODS

Experiment Design and Sample Collection

The main steps and bioinformatics used for data analysis in the present study is shown in **Supplementary Figure S1**. A total of sixty-nine clinically healthy XN cattle bulls from Kerchin Cattle Industry (Nanyang) Co., China was randomly selected. These animals were grouped into three groups based on their sexual maturity. The first group indicates the bulls are prepuberty (at birth, $n = 23$), the second group represents the bulls are puberty (about 1 year old showing heat for the first time, $n = 23$), and the last group represents the bulls are postpuberty (about 2 years of age, $n = 23$). In addition, the semen within 1 month of the bulls in puberty and postpuberty was taken by using artificial vagina. Sperm concentration was assessed using a haemocytometer (Bane, 1952). Sperm motility was evaluated based on the methods described (Björndahl et al., 2003). Further, the *t*-test was used to determine the significant difference levels of the semen quality parameters (semen volume, sperm motility and sperm concentration) between the puberty and postpuberty groups. For the puberty and postpuberty groups, the representative individuals of each group were selected in two ways: 1) the semen parameters existed significance differences between them; 2) the semen quality parameters closed to mean value for each group. In the prepuberty, the samples were

randomly chosen because the bulls have no semen parameters. Finally, a total of nine bulls (triplicate in each group) were selected based on the above-mentioned criterion. The selected animals were given general anesthesia (Zoletil 50, Virbac Co., France), a combination of zolazepam (5–9 mg/kg, i.m) and tiletamine, and xylazine hydrochloride (1.5–2 mg/kg, i.m) before sampling. Samples of the left testes were collected posterior to castration that performed by professional veterinarians. The length, width, and weight of the left testes were measured. Each testis was divided into three pieces and immediately subjected to snap-freezing in liquid nitrogen and stored at -80°C until RNA extraction.

RNA Isolation, Library Construction and Sequencing

Total RNA for each testis sample was isolated using the Trizol reagent (Invitrogen, CA, United States) following the manufacturer's protocols. The quality and quantity of total RNA were determined by Agilent Bioanalyzer 2100 system (Agilent Technologies Inc., CA, United States) and RNA 6000 Nano LabChip Kit (Agilent, Santa Clara, CA, United States) with RIN number >7.0 . Poly(A) RNA from total RNA was isolated with Arraystar Seq-Star™ poly(A) mRNA Isolation Kit (Arraystar, MD, United States). The RNA was further fragmented into fragments with an average length of 100 nt using RNA Fragmentation Reagents (Sigma, MO, United States). The fragmented RNA segments were divided into two groups. One group was used to perform m6A RNA immunoprecipitation (IP) using the GenSeq™ m6A RNA IP Kit (GenSeq Inc., China). The other group was utilized to construct the input samples without immunoprecipitation. The IP and input libraries were both constructed with NEBNext® Ultra II Directional RNA Library Prep Kit (New England Biolabs, Inc., MA, United States). The quality of all libraries was measured by the Agilent Bioanalyzer 2100 system (Agilent Technologies Inc., CA, United States). The sequencing of nine cDNA libraries was performed on the Illumina HiSeq™ 4000 by Gene Denovo Biotechnology Co., Ltd (Guangzhou, China). The raw data were deposited in the NCBI SRA database (BioProject ID: PRJNA776655).

Bioinformatics Analysis of m6A-Seq and RNA-Seq Data

TrimGalore v0.6.6 (Krueger, 2021) software was used to eliminate the reads containing adaptor contaminants, low-quality bases, and undetermined bases. Meanwhile, the sequence quality of IP and input of all samples were validated by the FASTP v0.20.1 (Chen et al., 2018) software. Subsequently, the high-quality clean reads were mapped to the *Bos taurus* reference genome (ARS-UCD1.2) by HISAT2 ver.2.1.0 (Kim et al., 2015) software with default parameters. Peak calling for mapped reads of IP and input libraries were performed using the exomePeak2 (Meng et al., 2014) package in R. The m6A intensity was visualized using the IGV software (<http://www.igv.org/>). The identified m6A peaks were carried out to conduct the motif enrichment analysis by

MEME (Bailey et al., 2009) and HOMER (Sven et al., 2010) software with default parameters. The ChIPseeker v1.0 (Guangchuang et al., 2015) software was used to annotate the called peaks by intersection with gene architecture. The differential m6A peaks [fold changes (FC) ≥ 2 and adjusted p -value < 0.05] between the pairwise comparison groups were analyzed using the exomePeak2 package in R. These differential peaks were annotated using the Ensembl database (*Bos taurus*/ARS-UCD1.2). Moreover, the expression level for all mRNAs from input libraries was calculated using StringTie ver. 1.3.5 (Pertea et al., 2016) software. The expression level of each transcript was normalized by the Trimmed Mean of M-values (TMM) implemented in the edgeR R-package. The differential expression analysis for pairwise contrasts was performed using the DESeq2 (Love et al., 2014) package in R. The adjusted p -value ≤ 0.05 and FoldChange > 1.5 were defined as the cutoff criteria for the differentially expressed mRNAs (DEGs). Gene enrichment analysis was performed by the Gene Ontology (GO) functional analysis and the Kyoto Encyclopedia of Genes and Genomics (KEGG) pathway enrichment using the KEGG Orthology-Based Annotation System (KOBAS) 3.0 with cutoff criteria of $p \leq 0.05$, aiming to identify their biological significance. The plot results were visualized using the ggplot2 (Wickham, 2016) package in R.

Quantitative Real-Time PCR Confirmation

Four differentially m6A methylated (DMGs) genes were selected and analyzed by qRT-PCR. Primers were designed using Primer 5.0 software (Supplementary Table S1) and synthesized by Sangon Biotech (Shanghai) Co. Ltd. RevertAid First Strand cDNA Synthesis Kit (Thermo Fisher Scientific, United States) was used to reverse transcribe the total RNAs into cDNA following the manufacturer's protocols. Then qPCR was conducted using QuantiNova SYBR Green PCR Kit (QIAGEN, Shanghai, China). The *GAPDH* gene was used for normalizing the relative abundance of genes. The $2^{-\Delta\Delta C_t}$ method (Livak and Schmittgen, 2001) was used to analyze the data for all samples in triplicate technical replicates.

Statistical Analysis

The data are expressed as mean \pm standard error of the mean (SEM). The student's t -test and one-way analysis of variance (ANOVA) was performed to determine the significance of the differences between the contrasting groups by using Graphpad Prism 8 software. Differences between means were considered statistically significant when adjusted pairwise comparison between means reached p -value ≤ 0.05 (Bonferroni).

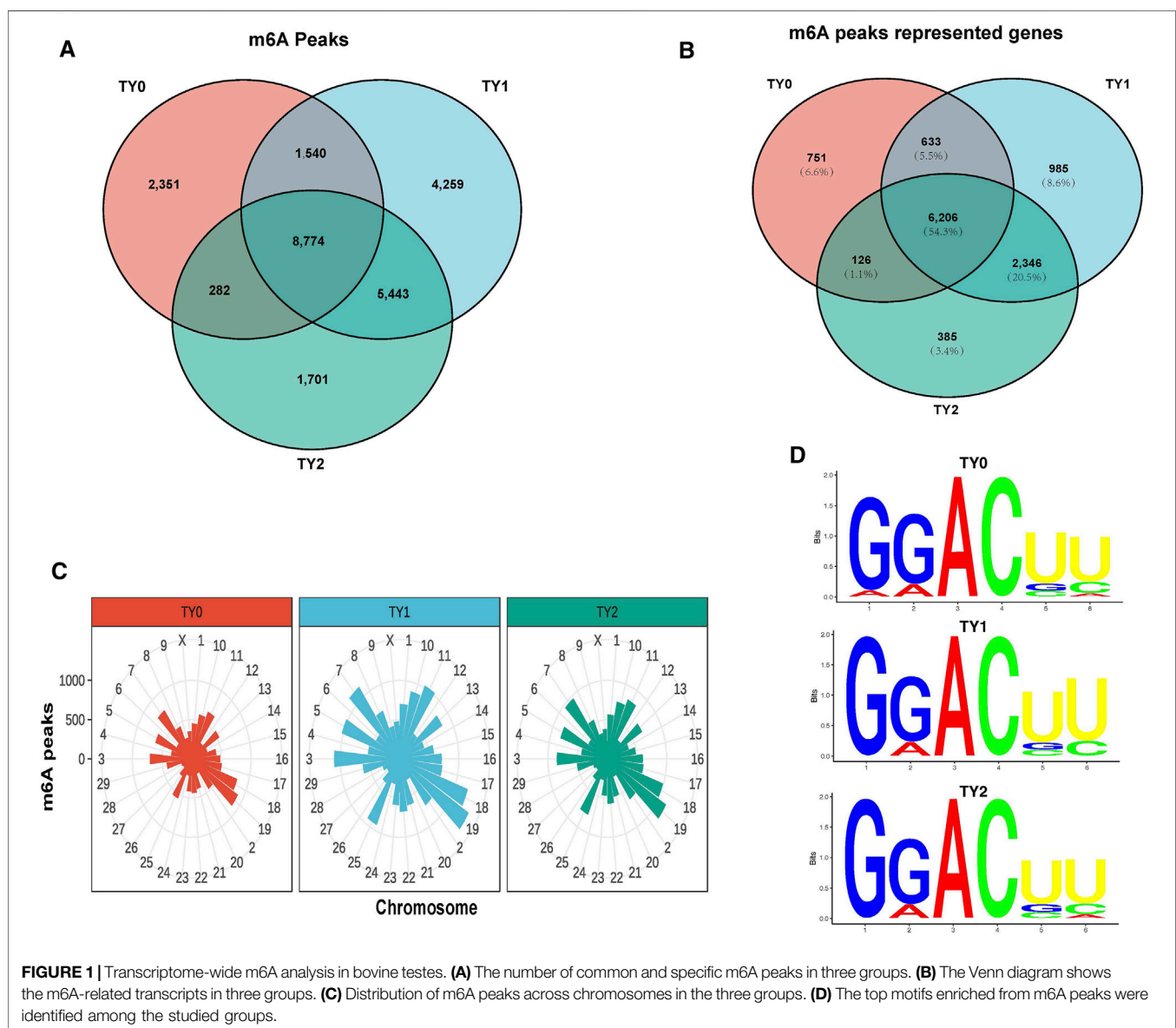
RESULTS

Testis Source Description

Semen quality parameters of the bulls in puberty and postpuberty, including the semen volume, sperm motility and sperm concentration were analyzed, and their results was listed in Table 1. Our data showed the semen volume and sperm motility in postpuberty were markedly higher ($p < 0.05$), while sperm concentration was not different as compared to bulls in

TABLE 1 | Evaluations of semen quality and testicular phenotypic parameters of XN bull testes at different ages (mean \pm SEM).

Indexes	Prepuberty	Groups ^a	
	prepuberty (<i>n</i> = 23)	Puberty (<i>n</i> = 23)	Postpuberty (<i>n</i> = 23)
Semen quality parameters			
Semen volume (ml)		4.96 \pm 0.26 ^b	6.21 \pm 0.23 ^c
Sperm motility (%)		0.61 \pm 0.02 ^b	0.67 \pm 0.01 ^c
Sperm concentration (billion/ml)		1.06 \pm 0.07	1.20 \pm 0.03
Physical attributed	TY0 (<i>n</i> = 3)	TY1 (<i>n</i> = 3)	TY2 (<i>n</i> = 3)
Weight (g)	4.84 \pm 0.89 ^b	168.73 \pm 5.04 ^c	322.81 \pm 12.34 ^d
Length (Cm)	4.07 \pm 0.46 ^b	9.97 \pm 0.68 ^c	13.27 \pm 0.44 ^d
Width (Cm)	1.70 \pm 0.15 ^b	5.73 \pm 0.09 ^c	7.23 \pm 0.23 ^d

^aTY0 = prepuberty; TY1 = puberty; TY2 = postpuberty.^bThe different superscript in the same row show significant differences ($p < 0.05$).^cThe different superscript in the same row show significant differences ($p < 0.05$).^dThe different superscript in the same row show significant differences ($p < 0.05$).**FIGURE 1** | Transcriptome-wide m6A analysis in bovine testes. **(A)** The number of common and specific m6A peaks in three groups. **(B)** The Venn diagram shows the m6A-related transcripts in three groups. **(C)** Distribution of m6A peaks across chromosomes in the three groups. **(D)** The top motifs enriched from m6A peaks were identified among the studied groups.

puberty. The **Supplementary Figure S2** further showed the detailed information on the semen volume, sperm motility and sperm concentration of bulls in puberty and postpuberty groups. Meanwhile, we selected six animals (three bulls for each group) to subsequently testes collection according to the principle that semen quality parameters closed to mean value. In addition, 3 bulls in prepuberty were randomly chosen.

For the above-selected 9 bulls, we measured their weight, length, and width of left testes, and their estimates are listed in **Table 1**. The results showed that all the tested testicular phenotypic parameters varied significantly ($p < 0.05$) among the groups studied. According to their semen quality and phenotypic difference, 9 testes samples of XN males at three developmental stages (prepuberty = TY0, in puberty = TY1, and postpuberty = TY2) were employed for further m6A-seq analysis. Each stage was in triplicate.

Transcriptome-Wide m6A-Seq Revealed m6A Modification Patterns During Testis Development

In the present study, the bull testes in prepuberty, puberty and postpuberty were used for m6A-Seq and RNA-Seq assays, with three replicates for each group. For the m6A-Seq, we obtained approximately 4.10 million raw reads for each sample, and about 3.39 million clean reads were mapped to the bovine reference genome for each animal (**Supplementary Table S2**). Regarding RNA-Seq, approximately 4.20 million raw reads for each individual were generated, and about 4.06 million valid reads were mapped to the reference genome for each individual (**Supplementary Table S2**). The proportions of mapped reads ranged from 86.39 to 97.12%, correspondingly (**Supplementary Table S2**). These results demonstrated that the high-quality sequence data obtained are proper to be used in subsequent analysis.

Using the exomePeak2 analysis, a total of 12,947, 20,016, and 16,200 m6A peaks were detected in the TY0, TY1, and TY2 groups, respectively (**Figure 1A**). Among them, a total of 2,351, 4,259, and 1,701 specific peaks were observed in the TY0, TY1, and TY2, respectively, reflecting the significant difference among the studied groups in total m6A modification trends. Likewise, a total of 7,716, 10,170, and 9,063 genes were annotated in the TY0, TY1, and TY2 groups, respectively (**Figure 1B**). In addition, 8,774 peaks were consistently observed in three groups, and 6,206 genes (54.3% of total genes) within the studied groups were modified by m6A.

Considering genome coverage pattern, the m6A distribution analysis revealed that the m6A peaks for each group differentially distributed on bovine chromosomes (**Figure 1C**). Most of the m6A peaks enriched in chromosome 19 in all studied groups. The motif analysis results indicated that the three studied groups had the classic m6A RRACH consensus sequences (**Figure 1D**). This enabled us to obtain the high credibility of the m6A peaks and revealed the presence of a prevailing methylated modification mechanism.

Analysis of m6A Modification Distribution in Testes Transcriptome

To investigate the preferential locations of m6A in transcripts, we explored the profiles of m6A peaks in the mRNA transcriptome by

coordinating the bovine reference genome. The transcript was divided into the following regions: the 5'untranslated regions (5'UTRs), near the start codon, CDS, near the stop codon, and the 3'untranslated regions (3'UTRs). The analysis revealed that enrichment of m6A modified peaks was highest in the CDS followed by the 3'UTRs, 5'UTRs, stop codon region, and start codon region in the studied groups (**Figure 2A**). The distribution of m6A peak density in each group exhibited similar trends (**Figure 2B**). In addition, we observed that the number of m6A modified peaks enriched in the CDS region was higher in the both puberty and postpuberty groups than in the prepuberty group, but the opposite trend was observed for enrichment near the stop codon. Thereafter, the enrichment degree of m6A peaks significantly varied among all the pairwise groups (p -value $< 2.21E-16$; **Figure 2C**). The distribution of m6A modified peaks with each gene was explored and it showed that almost >50% of affected genes hold only one m6A peak and the majority of genes harbored one to three m6A peaks (**Figure 2D**).

Differentially Methylated Gene Analysis

To explore the potential function of the m6A modification in bovine testes, a pairwise comparison was applied to scan the DMGs. Compared to the TY0 group, 2,495 significantly differential m6A peaks within 2,036 mRNAs were found in the TY1 group, while 2,047 differential peaks within 1,719 mRNAs were detected in the TY2 group (**Figure 3A**; **Supplementary Table S3**). In addition, we found 22 differential m6A peaks within 11 mRNAs in the TY2 group compared to the TY1 group. Several randomly selected mRNAs, including *SLU7*, *GOLGA7*, *METTL14*, and *TGFB1*, showed significantly hypermethylated peaks as presented in **Figure 3B**.

Moreover, the GO and KEGG enrichment analyses for all DMGs were performed to demonstrate the important function of m6A modification in bovine testes. GO analysis revealed that all the DMGs were mainly annotated into the nucleus, cytoplasm (ontology: cellular component), metal ion binding, RNA binding and ATP binding (ontology: molecular function), and protein ubiquitination, ubiquitin-dependent protein catabolic process (ontology: biological process) (**Figure 3C**). KEGG enrichment analysis demonstrated that the DMGs were significantly implicated with the MAPK signaling pathway, Herpes simplex virus 1 infection, Axon guidance, and FoxO signaling pathway, besides other methylated genes (**Figure 3D**).

RNA-Seq Identification of Differentially Expressed Genes

Using the RNA-Seq technique, a total of 8,280, 8,589, and 146 DEGs were detected between TY0 vs. TY1, TY0 vs. TY2, and TY1 vs. TY2, respectively (**Figure 4A**). Correspondingly, a set of 3,785, 4,001, and 77 up-regulated as well as 4,495, 4,588, and 69 down-regulated were found, respectively (**Figure 4B**). The hierarchical cluster expression pattern of the DEGs was shown in **Figure 4C**. Furthermore, all the DEGs were mainly enriched to 17 GO terms and 20 KEGG pathways (**Figure 4D**). Notably, most DEGs were highly annotated into the reproduction, reproductive process, multicellular organism reproduction, developmental

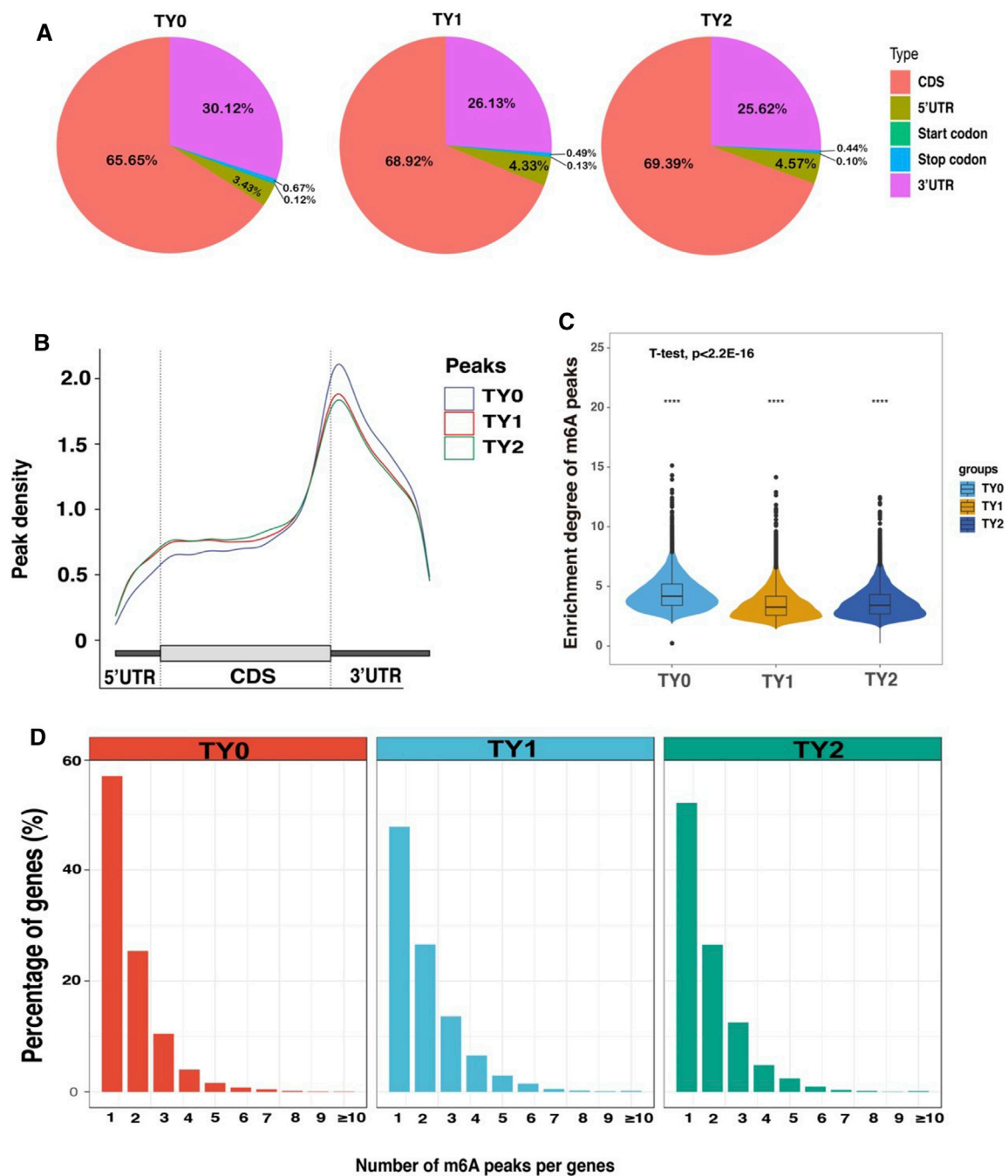


FIGURE 2 | Overview of m6A methylation profiles in bovine testes. **(A)** Pie charts demonstrating m6A peak distribution in the gene structures of mRNAs. **(B)** Metagene plots displaying the regions of m6A peaks identified across the transcripts in TY0, TY1, and TY2 groups. **(C)** Violin plot displays the distribution of enrichment degree of m6A peaks in each group. **(D)** The number of m6A peaks per gene in the TY0, TY1, and TY2 groups.

process involved in reproduction, sexual reproduction, spermatogenesis, male gamete generation (ontology: biological process) and motile cilium (ontology: cellular component) and calcium ion binding (ontology: molecular function) of GO

biological process. In addition, the PI3K-Akt signaling pathway is the most significant enrichment pathway for all DEGs identified, followed by MAPK signaling pathway and cAMP signaling pathway etc.

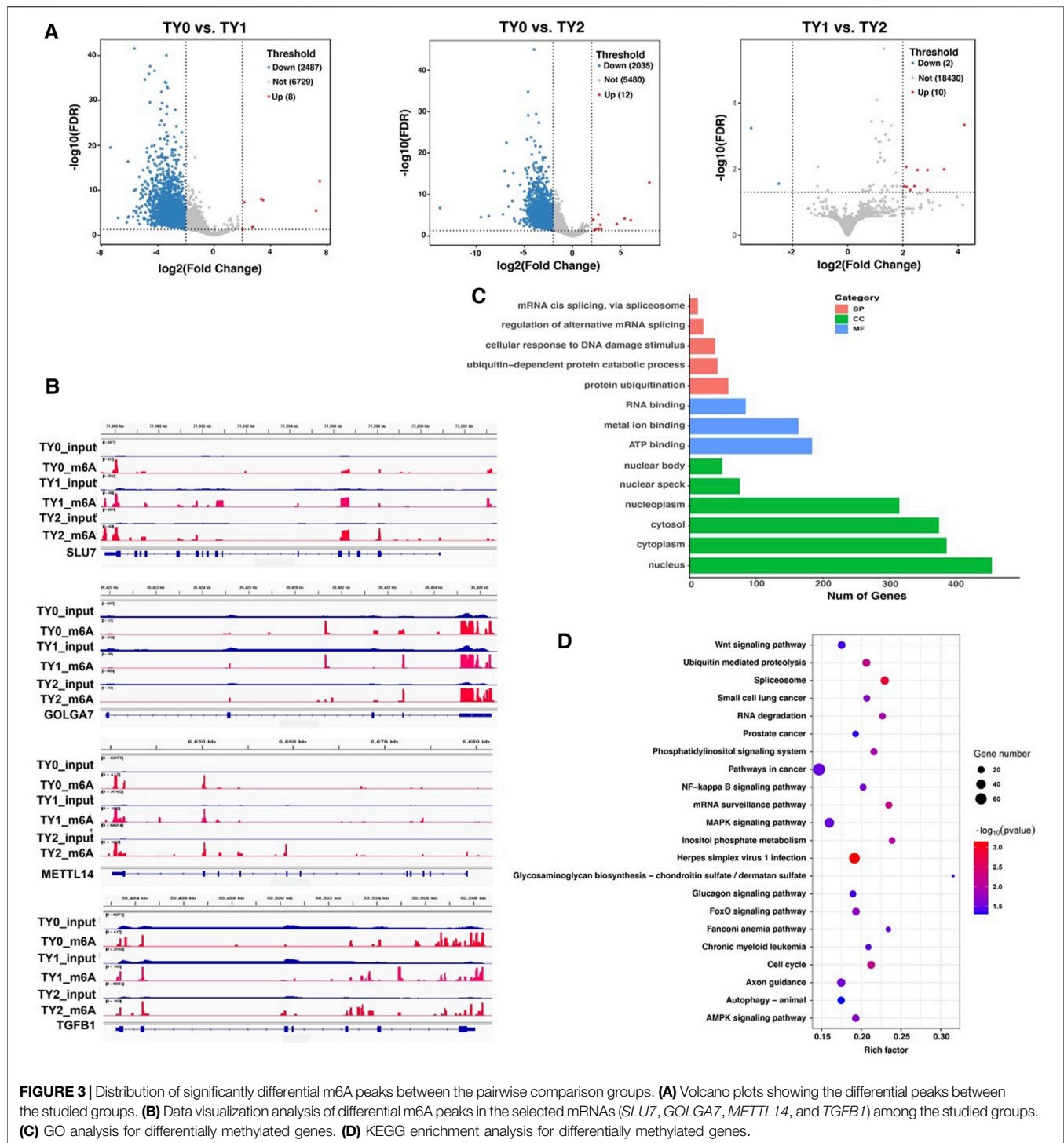
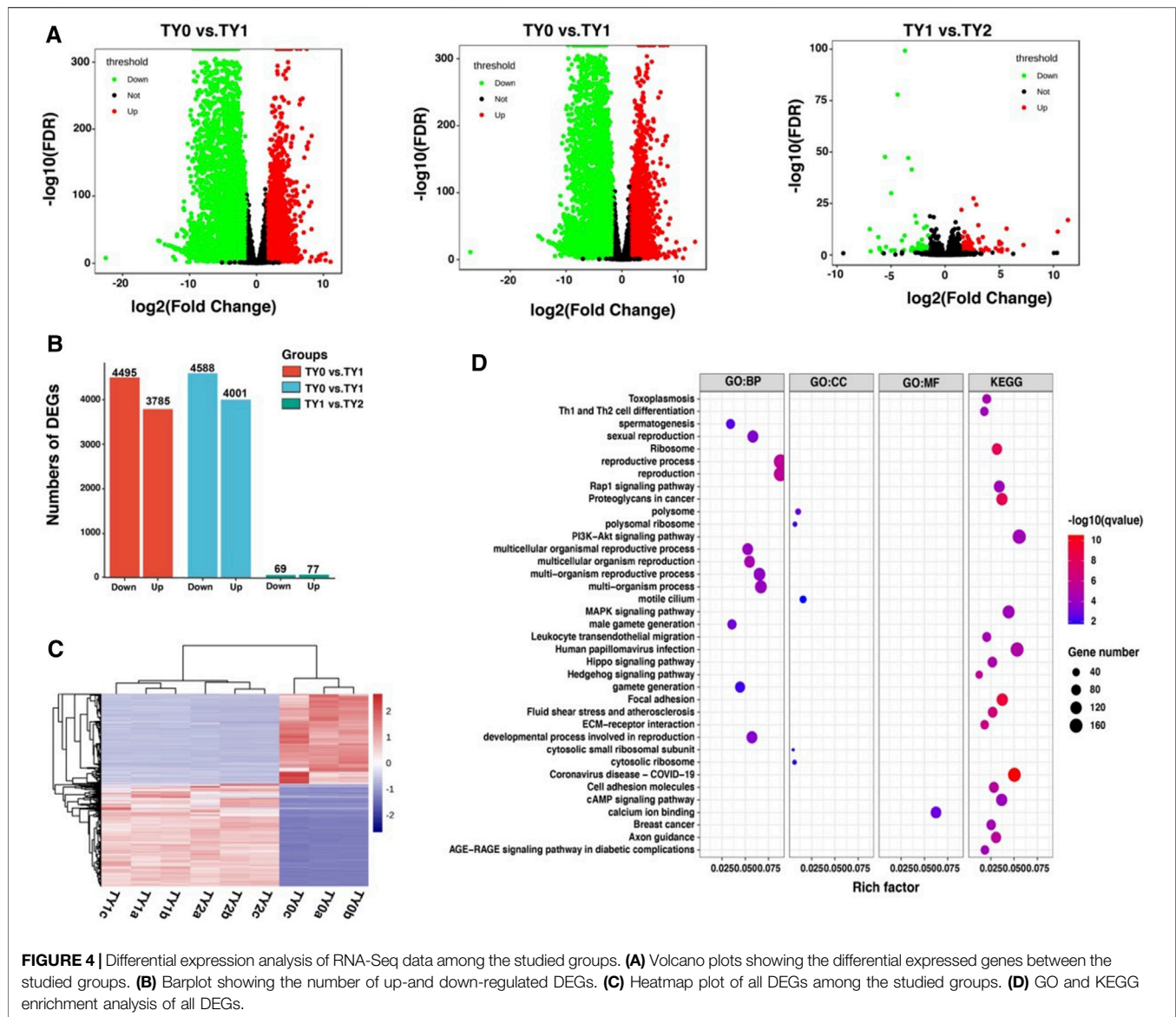


FIGURE 3 | Distribution of significantly differential m6A peaks between the pairwise comparison groups. **(A)** Volcano plots showing the differential peaks between the studied groups. **(B)** Data visualization analysis of differential m6A peaks in the selected mRNAs (*SLU7*, *GOLGA7*, *METTL14*, and *TGFB1*) among the studied groups. **(C)** GO analysis for differentially methylated genes. **(D)** KEGG enrichment analysis for differentially methylated genes.

Conjoint Analysis of m6A-Seq and RNA-Seq Data

To explore the potential relationship between m6A modification and gene expression, we performed a cross-analysis of the m6A-seq and RNA-seq data. As shown in **Figure 5A**, a positive correlation between differentially methylated peaks and gene

expression levels is obvious ($p = 0.0001$, Spearman $r = 0.1320$). Based on the principle that absolute value of both X and Y axes was greater than 2, the results of the four-quadrant diagram analysis revealed that there were 502 differentially methylated genes, of which 124 genes belonged to the hypo-up, 2 genes to the hyper-up, 368 genes to the hypo-down, and 8

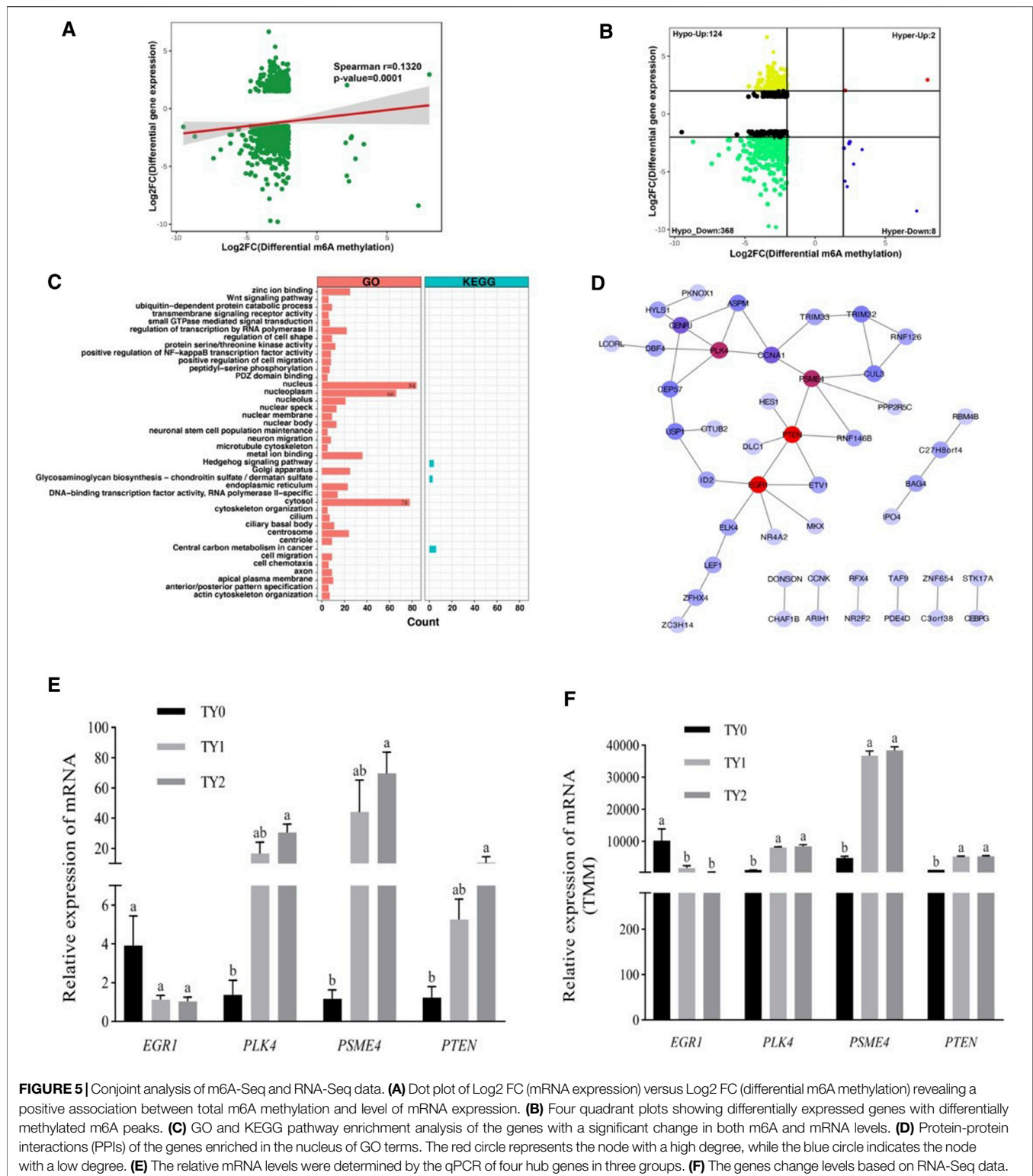


genes to the hyper-down quadrants (Figure 5B). Further, all of these genes were utilized for GO and KEGG pathway analyses (Figure 5C). Most of them were significantly enriched for 37 GO terms and 3 KEGG pathways. Interestingly, 84 genes were annotated into the nucleus of the GO term. The STRING analysis revealed that these genes were clustered into 8 PPIs networks (Figure 5D). Of them, 30 candidate genes were located in the largest PPIs network (Table 2). Further, 4 hub DMGs (*PLK4*, *PTEN*, *EGR1*, and *PSME4*) were selected and analyzed by RT-qPCR. The results of qPCR showed that the expression level of the 4 hub DMGs displayed a similar tendency with that of the RNA-Seq (Figures 5E,F). The above results suggested that these candidate genes may

have crucial roles in spermatogenesis during bovine testis development.

DISCUSSION

Improvement of our knowledge regarding the testis functions developments is vital for gaining our understating regard to the spermatogenesis process. The role of m6A modification influences the mechanisms underlying testis development and spermatogenesis. To our best knowledge, this work is the first comprehensive high-throughput study of RNA methylation in the testes of XN young calves and mature bulls. To explore the potential function of the m6A modification affecting



spermatogenesis, we specified three age points (TY0, TY1, and TY2) with significantly different physiological statuses in bovine testis development to analyze the transcriptome-wide m6A profile. The generated data in the present study displayed that

a diverse pattern of mRNA methylation have occurred over the testis development. These mRNA m6A sites were mainly concentrated around the CDS and 3'UTRs region (95.28%), in agreement with the distributional characteristics of the

TABLE 2 | List of 30 genes with significant changes in m6A and mRNA transcript abundance in bovine testes.

Gene	Symbol	Pattern	m6A level change				mRNA level change		
			Chr	Peak start	Peak end	diff.FC	diff.p	log2(FC)	Qvalue
ENSBTAG00000007860	ASPM	Hypo_Down	16	76,041,095	76,041,295	-2.340	0.010	-3.237	0.000
ENSBTAG00000007284	CCNA1	Hypo_Down	12	25,110,778	25,110,878	-2.405	0.000	-5.692	0.000
ENSBTAG000000017048	CENPJ	Hypo_Down	12	36,496,130	36,496,355	-4.685	0.000	-2.497	0.000
ENSBTAG000000016547	CEP57	Hypo_Down	15	14,448,587	14,448,637	-4.879	0.000	-3.235	0.000
ENSBTAG000000021769	CUL3	Hypo_Down	2	112,587,000	112,587,325	-3.625	0.000	-3.316	0.000
ENSBTAG000000014711	DBF4	Hypo_Down	4	32,288,748	32,288,948	-2.824	0.007	-3.584	0.000
ENSBTAG000000015541	DLC1	Hypo-Up	27	23,915,744	23,915,994	-2.733	0.000	2.021	0.000
ENSBTAG000000010069	EGR1	Hypo-Up	7	49,829,976	49,830,126	-2.566	0.007	2.527	0.000
ENSBTAG00000004953	ELK4	Hypo_Down	16	3,375,597	3,375,847	-2.808	0.000	-2.929	0.000
ENSBTAG000000015981	ETV1	Hypo_Down	4	22,100,027	22,100,077	-2.966	0.011	-2.703	0.000
ENSBTAG00000000569	HES1	Hypo-Up	1	73,362,983	73,363,058	-2.642	0.000	2.518	0.000
ENSBTAG000000010859	HYLS1	Hypo_Down	29	29,255,406	29,255,531	-3.612	0.000	-2.760	0.000
ENSBTAG000000021187	ID2	Hypo-Up	11	88,605,254	88,605,404	-2.933	0.005	2.841	0.000
ENSBTAG000000046561	LCORL	Hypo_Down	6	37,403,775	37,403,825	-6.199	0.001	-2.257	0.000
ENSBTAG000000006844	LEF1	Hyper-Down	6	17,083,863	17,084,113	3.340	0.000	-3.079	0.000
ENSBTAG000000007678	MXK	Hypo_Down	13	36,892,590	36,892,815	-2.628	0.017	-4.774	0.000
ENSBTAG000000003650	NR4A2	Hypo_Down	2	39,905,150	39,905,250	-3.755	0.001	-2.485	0.000
ENSBTAG000000014981	OTUB2	Hypo_Down	21	58,656,844	58,657,069	-4.620	0.000	-4.883	0.000
ENSBTAG000000014153	PKNOX1	Hypo_Down	1	143,202,058	143,202,108	-2.699	0.000	-2.689	0.000
ENSBTAG000000039552	PLK4	Hypo_Down	17	29,786,990	29,787,090	-6.151	0.000	-3.003	0.000
ENSBTAG000000020192	PPP2R5C	Hypo_Down	21	66,815,607	66,815,782	-2.345	0.000	-3.238	0.000
ENSBTAG000000020262	PSME4	Hypo_Down	11	36,573,366	36,573,416	-2.082	0.028	-3.020	0.000
ENSBTAG000000009498	PTEN	Hypo_Down	26	9,564,008	9,564,180	-3.981	0.000	-2.243	0.000
ENSBTAG000000014349	RNF126	Hypo_Down	7	43,262,899	43,262,949	-2.777	0.000	-2.273	0.000
ENSBTAG0000000034531	RNF146B	Hypo_Down	9	24,002,245	24,002,445	-2.178	0.000	-2.044	0.000
ENSBTAG000000017155	TRIM32	Hypo_Down	8	105,886,129	105,886,329	-2.293	0.000	-2.669	0.000
ENSBTAG0000000001499	TRIM33	Hypo_Down	3	28,977,136	28,977,286	-2.836	0.000	-2.356	0.000
ENSBTAG000000020451	USP1	Hypo_Down	3	83,118,601	83,118,801	-2.842	0.000	-2.755	0.000
ENSBTAG000000030453	ZC3H14	Hypo_Down	10	100,267,705	100,267,930	-3.124	0.000	-2.682	0.000
ENSBTAG000000033268	ZFXH4	Hypo_Down	14	40,040,613	40,040,713	-2.826	0.012	-2.833	0.000

Chr indicates the chromosome of cattle; diff.FC represents the differential log2 fold change estimates; diff.p indicates the differential p-values; FC represents Fold changes. All the data in diff.p and qvalue part are rounded.

mammalian transcriptomes (Wen et al., 2020). Our data showed that although the m6A peaks for each group markedly varied on different chromosomes, they had a highest expressed distribution in chromosome 19 within groups. The great differences in the genome coverage of reads among chromosomes observed in the present study may be attributed to the variation in the gene density of the bovine chromosomes. In addition, these m6A sites tended to occur in the conserved motif sequence “RRACH”, similar to that reported in other animals, such as the goat (Wang et al., 2020), sheep (Lu et al., 2019), and yak (Zhang et al., 2020a). This finding supported our hypothesis on the presence of a predominant methylated modification mechanism based on the m6A peaks identified.

In the study, a total of 2,278 unique DMGs were identified among all the pairwise groups. Differential m6A methylation has proved to be responsible for tissue or organ differentiation and development (Wen et al., 2020). Regarding the function and pathway of DMGs, we performed GO and KEGG enrichment analysis for DMGs. Importantly, GO analysis revealed that all the DMGs were mainly annotated into the nucleus, cytoplasm, metal ion binding, RNA binding, ATP binding, protein ubiquitination, and ubiquitin-dependent protein catabolic process. Earlier reports showed that metal ion binding was involved in porcine spermatogenesis (Luo et al., 2015) and horse testis development

(Han et al., 2020). A growing body of evidence supports the fact that protein ubiquitination also has a critical role in the regulation of spermatogenesis in testes of the mouse (Guo et al., 2021) and buffalo (Huang et al., 2020; Zhang et al., 2021). Similarly, RNA binding was also essential for spermatogenesis (Venables and Eperon, 1999; Paronetto and Sette, 2010; Jan et al., 2017). Moreover, KEGG enrichment analysis revealed that the DMGs were significantly implicated in the MAPK signaling pathway, Herpes simplex virus 1 infection, Axon guidance, and FoxO signaling pathway. Ni et al. (2019) found that the MAPK signaling pathway regulates dynamics of tight junctions and adherents junctions, proliferation, and meiosis of germ cells, proliferation and lactate production of Sertoli cells. Accumulating evidence has demonstrated that the FoxO signaling pathway was involved in the regulation of spermatogenesis process (Huang et al., 2016b; Ge et al., 2019; Hu et al., 2021). Therefore, above GO terms and pathways results suggested that the DMGs identified were related to bovine testis development and spermatogenesis process.

Likewise, our results showed that there are 8,952 unique DEGs were observed among all the pairwise groups. We observed that most DEGs were highly annotated into the reproduction, reproductive process, multicellular organism reproduction, developmental process involved in reproduction, sexual

reproduction, spermatogenesis, male gamete generation (ontology: biological process) of the GO biological process, indicating that the identified DEGs in the present study were reliable. Notably, the PI3K-Akt signaling pathway was found to be the most significant enrichment pathway for all DEGs. Many studies have demonstrated that the PI3K-Akt signaling pathway was involved in the regulation of spermatogenesis (Duan et al., 2016; Deng et al., 2020; Ni et al., 2020). In brief, our findings suggested that the DEGs were strongly associated with the testis development and spermatogenesis.

A surprising finding was that the enrichment degree of m6A peaks (Figure 2C), intensity of the DMGs (Figure 4A) and DEGs (Figure 5A) exhibited marked differences between before (TY0) and after puberty (TY1 and TY2 groups), suggesting that m6A modification and their gene expression mainly involved in the bovine testicular development and spermatogenesis. To further explore the potential genes underlying bovine testis development and spermatogenesis, the integrated analysis of m6A-Seq and mRNA-Seq data were performed. Results revealed that a positive correlation existed in differentially methylated peaks and gene expression levels, and 502 genes with concomitant changes in the mRNA expression and m6A modification. Interestingly, 84 genes were annotated into the nucleus of GO term, of which 30 candidate genes were located in the largest PPIs network. Importantly, four key node genes (*PLK4*, *PTEN*, *EGR1*, and *PSME4*) were observed on the largest PPIs network. Notably, the results of qPCR also supported that the expression level of the 4 selected DMGs exhibited marked differences between before and after puberty, which displayed a similar tendency with that of the RNA-Seq. These results indicated the putative role of these four genes in bovine testis development and spermatogenesis. It was noted that the four genes have already been reported to regulate the mammalian testis development and spermatogenesis. For example, the *PLK4* gene was highly expressed in testes during both pre- and post-natal stages and had a role in the initiation of spermatogenesis (Harris et al., 2011). Moreover, Miyamoto et al. (2016) reported that a mutation in *PLK4* causing azoospermia in a man with Sertoli cell-only syndrome. Dorostghoal et al. (2020) found that sperm *miR-26a-5p* and its target *PTEN* transcript content may contribute to the etiology of male infertility in unexplained infertile patients. More specifically, Neirijnck et al. (2019) reported that ablation of the *PTEN* appears dispensable for Sertoli cell proliferation and spermatogenesis, where inactivation of *PTEN* gene in the absence of *Insr* and *Igf1r* rescued the Sertoli cell proliferation rate during late fetal development, testis size, and sperm production. Besides, the *EGR1* gene has a role in maintaining spermatogonia stem cells' self-renewal and is a target to better understand the molecular basis of spermatogenesis (Sisakhtnezhad and Heshmati, 2018). Also, the *EGR1* gene can act as an activator of the sex-determining region Y box 18 promoter (Petrovic et al., 2010). Additionally, the loss of *PSME4* gene led to a marked reduction in male fertility, due to defects in spermatogenesis observed in meiotic spermatocytes and also during the maturation of postmeiotic haploid spermatids (Khor et al., 2006). Huang et al. (2016a) reported that the double knockout of *PSME3* and *PSME4* genes in mice resulted in completely

infertile males. These findings suggested that m6A modifications play an essential role during bovine testis development and spermatogenesis.

CONCLUSION

We identified 8,774 m6A peaks and 6,206 m6A genes among the studied groups by using MeRIP-Seq analysis. The cross-analysis of m6A and mRNA expression revealed 502 genes with concomitant changes in the mRNA expression and m6A modification. Further, 30 candidate genes were found to be located in the largest network of protein-protein interactions. Notably, four key node genes (*PLK4*, *PTEN*, *EGR1*, and *PSME4*) have been implicated in the regulation of mammalian testis development and spermatogenesis. The present study is pioneer to present a map of RNA m6A modification in bovine testes at different ages, and provides novel insights into m6A topology and associated molecular mechanisms underlying bovine spermatogenesis, and provides a basis for future research on mammalian testis development and spermatogenesis.

DATA AVAILABILITY STATEMENT

The datasets presented in this study can be found in online repositories. The names of the repository/repositories and accession number(s) can be found below: NCBI SRA; PRJNA776655.

ETHICS STATEMENT

The animal study was reviewed and approved by the Henan Agricultural University Animal Care and Use Committee. Written informed consent was obtained from the owners for the participation of their animals in this study.

AUTHOR CONTRIBUTIONS

S-HL, T-TY, Z-CW and Y-YG collected the phenotype data and testes tissue samples. S-HL, X-YM and T-TY isolated RNA. T-XD, S-HL, H-ER and X-YM, created and carried out the analysis, interpreted the data. S-HL, H-ER and T-XD wrote the manuscript. T-XD, S-HL, and X-LH developed the study and participated in its design and coordination. J-CL, K-LQ, TF, ML, FL, T-YG and L-GY reviewed the paper. All authors read and approved the manuscript.

FUNDING

This work was supported by the China Agriculture Research System of MOF and MARA and China Postdoctoral Science Foundation (2020M672233) and Henan Key Research and Development Program (192102110067).

ACKNOWLEDGMENTS

The authors thank Kerchin Cattle Industry (Nanyang) Co., Ltd. (China) for providing experimental animals and biological samples.

REFERENCES

- Bailey, T. L., Boden, M., Buske, F. A., Frith, M., Grant, C. E., Clementi, L., et al. (2009). MEME Suite: Tools for Motif Discovery and Searching. *Nucleic Acids Res.* 37 (Web Server issue), W202–W208. doi:10.1093/nar/gkp335
- Bane, A. (1952). A Study on the Technique of Hemocytometric Determination of Sperm Motility and Sperm Concentration in Bull Semen. *Cornell Vet.* 42 (4), 518–531. doi:10.1016/0035-9203(51)90016-8
- Björndahl, L., Söderlund, I., and Kvist, U. (2003). Evaluation of the One-step Eosin-Nigrosin Staining Technique for Human Sperm Vitality Assessment. *Hum. Reprod.* (4), 813–816. doi:10.1093/humrep/deg199
- Chen, S., Zhou, Y., Chen, Y., and Gu, J. (2018). Fastp: an Ultra-fast All-In-One FASTQ Preprocessor. *Bioinformatics* 34 (17), i884–i890. doi:10.1093/bioinformatics/bty560
- Deng, C.-Y., Lv, M., Luo, B.-H., Zhao, S.-Z., Mo, Z.-C., and Xie, Y.-J. (2020). The Role of the PI3K/AKT/mTOR Signalling Pathway in Male Reproduction. *Curr. Mol. Med.* 21 (7), 539–548. doi:10.2174/1566524020666201203164910
- Ding, H., Liu, M., Zhou, C., You, X., Su, T., Yang, Y., et al. (2020). Integrated Analysis of miRNA and mRNA Expression Profiles in Testes of Duroc and Meishan Boars. *BMC Genomics* 21 (1), 686. doi:10.1186/s12864-020-07096-7
- Dominissini, D., Moshitch-Moshkovitz, S., Schwartz, S., Salmon-Divon, M., Ungar, L., Osenberg, S., et al. (2012). Topology of the Human and Mouse m6A RNA Methylomes Revealed by m6A-Seq. *Nature* 485 (7397), 201–206. doi:10.1038/nature11112
- Dorstghoal, M., Galehdari, H., Moramezi, F., and Danyari, R. (2020). Sperm miR-26a-5p and its Target PTEN Transcripts Content in Men with Unexplained Infertility. *Andrologia* 8 (5), 1167–1173. doi:10.1111/andr.12801
- Duan, P., Quan, C., Huang, W. T., and Yang, K. D. (2016). PI3K-Akt/LKB1-AMPK-mTOR-p70S6K/4EBP1 Signaling Pathways Participate in the Regulation of Testis Development and Spermatogenesis: An Update. *Zhonghua Nan Ke Xue* 22 (11), 1016–1020. doi:10.13263/j.cnki.nja.2016.11.011
- Fu, Y., Dominissini, D., Rechavi, G., and He, C. (2014). Gene Expression Regulation Mediated through Reversible m6A RNA Methylation. *Nat. Rev. Genet.* 15 (5), 293–306. doi:10.1038/nrg3724
- Ge, P., Zhang, J., Zhou, L., Lv, M. Q., Li, Y. X., Wang, J., et al. (2019). CircRNA Expression Profile and Functional Analysis in Testicular Tissue of Patients with Non-obstructive Azoospermia. *Reprod. Biol. Endocrinol.* 17 (1), 100. doi:10.1186/s12958-019-0541-4
- Griswold, M. D. (2016). Spermatogenesis: The Commitment to Meiosis. *Physiol. Rev.* 96 (1), 1–17. doi:10.1152/physrev.00013.2015
- Guo, Y., Zhang, H., Yao, L., Li, Y., Situ, C., Sha, J., et al. (2021). Systematic Analysis of the Ubiquitome in Mouse Testis. *Proteomics*.
- Han, H., Chen, Q., Gao, Y., Li, J., Li, W., Dang, R., et al. (2020). Comparative Transcriptomics Analysis of Testicular miRNA from Cryptorchid and Normal Horses. *Animals (Basel)* 10 (2). doi:10.3390/ani10020338
- Harris, R. M., Weiss, J., and Jameson, J. L. (2011). Male Hypogonadism and Germ Cell Loss Caused by a Mutation in Polo-Like Kinase 4. *Endocrinology* 152 (10), 3975–3985. doi:10.1210/en.2011-1106
- Heinz, S., Benner, C., Spann, N., Bertolino, E., Lin, Y. C., Laslo, P., et al. 2010. Simple Combinations of Lineage-Determining Transcription Factors Prime Cis-Regulatory Elements Required for Macrophage and B Cell Identities. *Mol. Cell* 38(4):576–589. doi:10.1016/j.molcel.2010.05.004
- Hsu, P. J., Zhu, Y., Ma, H., Guo, Y., Shi, X., Liu, Y., et al. (2017). Ythdc2 Is an N6-Methyladenosine Binding Protein that Regulates Mammalian Spermatogenesis. *Cell Res* 27 (9), 1115–1127. doi:10.1038/cr.2017.99
- Hu, T., Luo, S., Xi, Y., Tu, X., Yang, X., Zhang, H., et al. (2021). Integrative Bioinformatics Approaches for Identifying Potential Biomarkers and Pathways Involved in Non-obstructive Azoospermia. *Transl. Androl. Urol.* 10 (1), 243–257. doi:10.21037/tau-20-1029
- Huang, L., Haratake, K., Miyahara, H., and Chiba, T. (2016a). Proteasome Activators, PA28γ and PA200, Play Indispensable Roles in Male Fertility. *Sci. Rep.* 6, 23171. doi:10.1038/srep23171
- Huang, P., Zhou, Z., Shi, F., Shao, G., Wang, R., Wang, J., et al. (2016b). Effects of the IGF-1/PTEN/Akt/FoxO Signaling Pathway on Male Reproduction in Rats Subjected to Water Immersion and Restraint Stress. *Mol. Med. Rep.* 14 (6), 5116–5124. doi:10.3892/mmr.2016.5880
- Huang, Y. L., Zhang, P. F., Hou, Z., Fu, Q., Li, M. X., Huang, D. L., et al. (2020). Ubiquitome Analysis Reveals the Involvement of Lysine Ubiquitination in the Spermatogenesis Process of Adult buffalo (Bubalus Bubalis) Testis. *Biosci. Rep.* 40. doi:10.1042/BSR20193537
- Jan, S. Z., Vormer, T. L., Jongejan, A., Röling, M. D., Silber, S. J., de Rooij, D. G., et al. (2017). Unraveling Transcriptome Dynamics in Human Spermatogenesis. *Development* 144 (20), 3659–3673. doi:10.1242/dev.152413
- Jia, G., Fu, Y., Zhao, X., Dai, Q., Zheng, G., Yang, Y., et al. (2011). N6-Methyladenosine in Nuclear RNA Is a Major Substrate of the Obesity-Associated FTO. *Nat. Chem. Biol.* 7 (12), 885–887. doi:10.1038/nchembio.687
- Khor, B., Bredemeyer, A. L., Huang, C.-Y., Turnbull, I. R., Evans, R., Maggi, L. B., et al. (2006). Proteasome Activator PA200 Is Required for normal Spermatogenesis. *Mol. Cell. Biol.* 26 (8), 2999–3007. doi:10.1128/mcb.26.8.2999-3007.2006
- Kim, D., Langmead, B., and Salzberg, S. L. (2015). HISAT: a Fast Spliced Aligner with Low Memory Requirements. *Nat. Methods* 12 (4), 357–360. doi:10.1038/nmeth.3317
- Krueger, F. (2021). Trim Galore! in. Available at: https://www.bioinformatics.babraham.ac.uk/projects/trim_galore/.
- Lin, Z., Hsu, P. J., Xing, X., Fang, J., Lu, Z., Zou, Q., et al. (2017). Mettl3-/Mettl14-mediated mRNA N6-Methyladenosine Modulates Murine Spermatogenesis. *Cel Res* 27 (10), 1216–1230. doi:10.1038/cr.2017.117
- Liu, J., Yue, Y., Han, D., Wang, X., Fu, Y., Zhang, L., et al. (2014). A METTL3-METTL14 Complex Mediates Mammalian Nuclear RNA N6-Adenosine Methylation. *Nat. Chem. Biol.* 10 (2), 93–95. doi:10.1038/nchembio.1432
- Livak, K. J., and Schmittgen, T. D. (2001). Analysis of Relative Gene Expression Data Using Real-Time Quantitative PCR and the 2-ΔΔCT Method. *Methods* 25 (4), 402–408. doi:10.1006/meth.2001.1262
- Love, M. I., Huber, W., and Anders, S. (2014). Moderated Estimation of Fold Change and Dispersion for RNA-Seq Data with DESeq2. *Genome Biol.* 15 (12), 550. doi:10.1186/s13059-014-0550-8
- Lu, Z., Ma, Y., Li, Q., Liu, E., Jin, M., Zhang, L., et al. (2019). The Role of N6-Methyladenosine RNA Methylation in the Heat Stress Response of Sheep (*Ovis aries*). *Cell Stress and Chaperones* 24 (2), 333–342. doi:10.1007/s12192-018-00965-x
- Luo, Z., Liu, Y., Chen, L., Ellis, M., Li, M., Wang, J., et al. (2015). microRNA Profiling in Three Main Stages during Porcine Spermatogenesis. *J. Assist. Reprod. Genet.* 32 (3), 451–460. doi:10.1007/s10815-014-0406-x
- Meng, J., Lu, Z., Liu, H., Zhang, L., Zhang, S., Chen, Y., et al. (2014). A Protocol for RNA Methylation Differential Analysis with MeRIP-Seq Data and exomePeak R/Bioconductor Package. *Methods* 69 (3), 274–281. doi:10.1016/j.jmeth.2014.06.008
- Miyamoto, T., Bando, Y., Koh, E., Tsujimura, A., Miyagawa, Y., Iijima, M., et al. (2016). APLK4 mutation Causing Azoospermia in a Man with Sertoli Cell-Only Syndrome. *Andrology* 4 (1), 75–81. doi:10.1111/andr.12113
- Neirijnck, Y., Kühne, F., Mayère, C., Pavlova, E., Sararols, P., Foti, M., et al. (2019). Tumor Suppressor PTEN Regulates Negatively Sertoli Cell Proliferation, Testis Size, and Sperm Production In Vivo. *Endocrinology* 160 (2), 387–398. doi:10.1210/en.2018-00892
- Ni, F.-D., Hao, S.-L., and Yang, W.-X. 2020. Molecular Insights into Hormone Regulation via Signaling Pathways in Sertoli Cells: With Discussion on Infertility and Testicular Tumor. *Gene* 753: 144812. doi:10.1016/j.gene.2020.144812

SUPPLEMENTARY MATERIAL

The Supplementary Material for this article can be found online at: <https://www.frontiersin.org/articles/10.3389/fcell.2021.791221/full#supplementary-material>

- Ni, F. D., Hao, S. L., and Yang, W. X. (2019). Multiple Signaling Pathways in Sertoli Cells: Recent Findings in Spermatogenesis. *Cell Death Dis* 10, 541. doi:10.1038/s41419-019-1782-z
- Niu, Y., Zhao, X., Wu, Y.-S., Li, M.-M., Wang, X.-J., and Yang, Y.-G. (2013). N6-methyl-adenosine (m6A) in RNA: An Old Modification with A Novel Epigenetic Function. *Genomics, Proteomics & Bioinformatics* 11 (1), 8–17. doi:10.1016/j.gpb.2012.12.002
- Paronetto, M. P., and Sette, C. (2010). Role of RNA-Binding Proteins in Mammalian Spermatogenesis. *Int. J. Androl.* 33 (1), 2–12. doi:10.1111/j.1365-2605.2009.00959.x
- Pertea, M., Kim, D., Pertea, G. M., Leek, J. T., and Salzberg, S. L. (2016). Transcript-level Expression Analysis of RNA-Seq Experiments with HISAT, StringTie and Ballgown. *Nat. Protoc.* 11 (9), 1650–1667. doi:10.1038/nprot.2016.095
- Petrovic, I., Kovacevic-Grujicic, N., and Stevanovic, M. (2010). Early Growth Response Protein 1 Acts as an Activator of SOX18 Promoter. *Exp. Mol. Med.* 42 (2), 132–142. doi:10.3858/em.2010.42.2.015
- Puglisi, R., Gaspa, G., Balduzzi, D., Severgnini, A., Vanni, R., Macciotta, N., et al. (2016). Genomewide Analysis of Bull Sperm Quality and Fertility Traits. *Reprod. Dom Anim.* 51 (5), 840–843. doi:10.1111/rda.12747
- Schwartz, S., Mumbach, M. R., Jovanovic, M., Wang, T., Maciag, K., Bushkin, G. G., et al. (2014). Perturbation of m6A Writers Reveals Two Distinct Classes of mRNA Methylation at Internal and 5' Sites. *Cel Rep.* 8 (1), 284–296. doi:10.1016/j.celrep.2014.05.048
- Shi, H., Wei, J., and He, C. (2019). Where, when, and How: Context-dependent Functions of RNA Methylation Writers, Readers, and Erasers. *Mol. Cel* 74 (4), 640–650. doi:10.1016/j.molcel.2019.04.025
- Sisakhtnezhad, S., and Heshmati, P. (2018). Comparative Analysis of Single-cell RNA Sequencing Data from Mouse Spermatogonial and Mesenchymal Stem Cells to Identify Differentially Expressed Genes and Transcriptional Regulators of Germline Cells. *J. Cel Physiol* 233 (7), 5231–5242. doi:10.1002/jcp.26303
- Venables, J., and Eperon, I. (1999). The Roles of RNA-Binding Proteins in Spermatogenesis and Male Infertility. *Curr. Opin. Genet. Dev.* 9 (3), 346–354. doi:10.1016/s0959-437x(99)80052-5
- Vendelbo, N. M., Mahmood, K., Sarup, P., Kristensen, P. S., Orabi, J., and Jahoor, A. (2021). Genomic Scan of Male Fertility Restoration Genes in a 'Gülzow' Type Hybrid Breeding System of Rye (*Secale Cereale* L.). *Int. J. Mol. Sci.* 22 (17). doi:10.3390/ijms22179277
- Wang, X., Lu, Z., Gomez, A., Hon, G. C., Yue, Y., Han, D., et al. (2014). N6-methyladenosine-dependent Regulation of Messenger RNA Stability. *Nature* 505 (7481), 117–120. doi:10.1038/nature12730
- Wang, Y., Zheng, Y., Guo, D., Zhang, X., Guo, S., Hui, T., et al. (2020). m6A Methylation Analysis of Differentially Expressed Genes in Skin Tissues of Coarse and Fine Type Liaoning Cashmere Goats. *Front. Genet.* 10, 1318. doi:10.3389/fgene.2019.01318
- Wen, K., Zhang, Y., Li, Y., Wang, Q., and Sun, J. (2020b). Comprehensive Analysis of Transcriptome-wide m6A Methylome in the Anterior Capsule of the Lens of High Myopia Patients. *Epigenetics*, 1–14. doi:10.1080/15592294.2020.1834917
- Wickham, H. (2016). *ggplot2: Elegant Graphics for Data Analysis*. Springer.
- Xiong, X., Hou, L., Park, Y. P., Molin, B., Ardlie, K. G., Aguet, F., et al. (2021). Genetic Drivers of m6A Methylation in Human Brain, Lung, Heart and Muscle. *Nat. Genet.* 53 (8), 1156–1165. doi:10.1038/s41588-021-00890-3
- Yu, G., Wang, L. G., and He, Q. Y. (2015). ChIPseeker: an R/Bioconductor Package for ChIP Peak Annotation, Comparison and Visualization. *Bioinformatics* 31 (14), 2382–2383. doi:10.1093/bioinformatics/btv145
- Zhang, P. f., Huang, Y. l., Fu, Q., He, W. t., Xiao, K., and Zhang, M. (2021). Integrated Analysis of Phosphoproteome and Ubiquitylome in Epididymal Sperm of buffalo (*Bubalus Bubalis*). *Mol. Reprod. Dev.* 88 (1), 15–33. doi:10.1002/mrd.23432
- Zhang, Y., Liang, C., Wu, X., Pei, J., and Yan, P. (2020a). *Integrated Study of Transcriptome-wide m6A Methylome Confirms a Potential Mechanism for Transcriptional Regulation during Yak Adipocytes Differentiation*.
- Zhang, Z., Luo, K., Zou, Z., Qiu, M., Tian, J., Sieh, L., et al. (2020b). Genetic Analyses Support the Contribution of mRNA N6-Methyladenosine (m6A) Modification to Human Disease Heritability. *Nat. Genet.* 52, 939–949. doi:10.1038/s41588-020-0644-z
- Zheng, G., Dahl, J. A., Niu, Y., Fedorcsak, P., Huang, C.-M., Li, C. J., et al. (2013). ALKBH5 Is a Mammalian RNA Demethylase that Impacts RNA Metabolism and Mouse Fertility. *Mol. Cel* 49 (1), 18–29. doi:10.1016/j.molcel.2012.10.015

Conflict of Interest: T-tY was employed by Henan Dairy Herd Improvement Co., Ltd., Y-yG was employed by Henan Dingyuan Cattle Breeding Co., Ltd.

The remaining authors declare that the research was conducted in the absence of any commercial or financial relationships that could be construed as a potential conflict of interest.

Publisher's Note: All claims expressed in this article are solely those of the authors and do not necessarily represent those of their affiliated organizations, or those of the publisher, the editors and the reviewers. Any product that may be evaluated in this article, or claim that may be made by its manufacturer, is not guaranteed or endorsed by the publisher.

Copyright © 2021 Liu, Ma, Yue, Wang, Qi, Li, Lin, Rushdi, Gao, Fu, Li, Gao, Yang, Han and Deng. This is an open-access article distributed under the terms of the Creative Commons Attribution License (CC BY). The use, distribution or reproduction in other forums is permitted, provided the original author(s) and the copyright owner(s) are credited and that the original publication in this journal is cited, in accordance with accepted academic practice. No use, distribution or reproduction is permitted which does not comply with these terms.



Current Advances in N6-Methyladenosine Methylation Modification During Bladder Cancer

Qiang Liu*

Department of Urology, Cancer Hospital of China Medical University, Liaoning Cancer Hospital and Institute, Shenyang, China

N6-methyladenosine (m6A) is a dynamic, reversible post-transcriptional modification, and the most common internal modification of eukaryotic messenger RNA (mRNA). Considerable evidence now shows that m6A alters gene expression, thereby regulating cell self-renewal, differentiation, invasion, and apoptotic processes. M6A methylation disorders are directly related to abnormal RNA metabolism, which may lead to tumor formation. M6A methyltransferase is the dominant catalyst during m6A modification; it removes m6A demethylase, promotes recognition by m6A binding proteins, and regulates mRNA metabolic processes. Bladder cancer (BC) is a urinary system malignant tumor, with complex etiology and high incidence rates. A well-differentiated or moderately differentiated pathological type at initial diagnosis accounts for most patients with BC. For differentiated superficial bladder urothelial carcinoma, the prognosis is normally good after surgery. However, due to poor epithelial cell differentiation, BC urothelial cell proliferation and infiltration may lead to invasive or metastatic BC, which lowers the 5-years survival rate and significantly affects clinical treatments in elderly patients. Here, we review the latest progress in m6A RNA methylation research and investigate its regulation on BC occurrence and development.

Keywords: N6-methyladenosine, “writers”, “erasers”, “readers”, methylation, bladder cancer

OPEN ACCESS

Edited by:

Yicheng Long,
Cornell University, United States

Reviewed by:

Kunqi Chen,
Fujian Medical University, China

*Correspondence:

Qiang Liu
lq174906097@outlook.com

Specialty section:

This article was submitted to
Epigenomics and Epigenetics,
a section of the journal
Frontiers in Genetics

Received: 30 November 2021

Accepted: 22 December 2021

Published: 11 January 2022

Citation:

Liu Q (2022) Current Advances in N6-Methyladenosine Methylation Modification During Bladder Cancer. *Front. Genet.* 12:825109. doi: 10.3389/fgene.2021.825109

INTRODUCTION

Bladder cancer (BC) is one of the most common malignant tumors of the urinary system; it ranks first among urological tumors in terms of incidence rate, and is the 9th highest incidence cancer in the world (Lenis et al., 2020; Li et al., 2021a). In recent years, BC treatment strategies have improved such that surgical resection combined with radiotherapy or chemotherapy are highly effective treatments (Jain et al., 2021; Tran et al., 2021). However, while immunotherapy has demonstrated strong prospects for solid tumor treatment, it remains to be clinically applied to BC (Afonso et al., 2020; van Puffelen et al., 2020; Wu and Abraham 2021). Immunotherapy is limited as it inhibits non-

Abbreviations: m6A, N6-methyladenosine; mRNA, messenger RNA; 3'UTR, 3'untranslated region; snRNA, small nuclear RNA; APC, adenomatous polyposis coli; METTL3, methyltransferase 3, N6-adenosine-methyltransferase complex catalytic subunit; METTL14, methyltransferase 14, N6-adenosine-methyltransferase subunit; WTAP, WT1 associated protein; VIRMA, vir like m6A methyltransferase associated; RBM15, RNA binding motif protein 15; ZC3H13, zinc finger CCCH-type containing 13; CBL1, Cbl proto-oncogene like 1; FTO, FTO alpha-ketoglutarate dependent dioxygenase; ALKBH5, alkB homolog 5, RNA demethylase; YTHDC1/2, YTH domain containing 1/2; YTHDF1/2/3, YTH N6-methyladenosine RNA binding protein 1/2/3; IGF2BP1/2/3, insulin like growth factor 2 mRNA binding protein 1/2/3.

muscular and muscular invasive BC at the laboratory level (Schneider et al., 2019; Witjes et al., 2021). For patients with non-muscle invasive tumors (NMIBC), transurethral resection combined with postoperative bladder perfusion chemotherapy or BCG treatment strategies is usually adopted (Charpentier et al., 2021; Li et al., 2021e). However, 20–30% of NMIBC patients will progress to muscle invasive bladder cancer (MIBC), and 50% will develop distant metastases within 2 years of radical surgery (Jiang et al., 2021a; Liu et al., 2021a). For locally advanced or advanced MIBC patients, gemcitabine combined with cisplatin (GC regimen) remains the standard treatment, however, BC fatality rates have only dropped by 1.5% in the past 15 years (Kaur et al., 2021; Roviello et al., 2021). Due to its high recurrence and metastasis rate, the 5-years survival rate for patients with MIBC remains very low (Meeks et al., 2020; Patel et al., 2020; Jiang et al., 2021a). Therefore, while novel treatment strategies must be explored and BC molecular mechanisms clarified, recent evidence has suggested that m6A mechanisms actively participate in BC (Mu et al., 2021).

N6-methyladenosine (m6A) is one of the most common internal transcription modifications in eukaryotic messenger RNA (mRNA) (Huang et al., 2021; Oerum et al., 2021). The molecule was first identified in the 1970s, but recent studies have shown that m6A-associated mutations are closely related to BC occurrence (Liu et al., 2021b). In 2011, the fat-mass and obesity-associated protein (FTO) was reported to have functions in m6A demethylase and suggested that m6A modification was dynamically reversible (Zheng et al., 2020; Gu et al., 2021a; Tan et al., 2021; Zhao et al., 2021). Studies have since summarized the related modifications of m6A as methyltransferase complexes, demethylases, and corresponding readers coordinated regulation, which are classified as “writers,” “erasers,” and “readers,” respectively (Tang et al., 2021). M6A is abundant in 3′ untranslated regions (UTRs), stop codons, and long exon regions. The process has a high degree of evolutionary conservation, but with unclear biological functions (Yao et al., 2021; Zhao et al., 2021). M6A is co-catalyzed by the methylation modification enzymes, METTL3 and METTL14. Also, WTAP and KIAA1429 function as m6A regulators to participate in catalytic processes (Wu et al., 2020; He and He 2021). Interestingly, the METTL3-METTL14 complex is more potent than individual components in catalyzing m6A formation (Song et al., 2021a; Uddin et al., 2021). M6A methylation is also demethylated by the FTO and AlkB homolog 5 (ALKBH5) demethylases (Ye et al., 2021). M6A modification is involved in all mRNA metabolic processes, including maturation, transport, splicing, translation, and degradation (Song et al., 2020; Li et al., 2021b; Li et al., 2021c; Lou et al., 2021). M6A RNA methylation exerts critical biological functions in mammals, such as tissue development, circadian rhythms, DNA damage responses, gender identification, and tumor occurrence and development (Xu et al., 2020a; Li et al., 2020; Ma and Ji 2020; Gu et al., 2021b; Wu and Wang 2021). In this review, we discuss the potential mechanisms of m6A methylation-related regulators in BC initiation and development.

M6A METHYLATION REGULATORS

M6A modification adds a methyl group to the N6 position of adenosine and is an evolutionarily conserved RNA modification (Han and Choe 2020; Zhang et al., 2020; Zhou et al., 2020). Approximately 0.3% of adenosine in mRNA is modified by m6A, with an average of three m6A modification sites in every transcript. M6A methylation mainly occurs in RRACH sequences (where R = A or G, H = A, C, or U), stop codons, 3′UTRs, and internal long exons, to regulate RNA transcription, processing, translation, and metabolism (Huang et al., 2020a; Chen and Wong 2020; Liang et al., 2020; Scarrow et al., 2020). The modification is controlled by m6A regulatory enzymes, amongst which, methyltransferases or m6A “writers” actively catalyze modifications, m6A “erasers,” with demethylase activity, eliminate m6A modifications, and m6A “readers” recognize modification (He et al., 2019; Huang et al., 2020b; Lee et al., 2020; Zhao et al., 2020) bases and convey information, thereby establishing an efficient and orderly m6A regulatory network (**Figure 1**).

The methyltransferase complex primarily includes methyltransferase-like 3 (METTL3), METTL14, vir like m6A methyltransferase associated (VIRMA), RNA binding motif protein 15 (RBM15), zinc finger CCCH-type containing 13 (ZC3H13), Cbl proto-oncogenes like 1 (CBLL1), and Wilm’s tumor 1-associated protein (WTAP). All proteins co-ordinate and regulate m6A control (Chen et al., 2019a; Ma et al., 2019; Williams et al., 2019). METTL3 functions as a core component where METTL14 combines with it to form a stable heterodimer to catalyze m6A RNA methylation *via* synergistic effects (Chen et al., 2019b; Yue et al., 2019). WTAP anchors the METTL3/14 complex on target RNA and promotes its nuclear accumulation (Lan et al., 2019; Liu et al., 2019). The KIAA1429-RBM15 complex was recently verified as a new component of the m6A “writer” complex, while RBM15 recruits the complex to target sites (Niu et al., 2018; Wang et al., 2018). METTL16 is also a novel m6A molecule targeting U6 small nuclear RNA (snRNA) and regulates S-adenosylmethionine homeostasis by elevating S-adenosylmethionine synthase expression during methionine starvation (Frye et al., 2018; Yang et al., 2018; Zhang 2018).

M6A demethylases include FTO and ALKBH5. FTO was identified as regulating steady-state energy levels and positively correlating with obesity risk (Deng et al., 2018a; Huang and Yin 2018). ALKBH5 is a homolog of FTO, and belongs to the Fe²⁺ and α -ketoglutarate-dependent AlkB oxygenase family (Deng et al., 2018b; Dai et al., 2018). FTO and ALKBH5 both recognize m6A-modified nuclear RNA as a substrate, and catalyze the removal of m6A methyl modifications (Meyer and Jaffrey 2017; Wang et al., 2017).

M6A reading proteins are divided into three categories: proteins contain an evolutionarily conserved YTH domain which folds into a hydrophobic aromatic structure directly binding to m6A (Liao et al., 2018; Patil et al., 2018). YTH domain proteins are composed of YTHDF (YTHDF1, YTHDF2, and YTHDF3) and YTHDC subtypes (YTHDC1 and YTHDC2). YTHDF subtype proteins are mainly distributed in the cytoplasm.

Heterogeneous nuclear ribonucleoproteins (hnRNPs) mainly include three types, namely hnRNPC, hnRNPG, and

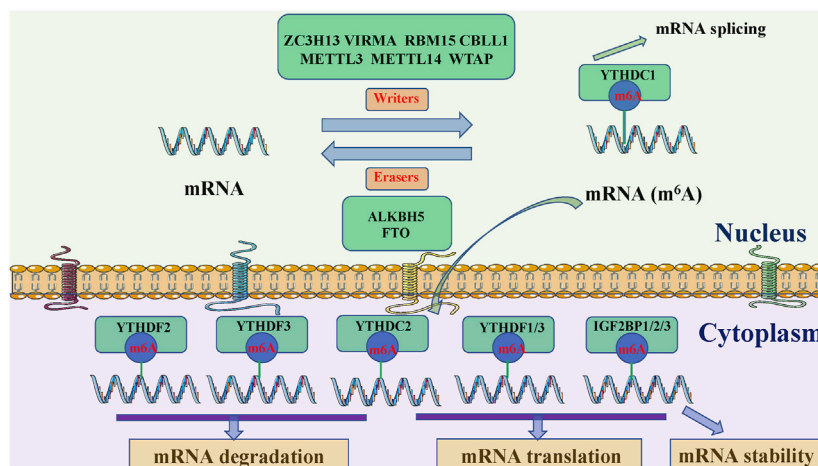


FIGURE 1 | Potential m6A methylation mechanisms in RNA. M6A methylation is catalyzed by the writer complex, including METTL3, METTL14, WTAP, VIRMA, RBM15, ZC3H13, and CBL1. The demethylases, FTO and ALKBH5 remove m6A modifications. Reader proteins (YTHDC1, YTHDF2, YTHDF3, YTHDC2, YTHDF1/3, and IGF2BP1/2/3) recognize m6A and determine target RNA targets. METTL3, methyltransferase 3, N6-adenosine-methyltransferase complex catalytic subunit; METTL14, methyltransferase 14, N6-adenosine-methyltransferase subunit; WTAP, WT1 associated protein; VIRMA, vir like m6A methyltransferase associated; RBM15, RNA binding motif protein 15; ZC3H13, zinc finger CCH-type containing 13; CBL1, Cbl proto-oncogene like 1; FTO, FTO α -ketoglutarate dependent dioxygenase; ALKBH5, alkB homolog 5, RNA demethylase; YTHDC1/2, YTH domain containing 1/2; YTHDF1/2/3, YTH N6-methyladenosine RNA binding protein 1/2/3; IGF2BP1/2/3, insulin like growth factor 2 mRNA binding protein 1/2/3.

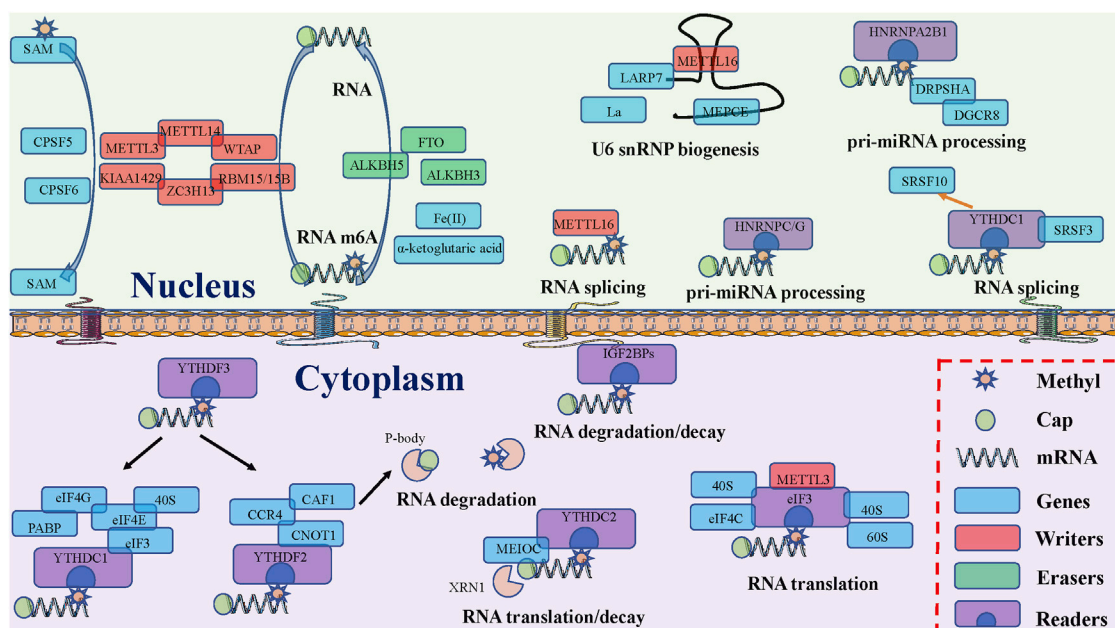


FIGURE 2 | The potential functions of RNA m6A modification related proteins. “Writers,” “Erasers,” and “Readers” rely on several crucial factors to install, remove, and recognize m6A modifications and participate in various RNA metabolism steps, including splicing, export, translation, degradation, and decay.

hnRNP2B1. The “m6A switch” phenomenon disrupts RNA hairpin structures and exposes single-stranded hnRNP binding motifs (Aguilo and Walsh 2017; Wu et al., 2017). These proteins bind to transcripts containing m6A via the m6A switch, thereby affecting mRNA localization and alternative splicing (Batista 2017; Roignant and Soller 2017).

Insulin-like growth factor 2 mRNA-binding proteins 1–3 (IGF2BP1–3) also recognize the GGC (m6A) sequences via the K homology domain, and enhance the stability and translation of downstream mRNAs in an m6A-dependent manner under normal and stress conditions (Adhikari et al., 2016).

M6A ROLES AND DISEASE MECHANISMS

The potential roles and mechanisms of m6A-related regulators are shown (Figure 2).

M6A Methyltransferases

RNA m6A methylation is controlled by METTL3, METTL14, WTAP, RBM15, RBM15B, and Cbl proto-oncogene E3, and is catalyzed by methyltransferase complexes composed of CBL1, VIRMA, and ZC3H13. Of these proteins, METTL3 and METTL14 exhibit m6A methyltransferase activity (Zhou et al., 2021a; Maldonado Lopez and Capell 2021; Pan et al., 2021). WTAP promotes m6A function by recruiting METTL3 and METTL14 into nuclear speckles (Deng et al., 2021). RBM15 and RBM15B bind METTL3 and WTAP and guides them to specific RNA sites for m6A modification (Meng et al., 2021). VIRMA preferentially mediates mRNA methylation near 3'UTR and stop codon regions (Zhu et al., 2021a). ZC3H13, together with other cofactors such as WTAP, control nuclear m6A methylation (Zhou et al., 2021b).

METTL16 is a novel RNA methyltransferase that independently induces the m6A modification of the 3'UTR of mRNAs (Satterwhite and Mansfield 2021), which have crucial roles in maintaining mRNA stability and splicing. M6A methyltransferases also display carcinogenic roles in several cancers. METTL3-induced miR-222-3p up-regulation suppresses STK4 and promotes malignant behaviors in thyroid carcinoma cells (Lin et al., 2021). METTL3 also up-regulates the m6A modification of adenomatous polyposis coli (APC), leading to its mRNA degradation. Decreased APC increases β -catenin, cyclin D1, c-Myc, and PKM2 expression, resulting in mouse aerobic glycolysis, cell proliferation, and enhanced esophageal squamous cell carcinoma (ESCC) formation (Wang et al., 2021a). METTL3 also induces PLX4032 resistance to melanoma by promoting m6A-dependent EGFR translation (Bhattacharai et al., 2021). METTL14 also aggravates podocyte injury and glomerulopathy progression via N-methyladenosine-dependent Sirt1 down-regulation (Lu et al., 2021). METTL14 promotes glomerular endothelial cell injury and diabetic nephropathy via m6A modification of the α -klotho protein (Li et al., 2021d). METTL16 promotes cell proliferation by up-regulating cyclin D1 expression in gastric cancer (Wang et al., 2021b). WTAP up-regulation reduces PERP levels via m6A modification, which in turn promotes pancreatic cancer growth and metastasis (Wang et al., 2020a). WTAP expression is significantly increased in HCC and promotes liver cancer development. WTAP-guided m6A modifications may also promote HCC progression via the HuR-ETS1-p21/p27 regulatory axis (Chen et al., 2019c).

M6A Demethyltransferase

RNA m6A methylation is a reversible process, with its demethylation reliant on demethylases. FTO catalyzes m6A demethylation and displays strict substrate selectivity near alternatively spliced exons and poly-A sites (Lan et al., 2020; Jiang et al., 2021b; He and He 2021). ALKBH5 functions with FTO to ensure balanced m6A modifications in the transcriptome

(Chen et al., 2021a; Purslow et al., 2021; Wu et al., 2021). ALKBH3 was identified as another m6A demethylase with easier binding to tRNA m6A sites than mRNA or rRNA sites (Esteve-Puig et al., 2021; Wollen et al., 2021). FTO expression is increased in breast cancer and promotes cell growth and metastasis (Niu et al., 2019). FTO also mediates m6A demethylation in the 3'UTR of BNIP3 mRNA and induces its degradation via a YTHDF2 independent manner. The FTO-mediated epigenetic up-regulation of LINC00022 also promotes tumorigenesis in ESCCs (Cui et al., 2021). ALKBH5-HOXA10 loop-mediated JAK2 m6A demethylation causes cisplatin resistance in epithelial ovarian cancer (Nie et al., 2021). ALKBH5 promotes the cadmium-induced transformation of human bronchial epithelial cells by regulating PTEN expression in an m6A-dependent manner (Li et al., 2021e). ALKBH5 was also identified in cell and animal models as related to patient prognoses and the suppression of esophageal cancer malignancies. The protein also demethylates pri-miR-194-2 and inhibits it in an m6A/DGCR8-dependent manner (Chen et al., 2021b).

M6A Binding Proteins

M6A modifications exert biological functions by binding to m6A-binding proteins (Dai et al., 2021; Tsuchiya et al., 2021). YTHDF1 knockout reduces the overall level of IFN-induced A-to-I RNA editing, thereby activating the Double stranded RNA sensing pathway and promoting IFN-stimulated gene expression (Terajima et al., 2021). YTHDF1 deficiency also inhibits viral replication in cells by modulating IFN responses. YTHDF2 inhibits cardiac hypertrophy through a Myh7 mRNA decoy in an m6A-dependent manner (Xu et al., 2021). YTHDF1 also correlates with the immune microenvironment and predicts clinical outcomes and therapeutic efficacy in breast cancer (Hu et al., 2021). YTHDF1 and YTHDF2 are associated with better patient survival rates and an inflamed tumor-immune microenvironment in non-small-cell lung cancer (Tsuchiya et al., 2021). Highly expressed YTHDF3 promotes cancer cell interactions with brain endothelial cells and astrocytes, blood-brain barrier extravasation, angiogenesis, and growth (Chang et al., 2020). Mechanistically, YTHDF3 enhances the translation of m6A-rich ST6GALNAC5, GJA1, and EGFR transcripts. MiR-30d is a new target modified by YTHDC1 via m6A, with miR-30d inhibiting pancreatic tumors by inhibiting aerobic glycolysis (Hou et al., 2021). YTHDC2 contains an RNA helicase domain, recognizes m6A methylated adenosine at nucleotide 331, and cooperates with the cellular La antigen to support HCV IRES-dependent translation (Kim and Siddiqui 2021).

M6A ROLES AND MECHANISMS IN BC

Recent studies reported that m6A-modified mRNA is dysregulated in several cancers, with *in vivo* and *in vitro* anti-cancer effects identified. Dysregulated m6A-related factors may alter m6A modifications in tumors and interfere with cancer

TABLE 1 | The role of RNA m6A modification in bladder cancer.

Type	m6A regulator	Role in cancer	Biological function	Mechanism	References
m6A writer	METTL3	Oncogene	Promotes cell growth and invasion	METTL3/AFF4/NF-κB/MYC	Lan et al. (2020)
	METTL3	Oncogene	Promotes malignant transformation and tumorigenesis	METTL3-m6A-CDCP1	Purslow et al. (2021)
	METTL3	Oncogene	Promotes cell proliferation	METTL3-DGCR8-PTEN	Chen et al. (2021b)
				METTL3/pri-miR221/222	
	METTL3	Oncogene	Promotes cancer proliferation and metastasis	METTL3/YTHDF2/SETD7/KLF4	Wu et al. (2021)
	METTL3	Oncogene	Promotes bladder cancer development	METTL3-m6A-CDCP1	Wollen et al. (2021)
	METTL3	Oncogene	Promotes oncogenesis and tumor angiogenesis	METTL3/TEK/VEGF-A	Esteve-Puig et al. (2021)
	METTL3 METTL14	Oncogene Tumor suppressor	Promotes tumor proliferation and metastasis Inhibits the proliferation, self-renewal, metastasis and tumor initiating capacity of bladder TICs	cisplatin/METTL3/G-CSF METTL14/m6A/NOTCH1	Niu et al. (2019) Cui et al. (2021)
m6A eraser	METTL14	Tumor suppressor	Inhibits cell invasion	ISO/FOXO3a/METTL14/Vimentin	Nie et al. (2021)
	FTO	Tumor suppressor	Inhibits cell proliferation and invasion	—	Li et al.(2021b)
	FTO	Oncogene	Promotes cancer initiation and progression	UPS18/FTO/PYCR1	Dai et al. (2021)
	FTO	Oncogene	Stimulates cell viability and tumorigenicity	FTO/MALAT/miR-384/MAL2	Tsuchiya et al. (2021)
	ALKBH5	Tumor suppressor	Inhibits bladder cancer growth and progression	ALKBH5/ITGA6/YTHDF1/3	Terajima et al. (2021)
m6A reader	ALKBH5	Tumor suppressor	Inhibits cell proliferation, migration, invasion and increases cisplatin chemosensitivity	ALKBH5/m6A/CK2a	Xu et al. (2021)
	YTHDF1/3	Oncogene	Promotes bladder cancer growth and progression	METTL3/ITGA6/YTHDF1/3	Hu et al. (2021)
	YTHDF2	Oncogene	Promotes cancer proliferation and metastasis	METTL3/YTHDF2/SETD7/KLF4	Chang et al. (2021)
	IGF2BP1	Oncogene	Promotes bladder cancer cell invasion, metastasis and cell cycle progression	circPTPRA/IGF2BP1/FSCN1- MYC	Hou et al. (2021)
	IGF2BP3	Oncogene	Promotes cell proliferation, cell cycle and inhibit apoptosis	IGF2BP3/JAK/STAT	Kim and Siddiqui (2021)

progression. In the following sections, we summarize m6A regulatory factor roles in BC (Table 1).

M6A Modification of Related Protein Expression Up-Regulates METTL3 in BC

METTL3 was the first discovered methyltransferase and forms a complex with METTL14 and WTAP to promote RNA methylation. METTL3 in human tissue is highly expressed and conserved, especially in the testes. Recent studies reported that METTL3 is significantly highly expressed in chronic myeloid leukemia (Ianniello et al., 2021), thymic epithelial tumors (Iaiza et al., 2021), esophageal cancer (Han et al., 2021), and prostate cancer (Chen et al., 2021b), suggesting a close relationship with malignant tumor development. Previous studies also suggested that METTL3 is significantly up-regulated in BC. METTL3 knockdown significantly reduces BC proliferation, invasion, and survival rates *in vitro*, and tumorigenicity *in vivo*. In contrast, METTL3 overexpression promotes BC cell growth and invasion (Cheng et al., 2019). AF4/FMR2 are two critical regulators of the NF-κB pathway (IKBKB and RELA) and MYC and were verified as downstream targets of METTL3-mediated m6A modification. Yang et al. reported that METTL3 and CDCP1 were up-regulated in BC tissue, and their expression

levels were interrelated with respect to BC progression (Yang et al., 2019). METTL3-m6A-CDCP1 axis repression inhibits the growth and progression of chemically transformed and BC cells. This axis and chemical carcinogens exert a synergistic impact on promoting the malignant transformation of urothelial cells and BC occurrence. Han et al. (2019) indicated that METTL3 exerts carcinogenic effects in BC by interacting with DGCR8 and positively regulating pri-miR221/222 processes in an m6A-dependent manner. Xie et al. (2020) discovered that the tumor-promoting functions and specific regulatory mechanisms of the m6A axis are composed of the core “writer” protein, METTL3 and the main “reading” protein, YTHDF2. METTL3 consumption damages cancer proliferation and metastasis. The METTL3/YTHDF2 m6A axis directly degrades the mRNA of the tumor suppressors, SETD7 and KLF4 and promotes BC development. Ying et al. (2020) showed that the RCas9-METTL3 system mediates the effective site-specific m6A installation on CDCP1 mRNA and promotes BC progression. Wang et al. (2021c) suggested that METTL3 absence inhibits tyrosine kinase endothelium (TEK) and vascular endothelial growth factor A (VEGF-A) by reducing the abundance of m6A peaks at specific sites. METTL3 consumption down-regulates mRNA and protein expression levels of TEK and VEGF-A. Also, activation of TEK-VEGF-A-

mediated tumor development and angiogenesis requires METTL3-mediated m6A modification. Mu et al. reported that cisplatin blocks G-CSF methylation by targeting METTL3 and reducing fibrocystic-myeloid-derived suppressor cells during IAIC (Mu, et al., 2021).

4.1.1 FTO

FTO is the first obesity susceptibility gene confirmed by whole genome scanning and is localized to human chromosome 16q12.2, is approximately 430 kb, and contains nine exons and eight introns. The protein is widely expressed in the hypothalamus, adipose tissue, pancreatic islets, and other tissues (Zarza-Rebollo et al., 2021) (Zhou et al., 2021b). Song et al. (2021b) showed that USP18 post-translational deubiquitination up-regulates FTO protein expression, while FTO promotes BC occurrence and progression *via* its demethylase activity on PYCR1 to stabilize its transcript. Thus, the UPS18/FTO/PYCR1 signaling network could act as a potential therapeutic target for BC. In addition, FTO regulates the MALAT1/miR-384/MAL2 axis via m6A RNA modification to initiate BC. Thus, FTO has the potential to be a prognostic biomarker for BC (Tao et al., 2021).

4.1.2 IGF2BP1

Several IGF2BP molecules were identified thanks to molecular detection and proteomic approaches. These proteins exert key biological roles in cell polarization, proliferation, migration, and differentiation, and are closely related to the development of many tumors (Bell et al., 2013). The IGF2BP family includes IGF2BP1, IGF2BP2, and IGF2BP3, and all of which are highly conserved onco-embryonic proteins mainly expressed in embryonic tissue. Their expression levels are extremely low, or negligible in adult tissue (Du et al., 2021). Xie et al. (2021) showed that IGF2BP1 binds circPTPRA in the BC cell cytoplasm, with the ectopic expression of circPTPRA eliminating the promotion of IGF2BP1-induced growth and metastasis in BC cells.

4.1.3 IGF2BP3

Huang et al. (2020c) reported that IGF2BP3 expression is elevated in BC tissue and is closely related to a poor prognosis in BC patients. Overexpressed IGF2BP3 significantly promotes cell cycle and BC cell proliferation by activating the JAK/STAT signaling pathway and inhibiting apoptosis.

4.2 M6A Modification of Related Protein Expression Down-Regulates METTL14 in BC

Gu et al. reported that METTL14 expression decreases in BC and bladder tumor-initiating cells (TIC). METTL14 knockout significantly promotes cell proliferation, self-renewal, metastasis, and tumor initiation of bladder TIC (Gu et al., 2019). METTL14 and m6A modifications are involved in Notch1 mRNA stability. In addition, isorhapontigenin reduces vimentin protein levels by increasing METTL14 expression and up-regulating METTL14 mRNA by activating the transcription factor, FOXO3a, thereby impacting on BC progression (Zhang et al., 2021).

4.2.1 FTO

Using real-time fluorescent quantitative PCR and TCGA analysis, Wen et al. (2020) observed that FTO mRNA expression levels in urothelial BC are significantly lower than normal tissue. FTO knockdown significantly promotes the proliferation and migration of 5,637 and T24 cells (Wen et al., 2020).

4.2.2 ALKBH5

ALKBH5 is an RNA demethylation modification enzyme during m6A modification processes (Cai et al., 2021; Peng et al., 2021; Wu, et al., 2021) and mainly reverses m6A methylation (Wang et al., 2020b; Cai et al., 2021). ALKBH5 is an Fe²⁺ and Q-ketoglutarate-dependent non-heme oxygenase, belongs to the ALKB family, and only displays demethylation activity for m6A modifications on single-stranded RNA/DNA. ALKBH5 exerts essential biological functions in several tumors and cancers. Jin et al. (2019) reported that METTL3 and ALKBH5 modulate ITGA6 expression in BC cells to alter cell adhesion, thereby indicating the carcinogenic effects of m6A-modified ITGA6 and its regulatory mechanisms on BC initiation and development. In addition, down-regulated ALKBH5 expression in BC tissue and cell lines is related to a poor prognosis in patients with BC. ALKBH5 knockdown promotes BC cell proliferation, migration, and invasion, and reduces cisplatin chemosensitivity (Yu et al., 2021). ALKBH5 inhibits cancer progression in an m6A-dependent manner via the glycolytic pathway as mediated by casein kinase 2, and promotes BC cell sensitivity to cisplatin.

4.3 M6A Methylation is a Putative Prognostic Biomarker for BC

The diagnostic value of m6A-related regulatory proteins in BC is summarized (Table 2). Chen et al. collected 62 fresh bladder transitional BC samples (BC group) and 20 normal bladder mucosa specimens (controls). When compared with controls, WTAP expression was significantly increased in the BC group (Chen and Wang 2018). These authors identified a significant difference in the risk of disease recurrence between patients with negative WTAP protein expression levels and those with positive expression. In addition, METTL3 (Han, et al., 2019), ALKBH5 (Yu, et al., 2021), m6A (Gu, et al., 2019), IGF2BP3 (Huang et al., 2020c), and FTO (Tao, et al., 2021) levels are closely related to prognosis in BC patients. However, no research has yet analyzed the diagnostic potential of m6A-related regulatory protein expression levels in urine and plasma.

5 PERSPECTIVES AND CONCLUSION

M6A methylation mechanism have greatly contributed to the field of epigenetics. Methyltransferases, demethylases, and reading proteins jointly regulate m6A levels in downstream genes, thereby promoting tumor initiation and progression (Xu et al., 2020b; Yan et al., 2021). M6A RNA methylation comprises the m6A methyltransferase, m6A demethylase, and m6A binding proteins which regulate mRNA precursor shear,

TABLE 2 | The potential of m6A as a diagnostic and prognostic tool in bladder cancer.

m6A regulator	Source	Detection method	Biomarker potential	References
WTAP	tissues	qRT-PCR, WB and IHC	A biomarker for prognosis	Hou et al. (2021)
METTL3	tissues	IHC	A biomarker for prognosis	Chen et al. (2021b)
ALKBH5	tissues	IHC	A biomarker for prognosis	Chang et al. (2021)
m6A	tissues	IHC	A biomarker for prognosis	Tsuchiya et al. (2021)
IGF2BP3	tissues	IHC	A biomarker for prognosis	Dai et al. (2021)
FTO	tissues	IHC	A biomarker for prognosis	Nie et al. (2021)

bladder cancer, BC; WTAP, WT1 associated protein; METTL3, methyltransferase 3, N6-adenosine-methyltransferase complex catalytic subunit. METTL14, methyltransferase 14, N6-adenosine-methyltransferase subunit; ALKBH5, alkB homolog 5, RNA demethylase. IGF2BP3, insulin like growth factor 2 mRNA binding protein 3; FTO, FTO alpha-ketoglutarate dependent dioxygenase. qRT-PCR, quantitative real-time PCR; WB, Western blot; IHC, Immunohistochemistry.

mRNA stability, and translation. M6A RNA methylation is related to tumor cell growth, metastasis, and drug resistance. There is no doubt that m6A methylation has significant potential for the development of new human cancer therapies. Additionally, bioinformatics show that m6A participates in BC *via* multiple biological processes: m6A regulators contribute to malignant progression and impact on prognoses (Chen et al., 2019d), m6A contributes to tumor microenvironments (Zhu et al., 2021b), and m6A regulates lncRNA in BC carcinogenesis (Li et al., 2021f). Moreover, bioinformatics tools can be used to study associations between m6A and BC. RMVar (Luo et al., 2021) and RMdisease (Chen et al., 2021c) presented the m6A-associated mutations in BC, and the BC-associated m6A sites were estimated by the heterogeneous network in DURM (Tang et al., 2019). However, challenges remain. Mechanisms underpinning m6A modulators in certain cancers are unclear, especially as so few studies on m6A modified “readers” exist. The evidence suggests that m6A modulators and related pathways could function as therapeutic targets, therefore, more input from the clinic is required to verify these therapeutic effects. Moreover, m6A modified proteins have the dual effect of suppressing or causing cancer, thus controversial research results must be fully explored to characterize these discrepancies. However, in the era of next-generation sequencing, the generation and analysis of big data (omics) will expand and transform cancer biology.

In summary, thanks to high-throughput sequencing and other biotechnologies, a clear role of m6A methylation during BC has emerged. METTL3, METTL14, ALKBH5, FTO, YTHDF1/3,

YTHDF2, IGF2BP1, and IGF2BP3 aberrant expression occur in BC, mainly affect mRNA stability, and regulate the growth and metastasis of tumor cells. However, many challenges remain. The role of epigenetic networks in BC initiation and progression requires further exploration. It is vital to fully evaluate the safety and effectiveness of m6A-related regulatory factors and pathways as novel tumor therapy targets. Furthermore, exploring correlations between m6A and BC drug sensitivity and long-term prognostics is also essential.

AUTHOR CONTRIBUTIONS

Original draft preparation, allocation, revision, supplementation and editing: QL. All authors read and agreed to the final published version of the manuscript.

ACKNOWLEDGMENTS

We thank the Liaoning Cancer Hospital and Institute (Shenyang).

SUPPLEMENTARY MATERIAL

The Supplementary Material for this article can be found online at: <https://www.frontiersin.org/articles/10.3389/fgene.2021.825109/full#supplementary-material>

REFERENCES

Adhikari, S., Xiao, W., Zhao, Y.-L., and Yang, Y.-G. (2016). m6A: Signaling for mRNA Splicing. *RNA Biol.* 13, 756–759. doi:10.1080/15476286.2016.1201628

Afonso, J., Santos, L. L., Longatto-Filho, A., and Baltazar, F. (2020). Competitive Glucose Metabolism as a Target to Boost Bladder Cancer Immunotherapy. *Nat. Rev. Urol.* 17, 77–106. doi:10.1038/s41585-019-0263-6

Aguilo, F., and Walsh, M. J. (2017). The N6-Methyladenosine RNA Modification in Pluripotency and Reprogramming. *Curr. Opin. Genet. Development* 46, 77–82. doi:10.1016/j.gde.2017.06.006

Batista, P. J. (2017). The RNA Modification N 6 -methyladenosine and its Implications in Human Disease. *Genomics, Proteomics & Bioinformatics* 15 (3), 154–163. doi:10.1016/j.gpb.2017.03.002

Bell, J. L., Wächter, K., Mühleck, B., Pazaitis, N., Köhn, M., Lederer, M., et al. (2013). Insulin-like Growth Factor 2 mRNA-Binding Proteins (IGF2BPs): post-transcriptional Drivers of Cancer Progression? *Cell. Mol. Life Sci.* 70, 2657–2675. doi:10.1007/s00018-012-1186-z

Bhattarai, P. Y., Kim, G., Poudel, M., Lim, S.-C., and Choi, H. S. (2021). METTL3 Induces PLX4032 Resistance in Melanoma by Promoting m6A-dependent EGFR Translation. *Cancer Lett.* 522, 44–56. doi:10.1016/j.canlet.2021.09.015

Cai, Y., Wu, G., Peng, B., Li, J., Zeng, S., Yan, Y., et al. (2021). Expression and Molecular Profiles of the AlkB Family in Ovarian Serous Carcinoma. *Aging* 13, 9679–9692. doi:10.18632/aging.202716

Chang, G., Shi, L., Ye, Y., Shi, H., Zeng, L., Tiwary, S., et al. (2020). YTHDF3 Induces the Translation of m6A-Enriched Gene Transcripts to Promote Breast Cancer Brain Metastasis. *Cancer Cell* 38, 857–871. doi:10.1016/j.ccell.2020.10.004

- Charpentier, M., Gutierrez, C., Guillaudeux, T., Verhoest, G., and Pedoux, R. (2021). Noninvasive Urine-Based Tests to Diagnose or Detect Recurrence of Bladder Cancer. *Cancers (Basel)* 13 (7), 1650. doi:10.3390/cancers13071650
- Chen, J., Fang, X., Zhong, P., Song, Z., and Hu, X. (2019a). N6-methyladenosine Modifications: Interactions with Novel RNA-Binding Proteins and Roles in Signal Transduction. *RNA Biol.* 16, 991–1000. doi:10.1080/15476286.2019.1620060
- Chen, K., Song, B., Tang, Y., Wei, Z., Xu, Q., Su, J., et al. (2021a). RMDisease: a Database of Genetic Variants that Affect RNA Modifications, with Implications for Epitranscriptome Pathogenesis. *Nucleic Acids Res.* 49, D1396–D1404. doi:10.1093/nar/gkaa790
- Chen, L., and Wang, X. (2018). Relationship between the Genetic Expression of WTAP and Bladder Cancer and Patient Prognosis. *Oncol. Lett.* 16, 6966–6970. doi:10.3892/ol.2018.9554
- Chen, M., Nie, Z. Y., Wen, X. H., Gao, Y. H., Cao, H., and Zhang, S. F. (2019b). m6A RNA Methylation Regulators Can Contribute to Malignant Progression and Impact the Prognosis of Bladder Cancer. *Biosci. Rep.* 39, 12. doi:10.1042/BSR20192892
- Chen, M., and Wong, C.-M. (2020). The Emerging Roles of N6-Methyladenosine (m6A) Deregulation in Liver Carcinogenesis. *Mol. Cancer* 19, 44. doi:10.1186/s12943-020-01172-y
- Chen, P., Li, S., Zhang, K., Zhao, R., Cui, J., Zhou, W., et al. (2021b). N(6)-methyladenosine Demethylase ALKBH5 Suppresses Malignancy of Esophageal Cancer by Regulating microRNA Biogenesis and RAI1 Expression. *Oncogene* 40 (37), 5600–5612. doi:10.1038/s41388-021-01966-4
- Chen, X.-Y., Zhang, J., and Zhu, J.-S. (2019c). The Role of m6A RNA Methylation in Human Cancer. *Mol. Cancer* 18, 103. doi:10.1186/s12943-019-1033-z
- Chen, Y., Pan, C., Wang, X., Xu, D., Ma, Y., Hu, J., et al. (2021c). Silencing of METTL3 Effectively Hinders Invasion and Metastasis of Prostate Cancer Cells. *Theranostics* 11, 7640–7657. doi:10.7150/thno.61178
- Chen, Y., Peng, C., Chen, J., Chen, D., Yang, B., He, B., et al. (2019d). WTAP Facilitates Progression of Hepatocellular Carcinoma via m6A-HuR-dependent Epigenetic Silencing of ETS1. *Mol. Cancer* 18, 127. doi:10.1186/s12943-019-1053-8
- Cheng, M., Sheng, L., Gao, Q., Xiong, Q., Zhang, H., Wu, M., et al. (2019). The m6A Methyltransferase METTL3 Promotes Bladder Cancer Progression via AFF4/NF-KB/MYC Signaling Network. *Oncogene* 38, 3667–3680. doi:10.1038/s41388-019-0683-z
- Cui, Y., Zhang, C., Ma, S., Li, Z., Wang, W., Li, Y., et al. (2021). RNA m6A Demethylase FTO-Mediated Epigenetic Up-Regulation of LINC00022 Promotes Tumorigenesis in Esophageal Squamous Cell Carcinoma. *J. Exp. Clin. Cancer Res.* 40, 294. doi:10.1186/s13046-021-02096-1
- Dai, D., Wang, H., Zhu, L., Jin, H., and Wang, X. (2018). N6-methyladenosine Links RNA Metabolism to Cancer Progression. *Cell Death Dis* 9, 124. doi:10.1038/s41419-017-0129-x
- Dai, X.-Y., Shi, L., Li, Z., Yang, H.-Y., Wei, J.-F., and Ding, Q. (2021). Main N6-Methyladenosine Readers: YTH Family Proteins in Cancers. *Front. Oncol.* 11, 635329. doi:10.3389/fonc.2021.635329
- Deng, J., Zhang, J., Ye, Y., Liu, K., Zeng, L., Huang, J., et al. (2021). N6-methyladenosine-mediated Upregulation of WTAPP1 Promotes WTAP Translation and Wnt Signaling to Facilitate Pancreatic Cancer Progression. *Cancer Res.* doi:10.1158/0008-5472.can-21-0494
- Deng, X., Su, R., Feng, X., Wei, M., and Chen, J. (2018a). Role of N6-Methyladenosine Modification in Cancer. *Curr. Opin. Genet. Development* 48, 1–7. doi:10.1016/j.gde.2017.10.005
- Deng, X., Su, R., Weng, H., Huang, H., Li, Z., and Chen, J. (2018b). RNA N6-Methyladenosine Modification in Cancers: Current Status and Perspectives. *Cell Res* 28, 507–517. doi:10.1038/s41422-018-0034-6
- Du, Q. Y., Zhu, Z. M., and Pei, D. S. (2021). The Biological Function of IGF2BPs and Their Role in Tumorigenesis. *Invest. New Drugs* 39 (6), 1682–1693. doi:10.1007/s10637-021-01148-9
- Esteve-Puig, R., Climent, F., Piñeyro, D., Domingo-Domènech, E., Davalos, V., Encuentra, M., et al. (2021). Epigenetic Loss of m1A RNA Demethylase ALKBH3 in Hodgkin Lymphoma Targets Collagen, Conferring Poor Clinical Outcome. *Blood* 137 (7), 994–999. doi:10.1182/blood.2020005823
- Frye, M., Harada, B. T., Behm, M., and He, C. (2018). RNA Modifications Modulate Gene Expression during Development. *Science* 361, 1346–1349. doi:10.1126/science.aau1646
- Gu, C., Wang, Z., Zhou, N., Li, G., Kou, Y., Luo, Y., et al. (2019). METTL14 Inhibits Bladder TIC Self-Renewal and Bladder Tumorigenesis through N6-Methyladenosine of Notch1. *Mol. Cancer* 18, 168. doi:10.1186/s12943-019-1084-1
- Gu, J., Zhan, Y., Zhuo, L., Zhang, Q., Li, G., Li, Q., et al. (2021a). Biological Functions of m6A Methyltransferases. *Cell Biosci* 11, 15. doi:10.1186/s13578-020-00513-0
- Gu, Y., Wu, X., Zhang, J., Fang, Y., Pan, Y., Shu, Y., et al. (2021b). The Evolving Landscape of N6-Methyladenosine Modification in the Tumor Microenvironment. *Mol. Ther.* 29 (5), 1703–1715. doi:10.1016/j.jymthe.2021.04.009
- Han, H., Yang, C., Zhang, S., Cheng, M., Guo, S., Zhu, Y., et al. (2021). METTL3-mediated m6A mRNA Modification Promotes Esophageal Cancer Initiation and Progression via Notch Signaling Pathway. *Mol. Ther. - Nucleic Acids* 26, 333–346. doi:10.1016/j.omtn.2021.07.007
- Han, J., Wang, J.-z., Yang, X., Yu, H., Zhou, R., Lu, H.-C., et al. (2019). METTL3 Promote Tumor Proliferation of Bladder Cancer by Accelerating Pri-miR221/222 Maturation in m6A-dependent Manner. *Mol. Cancer* 18, 110. doi:10.1186/s12943-019-1036-9
- Han, S. H., and Choe, J. (2020). Diverse Molecular Functions of m6A mRNA Modification in Cancer. *Exp. Mol. Med.* 52, 738–749. doi:10.1038/s12276-020-0432-y
- He, L., Li, H., Wu, A., Peng, Y., Shu, G., and Yin, G. (2019). Functions of N6-Methyladenosine and its Role in Cancer. *Mol. Cancer* 18, 176. doi:10.1186/s12943-019-1109-9
- He, P. C., and He, C. (2021). m6 A RNA Methylation: from Mechanisms to Therapeutic Potential. *EMBO J.* 40 (3), e105977. doi:10.15252/embj.2020105977
- Hou, Y., Zhang, Q., Pang, W., Hou, L., Liang, Y., Han, X., et al. (2021). YTHDC1-mediated Augmentation of miR-30d in Repressing Pancreatic Tumorigenesis via Attenuation of RUNX1-Induced Transcriptional Activation of Warburg Effect. *Cell Death Differ* 28 (11), 3105–3124. doi:10.1038/s41418-021-00804-0
- Hu, Y., Pan, Q., Wang, M., Ai, X., Yan, Y., Tian, Y., et al. (2021). m6A RNA Methylation Regulator YTHDF1 Correlated with Immune Microenvironment Predicts Clinical Outcomes and Therapeutic Efficacy in Breast Cancer. *Front. Med.* 8, 667543. doi:10.3389/fmed.2021.667543
- Huang, H., Weng, H., and Chen, J. (2020b). m6A Modification in Coding and Non-coding RNAs: Roles and Therapeutic Implications in Cancer. *Cancer Cell* 37, 270–288. doi:10.1016/j.ccell.2020.02.004
- Huang, H., Weng, H., and Chen, J. (2020a). The Biogenesis and Precise Control of RNA m6A Methylation. *Trends Genet.* 36, 44–52. doi:10.1016/j.tig.2019.10.011
- Huang, J., and Yin, P. (2018). Structural Insights into N 6 -methyladenosine (m6A) Modification in the Transcriptome. *Genomics, Proteomics & Bioinformatics* 16, 85–98. doi:10.1016/j.gpb.2018.03.001
- Huang, W., Chen, T.-Q., Fang, K., Zeng, Z.-C., Ye, H., and Chen, Y.-Q. (2021). N6-methyladenosine Methyltransferases: Functions, Regulation, and Clinical Potential. *J. Hematol. Oncol.* 14, 117. doi:10.1186/s13045-021-01129-8
- Huang, W., Li, Y., Zhang, C., Zha, H., Zhou, X., Fu, B., et al. (2020c). IGF2BP3 Facilitates Cell Proliferation and Tumorigenesis via Modulation of JAK/STAT Signalling Pathway in Human Bladder Cancer. *J. Cell. Mol. Med.* 24, 13949–13960. doi:10.1111/jcmm.16003
- Iaiza, A., Tito, C., Ianniello, Z., Ganci, F., Laquintana, V., Gallo, E., et al. (2021). METTL3-dependent MALAT1 Delocalization Drives C-Myc Induction in Thymic Epithelial Tumors. *Clin. Epigenet* 13, 173. doi:10.1186/s13148-021-01159-6
- Ianniello, Z., Sorci, M., Ceci Ginistrelli, L., Iaiza, A., Marchioni, M., Tito, C., et al. (2021). New Insight into the Catalytic -dependent and -independent Roles of METTL3 in Sustaining Aberrant Translation in Chronic Myeloid Leukemia. *Cel Death Dis* 12, 870. doi:10.1038/s41419-021-04169-7
- Jain, P., Kathuria, H., and Momin, M. (2021). Clinical Therapies and Nano Drug Delivery Systems for Urinary Bladder Cancer. *Pharmacol. Ther.* 226, 107871. doi:10.1016/j.pharmthera.2021.107871
- Jiang, D. M., Gupta, S., Kitchlu, A., Meraz-Munoz, A., North, S. A., Alimohamed, N. S., et al. (2021a). Defining Cisplatin Eligibility in Patients with Muscle-Invasive Bladder Cancer. *Nat. Rev. Urol.* 18, 104–114. doi:10.1038/s41585-020-00404-6
- Jiang, X., Liu, B., Nie, Z., Duan, L., Xiong, Q., Jin, Z., et al. (2021b). The Role of m6A Modification in the Biological Functions and Diseases. *Sig Transduct Target. Ther.* 6, 74. doi:10.1038/s41392-020-00450-x

- Jin, H., Ying, X., Que, B., Wang, X., Chao, Y., Zhang, H., et al. (2019). N6-methyladenosine Modification of ITGA6 mRNA Promotes the Development and Progression of Bladder Cancer. *EBioMedicine* 47, 195–207. doi:10.1016/j.ebiom.2019.07.068
- Kaur, J., Choi, W., Geynisman, D. M., Plimack, E. R., and Ghatalia, P. (2021). Role of Immunotherapy in Localized Muscle Invasive Urothelial Cancer. *Ther. Adv. Med. Oncol.* 13, 17588359211045858. doi:10.1177/17588359211045858
- Kim, G. W., and Siddiqui, A. (2021). N6-methyladenosine Modification of HCV RNA Genome Regulates Cap-independent IRES-Mediated Translation via YTHDC2 Recognition. *Proc. Natl. Acad. Sci. U S A.* 118, 10. doi:10.1073/pnas.2022024118
- Lan, N., Lu, Y., Zhang, Y., Pu, S., Xi, H., Nie, X., et al. (2020). FTO - A Common Genetic Basis for Obesity and Cancer. *Front. Genet.* 11, 559138. doi:10.3389/fgene.2020.559138
- Lan, Q., Liu, P. Y., Haase, J., Bell, J. L., Hüttelmaier, S., and Liu, T. (2019). The Critical Role of RNA m6A Methylation in Cancer. *Cancer Res.* 79, 1285–1292. doi:10.1158/0008-5472.can-18-2965
- Lee, Y., Choe, J., Park, O. H., and Kim, Y. K. (2020). Molecular Mechanisms Driving mRNA Degradation by m6A Modification. *Trends Genet.* 36, 177–188. doi:10.1016/j.tig.2019.12.007
- Lenis, A. T., Lec, P. M., Chamie, K., and Mshs, M. (2020). Bladder Cancer. *JAMA* 324, 1980–1991. doi:10.1001/jama.2020.17598
- Li, H., Wu, H., Wang, Q., Ning, S., Xu, S., and Pang, D. (2021a). Dual Effects of N6-Methyladenosine on Cancer Progression and Immunotherapy. *Mol. Ther. - Nucleic Acids* 24, 25–39. doi:10.1016/j.omtn.2021.02.001
- Li, L., Zhou, M., Chen, B., Wang, Q., Pan, S., Hou, Y., et al. (2021b). ALKBH5 Promotes Cadmium-Induced Transformation of Human Bronchial Epithelial Cells by Regulating PTEN Expression in an m6A-dependent Manner. *Ecotoxicology Environ. Saf.* 224, 112686. doi:10.1016/j.ecoenv.2021.112686
- Li, M., Deng, L., and Xu, G. (2021c). METTL14 Promotes Glomerular Endothelial Cell Injury and Diabetic Nephropathy via m6A Modification of α -klotho. *Mol. Cell* 27, 106. doi:10.1186/s10020-021-00365-5
- Li, M., Zha, X., and Wang, S. (2021d). The Role of N6-Methyladenosine mRNA in the Tumor Microenvironment. *Biochim. Biophys. Acta (Bba) - Rev. Cancer* 1875, 188522. doi:10.1016/j.bbcan.2021.188522
- Li, R., Zhang, J., Gilbert, S. M., Conejo-Garcia, J., and Mule, J. J. (2021e). Using Oncolytic Viruses to Ignite the Tumour Immune Microenvironment in Bladder Cancer. *Nat. Rev. Urol.* 18 (9), 543–555. doi:10.1038/s41585-021-00483-z
- Li, Y., Ge, Y.-z., Xu, L., Xu, Z., Dou, Q., and Jia, R. (2020). The Potential Roles of RNA N6-Methyladenosine in Urological Tumors. *Front. Cel Dev. Biol.* 8, 579919. doi:10.3389/fcell.2020.579919
- Li, Z., Li, Y., Zhong, W., and Huang, P. (2021f). m6A-Related lncRNA to Develop Prognostic Signature and Predict the Immune Landscape in Bladder Cancer. *J. Oncol.* 2021, 7488188. doi:10.1155/2021/7488188
- Liang, Z., L. Kidwell, R., Deng, H., and Xie, Q. (2020). Epigenetic N6-Methyladenosine Modification of RNA and DNA Regulates Cancer. *Cancer Biol. Med.* 17, 9–19. doi:10.20892/j.issn.2095-3941.2019.0347
- Liao, S., Sun, H., and Xu, C. (2018). YTH Domain: A Family of N 6 - methyladenosine (M 6 A) Readers. *Genomics, Proteomics & Bioinformatics* 16, 99–107. doi:10.1016/j.gpb.2018.04.002
- Lin, S., Zhu, Y., Ji, C., Yu, W., Zhang, C., Tan, L., et al. (2021). METTL3-Induced miR-222-3p Upregulation Inhibits STK4 and Promotes the Malignant Behaviors of Thyroid Carcinoma Cells. *J. Clin. Endocrinol. Metab.* dgab480. doi:10.1210/clinem/dgab480
- Liu, H., Gu, J., Jin, Y., Yuan, Q., Ma, G., Du, M., et al. (2021a). Genetic Variants in N6-Methyladenosine Are Associated with Bladder Cancer Risk in the Chinese Population. *Arch. Toxicol.* 95, 299–309. doi:10.1007/s00204-020-02911-2
- Liu, J., Harada, B. T., and He, C. (2019). Regulation of Gene Expression by N-Methyladenosine in Cancer. *Trends Cel Biol.* 29, 487–499. doi:10.1016/j.tcb.2019.02.008
- Liu, S., Chen, X., and Lin, T. (2021b). Lymphatic Metastasis of Bladder Cancer: Molecular Mechanisms, Diagnosis and Targeted Therapy. *Cancer Lett.* 505, 13–23. doi:10.1016/j.canlet.2021.02.010
- Lou, X., Wang, J.-J., Wei, Y.-Q., and Sun, J.-J. (2021). Emerging Role of RNA Modification N6-Methyladenosine in Immune Evasion. *Cel Death Dis* 12, 300. doi:10.1038/s41419-021-03585-z
- Lu, Z., Liu, H., Song, N., Liang, Y., Zhu, J., Chen, J., et al. (2021). METTL14 Aggravates Podocyte Injury and Glomerulopathy Progression through N6-methyladenosine-dependent Downregulating of Sirt1. *Cel Death Dis* 12, 881. doi:10.1038/s41419-021-04156-y
- Luo, X., Li, H., Liang, J., Zhao, Q., Xie, Y., Ren, J., et al. (2021). RMVar: an Updated Database of Functional Variants Involved in RNA Modifications. *Nucleic Acids Res.* 49, D1405–D1412. doi:10.1093/nar/gkaa811
- Ma, S., Chen, C., Ji, X., Liu, J., Zhou, Q., Wang, G., et al. (2019). The Interplay between m6A RNA Methylation and Noncoding RNA in Cancer. *J. Hematol. Oncol.* 12, 121. doi:10.1186/s13045-019-0805-7
- Ma, Z., and Ji, J. (2020). N6-methyladenosine (m6A) RNA Modification in Cancer Stem Cells. *Stem Cells* 38, 1511–1519. doi:10.1002/stem.3279
- Maldonado López, A., and Capell, B. C. (2021). The METTL3-m6A Epitranscriptome: Dynamic Regulator of Epithelial Development, Differentiation, and Cancer. *Genes (Basel)* 12 (7), 1019. doi:10.3390/genes12071019
- Meeks, J. J., Al-Ahmadie, H., Faltas, B. M., Taylor, J. A., 3rd, Flaig, T. W., DeGraff, D. J., et al. (2020). Genomic Heterogeneity in Bladder Cancer: Challenges and Possible Solutions to Improve Outcomes. *Nat. Rev. Urol.* 17, 259–270. doi:10.1038/s41585-020-0304-1
- Meng, Y., Zhang, Q., Wang, K., Zhang, X., Yang, R., Bi, K., et al. (2021). RBM15-mediated N6-Methyladenosine Modification Affects COVID-19 Severity by Regulating the Expression of Multitarget Genes. *Cel Death Dis* 12, 732. doi:10.1038/s41419-021-04012-z
- Meyer, K. D., and Jaffrey, S. R. (2017). Rethinking m6A Readers, Writers, and Erasers. *Annu. Rev. Cel Dev. Biol.* 33, 319–342. doi:10.1146/annurev-cellbio-100616-060758
- Mu, X., Wu, K., Zhu, Y., Zhu, Y., Wang, Y., Xiao, L., et al. (2021). Intra-arterial Infusion Chemotherapy Utilizing Cisplatin Inhibits Bladder Cancer by Decreasing the Flbrocytic Myeloid-Derived Suppressor Cells in an m6A-dependent Manner. *Mol. Immunol.* 137, 28–40. doi:10.1016/j.molimm.2021.06.012
- Nie, S., Zhang, L., Liu, J., Wan, Y., Jiang, Y., Yang, J., et al. (2021). ALKBH5-HOXA10 Loop-Mediated JAK2 m6A Demethylation and Cisplatin Resistance in Epithelial Ovarian Cancer. *J. Exp. Clin. Cancer Res.* 40, 284. doi:10.1186/s13046-021-02088-1
- Niu, Y., Lin, Z., Wan, A., Chen, H., Liang, H., Sun, L., et al. (2019). RNA N6-Methyladenosine Demethylase FTO Promotes Breast Tumor Progression through Inhibiting BNIP3. *Mol. Cancer* 18, 46. doi:10.1186/s12943-019-1004-4
- Niu, Y., Wan, A., Lin, Z., Lu, X., and Wan, G. (2018). N6-Methyladenosine Modification: a Novel Pharmacological Target for Anti-cancer Drug Development. *Acta Pharmaceutica Sinica B* 8, 833–843. doi:10.1016/j.japsb.2018.06.001
- Oerum, S., Meynier, V., Catala, M., and Tisné, C. (2021). A Comprehensive Review of m6A/m6Am RNA Methyltransferase Structures. *Nucleic Acids Res.* 49, 7239–7255. doi:10.1093/nar/gkab378
- Pan, F., Lin, X.-R., Hao, L.-P., Chu, X.-Y., Wan, H.-J., and Wang, R. (2021). The Role of RNA Methyltransferase METTL3 in Hepatocellular Carcinoma: Results and Perspectives. *Front. Cel Dev. Biol.* 9, 674919. doi:10.3389/fcell.2021.674919
- Patel, V. G., Oh, W. K., and Galsky, M. D. (2020). Treatment of Muscle-invasive and Advanced Bladder Cancer in 2020. *CA A. Cancer J. Clin.* 70, 404–423. doi:10.3322/caac.21631
- Patil, D. P., Pickering, B. F., and Jaffrey, S. R. (2018). Reading m6A in the Transcriptome: m6A-Binding Proteins. *Trends Cel Biol.* 28, 113–127. doi:10.1016/j.tcb.2017.10.001
- Peng, B., Yan, Y., and Xu, Z. (2021). The Bioinformatics and Experimental Analysis of AlkB Family for Prognosis and Immune Cell Infiltration in Hepatocellular Carcinoma. *PeerJ* 9, e12123. doi:10.7717/peerj.12123
- Purslow, J. A., Nguyen, T. T., Khatiwada, B., Singh, A., and Venditti, V. (2021). N 6-methyladenosine Binding Induces a Metal-Centered Rearrangement that Activates the Human RNA Demethylase Alkbh5. *Sci. Adv.* 7, 34. doi:10.1126/sciadv.abi8215
- Roignant, J.-Y., and Soller, M. (2017). m 6 A in mRNA: An Ancient Mechanism for Fine-Tuning Gene Expression. *Trends Genet.* 33, 380–390. doi:10.1016/j.tig.2017.04.003
- Roviello, G., Catalano, M., Santi, R., Palmieri, V. E., Vannini, G., Galli, I. C., et al. (2021). Immune Checkpoint Inhibitors in Urothelial Bladder Cancer: State of the Art and Future Perspectives. *Cancers* 13, 4411. doi:10.3390/cancers13174411

- Satterwhite, E. R., and Mansfield, K. D. (2021). *RNA Methyltransferase METTL16: Targets and Function*. Wiley Interdiscip Rev RNA, e1681. doi:10.1002/wrna.1681
- Scarrow, M., Chen, N., and Sun, G. (2020). Insights into the N6-Methyladenosine Mechanism and its Functionality: Progress and Questions. *Crit. Rev. Biotechnol.* 40, 639–652. doi:10.1080/07388551.2020.1751059
- Schneider, A. K., Chevalier, M. F., and Derré, L. (2019). The Multifaceted Immune Regulation of Bladder Cancer. *Nat. Rev. Urol.* 16, 613–630. doi:10.1038/s41585-019-0226-y
- Song, P., Tayier, S., Cai, Z., and Jia, G. (2021a). RNA Methylation in Mammalian Development and Cancer. *Cell Biol Toxicol* 37 (6), 811–831. doi:10.1007/s10565-021-09627-8
- Song, T., Yang, Y., Jiang, S., and Peng, J. (2020). Novel Insights into Adipogenesis from the Perspective of Transcriptional and RNA N6-Methyladenosine-Mediated Post-Transcriptional Regulation. *Adv. Sci.* 7, 2001563. doi:10.1002/advs.202001563
- Song, W., Yang, K., Luo, J., Gao, Z., and Gao, Y. (2021b). Dysregulation of USP18/FTO/PYCR1 Signaling Network Promotes Bladder Cancer Development and Progression. *Aging* 13, 3909–3925. doi:10.18632/aging.202359
- Tan, F., Zhao, M., Xiong, F., Wang, Y., Zhang, S., Gong, Z., et al. (2021). N6-methyladenosine-dependent Signalling in Cancer Progression and Insights into Cancer Therapies. *J. Exp. Clin. Cancer Res.* 40, 146. doi:10.1186/s13046-021-01952-4
- Tang, L., Wei, X., Li, T., Chen, Y., Dai, Z., Lu, C., et al. (2021). Emerging Perspectives of RNA N6-Methyladenosine (m6A) Modification on Immunity and Autoimmune Diseases. *Front. Immunol.* 12, 630358. doi:10.3389/fimmu.2021.630358
- Tang, Y., Chen, K., Wu, X., Wei, Z., Zhang, S.-Y., Song, B., et al. (2019). DRUM: Inference of Disease-Associated m6A RNA Methylation Sites from a Multi-Layer Heterogeneous Network. *Front. Genet.* 10, 266. doi:10.3389/fgene.2019.00266
- Tao, L., Mu, X., Chen, H., Jin, D., Zhang, R., Zhao, Y., et al. (2021). FTO Modifies the m6A Level of MALAT and Promotes Bladder Cancer Progression. *Clin. Transl Med.* 11, e310. doi:10.1002/ctm2.310
- Terajima, H., Lu, M., Zhang, L., Cui, Q., Shi, Y., Li, J., et al. (2021). N6-methyladenosine Promotes Induction of ADAR1-Mediated A-To-I RNA Editing to Suppress Aberrant Antiviral Innate Immune Responses. *Plos Biol.* 19, e3001292. doi:10.1371/journal.pbio.3001292
- Tran, L., Xiao, J.-F., Agarwal, N., Duex, J. E., and Theodorescu, D. (2021). Advances in Bladder Cancer Biology and Therapy. *Nat. Rev. Cancer* 21, 104–121. doi:10.1038/s41568-020-00313-1
- Tsuchiya, K., Yoshimura, K., Inoue, Y., Iwashita, Y., Yamada, H., Kawase, A., et al. (2021). YTHDF1 and YTHDF2 Are Associated with Better Patient Survival and an Inflamed Tumor-Immune Microenvironment in Non-small-cell Lung Cancer. *Oncimmunology* 10, 1962656. doi:10.1080/2162402x.2021.1962656
- Uddin, M. B., Wang, Z., and Yang, C. (2021). The m6A RNA Methylation Regulates Oncogenic Signaling Pathways Driving Cell Malignant Transformation and Carcinogenesis. *Mol. Cancer* 20, 61. doi:10.1186/s12943-021-01356-0
- van Puffelen, J. H., Keating, S. T., Oosterwijk, E., van der Heijden, A. G., Netea, M. G., Joosten, L. A. B., et al. (2020). Trained Immunity as a Molecular Mechanism for BCG Immunotherapy in Bladder Cancer. *Nat. Rev. Urol.* 17, 513–525. doi:10.1038/s41585-020-0346-4
- Wang, G., Dai, Y., Li, K., Cheng, M., Xiong, G., Wang, X., et al. (2021a). Deficiency of Mettl3 in Bladder Cancer Stem Cells Inhibits Bladder Cancer Progression and Angiogenesis. *Front. Cell Dev. Biol.* 9, 627706. doi:10.3389/fcell.2021.627706
- Wang, J., Wang, J., Gu, Q., Ma, Y., Yang, Y., Zhu, J., et al. (2020a). The Biological Function of m6A Demethylase ALKBH5 and its Role in Human Disease. *Cancer Cell Int* 20, 347. doi:10.1186/s12935-020-01450-1
- Wang, M., Liu, J., Zhao, Y., He, R., Xu, X., Guo, X., et al. (2020b). Upregulation of METTL14 Mediates the Elevation of PERP mRNA N6 Adenosine Methylation Promoting the Growth and Metastasis of Pancreatic Cancer. *Mol. Cancer* 19, 130. doi:10.1186/s12943-020-01249-8
- Wang, S., Chai, P., Jia, R., and Jia, R. (2018). Novel Insights on m6A RNA Methylation in Tumorigenesis: a Double-Edged Sword. *Mol. Cancer* 17, 101. doi:10.1186/s12943-018-0847-4
- Wang, S., Sun, C., Li, J., Zhang, E., Ma, Z., Xu, W., et al. (2017). Roles of RNA Methylation by Means of N6-Methyladenosine (m6A) in Human Cancers. *Cancer Lett.* 408, 112–120. doi:10.1016/j.canlet.2017.08.030
- Wang, W., Shao, F., Yang, X., Wang, J., Zhu, R., Yang, Y., et al. (2021b). METTL3 Promotes Tumour Development by Decreasing APC Expression Mediated by APC mRNA N6-methyladenosine-dependent YTHDF Binding. *Nat. Commun.* 12, 3803. doi:10.1038/s41467-021-23501-5
- Wang, X. K., Zhang, Y. W., Wang, C. M., Li, B., Zhang, T. Z., Zhou, W. J., et al. (2021c). METTL16 Promotes Cell Proliferation by Up-regulating Cyclin D1 Expression in Gastric Cancer. *J. Cel Mol Med* 25, 6602–6617. doi:10.1111/jcmm.16664
- Wen, L., Pan, X., Yu, Y., and Yang, B. (2020). Down-regulation of FTO Promotes Proliferation and Migration, and Protects Bladder Cancer Cells from Cisplatin-Induced Cytotoxicity. *BMC Urol.* 20, 39. doi:10.1186/s12894-020-00612-7
- Williams, G. D., Gokhale, N. S., and Horner, S. M. (2019). Regulation of Viral Infection by the RNA Modification N6-Methyladenosine. *Annu. Rev. Virol.* 6, 235–253. doi:10.1146/annurev-virology-092818-015559
- Witjes, J. A., Bruins, H. M., Cathomas, R., Compérat, E. M., Cowan, N. C., Gakis, G., et al. (2021). European Association of Urology Guidelines on Muscle-Invasive and Metastatic Bladder Cancer: Summary of the 2020 Guidelines. *Eur. Urol.* 79, 82–104. doi:10.1016/j.eururo.2020.03.055
- Wollen, K. L., Hagen, L., Vågbø, C. B., Rabe, R., Iveland, T. S., Aas, P. A., et al. (2021). ALKBH3 Partner ASCC3 Mediates P-Body Formation and Selective Clearance of MMS-Induced 1-methyladenosine and 3-methylcytosine from mRNA. *J. Transl Med.* 19, 287. doi:10.1186/s12967-021-02948-6
- Wu, B., Li, L., Huang, Y., Ma, J., and Min, J. (2017). Readers, Writers and Erasers of N6-Methylated Adenosine Modification. *Curr. Opin. Struct. Biol.* 47, 67–76. doi:10.1016/j.sbi.2017.05.011
- Wu, G., Yan, Y., Cai, Y., Peng, B., Li, J., Huang, J., et al. (2021). ALKBH1-8 and FTO: Potential Therapeutic Targets and Prognostic Biomarkers in Lung Adenocarcinoma Pathogenesis. *Front. Cell Dev. Biol.* 9, 633927. doi:10.3389/fcell.2021.633927
- Wu, J., and Abraham, S. N. (2021). The Roles of T Cells in Bladder Pathologies. *Trends Immunol.* 42, 248–260. doi:10.1016/j.it.2021.01.003
- Wu, R., and Wang, X. (2021). Epigenetic Regulation of Adipose Tissue Expansion and Adipogenesis by N6 -methyladenosine. *Obes. Rev.* 22 (2), e13124. doi:10.1111/obr.13124
- Wu, S., Zhang, S., Wu, X., and Zhou, X. (2020). m6A RNA Methylation in Cardiovascular Diseases. *Mol. Ther.* 28, 2111–2119. doi:10.1016/j.jymth.2020.08.010
- Xie, F., Huang, C., Liu, F., Zhang, H., Xiao, X., Sun, J., et al. (2021). CircPTPRA Blocks the Recognition of RNA N6-Methyladenosine through Interacting with IGF2BP1 to Suppress Bladder Cancer Progression. *Mol. Cancer* 20, 68. doi:10.1186/s12943-021-01359-x
- Xie, H., Li, J., Ying, Y., Yan, H., Jin, K., Ma, X., et al. (2020). METTL3/YTHDF2 M6 A axis Promotes Tumorigenesis by Degrading SETD7 and KLF4 mRNAs in Bladder Cancer. *J. Cel Mol Med* 24, 4092–4104. doi:10.1111/jcmm.15063
- Xu, H., Wang, Z., Chen, M., Zhao, W., Tao, T., Ma, L., et al. (2021). YTHDF2 Alleviates Cardiac Hypertrophy via Regulating Myh7 mRNA Decoy. *Cel Biosci* 11, 132. doi:10.1186/s13578-021-00649-7
- Xu, Y., Liu, J., Chen, W.-J., Ye, Q.-Q., Chen, W.-T., Li, C.-L., et al. (2020a). Regulation of N6-Methyladenosine in the Differentiation of Cancer Stem Cells and Their Fate. *Front. Cell Dev. Biol.* 8, 561703. doi:10.3389/fcell.2020.561703
- Xu, Z., Peng, B., Cai, Y., Wu, G., Huang, J., Gao, M., et al. (2020b). N6-methyladenosine RNA Modification in Cancer Therapeutic Resistance: Current Status and Perspectives. *Biochem. Pharmacol.* 182, 114258. doi:10.1016/j.bcp.2020.114258
- Yan, Y., Liang, Q., Xu, Z., and Yi, Q. (2021). Integrative Bioinformatics and Experimental Analysis Revealed Down-Regulated CDC42EP3 as a Novel Prognostic Target for Ovarian Cancer and its Roles in Immune Infiltration. *PeerJ* 9, e12171. doi:10.7717/peerj.12171
- Yang, F., Jin, H., Que, B., Chao, Y., Zhang, H., Ying, X., et al. (2019). Dynamic m6A mRNA Methylation Reveals the Role of METTL3-m6A-CDCP1 Signaling axis in Chemical Carcinogenesis. *Oncogene* 38, 4755–4772. doi:10.1038/s41388-019-0755-0
- Yang, Y., Hsu, P. J., Chen, Y.-S., and Yang, Y.-G. (2018). Dynamic Transcriptomic m6A Decoration: Writers, Erasers, Readers and Functions in RNA Metabolism. *Cel Res* 28, 616–624. doi:10.1038/s41422-018-0040-8
- Yao, L., Yin, H., Hong, M., Wang, Y., Yu, T., Teng, Y., et al. (2021). RNA Methylation in Hematological Malignancies and its Interactions with Other Epigenetic Modifications. *Leukemia* 35 (5), 1243–1257. doi:10.1038/s41375-021-01225-1

- Ye, F., Hu, Y., Gao, J., Liang, Y., Liu, Y., Ou, Y., et al. (2021). Radiogenomics Map Reveals the Landscape of m6A Methylation Modification Pattern in Bladder Cancer. *Front. Immunol.* 12, 722642. doi:10.3389/fimmu.2021.722642
- Ying, X., Jiang, X., Zhang, H., Liu, B., Huang, Y., Zhu, X., et al. (2020). Programmable N6-Methyladenosine Modification of CDCP1 mRNA by RCas9-Methyltransferase like 3 Conjugates Promotes Bladder Cancer Development. *Mol. Cancer* 19, 169. doi:10.1186/s12943-020-01289-0
- Yu, H., Yang, X., Tang, J., Si, S., Zhou, Z., Lu, J., et al. (2021). ALKBH5 Inhibited Cell Proliferation and Sensitized Bladder Cancer Cells to Cisplatin by m6A-Ck2 α -Mediated Glycolysis. *Mol. Ther. - Nucleic Acids* 23, 27–41. doi:10.1016/j.omtn.2020.10.031
- Yue, H., Nie, X., Yan, Z., and Weining, S. (2019). N6-methyladenosine Regulatory Machinery in Plants: Composition, Function and Evolution. *Plant Biotechnol. J.* 17, 1194–1208. doi:10.1111/pbi.13149
- Zarza-Rebollo, J. A., Molina, E., and Rivera, M. (2021). The Role of the FTO Gene in the Relationship between Depression and Obesity. A Systematic Review. *Neurosci. Biobehavioral Rev.* 127, 630–637. doi:10.1016/j.neubiorev.2021.05.013
- Zhang, L., Hou, C., Chen, C., Guo, Y., Yuan, W., Yin, D., et al. (2020). The Role of N6-Methyladenosine (m6A) Modification in the Regulation of circRNAs. *Mol. Cancer* 19, 105. doi:10.1186/s12943-020-01224-3
- Zhang, N., Hua, X., Tu, H., Li, J., Zhang, Z., and Max, C. (2021). Isorhapontigenin (ISO) Inhibits EMT through FOXO3A/METTL14/VIMENTIN Pathway in Bladder Cancer Cells. *Cancer Lett.* 520, 400–408. doi:10.1016/j.canlet.2021.07.041
- Zhang, S. (2018). Mechanism of N6-Methyladenosine Modification and its Emerging Role in Cancer. *Pharmacol. Ther.* 189, 173–183. doi:10.1016/j.pharmthera.2018.04.011
- Zhao, W., Qi, X., Liu, L., Ma, S., Liu, J., and Wu, J. (2020). Epigenetic Regulation of m6A Modifications in Human Cancer. *Mol. Ther. - Nucleic Acids* 19, 405–412. doi:10.1016/j.omtn.2019.11.022
- Zhao, Y., Chen, Y., Jin, M., and Wang, J. (2021). The Crosstalk between m6A RNA Methylation and Other Epigenetic Regulators: a Novel Perspective in Epigenetic Remodeling. *Theranostics* 11, 4549–4566. doi:10.7150/thno.54967
- Zheng, H.-x., Zhang, X.-s., and Sui, N. (2020). Advances in the Profiling of N6-Methyladenosine (m6A) Modifications. *Biotechnol. Adv.* 45, 107656. doi:10.1016/j.biotechadv.2020.107656
- Zhou, G., Yan, K., Liu, J., Gao, L., Jiang, X., and Fan, Y. (2021a). FTO Promotes Tumour Proliferation in Bladder Cancer via the FTO/miR-576/CDK6 axis in an m6A-dependent Manner. *Cell Death Discov.* 7, 329. doi:10.1038/s41420-021-00724-5
- Zhou, H., Yin, K., Zhang, Y., Tian, J., and Wang, S. (2021b). The RNA m6A Writer METTL14 in Cancers: Roles, Structures, and Applications. *Biochim. Biophys. Acta (Bba) - Rev. Cancer* 1876, 188609. doi:10.1016/j.bbcan.2021.188609
- Zhou, Z., Lv, J., Yu, H., Han, J., Yang, X., Feng, D., et al. (2020). Mechanism of RNA Modification N6-Methyladenosine in Human Cancer. *Mol. Cancer* 19, 104. doi:10.1186/s12943-020-01216-3
- Zhu, H., Jia, X., Wang, Y., Song, Z., Wang, N., Yang, Y., et al. (2021a). M6A Classification Combined with Tumor Microenvironment Immune Characteristics Analysis of Bladder Cancer. *Front. Oncol.* 11, 714267. doi:10.3389/fonc.2021.714267
- Zhu, W., Wang, J.-Z., Wei, J.-F., and Lu, C. (2021b). Role of m6A Methyltransferase Component VIRMA in Multiple Human Cancers (Review). *Cancer Cel Int* 21, 172. doi:10.1186/s12935-021-01868-1

Conflict of Interest: The author declares that the research was conducted in the absence of any commercial or financial relationships that could be construed as a potential conflict of interest.

Publisher's Note: All claims expressed in this article are solely those of the authors and do not necessarily represent those of their affiliated organizations, or those of the publisher, the editors and the reviewers. Any product that may be evaluated in this article, or claim that may be made by its manufacturer, is not guaranteed or endorsed by the publisher.

Copyright © 2022 Liu. This is an open-access article distributed under the terms of the Creative Commons Attribution License (CC BY). The use, distribution or reproduction in other forums is permitted, provided the original author(s) and the copyright owner(s) are credited and that the original publication in this journal is cited, in accordance with accepted academic practice. No use, distribution or reproduction is permitted which does not comply with these terms.



Transcriptomic and Metabolomic Analyses Reveal Inhibition of Hepatic Adipogenesis and Fat Catabolism in Yak for Adaptation to Forage Shortage During Cold Season

Juanshan Zheng^{1†}, Mei Du^{1†}, Jianbo Zhang¹, Zeyi Liang¹, Anum Ali Ahmad², Jiahao Shen¹, Ghasem Hosseini Salekdeh^{3*} and Xuezhi Ding^{1,4*}

¹Key Laboratory of Veterinary Pharmaceutical Development, Ministry of Agricultural and Rural Affairs & Key Laboratory of Yak Breeding Engineering, Lanzhou Institute of Husbandry and Pharmaceutical Sciences, Chinese Academy of Agricultural Sciences, Lanzhou, China, ²State Key Laboratory of Grassland Agro-Ecosystems, School of Life Sciences, Lanzhou University, Lanzhou, China, ³Department of Systems Biology, Agricultural Biotechnology Research Institute of Iran, Agricultural Research, Education, and Extension Organization, Karaj, Iran, ⁴Key Laboratory of Veterinary Pharmaceutical Development, Ministry of Agricultural and Rural Affairs, Lanzhou Institute of Husbandry and Pharmaceutical Sciences, Chinese Academy of Agricultural Sciences, Lanzhou, China

OPEN ACCESS

Edited by:

A. Rasim Barutcu,
University of Toronto, Canada

Reviewed by:

Qiang Qiu,
Northwestern Polytechnical
University, China
Shaobin Li,
Gansu Agricultural University, China

*Correspondence:

Ghasem Hosseini Salekdeh
hosseini.salekdeh@mq.edu.au
Xuezhi Ding
dingxuezhi@caas.cn

[†]These authors have contributed
equally to this work

Specialty section:

This article was submitted to
Epigenomics and Epigenetics,
a section of the journal
Frontiers in Cell and Developmental
Biology

Received: 16 August 2021

Accepted: 02 December 2021

Published: 17 January 2022

Citation:

Zheng J, Du M, Zhang J, Liang Z,
Ahmad AA, Shen J, Salekdeh GH and
Ding X (2022) Transcriptomic and
Metabolomic Analyses Reveal
Inhibition of Hepatic Adipogenesis and
Fat Catabolism in Yak for Adaptation to
Forage Shortage During Cold Season.
Front. Cell Dev. Biol. 9:759521.
doi: 10.3389/fcell.2021.759521

Animals have adapted behavioral and physiological strategies to conserve energy during periods of adverse conditions. Hepatic glucose is one such adaptation used by grazing animals. While large vertebrates have been shown to have feed utilization and deposition of nutrients—fluctuations in metabolic rate—little is known about the regulating mechanism that controls hepatic metabolism in yaks under grazing conditions in the cold season. Hence, the objective of this research was to integrate transcriptomic and metabolomic data to better understand how the hepatic responds to chronic nutrient stress. Our analyses indicated that the blood parameters related to energy metabolism (glucose, total cholesterol, low-density lipoprotein cholesterol, high-density lipoprotein cholesterol, lipoprotein lipase, insulin, and insulin-like growth factor 1) were significantly ($p < 0.05$) lower in the cold season. The RNA-Seq results showed that malnutrition inhibited lipid synthesis (particularly fatty acid, cholesterol, and steroid synthesis), fatty acid oxidation, and lipid catabolism and promoted gluconeogenesis by inhibiting the peroxisome proliferator-activated receptor (PPAR) and PI3K-Akt signaling pathways. For metabolite profiles, 359 metabolites were significantly altered in two groups. Interestingly, the cold season group remarkably decreased glutathione and phosphatidylcholine (18:2 (2E, 4E)/0:0). Moreover, integrative analysis of the transcriptome and metabolome demonstrated that glycolysis or gluconeogenesis, PPAR signaling pathway, fatty acid biosynthesis, steroid biosynthesis, and glutathione metabolism play an important role in the potential relationship between differential expression genes and metabolites. The reduced lipid synthesis, fatty acid oxidation, and fat catabolism facilitated gluconeogenesis by inhibiting the PPAR and PI3K-Akt signaling pathways to maintain the energy homeostasis of the whole body in the yak, thereby coping with the shortage of forages and adapting to the extreme environment of the Qinghai-Tibetan Plateau (QTP).

Keywords: forage shortage, yak, liver, energy metabolism, transcriptome, metabolomics

HIGHLIGHTS

- Nutritional stress caused differential alterations of various hepatic metabolites, genes, and related pathways.
- The facilitated gluconeogenesis and fatty acid oxidation and reduced the fat catabolism by inhibiting the peroxisome proliferator-activated receptor signaling pathway and PI3K-Akt signaling pathway to cope with the shortage of forages.
- Cold season grazing inhibited the expression of genes responsible for *de novo* fatty acids synthesis (ACACA, ACACB, and FASN), fatty acid uptake (LPL, OLR1), FA desaturation (SCD), and FA transportation (LDLR), fatty acid oxidation (CPT1C), and lipolysis (FABP4).

INTRODUCTION

The Qinghai-Tibetan Plateau (QTP), China's largest and highest region, is a significant livestock production area and a global biodiversity hotspot (Jing et al., 2021). It is characterized by hypoxia, high altitude, short forage growing, and long-term cold season that extends from October to May, average temperature -5°C to -15°C (Hu et al., 2019). Yak (*Bos grunniens*), a unique livestock species found mostly at high altitudes (over 4,000 m) on the QTP, plays an important role in the daily lives of local herders by providing basic production and living materials such as animal-derived food, shelter, and fuel (Hu et al., 2019). As traditional grazing livestock, yaks graze without supplementary feeding all year round; consequently, they suffer from nutritional stress for a long time due to a shortage of forage during the long-term cold season. However, yaks have lived on the QTP for thousands of years and are well adapted to cope with the harsh conditions of the QTP. It is possible that the regulation of hepatic gene expression reduced metabolic rate, and energy requirements may be adjusted in response to harsh environment by changing the capacity of enzymes (Weber et al., 2017; Jing et al., 2020; Jing et al., 2021). The liver is the main metabolic site of glucose, fatty acids, and protein and plays an important role in regulating the composition of peripheral blood nutrients and the energy metabolism balance of the animal body (Costa et al., 2014; Rui, 2014; Jing et al., 2021). The warm season pastures on the QTP grow luxuriantly, and the supply is sufficient. Yaks, like other livestock, synthesize fatty acids through *de novo* lipogenesis (DNL), and long-chain fatty acids are contributed in hepatocytes for triglycerides (TG), phospholipids, or cholesterol esters (Rui, 2014). These complex lipids are stored in lipid droplets or secreted into the circulation as intestinally derived chylomicrons (CMs) and very low-density lipoprotein (VLDL) particles. The genes involved in lipid synthesis were down-regulated, whereas the pathways gluconeogenesis (Yu et al., 2016), fatty acid oxidation (Yu et al., 2016; Ren et al., 2019), and peroxisome proliferator-activated receptor A (PPAR-A) target genes (involved in lipolysis) (Laporta et al., 2014) were up-regulated in ruminants under nutritional deprivation. However, the recent study suggests that lipid catabolism, fatty acid synthesis, glucose intake, and fatty acid oxidation in yaks were all inhibited by regulating the AMPK (adenosine 5'-

monophosphate-activated protein kinase) signaling over cold seasons (Xiong et al., 2020). Consequently, we speculate that the extreme long-term environment and nutritional stress caused by yak has formed a unique metabolic mechanism in the liver to help the host reduce energy consumption under the traditional grazing regime and maintain the body's energy homeostasis to effectively cope with the long-term withered grass period. However, the regulating mechanism of hepatic metabolism in yaks remains unknown under grazing conditions in cold seasons.

Lipid catabolism is a biochemical process that begins with fatty acid oxidation and ends with glucose production. It is influenced by nutrients, key hormones, transcriptional factors, and lipolytic enzymes (Li Y. et al., 2020). The genes such as stearoyl-CoA desaturase (SCD), fatty acid synthase (FASN), lipoprotein lipase (LPL), insulin (INS), acetyl-CoA carboxylase (ACC), and ACSL (acyl-CoA synthetase long-chain), all of which take part in lipogenesis, lipolysis, fatty acid transport, and cholesterol metabolism (Zhong et al., 2020). It is reported that the activity of LPL and INS in yak was sensitive as a result of alterations in nutritional conditions and seasons (Ding et al., 2012). Therefore, further research on the expression and regulation of genes is necessary for different seasons. Studies have revealed that the regulation of hepatic gene expression plays a crucial role in hepatic metabolism by changing the capacity of enzymes in relevant metabolic pathways (Pamela A. Alexandre et al., 2015; Ren et al., 2019). Furthermore, results of the recent studies suggest that the genes involved in hepatic lipid synthesis (ACACA, FASN, LPL, SCD1, FADS1, and FADS2) were down-regulated over nutritional deficiency (Kaufmann et al., 2012; Laporta et al., 2014; Vailati Riboni et al., 2015). Our previous study in yak also indicated the expression of genes FASN, LPL, ACACA, PPAR γ , and SREBP-1c with increasing energy levels, whereas there was low expression of HSL, CPT-1, and ATGL (Yang et al., 2020). However, most of the current research is based on specific functional genes and enzymes, and the regulation of target pathways in the hepatic response of yak is less well understood under grazing conditions. The hepatic response in ruminants has been performed to reveal the pathways such as glycolysis or gluconeogenesis, fatty acid biosynthesis, extracellular matrix-receptor interaction, protein digestion and absorption, and cholesterol homeostasis, which play an essential role in nutritional metabolism (Ren et al., 2018; Lu et al., 2019; Ren et al., 2019; Yu et al., 2019). Little information has been published concerning gene expression and target pathways in hepatic energy metabolism in yaks under natural grazing. In addition, knowledge about hepatic energy metabolism in the cold season may help explore yak's modulatory molecular mechanisms to adapt to the long-term withered grass period.

In recent years, the emerging "omics" technologies, including transcriptomics, metabolomics, and proteomics, have greatly accelerated research on the interactions between nutrients and diet in a biological system (Laporta et al., 2014; Alexandre et al., 2015). Transcriptomic and metabolomics have become the focus of nutrition research. The modulatory mechanisms of hepatic metabolism can be revealed by integrating transcriptomics and metabolomics (Yu et al., 2019). There have been extensive studies that demonstrated marked changes in ruminant's hepatic

transcriptome and metabolite profiles due to changes in different feeding regimes, particularly genes, metabolites, and pathways related to lipid metabolism (Laporta et al., 2014; Sun et al., 2018). So far, however, studies for hepatic energy metabolism in yaks based on transcriptomics and metabolomics in the nutrition stress state are rarely reported.

Therefore, we hypothesize that yak has developed a core metabolic mechanism that helps the host to adapt to the harsh environment and long-term withered grass period of the Qinghai-Tibet Plateau. In the present study, we integrated transcriptomic, metabolomic and animal serum parameters to provide new insights into the hepatic metabolism and nutritional strategies in yak for adaptation to harsh environment.

MATERIALS AND METHODS

Study Site

All yaks were grazing on the natural alpine pasture under a traditional farming system on the Qinghai-Tibetan Plateau with free access to water. Six grass species predominate the natural vegetation, namely, *Kobresia pygmaea*, *Elymus nutans*, *Kobresia humilis*, *Kobresia capillifolia*, *Stipa purpurea*, and *Potentilla acaulis*. This study was conducted at Haibei Demonstration Zone of Plateau Modern Ecological Animal Husbandry Scientific and Technology in Haibei Prefecture, Haiyan County (36° 44' to 39° 05' N, 102° 41' to 102° 57' E), Qinghai Province, China. This area has an average altitude of more than 3,000 m above sea level, an average annual temperature of 0.45°C, average annual precipitation of 277.8 to 499.5 mm, and a dry, cold winter climate. Alpine and subalpine herbage meadows in the region are important for yak production, with seasonal migration between different grazing areas. Typically, transhumance farming defined by switching between different seasonal pasture sites is practiced, with cold season and warm season pastures belonging to one type but being divided by fences as different seasonal pastures (Ding et al., 2012).

Animals and Management

A total of twelve 4-year-old healthy adult female yaks with initial average body weight (BW) 270 ± 10.6 kg were selected and randomly divided into a warm-season group (YW) and cold season (YC) group, with six yaks each group, and properly marked with ear tags for identification. The warm season group was grazed on the natural alpine pasture in the Qinghai-Tibetan Plateau from May to September, whereas the yaks in cold season were grazed from October to the following April, which was thought to correspond to the increasing stage of alpine grasses and changes in the nutritional status of yaks in a whole production year. Moreover, the experimental procedures in animal care in this study were approved by the Animal Care and Use Committee of Lanzhou Institute of Husbandry and Pharmaceutical Sciences, CAAS, and China [SYXK-2018-0011]. Meanwhile, all yaks care procedures were consistent with the Guide, local animal welfare laws for the Care and Use of Laboratory Animals (Gansu Province Animal Care Committee, Lanzhou, and China).

The forage samples were collected with the previous method in mid-month; vegetation samples were cut within a 10×10 -cm

quadrat frame. Each plot was randomly sampled for 30 small samples, mixed into a large sample, and each plot was repeated five times. The feces of the yaks were collected each month; in each plot, 15 fresh feces were randomly selected as small samples, mixed into a large sample, with five replicates for each plot. The dry matter (DM), crude protein (CP), neutral detergent fiber (NDF), ether extract (EE), and acid detergent fiber (ADF) were measured according to previous methods (Van Soest et al., 1991). The nutritional composition of pasture herbage is listed in **Supplementary Table S1**. The DM intake (DMI), metabolic energy intake, DM digestibility, CP digestibility, NDF digestibility, and ADF digestibility was measured by previous studies (Oba and Allen, 1999). The results are presented in **Supplementary Table S2**.

Sample Collection

Following fasting for 8 h, blood samples were collected from the jugular vein into EDTA tubes and chilled on ice. After centrifugation ($2,000 \times g$, 4°C, and 20 min) of the blood samples, the plasma was divided into portions and frozen at -20°C and used for measurement of glucose, INS, total cholesterol, nonesterified fatty acids, triglyceride, and so on. The liver tissue was collected after slaughtering and immediately washed with 0.90% NaCl solution and stored in liquid nitrogen for gene expression and metabolome analysis.

Measurement of Blood Biochemical and Hormonal Parameters

Triglyceride (TG), cholesterol (CH), high-density lipoprotein cholesterol (HDL-C), low-density lipoprotein cholesterol (LDL-C), lactate dehydrogenase (LDH), glucose, nonesterified fatty acids (NEFAs), and creatine kinase (CK) levels, of plasma, were determined with an automatic biochemical analyzer (TG, Cat #: A110-1-1; CH, Cat #: A111-1-1; HDL-C, Cat #: A020-1-2; LDL-C, Cat #: A113-1-1; LDH, Cat #: A110-1-1; NEFAs, Cat #: A042-1; CK, Cat #: A032-1-1; Shenzhen Mindray Bio-Medical Electronics Company Limited, Shenzhen, and China).

The concentrations of FAS, growth hormone (GH), INS-like growth factor 1 (IGF-1), INS-like growth factor 2 (IGF-2), glutathione peroxidase (GSH-PX), LPL, INS, malondialdehyde (MDA), superoxide dismutase (SOD), and total antioxidant capacity (T-AOC) were measured according to the manufacturer's instructions (FAS, bovine FAS ELISA KIT, Cat #: ZC-50645; GH, bovine GH ELISA KIT, Cat #: ZC-50478; IGF-1, bovine IGF-1 ELISA KIT, Cat #: ZC-50596; IGF-2, bovine IGF-2 ELISA KIT, Cat #: ZC-54217; GSH-PX, bovine GSH-PX ELISA KIT, Cat #: ZC-54011; LPL, bovine LPL ELISA KIT, Cat #: ZC-50640; INS, bovine INS ELISA KIT, Cat #: ZC-50594; MDA, bovine MDA ELISA KIT, Cat #: ZC-50180; SOD, bovine SOD ELISA KIT, Cat #: ZC-50189; T-AOC, bovine T-AOC ELISA KIT, Cat #: ZC-53993; Chengdu Li Lai Biotechnology Company Limited, Chengdu, and China).

Metabolomic Profiling Analysis

The hepatic metabolome was analyzed using a Vanquish UHPLC system (Thermo Fisher) coupled with an Orbitrap Q Exactive HF-X mass spectrometer (Thermo Fisher). Samples were separated on a

Hyperil Gold column (100 × 2.1 mm, 1.9 μm) at a 0.2 mL/min flow rate. The eluents for the positive polarity mode and the negative polarity mode were eluent A (0.1% FA in water, 5 mM ammonium acetate, pH 9.0) and eluent B (methanol). The solvent gradient was as follows: 1.5 min, 2% B; 12.0 min, 2%–100% B; 14.0 min, 100% B; 14.1 min, 100%–2% B; 16 min, 2% B. Q Exactive HF-X mass spectrometer was performed in positive/negative polarity mode with a spray voltage of 3.2 kV, the capillary temperature of 320°C, and sheath gas and aux gas flow rate of 35 and 10 arb, respectively.

Progenesis QI (Waters Corporation, Milford, MA, USA) data processing software was used to identify metabolites. The metabolic alterations among experimental groups were visualized by principal component analysis (PCA) and (orthogonal) partial least-squares discriminant analysis (O) PLS-DA, after data preprocessing by mean centering (Ctr), and Pareto variance (Par) scaling, respectively. Metabolites were identified with variable importance in the projection (VIP) values larger than 1.0 and *p* values less than 0.05, and FC less than or equal to 0.67 or FC larger than or equal to 1.5 were considered differential metabolites. The metabolic pathways and metabolite set enrichment analysis were analyzed using MetaboAnalyst 5.0 (<https://www.metaboanalyst.ca/>).

RNA Preparation and Transcriptome Sequencing

Liver tissues of yak were used to total RNA extraction using TRIzol reagent (Invitrogen, Carlsbad, CA, USA) following the manufacturer's protocol. The Agilent 2,100 Bioanalyzer was performed to detect RNA integrity (Agilent Technologies, Santa Clara, CA, USA). All samples with RNA Integrity Number ≥ 7 were subsequently analyzed. The mRNA was established sequencing libraries using TruSeq RNA Sample Preparation Kit (Illumina, San Diego, CA, USA). Then cDNA libraries were sequenced on the Illumina sequencing platform (HiSeqTM 2,500), which generated paired-end reads of 125 bp/150 bp. FPKM (Roberts et al., 2011) value of each gene was calculated using cufflinks (Trapnell et al., 2010), and the htseq count was used to obtain the read counts of each gene (Anders et al., 2015). The differential expression genes (DEGs) between YW and YC groups were detected using DESeq (Anders and Huber, 2012) R package. The false discovery rate (FDR) < 0.05 and the absolute value of the log₂ (fold change) with FPKM ≥ 1 were used as the threshold for significantly different expression (Liu et al., 2021). Hierarchical cluster analysis of DEGs was performed to explore gene expression patterns. Gene Ontology (GO) and Kyoto Encyclopedia of Genes and Genomes (KEGG) (Kanehisa et al., 2007) pathway enrichment analysis of DEGs were respectively performed using R based on the hypergeometric distribution. GO terms and the pathways of KEGG with FDR < 0.05 were considered remarkably enriched. The raw data of transcriptome sequencing for livers of yaks in YC and YW groups have been deposited in the National Center for Biotechnology Information (NCBI) at Sequence Read Archive with the accession number PRJNA756146.

Real-Time Quantitative PCR

Real-time quantitative reverse transcriptase–polymerase chain reaction (qRT-PCR) assay was performed as described in our

TABLE 1 | The effects of different seasons on serum biochemical parameters.

Item	Treatment		SEM	<i>p</i> value
	YC	YW		
TG (mmol/L)	0.18 ^b	0.30 ^a	0.10	0.022
LDH (U/L)	839.14	993.62	91.92	0.433
GLU (mmol/L)	3.68 ^b	5.24 ^a	0.52	0.044
LDL-C (mmol/L)	0.16 ^b	0.41 ^a	0.05	0.006
HDL-C (mmol/L)	1.04 ^b	1.71 ^a	0.16	0.025
CH (mmol/L)	1.11 ^b	2.21 ^a	0.22	0.003
CK (U/L)	742.50 ^a	171.32 ^b	116.74	0.015
NEFAs (μmol/L)	835.90 ^a	545.64 ^b	58.24	0.012

Note: TG, triglycerides; LDH, lactate dehydrogenase; GLU, glucose; LDL-C, low-density lipoprotein cholesterol; HDL-C, high-density lipoprotein cholesterol; CH, cholesterol; CK, creatine kinase; NEFAs, nonesterified fatty acids.

previous study (Yang et al., 2020). The β-actin was used as a reference gene to normalize gene expression. Primers used for qRT-PCR are listed in **Supplementary Table S3**. The qRT-PCR was performed in triplicate reactions to determine relative mRNA levels using SYBR® Premix Ex Taq™ II (TaRaKa, Dalian, and China). Fold change was calculated for each candidate gene, and sample was calculated by means of the formula the $2^{-\Delta\Delta Ct}$ (Schmittgen and Livak, 2008).

Statistical Analysis

Data are presented as means ± SEM. All statistical analyses were performed by the one-way analysis of variance test, and the differences were compared using Tukey multiple-comparisons test, and *P* < 0.05 was considered to be statistically significant. Moreover, integrative analysis of DEGs and differential metabolites that involved hepatic energy metabolism was performed by MetaboAnalyst 5.0 (<https://www.metaboanalyst.ca/>). Pearson correlation algorithm was used to calculate the associations between discriminant gene expression and metabolites, when $|r| > 0.60$ and *p* < 0.05 were considered as a significant correlation.

RESULTS

Serum Biochemical Parameters

Live BW fell through the whole winter as food accessibility decreased with decreasing above-ground herbage mass. Still, during the warm season, compensatory growth led to early and increasing benefits for mitigating body mass loss over the winter. The levels of GLU, CH, and TG were significantly higher in the YW group than those in the YC group (*p* = 0.044, *p* = 0.003, and *p* = 0.022; **Table 1**), indicating that the energy produced by glucose from forage cannot maintain the energy homeostasis of the body in the case of the shortage of forage. The yak needs to consume higher levels of GLU to maintain normal physiological function. Conversely, the concentration of NEFAs and CK in the YC group was significantly higher than that in the YW group (*p* = 0.012, *p* = 0.015), whereas differences were not statistically significant in the concentration of LDH (*p* > 0.05). Similarly, no significant differences in FAS, HSL, and IGF-2 were observed between the considered groups (*p* > 0.05; **Table 2**). However, the

TABLE 2 | The effects of different seasons on serum hormone of the yak.

Item	Treatment		SEM	p value
	YC	YW		
FAS (nmol/L)	2.93	1.94	0.33	0.145
GH (ng/mL)	3.66 ^a	2.36 ^b	0.42	0.018
HSL (ng/mL)	1.14	1.74	0.21	0.173
IGF-1 (ng/mL)	48.21 ^b	55.15 ^a	2.70	0.012
IGF-2 (ng/mL)	4.45	7.11	0.97	0.185
INS (mIU/L)	3.36 ^b	5.10 ^a	0.68	0.002
LPL (U/L)	96.31 ^b	148.72 ^a	13.96	0.020

Note: FAS, fatty acid synthetase; GH, growth hormone; HSL, Hormone-sensitive fatty lipase; IGF-1, insulin-like growth factor 1; IGF-2, insulin-like growth factor 2; INS, insulin; LPL, lipoprotein lipase.

levels of LDL-C, HDL-C, IGF-1, INS, and LPL tended to be higher in warm season than those in cold season ($p = 0.006$, $p = 0.025$, $p = 0.012$, $p = 0.002$, and $p = 0.020$), whereas GH concentration was higher for the YC group than the YW group ($p = 0.018$) (Tables 1, 2). In addition, compared with the YC group, there was an increasing trend but no significant differences in serum antioxidant index, including T-AOC, GSH-PX, MDA, and SOD in the YW group ($p > 0.05$; Table 3)

Metabolomic Profiling

An untargeted metabolomics approach studied the specific impact of seasonal changes in external conditions, especially food availability, and on metabolomic profiling. Based on the extracted ion peaks, differential metabolites in yak liver were discriminated by the scatterplots, including the quality control samples (Figure 1A), which demonstrated the precision and repeatability of the untargeted liquid chromatography-mass spectrometry (LC-MS) detection. A total of 4,953 metabolites (3,311 in positive mode and 1,642 in negative mode) were detected and used for multivariate analysis of hepatic metabolites (Supplementary Figure S1). The OPLS-DA for the two groups reveals a clear distinction (Figure 1B); cumulative variation modeled in the component in the Y matrix (R^2Y_{cum}) was 0.986, and the cumulative estimate of the predictive ability of the model (Q^2_{cum}) was 0.957, which was validated by the permutation analysis ($Q^2 = -0.493$). Importantly, 306 main metabolites (213 up-regulated and 93 down-regulated) were considerably significantly altered from each other, especially under the different seasons ($VIP > 1$, $p < 0.05$, and $FC \leq 0.67$ or ≥ 1.5 ; Supplementary File S1).

To show the expression differences of metabolites in different samples more intuitively, we performed Hierarchical Clustering on all significantly different metabolites ($p < 0.05$) and conducted a visual analysis of differential metabolite expression levels based on VIP value. We found that metabolites had a significant difference in the YC and YW groups from in Figure 1C. And results showed that the YC group contained lower contents of the expression abundance of metabolites YC ($p < 0.05$), including phosphatidylcholine (PC) (18:2 (2E, 4E)/0:0), glutamylcysteine, glutathione, Lyso PC (18:1 (11Z)), phosphocholine, and Glu-Cys. In comparison, the YW group accumulated higher contents of glycochenodeoxycholic acid 3-glucuronide, TG (20:0/18:3 (9Z, 12Z, 15Z)/o-18:0), and allocholic acid. These results indicated

TABLE 3 | The effects of different seasons on plasma antioxidant index of the yak.

Item	Treatment		SEM	p value
	YC	YW		
T-AOC (U/mL)	9.09	5.95	1.19	0.206
GSH-PX (ng/mL)	970.15	523.30	129.47	0.082
MDA (nmol/mL)	2.04	1.36	0.25	0.181
SOD (ng/mL)	1.83	1.07	0.23	0.104

Note: T-AOC, bovine total antioxidant capability; GSH-PX, glutathione peroxidase; MDA, malondialdehyde; SOD, superoxide dismutase.

that nutritional stress increased oxidative stress, reduced lipid transport metabolism, and boosted VLDL synthesis. In addition, KEGG pathway enrichment analysis was performed to screen the differential pathways in the liver of yaks with the effect of malnutrition (Figure 1D). The results revealed that the most abundant metabolites were mainly enriched in pentose and glucuronate interconversions, glutathione metabolism, ABC transporters. Meanwhile, glycerophospholipid metabolism and fructose and mannose metabolism were similarly enriched.

Analysis of Different Expression Genes

To obtain a global view of the hepatic transcriptome responses in yak under different seasons, the hepatic transcriptomes were analyzed by comparative RNA-Seq. cDNA libraries were constructed using total RNA isolated from the same experimental materials as metabolic profiling. Using an Illumina HiSeq 2,500 sequencer, we obtained approximately 52.90 and 50.76 million high-quality clean reads from YW and YC groups, respectively. For each sample, 94.71% and 94.99% of reads could be mapped to the YW and YC yak reference genome, respectively, in which 90.54% and 91.10% aligned with unique genes unambiguously (Table 4). In total, 10,955 and 10,296 expressed genes (average FPKM > 1) were detected in the livers of YW and YC yaks, respectively. The PCA approach showed that the samples were grouped closely, respectively (Figure 2A). DEGs were screened via DEGSeq with an FDR < 0.05 and the absolute value of the \log_2 (fold change) with an FPKM ≥ 1 . We identified 1,870 DEGs (487 up-regulated and 1,383 down-regulated) from the total of 17,724 genes (Figure 2B, C; DEG list is provided in Supplementary File S2). A heat map for hierarchical cluster analysis of DEGs between the two groups was more intuitive to support the view (Figure 2D).

GO Enrichment and Pathway Analysis of DEGs

GO enrichment analysis and the terms of top30 DEGs indicated that the energy metabolism and glutathione metabolism processes dominated the biological processes between the different seasons (FDR < 0.05 ; Figure 2E). The GO terms of glutathione transferase activity and glutathione metabolic process were related to the glutathione metabolism. Notably, the GO terms of cholesterol biosynthetic process, sterol biosynthetic process, cholesterol homeostasis, IGF-2 binding, long-chain fatty acid import, and IGF-1 binding were closely related to energy metabolism.

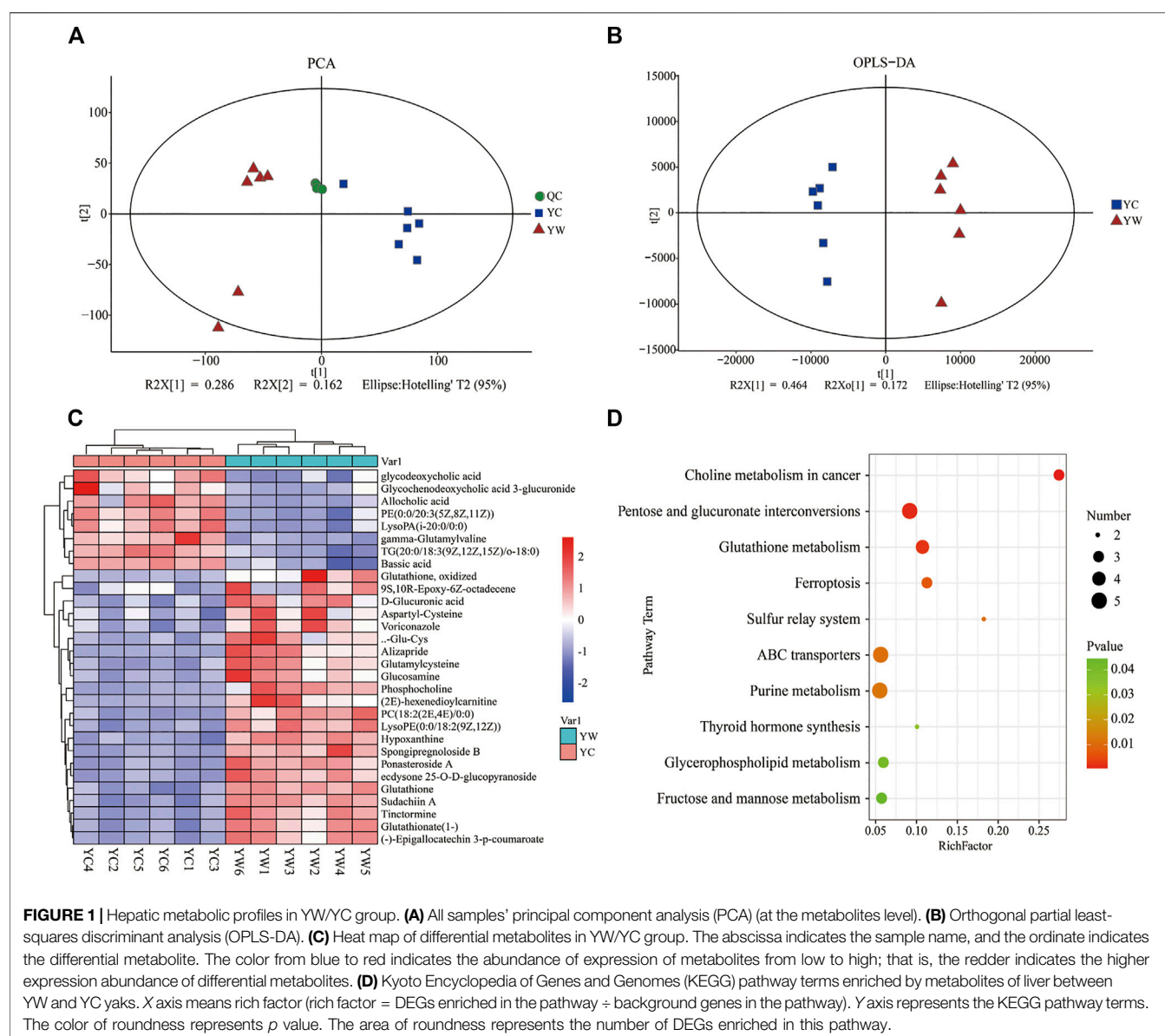
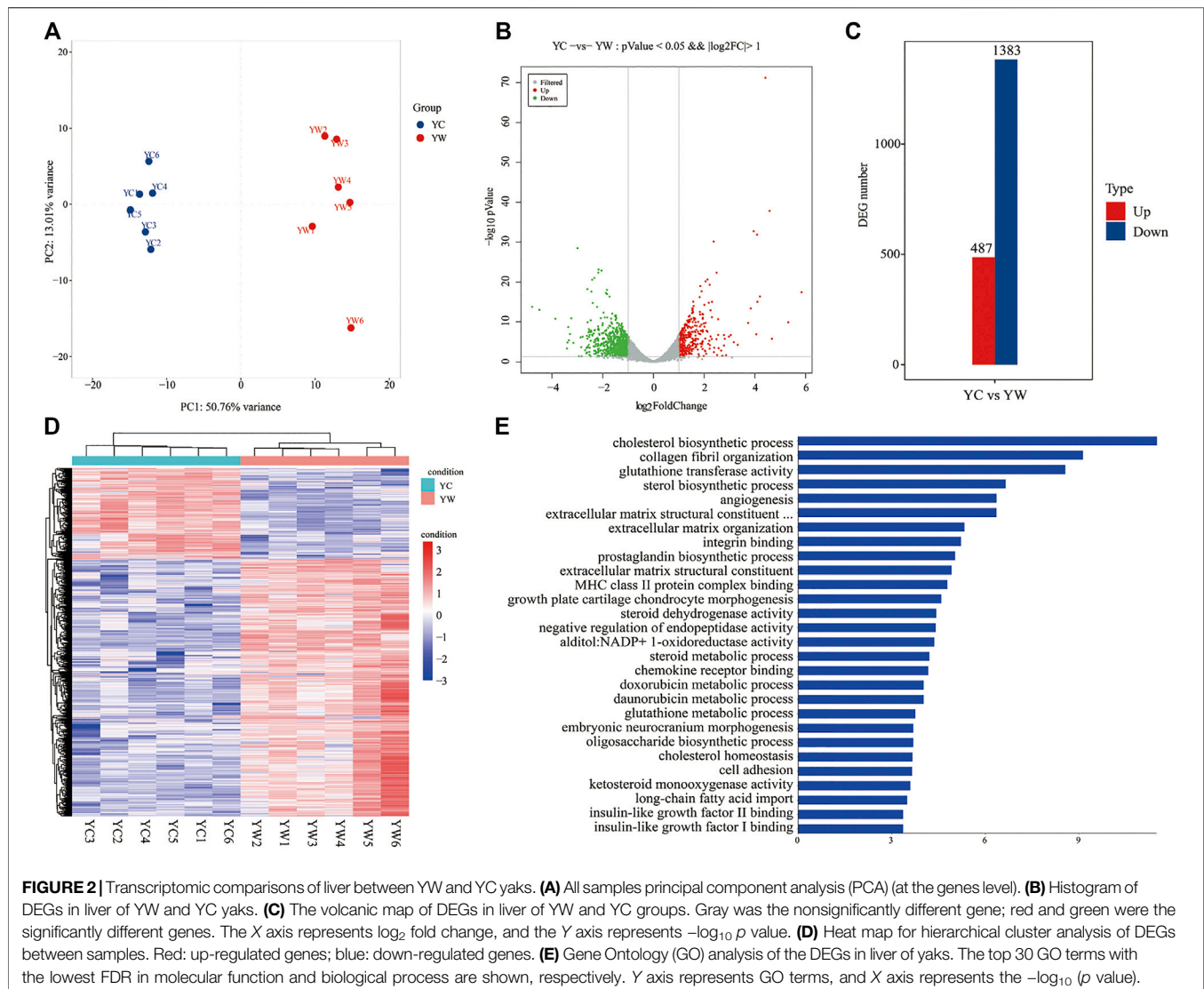


TABLE 4 | Summary of the sequencing reads alignment to the reference genome.

Statistics term	YW	YC
Clean reads	50.76	52.90
Total reads	50,760,057	52,896,499
Total mapped reads	94.99%	94.71%
Uniquely mapped	91.0%	90.54%
Nonsplice reads	49.39%	50.28%
Splice reads	41.70%	40.26%
Reads mapped in proper pairs	87.66%	87.11%

Furthermore, the KEGG analysis remarkably enriched 50 pathways for the identified DEGs (FDR <0.05; **Figure 3B**). ECM–receptor interaction (30 genes, adjusted $p = 8.57 \times 10^{-9}$), focal adhesion (47 genes, adjusted $p = 2.53 \times 10^{-5}$), protein digestion and absorption (34

genes, adjusted $p = 9.50 \times 10^{-5}$), metabolism of xenobiotics by cytochrome P450 (21 genes, adjusted $p = 2.18 \times 10^{-6}$), drug metabolism—cytochrome P450 (19 genes, adjusted $p = 8.94 \times 10^{-6}$), and glutathione metabolism (14 genes, adjusted $p = 0.004$) were significantly enriched. Typically, the expression levels of the genes including THBS1, COL4A4, SLC38A2, COL4A3, GSTK1, and GSTM3 were remarkably lower expressed in the liver of YC yaks compared with YW yaks, whereas ITGA1 had a higher expression. The bile secretion was significantly enriched with 23 genes (adjusted $p = 0.0001$), in which LDLR, HMGCR, and ABCB11 were highly expressed in YW yaks than YC yaks. Meanwhile, there were nine DEGs enriched in ovarian steroidogenesis (adjusted $p = 0.004$) and 10 DEGs enriched in steroid biosynthesis (adjusted $p = 8.94 \times 10^{-6}$). Mainly, including LDLR, IGF1R, FDFT1, and DHCR7 were weakly expressed in YC yaks. Interestingly, PI3K–Akt signaling pathway (53 genes, adjusted $p = 0.004$) were also enriched. Notably, the PPAR signaling



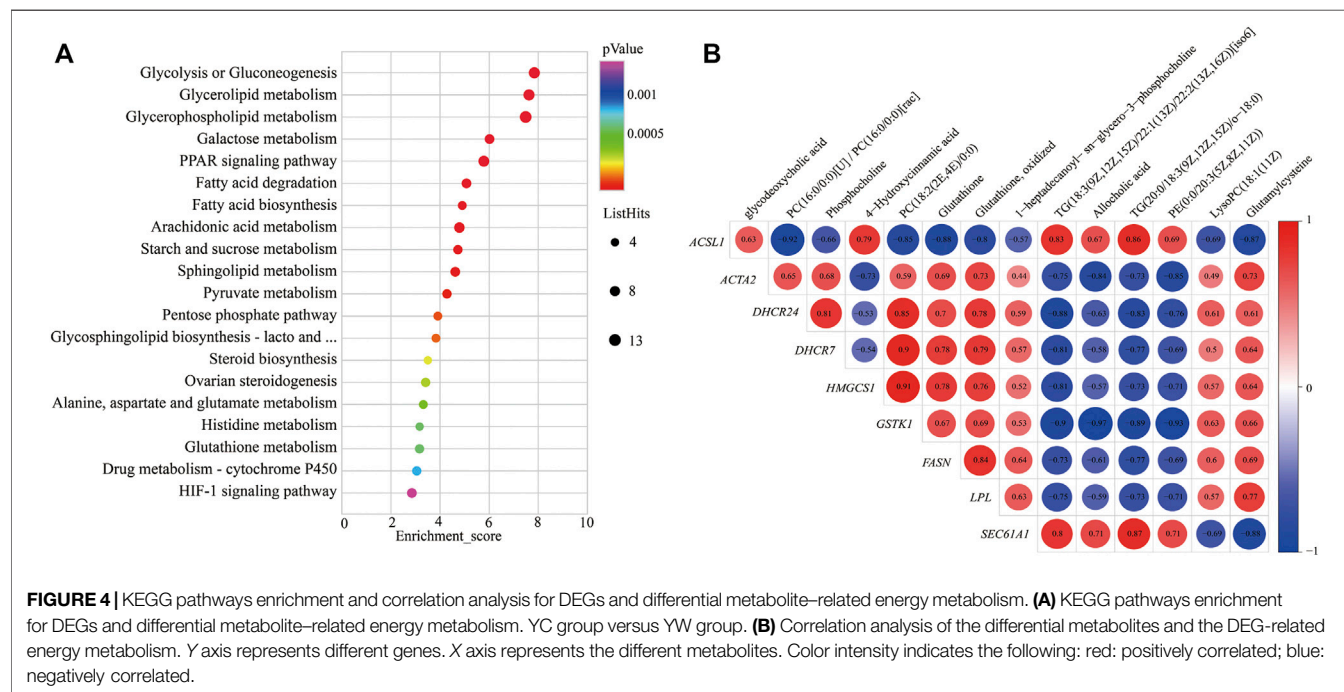
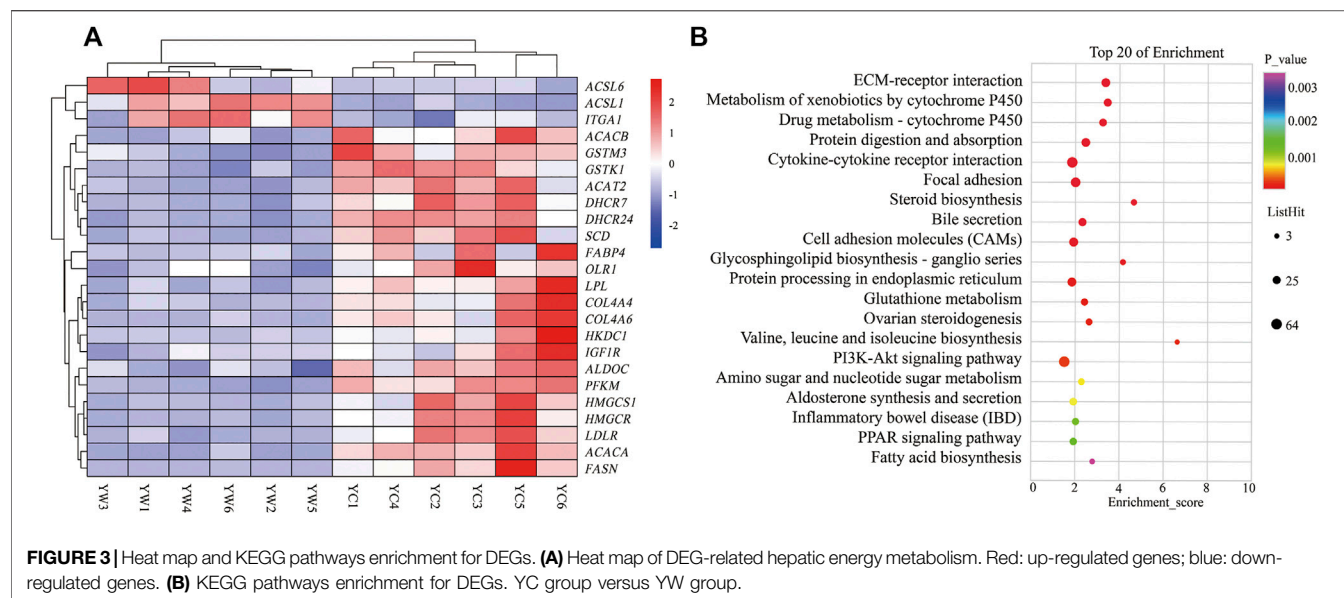
pathway (16 genes, adjusted $p = 0.01$) and fatty acid biosynthesis (5 genes, adjusted $p = 0.03$) were significantly enriched. Typically, ACSL6 and ACSL1 had higher expression in YC yaks, whereas FABP4, SCD, HMGCS1, SLC27A2, HKDC1, LPL, OLR1, ACACA, ACACB, and FASN had lower expression (Figure 3A).

qRT-PCR Validation of Functional Gene Expression

To validate the reliability gene expression from RNA-Seq, the transcriptome levels of 10 genes (ACACB, ALDOC, ACSL1, ACAT2, HK2, ACSL6, SEC61A1, GMPPB, SDS, and HKDC1) among the DEGs were determined by qRT-PCR with three replicates (Supplementary Figure S2). Of these, the expression trends were consistent with those obtained in the RNA-Seq analysis. In addition, the RNA-Seq and qRT-PCR results demonstrated that the data could be used to assess the up-regulation and down-regulation of gene expression.

Integrative Analysis of Transcriptome and Metabolome

To further study the potential relationship between DEGs and metabolites. The metabolomic and transcriptomic data were combined and analyzed by MetaboAnalyst 5.0. As shown in Figure 4A, the results demonstrated that the pathways, such as glycolysis or gluconeogenesis, PPAR signaling pathway, fatty acid degradation, fatty acid biosynthesis, arachidonic acid metabolism, pyruvate metabolism, pentose phosphate pathway, steroid biosynthesis, alanine, aspartate, and glutamate metabolism, glutathione metabolism, drug metabolism—cytochrome P450, and HIF-1 signaling pathway, were significantly enriched. Indicating energy metabolism plays an important role in yaks to adapt to nutritional stress due to a shortage of forage. Meanwhile, correlation analysis was performed to examine the association of differential metabolites with DEGs. The correlation analysis between DEGs and differential metabolites related to energy metabolism also showed that PC (18:2 (2E, 4E)/0:0), phosphocholine, glutathione,



and glutamylcysteine were positively correlated with DHCR24, DHCR7, HMGCS1, LPL, FASN, ACAT2, and GSTK1, whereas glycodeoxycholic acid, TG (20:0/18:3 (9Z, 12Z, 15Z)/o-18:0), and 4-hydroxycinnamic acid displayed negative correlation (Figure 4B).

DISCUSSION

The present study revealed a potential mechanism of yak adaption to the long-term withered grass period by regulating

hepatic energy metabolism to alter related metabolite and gene pathways to reduce fat catabolism as possible, to maintain the energy homeostasis of whole-body in the yak, further coping with a shortage of forages and adapting to the extreme environment of the QTP.

With the extension of the cold season, the content of CP and EE in herbage decreased, and that of PDF and ADF increased in a previous study (Saul et al., 2009; Zhou et al., 2020), which is consistent with our research results. In this present, compared within a warm season, the content of DM and ADF increased in

the cold season, whereas the content of CP and EE in herbage decreased. Therefore, it could be inferred that the BW loss during the cold season resulted from low nutrient contents in forage, which were insufficient to meet the maintenance requirement of growing yaks during the cold season. Meanwhile, the levels of GLU, NEFAs, INS, and IGF-1 in the blood can reflect the energy metabolism of the animal body. Studies have shown that the concentrations of GLU and NEFAs in serum are regulated by the hormones GH, INS, and IGF-1, which play an important role in the synthesis, decomposition, and utilization of sugars and lipids (McGillicuddy et al., 2009). Results of the present study suggest that the levels of glucose (GLU) were remarkably decreased in the cold season; this may be due to when yaks are in a state of starvation or hypoxia, the energy produced by glucose from grass is unable to maintain the normal physiological function of yak, and the demand for glucose exceeds the gluconeogenesis in the liver, and the concentration of GLU decreases accordingly (Giulia Esposito et al., 2014). Previous studies have found that in dairy cows, serum IGF-1 concentration increased with an increase in nutrient intake, whereas the concentration of GH decreased with an increase in nutrient intake (Weller et al., 2016). This experimental result also found that the serum IGF-1 concentration was observably lower in the cold season than in the warm season. Meanwhile, the concentration of GH was significantly higher in the cold season. The possible reasons may be the abundant grass in the warm season, the average daily gain of the yak has been improved, and the growth and development of the animal body tend to mature with the increase in ADG, which gradually reduces the amount of protein synthesis in the body and increases fat deposition. Therefore, the role of GH is relatively weakened, and the serum GH concentration also decreases (Firmenich et al., 2020). Serum triglyceride, total cholesterol, LDL, and HDL reflect the status or rate of lipid metabolism (Huang et al., 2013). Compared with the warm season in this study, the concentration of CH, HDL-C, and LDL-C was significantly decreased in the cold season, implying that the synthesis of lipid metabolism was inhibited during the cold season. Also, INS and LPL were remarkably lower in the cold season than in the warm season; a report from the literature indicated that plasma INS levels were low during energy restriction in most species (Radcliff et al., 2004), consistent with our results, indicating that gluconeogenesis was promoted by the INS signaling pathway to maintain glucose homeostasis during the shortage of forage (Feng et al., 2020). Moreover, our previous study also showed that in the yak, the levels of INS and LPL were significantly higher in the warm season than those in the cold season, which may be used for compensatory growth involved in the supplement of extrahepatic lipid depots and maintenance of body energy of yak in the cold season (Ding et al., 2012).

In the present study, we evaluated hepatic metabolomic alterations through different seasons using LC-MS and found that 306 metabolites were significantly altered between the YC group and the YW group ($VIP > 1$, $p < 0.05$, and $FC \leq 0.67$ or ≥ 1.5), of which 213 metabolites were up-regulated, and 93 metabolites were down-regulated in the cold season. A most important finding was that glutathione and PC (18:2 (2E, 4E)/0:0) were remarkably decreased in the YC group, whereas TG

increased. Glutathione is a tripeptide that plays a pivotal role in reducing oxidative stress, maintaining redox balance, enhancing metabolic detoxification, and regulating immune system function (Minich and Brown, 2019). PC, a glycerophospholipid and principal component of the VLDL monolayer, is the major phospholipid component of all plasma lipoprotein classes (Cole et al., 2012), which may help in lipid transport and metabolism and boost VLDL synthesis in the liver of yak (Zhou et al., 2020), indicating that a decrease in the levels of circulating VLDLs and HDLs (Cole et al., 2012; Mcfadden, 2020) was in agreement with the low levels of LDL and HDL in the serum; these results implied free fatty acids as triglyceride for tissues as energy source storage for utilization (Hocquette et al., 1998). Of note, we also observed a significant decrease in metabolites involved in glutathione metabolism, implying that the shortage of forage may increase yak exercise and physical activity, thereby inducing oxidative stress. This result agrees with Godin and Wohieb's findings, which suggested that a strong ultraviolet and low oxygen environment on the Qinghai Tibet Plateau would increase the formation of free radicals in animals. In contrast, oxidative stress was increased under nutritional deficiency (Godin and Wohieb, 1988).

The adaptive response to food deprivation is associated with major transcriptional and metabolic alterations; one of the most major metabolic changes observed during starvation is increased lipid catabolism in the liver (Settembre et al., 2013). In this study, the gene expression profiles showed that DEGs were significantly enriched in the bile secretion, steroid biosynthesis, PPAR signaling pathway, and fatty acid biosynthesis. In these pathways, *ACSL6* and *ACSL1* were up-regulated, whereas *LDLR*, *HMGCR*, *IGF1R*, *DHCR7*, *FABP4*, *SCD*, *HMGCS1*, *SLC27A2*, *HKDC1*, *LPL*, *OLR1*, *ACACA*, *ACACB*, and *FASN* were down-regulated in the YC group. The ACC- α (*ACC1/ACACA*), which catalyzes the carboxylation of acetyl-CoA to malonyl-CoA, is a key rate-limiting enzyme of DNL synthesis in the mammalian cytosol (Ma et al., 2011). The ACC- β (*ACC2/ACACB*) is a regulator of mitochondrial fat oxidation, and *ACACB* knockout in mice has reportedly increased fat oxidation and total energy expenditure and reduced fat mass (Ma et al., 2011). *FASN* and *SCD* are important lipogenic enzymes, and changes in their activities can change the biosynthesis rate of fatty acids (Cogburn et al., 2020). The *LPL* is the major enzyme responsible for hydrolyzing triglycerides present in the triglyceride-rich lipoproteins VLDL and CMs to provide free fatty acids for tissue utilization or storage (Kersten, 2014; Nyrén et al., 2019). Oxidized low-density lipoprotein receptor 1 (*OLR1*) is one of the most vital lipoprotein receptors regulating fat deposition, which overexpression could augment free fatty acid uptake and cholesterol content (Chui et al., 2005). Solute carrier family 27 member 2 (*SLC27A2*) is a transmembrane protein, which plays a crucial role in fatty acid degradation and lipid biosynthesis (Caimari et al., 2010). Moreover, our previous study in yak showed the expression of genes *FASN*, *LPL*, *ACACA*, *PPAR γ* , and *SREBP-1c* with increasing energy levels during the cold season, whereas there was low expression of *HSL*, *CPT-1*, and *ATGL* (Yang et al., 2020).

Similar to our results, in comparison with the warm season, the expressions of genes responsible for *de novo* fatty acids synthesis (ACACA, ACACB, and FASN), fatty acid uptake (LPL, OLR1), the rate-limiting steps of fatty acid uptake (SLC27A2), FA desaturation (SCD), and FA transportation (LDLR) were significantly down-regulated in the liver of cold season grazing yak, indicating that malnutrition reduced the capacity of liver for synthesis, and degradation of *de novo* fatty acid and FA uptake as well as the transportation of fatty acids from the liver to other parts of the body in the form of VLDL. It may be used for compensatory growth and to maintain the body's energy homeostasis, thereby coping with the harsh conditions of the QTP (Ding et al., 2012). This speculation was further supported by the serum levels of LDL-C, LPL, and total cholesterol, which were remarkably lower for the YC group than the YW group. And also consistent with the study by Vahmani et al. (2014), who reported that the genes involved in lipid synthesis, including ACACA, FASN, LPL, SCD1, FADS1, and FADS2, were down-regulated under nutritional deficiency.

Long-chain acyl-CoA synthetases (ACSL 1–6) are key enzymes regulating the partitioning of acyl-CoA species in lipid metabolism and take part in lipid synthesis or β -oxidation (Ellis et al., 2010). ACSL1 plays a key role in the synthesis of triglycerides, phospholipids, and cholesterol esters. It was reported that high expression of ACSL1 reduced fatty acid β -oxidation through the PPAR γ pathway, further increasing triglyceride levels (Li Y. et al., 2020). Fasting and exercise decreased the expression levels of ACSL6 and other lipid synthesis genes (Teodoro et al., 2017). We observed in the liver the ACSL1, and the ACSL6 gene was up-regulated in the cold season, which was not in agreement with previous results. Previous research indicated in rat fasting up-regulated ACSL1 and ACSL4 mRNA expression levels and down-regulated expression of ACSL6 (Mashek et al., 2006). The possible reasons may be that ACSL6 was regulated by INS and speculated that biological circumstances that promote increased INS sensitivity would be corrected with higher levels of ACSL6 in the liver (Teodoro et al., 2017).

Cholesterol homeostasis in the liver of mammals is maintained through exogenous absorption, endogenous synthesis, and excretion or conversion of cholesterol into bile acids. A reciprocal relationship between these processes regulates circulating cholesterol levels in response to dietary interventions (Liu et al., 2017; Oczkowicz et al., 2020). Bile acid, a steroid acid synthesized in the liver, is responsible for fat metabolisms, such as digestion and absorption (Li R. et al., 2020). A previous study has shown that lipid metabolism (particularly cholesterol and steroid metabolism) was significantly increased with increasing dietary forage levels and the genes (HMGCS1, HMGCR, MSMO1, and DHCR7) enriched in the related pathways (Shi et al., 2018). Similar to our results, in the current study, the GO and KEGG enrichment analysis found that DEGs (HMGCR, HMGCS1, and DHCR7) involved in the cholesterol biosynthetic process, the bile secretion, and sterol metabolism were significantly down-regulated in the absence of forage. Decreased cholesterol synthesis, steroid biosynthesis, and bile secretion in the liver might be responsible for the increased energy utilization and adaption to a harsh QTP environment in the cold season (Miron and Tirosh, 2019).

Meanwhile, we also observed that glutathione metabolism was significantly involved in liver transcriptome and metabolome of grazing yaks in the cold season. The glutathione S-transferases (GSTs) are a superfamily of isoenzymes that play important roles in the diminution of antioxidant injury, immune system function regulation, signaling pathways, and enhancement of metabolic detoxification. It has been demonstrated that GSTM3 and GSTK1 contributed to oxidative stress-mediated liver damage (Uno et al., 2020). We observed that down-regulation of GSTM3 and GSTK1 expression in the liver of cold season grazing yaks, which may be due to shortage of forage and low temperature in the cold season, induced excessive physical activity and negative nutrient balance, thereby inducing oxidative stress and immune response (Ren et al., 2019).

The PPAR signaling pathway is vital in metabolism, lipolysis, adipogenesis, angiogenesis, INS sensitivity, inflammatory response, and cell growth. A recent study showed that the PPAR signaling pathway (related to lipolysis) was up-regulated in grazing conditions (Laporta et al., 2014; Vahmani et al., 2014; Ren et al., 2019). Strangely, The finding from the present study was the observation that DEGs were significantly enriched in the PPAR signaling pathway, the genes related to fatty acid uptake (LPL, OLR1), adipogenesis (SCD, FASN, and FADS2), lipolysis (FABP4), the rate-limiting steps of fatty acid uptake (SLC27A2), and fatty acid oxidation (CPT1C) were all down-regulated, indicating the inhibition of fatty acid synthesis, adipogenesis, fat catabolism, and fatty acid oxidation in grazing of the cold season. It is not consistent with the results of hepatic metabolism in other ruminants. In addition, the PI3K-Akt signaling pathway plays an essential role in regulating hepatic glucose homeostasis and INS sensitivity. PI3K activates Akt and accelerates the phosphorylation of PDK1, thereby suppressing hepatic gluconeogenesis and accelerating glycogen synthesis (Pitaloka et al., 2019). Our results showed that the PI3K-Akt signaling pathway was significantly inhibited in the cold season, implying that the decreased gene expression levels involved in the PI3K-Akt pathway may enhance hepatic glycogenolysis and gluconeogenesis to maintain energy homeostasis of the body (Rui, 2014). The study reported that compared with small-tailed Han sheep, Tibetan sheep had higher gluconeogenesis and ketogenesis in the liver in negative energy balance to cope with low energy intake and regulate whole-body energy homeostasis under the harsh environment of the QTP (Jing et al., 2021). These physiological characteristics in yak are similar to those in Tibetan sheep, presenting low fatty acid oxidation and fat catabolism and high gluconeogenesis to maintain whole-body energy homeostasis under grazing conditions in the cold season. The regulatory mechanism of the PPAR signaling pathway and PI3K-Akt signaling pathway in the liver of yak under long-term nutritional stress is shown in **Figure 5**.

In addition, the correlation analysis between DEGs and differential metabolites related to energy metabolism showed that PC, phosphocholine, glutathione, and glutamylcysteine were positively correlated with DHCR24, DHCR7, HMGCS1, LPL, FASN, ACAT2, and GSTK1. At the same time, TG displayed a negative correlation; this may be due to yak to cope with the shortage of forages and maintain the energy homeostasis of whole-body during the cold season; the LPL catalyzes the hydrolysis of VLDL and CMs to provide free fatty acids for tissue utilization. This process increased the metabolite TG. It

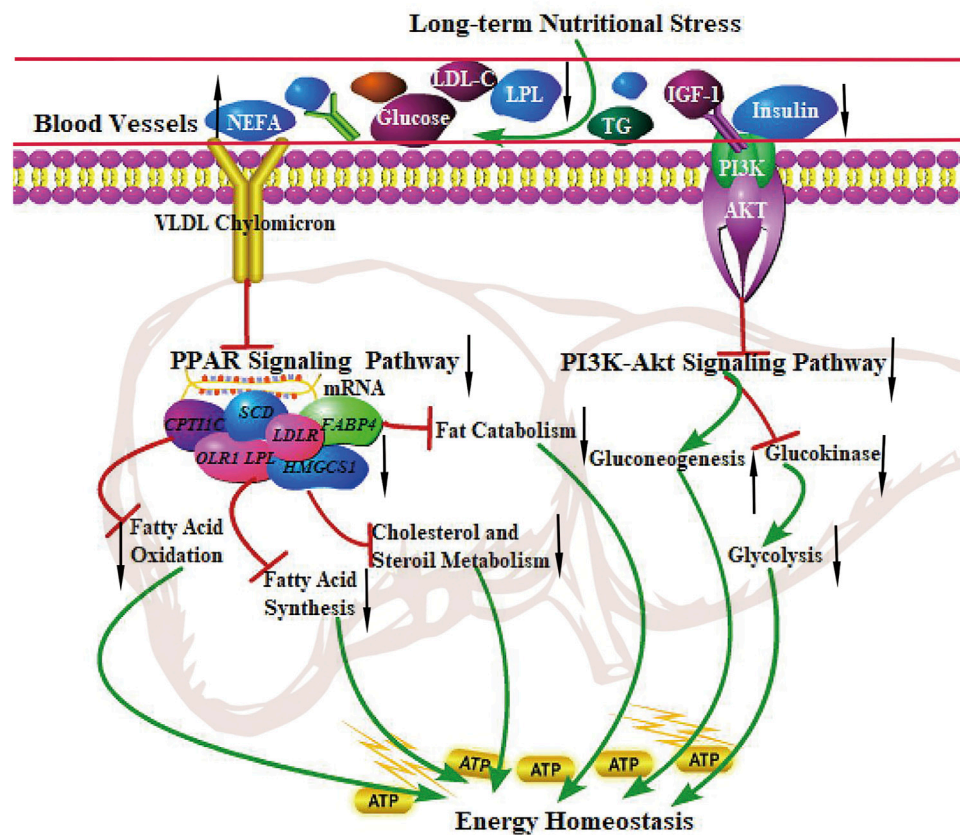


FIGURE 5 | The regulation of the PPAR signaling pathway and PI3K-Akt signaling pathway in the liver of the yak under long-term nutritional stress. ↑: up-regulation of genes expression or enhanced the pathways; ↓: down-regulation of genes expression or diminished the pathways. →: promote or result in. ⊥: the genes expression or metabolic pathways were inhibited.

decreased the expression of genes of LPL and VLDL. PC is a principal component of the VLDL monolayer and helps lipid transport metabolism and boost VLDL synthesis in the liver of yak (Zhou et al., 2020). Therefore, the low expression of the VLDL causes to decrease in the metabolite PC and thereby inhibits lipid metabolism. So, it was speculated that the decrease in LPL may affect the production of metabolite PC and expression of genes LPL and VLDL, which further affects the expression of genes FASN, DHCR24, DHCR7, HMGCS1, and ACAT2.

CONCLUSION

The study investigated the potential mechanism of yak adaption to the long-term withered grass period by transcriptomics and metabolomics under natural grazing. The metabolome and transcriptome analysis showed that nutritional stress caused differential alterations of various hepatic metabolites, genes and related pathways, such as glycolysis or gluconeogenesis, lipid metabolism (particularly fatty acid, cholesterol, and steroid metabolism), and glutathione metabolism. But most importantly, the reduced fatty acid synthesis, fatty acid oxidation, adipogenesis,

and fat catabolism facilitated gluconeogenesis by regulating the PPAR signaling pathway and PI3K-Akt signaling pathway to maintain the energy homeostasis of whole body in the yak, thereby coping with the shortage of forages and adapting to the extreme environment of the QTP.

DATA AVAILABILITY STATEMENT

The datasets presented in this study can be found in online repositories. The names of the repository/repositories and accession number(s) can be found in the article/ Supplementary Material.

ETHICS STATEMENT

The animal study was reviewed and approved by the experimental procedures in animal care in this study were approved by the Animal Care and Use Committee (IACUC) of Lanzhou Institute of Husbandry and Pharmaceutical Sciences, CAAS, China [SYXK-2018-0011]. Written informed consent was obtained from the owners for the participation of their animals in this study.

AUTHOR CONTRIBUTIONS

JZ and MD conceived and designed the research, Writing—original draft and analyzed data, JZ, ZL, AA, and JS collected samples, analyzed data, XD and GH designed the research and revised the manuscript.

FUNDING

This study was supported by the international cooperation and exchange program of the National Natural Science Foundation of

China (No. 31461143020), National Key R&D Project of “13th Five-Year” (No.31461143020), and the Young Talents Special Foundation of Chinese Academy of Agricultural Sciences.

SUPPLEMENTARY MATERIAL

The Supplementary Material for this article can be found online at: <https://www.frontiersin.org/articles/10.3389/fcell.2021.759521/full#supplementary-material>

REFERENCES

- Alexandre, P. A., Kogelman, L. J. A., Santana, M. H. A., Passarelli, D., Pulz, L. H., Fantinato-Neto, P., et al. (2015). Liver Transcriptomic Networks Reveal Main Biological Processes Associated with Feed Efficiency in Beef Cattle. *BMC Genomics* 16, 1073. doi:10.1186/s12864-015-2292-8
- Anders, S., and Huber, W. (2012). *Differential Expression of RNA-Seq Data at the Gene Level—The DESeq Package*, 10. Heidelberg, Germany: European Molecular Biology Laboratory EMBL, f1000.
- Anders, S., Pyl, P. T., and Huber, W. (2015). HTSeq—a Python Framework to Work with High-Throughput Sequencing Data. *Bioinformatics* 31 (2), 166–169. doi:10.1093/bioinformatics/btu638
- Caimari, A., Oliver, P., Rodenburg, W., Keijer, J., and Palou, A. (2010). *Slc27a2* Expression in Peripheral Blood Mononuclear Cells as a Molecular Marker for Overweight Development. *Int. J. Obes.* 34 (5), 831–839. doi:10.1038/ijo.2010.17
- Chui, P. C., Guan, H.-P., Lehrke, M., and Lazar, M. A. (2005). PPAR γ Regulates Adipocyte Cholesterol Metabolism via Oxidized LDL Receptor 1. *J. Clin. Invest.* 115 (8), 2244–2256. doi:10.1172/jci24130
- Cogburn, L. A., Trakooljul, N., Wang, X., Ellestad, L. E., and Porter, T. E. (2020). Transcriptome Analyses of Liver in Newly-Hatched Chicks during the Metabolic Perturbation of Fasting and Re-feeding Reveals THRSPA as the Key Lipogenic Transcription Factor. *BMC Genomics* 21 (1), 109. doi:10.1186/s12864-020-6525-0
- Cole, L. K., Vance, J. E., and Vance, D. E. (2012). Phosphatidylcholine Biosynthesis and Lipoprotein Metabolism. *Biochim. Biophys. Acta (Bba) - Mol. Cel Biol. Lipids* 1821 (5), 754–761. doi:10.1016/j.bbalip.2011.09.009
- da Costa, A. S. H., Bessa, R. J. B., Pires, V. M. R., Rolo, E. A., Pinto, R. M. A., Andrade Fontes, C. M. G., et al. (2014). Is Hepatic Lipid Metabolism of Beef Cattle Influenced by Breed and Dietary Silage Level? *BMC Vet. Res.* 10 (1), 65. doi:10.1186/1746-6148-10-65
- Ding, X. Z., Guo, X., Yan, P., Liang, C. N., Bao, P. J., and Chu, M. (2012). Seasonal and Nutrients Intake Regulation of Lipoprotein Lipase (LPL) Activity in Grazing Yak (*Bos Grunniens*) in the Alpine Regions Around Qinghai Lake. *Livestock Sci.* 143 (1), 29–34. doi:10.1016/j.livsci.2011.08.004
- Ellis, J. M., Li, L. O., Wu, P.-C., Koves, T. R., Ilkayeva, O., Stevens, R. D., et al. (2010). Adipose Acyl-CoA Synthetase-1 Directs Fatty Acids toward β -Oxidation and Is Required for Cold Thermogenesis. *Cel Metab.* 12 (1), 53–64. doi:10.1016/j.cmet.2010.05.012
- Esposito, G., Irons, P. C., Webb, E. C., and Chapwanya, A. (2014). Interactions between Negative Energy Balance, Metabolic Diseases, Uterine Health and Immune Response in Transition Dairy Cows. *Anim. Reprod. Sci.* 144 (3–4), 60–71. doi:10.1016/j.anireprosci.2013.11.007
- Feng, S., Ma, J., Long, K., Zhang, J., Qiu, W., Li, Y., et al. (2020). Comparative microRNA Transcriptomes in Domestic Goats Reveal Acclimatization to High Altitude. *Front. Genet.* 11, 809. doi:10.3389/fgene.2020.00809
- Firmenich, C. S., Schnepel, N., Hansen, K., Schmicke, M., and Muscher-Banse, A. S. (2020). Modulation of Growth Hormone Receptor-insulin-like Growth Factor 1 axis by Dietary Protein in Young Ruminants. *Br. J. Nutr.* 123 (6), 652–663. doi:10.1017/s0007114519003040
- China (No. 31461143020), National Key R&D Project of “13th Five-Year” (No.31461143020), and the Young Talents Special Foundation of Chinese Academy of Agricultural Sciences.
- Godin, D., and Wohaieb, S. (1988). Nutritional Deficiency, Starvation, and Tissue Antioxidant Status. *Free Radic. Biol. Med.* 5 (3), 165–176. doi:10.1016/0891-5849(88)90079-2
- Hocquette, J.-F., Graulet, B., and Olivecrona, T. (1998). Lipoprotein Lipase Activity and mRNA Levels in Bovine Tissues. *Comp. Biochem. Physiol. B: Biochem. Mol. Biol.* 121, 201–212. doi:10.1016/S0305-0491(98)10090-1
- Hu, R., Zou, H., Wang, Z., Cao, B., Peng, Q., Jing, X., et al. (2019). Nutritional Interventions Improved Rumen Functions and Promoted Compensatory Growth of Growth-Retarded Yaks as Revealed by Integrated Transcripts and Microbiome Analyses. *Front. Microbiol.* 10, 318. doi:10.3389/fmicb.2019.00318
- Huang, J., Zhang, Y., Zhou, Y., Zhang, Z., Xie, Z., Zhang, J., et al. (2013). Green tea Polyphenols Alleviate Obesity in Broiler Chickens through the Regulation of Lipid-Metabolism-Related Genes and Transcription Factor Expression. *J. Agric. Food Chem.* 61 (36), 8565–8572. doi:10.1021/jf402004x
- Jing, X. P., Wang, W. J., Degen, A. A., Guo, Y. M., Kang, J. P., Liu, P. P., et al. (2021). Energy Substrate Metabolism in Skeletal Muscle and Liver when Consuming Diets of Different Energy Levels: Comparison between Tibetan and Small-Tailed Han Sheep. *Animal* 15, 100162. doi:10.1016/j.animal.2020.100162
- Jing, X., Zhou, J., Degen, A., Wang, W., Guo, Y., Kang, J., et al. (2020). Comparison between Tibetan and Small-Tailed Han Sheep in Adipocyte Phenotype, Lipid Metabolism and Energy Homeostasis Regulation of Adipose Tissues when Consuming Diets of Different Energy Levels. *Br. J. Nutr.* 124 (7), 668–680. doi:10.1017/s0007114520001701
- Kanehisa, M., Araki, M., Goto, S., Hattori, M., Hirakawa, M., Itoh, M., et al. (2007). KEGG for Linking Genomes to Life and the Environment. *Nucleic Acids Res.* 36 (Suppl. 1), D480–D484. doi:10.1017/10.1093/nar/gkm882
- Kaufmann, L. D., Dohme-Meier, F., Munger, A., Bruckmaier, R. M., and van Dorland, H. A. (2012). Metabolism of Grazed vs. Zero-Grazed Dairy Cows throughout the Vegetation Period: Hepatic and Blood Plasma Parameters. *J. Anim. Physiol. Anim. Nutr.* 96 (2), 228–236. doi:10.1111/j.1439-0396.2011.01142.x
- Kersten, S. (2014). Physiological Regulation of Lipoprotein Lipase. *Biochim. Biophys. Acta (Bba) - Mol. Cel Biol. Lipids* 1841 (7), 919–933. doi:10.1016/j.bbalip.2014.03.013
- Laporta, J., Rosa, G. J. M., Naya, H., and Carriquiry, M. (2014). Liver Functional Genomics in Beef Cows on Grazing Systems: Novel Genes and Pathways Revealed. *Physiol. Genomics* 46 (4), 138–147. doi:10.1152/physiolgenomics.00120.2013
- Li, R., Huang, X., Liang, X., Su, M., Lai, K. P., and Chen, J. (2020a). Integrated Omics Analysis Reveals the Alteration of Gut Microbe-Metabolites in Obese Adults. *Brief Bioinform* 22 (3), 1–16. doi:10.1038/s41467-020-19754-110.1093/bib/bbaa165
- Li, Y., Ding, W., Li, C.-Y., and Liu, Y. (2020b). HLH-11 Modulates Lipid Metabolism in Response to Nutrient Availability. *Nat. Commun.* 11 (1), 5959. doi:10.1038/s41467-020-19754-1
- Liu, X., Chen, L., Shi, W., Xu, X., Li, Z., Liu, T., et al. (2021). Comparative Transcriptome Reveals Distinct Starch-Sugar Interconversion Patterns in Potato Genotypes Contrasting for Cold-Induced Sweetening Capacity. *Food Chem.* 334, 127550. doi:10.1016/j.foodchem.2020.127550
- Liu, Y., Zhang, Y., Zhang, X., Xu, Q., Yang, X., and Xue, C. (2017). Medium-chain Fatty Acids Reduce Serum Cholesterol by Regulating the Metabolism of Bile Acid in C57BL/6J Mice. *Food Funct.* 8 (1), 291–298. doi:10.1039/c6fo01207h

- Lu, X., Wen, H., Li, Q., Wang, G., Li, P., Chen, J., et al. (2019). Comparative Analysis of Growth Performance and Liver Transcriptome Response of Juvenile Ancherythroculter Nigrocauda Fed Diets with Different Protein Levels. *Comp. Biochem. Physiol. D: Genomics Proteomics* 31, 100592. doi:10.1016/j.cbd.2019.05.002
- Ma, L., Mondal, A. K., Murea, M., Sharma, N. K., Tönjes, A., Langberg, K. A., et al. (2011). The Effect of ACACB Cis-Variants on Gene Expression and Metabolic Traits. *PLoS One* 6 (8), e23860. doi:10.1371/journal.pone.0023860
- Mashek, D. G., Li, L. O., and Coleman, R. A. (2006). Rat Long-Chain Acyl-CoA Synthetase mRNA, Protein, and Activity Vary in Tissue Distribution and in Response to Diet. *J. Lipid Res.* 47 (9), 2004–2010. doi:10.1194/jlr.M600150-JLR200
- McFadden, J. W. (2020). Review: Lipid Biology in the Periparturient Dairy Cow: Contemporary Perspectives. *Animal* 14 (S1), s165–s175. doi:10.1017/S1751731119003185
- McGillicuddy, F. C., Chiquoine, E. H., Hinkle, C. C., Kim, R. J., Shah, R., Roche, H. M., et al. (2009). Interferon γ Attenuates Insulin Signaling, Lipid Storage, and Differentiation in Human Adipocytes via Activation of the JAK/STAT Pathway. *J. Biol. Chem.* 284 (46), 31936–31944. doi:10.1074/jbc.M109.061655
- Minich, D. M., and Brown, B. I. (2019). A Review of Dietary (Phyto)nutrients for Glutathione Support. *Nutrients* 11 (9), 2073–2118. doi:10.3390/nu11092073
- Miron, N., and Tirosh, O. (2019). Cholesterol Prevents Hypoxia-Induced Hypoglycemia by Regulation of a Metabolic Ketogenic Shift. *Oxidative Med. Cell Longevity* 2019, 1–11. doi:10.1155/2019/5829357
- Nyrén, R., Makoveichuk, E., Malla, S., Kersten, S., Nilsson, S. K., Ericsson, M., et al. (2019). Lipoprotein Lipase in Mouse Kidney: Effects of Nutritional Status and High-Fat Diet. *Am. J. Physiology-Renal Physiol.* 316 (3), F558–F571. doi:10.1152/ajprenal.00474.2018
- Oba, M., and Allen, M. S. (1999). Evaluation of the Importance of the Digestibility of Neutral Detergent Fiber from Forage: Effects on Dry Matter Intake and Milk Yield of Dairy Cows. *J. Dairy Sci.* 82 (3), 589–596. doi:10.3168/jds.S0022-0302(99)75271-9
- Oczkowicz, M., Szmatoła, T., Świątkiewicz, M., Koseniuk, A., Smółucha, G., Witarski, W., et al. (2020). 3'quant mRNA-Seq of Porcine Liver Reveals Alterations in UPR, Acute Phase Response, and Cholesterol and Bile Acid Metabolism in Response to Different Dietary Fats. *Genes* 11 (9), 1087. doi:10.3390/genes11091087
- Pitaloka, D. M. I., Ko, C.-H., Lin, M.-T., Yeh, S.-L., and Yeh, C.-L. (2019). Glutamine Administration Promotes Hepatic Glucose Homeostasis through Regulating the PI3K/Akt Pathway in High-Fat Diet-Induced Obese Mice with Limb Ischemia. *Nutr. Res.* 68, 45–53. doi:10.1016/j.nutres.2019.05.008
- Radcliff, R. P., Vandehaar, M. J., Kobayashi, Y., Sharma, B. K., Tucker, H. A., and Lucy, M. C. (2004). Effect of Dietary Energy and Somatotropin on Components of the Somatotrophic Axis in Holstein Heifers. *J. Dairy Sci.* 87 (5), 1229–1235. doi:10.3168/jds.S0022-0302(04)73273-7
- Ren, E., Chen, X., Yu, S., Xu, J., Su, Y., and Zhu, W. (2018). Transcriptomic and Metabolomic Responses Induced in the Livers of Growing Pigs by a Short-Term Intravenous Infusion of Sodium Butyrate. *Animal* 12 (11), 2318–2326. doi:10.1017/S1751731118000174
- Ren, W., Badgery, W., Ding, Y., Guo, H., Gao, Y., and Zhang, J. (2019). Hepatic Transcriptome Profile of Sheep (*Ovis aries*) in Response to Overgrazing: Novel Genes and Pathways Revealed. *BMC Genet.* 20 (1), 54. doi:10.1186/s12863-019-0760-x
- Roberts, A., Trapnell, C., Donaghey, J., Rinn, J. L., and Pachter, L. (2011). Improving RNA-Seq Expression Estimates by Correcting for Fragment Bias. *Genome Biol.* 12 (3), R22–R14. doi:10.1186/gb-2011-12-3-r22
- Rui, L. (2014). Energy Metabolism in the Liver. *Compr. Physiol.* 4 (1), 177–197. doi:10.1002/cphy.c130024
- Saul, G., Kearney, G., and Borg, D. (2009). Pasture Systems to Improve Productivity of Sheep in South-Western Victoria. 1. Growth, Composition, Nutritive Value and Persistence of Resown Pastures. *Anim. Prod. Sci.* 49, 9–13. doi:10.1071/EA06142
- Schmittgen, T. D., and Livak, K. J. (2008). Analyzing Real-Time PCR Data by the Comparative CT Method. *Nat. Protoc.* 3 (6), 1101–1108. doi:10.1038/nprot.2008.73
- Settembre, C., De Cegli, R., Mansueto, G., Saha, P. K., Vetrini, F., Visvikis, O., et al. (2013). TFEB Controls Cellular Lipid Metabolism through a Starvation-Induced Autoregulatory Loop. *Nat. Cell Biol.* 15 (6), 647–658. doi:10.1038/ncb2718
- Shi, H., Zhang, J., Li, S., Ji, S., Cao, Z., Zhang, H., et al. (2018). Effects of a Wide Range of Dietary Forage-To-Concentrate Ratios on Nutrient Utilization and Hepatic Transcriptional Profiles in Limit-Fed Holstein Heifers. *BMC Genomics* 19 (1), 148. doi:10.1186/s12864-018-4529-9
- Sun, H.-Z., Wang, D.-M., Liu, H.-Y., and Liu, J.-X. (2018). Metabolomics Integrated with Transcriptomics Reveals a Subtle Liver Metabolic Risk in Dairy Cows Fed Different Crop By-Products. *Proteomics* 18 (16), 1800122. doi:10.1002/pmic.201800122
- Teodoro, B. G., Sampaio, I. H., Bomfim, L. H. M., Queiroz, A. L., Silveira, L. R., Souza, A. O., et al. (2017). Long-chain Acyl-CoA Synthetase 6 Regulates Lipid Synthesis and Mitochondrial Oxidative Capacity in Human and Rat Skeletal Muscle. *J. Physiol.* 595 (3), 677–693. doi:10.1113/jp272962
- Trapnell, C., Williams, B. A., Pertea, G., Mortazavi, A., Kwan, G., Van Baren, M. J., et al. (2010). Transcript Assembly and Quantification by RNA-Seq Reveals Unannotated Transcripts and Isoform Switching during Cell Differentiation. *Nat. Biotechnol.* 28 (5), 511–515. doi:10.1038/nbt.1621
- Uno, Y., Uehara, S., Tanaka, S., Murayama, N., and Yamazaki, H. (2020). Systematic Characterization of Glutathione S-Transferases in Common Marmosets. *Biochem. Pharmacol.* 174, 113835. doi:10.1016/j.bcp.2020.113835
- Vahmani, P., Glover, K. E., and Fredeen, A. H. (2014). Effects of Pasture versus Confinement and marine Oil Supplementation on the Expression of Genes Involved in Lipid Metabolism in Mammary, Liver, and Adipose Tissues of Lactating Dairy Cows. *J. Dairy Sci.* 97 (7), 4174–4183. doi:10.3168/jds.2013-7290
- Vailati Riboni, M., Meier, S., Priest, N. V., Burke, C. R., Kay, J. K., McDougall, S., et al. (2015). Adipose and Liver Gene Expression Profiles in Response to Treatment with a Nonsteroidal Antiinflammatory Drug after Calving in Grazing Dairy Cows. *J. Dairy Sci.* 98 (5), 3079–3085. doi:10.3168/jds.2014-8579
- Van Soest, P. J., Robertson, J. B., and Lewis, B. A. (1991). Methods for Dietary Fiber, Neutral Detergent Fiber, and Nonstarch Polysaccharides in Relation to Animal Nutrition. *J. Dairy Sci.* 74 (10), 3583–3597. doi:10.3168/jds.S0022-0302(91)78551-2
- Weber, C., Schäff, C. T., Kautzsch, U., Börner, S., Erdmann, S., Bruckmaier, R. M., et al. (2017). Variable Liver Fat Concentration as a Proxy for Body Fat Mobilization Postpartum Has Minor Effects on Insulin-Induced Changes in Hepatic Gene Expression Related to Energy Metabolism in Dairy Cows. *J. Dairy Sci.* 100 (2), 1507–1520. doi:10.3168/jds.2016-11808
- Weller, M. M. D. C. A., Albino, R. L., Marcondes, M. I., Silva, W., Daniels, K. M., Campos, M. M., et al. (2016). Effects of Nutrient Intake Level on Mammary Parenchyma Growth and Gene Expression in Crossbred (Holstein \times Gyr) Prepubertal Heifers. *J. Dairy Sci.* 99 (12), 9962–9973. doi:10.3168/jds.2016-11532
- Xiong, L., Pei, J., Wu, X., Kalwar, Q., Liang, C., Guo, X., et al. (2020). The Study of the Response of Fat Metabolism to Long-Term Energy Stress Based on Serum, Fatty Acid and Transcriptome Profiles in Yaks. *Animals* 10 (7), 1150. doi:10.3390/ani10071150
- Yang, C., Ahmad, A. A., Bao, P. J., Guo, X., Wu, X. Y., Liu, J. B., et al. (2020). Increasing Dietary Energy Level Improves Growth Performance and Lipid Metabolism through Up-Regulating Lipogenic Gene Expression in Yak (*Bos Grunniens*). *Anim. Feed Sci. Technology* 263, 114455. doi:10.1016/j.anifeedsci.2020.114455
- Yu, K., Zhang, Y., Chen, H., and Zhu, W. (2019). Hepatic Metabolomic and Transcriptomic Responses Induced by Cecal Infusion of Sodium Propionate in a Fistula Pig Model. *J. Agric. Food Chem.* 67 (47), 13073–13081. doi:10.1021/acs.jafc.9b05070
- Yu, X., Peng, Q., Luo, X., An, T., Guan, J., and Wang, Z. (2016). Effects of Starvation on Lipid Metabolism and Gluconeogenesis in Yak. *Asian Australas. J. Anim. Sci.* 29 (11), 1593–1600. doi:10.5713/ajas.15.0868
- Zhong, H., Hu, J., and Zhou, Y. (2021). Transcriptomic Evidence of Luteinizing Hormone-Releasing Hormone Agonist (LHRH-A) Regulation on Lipid Metabolism in Grass Carp (*Ctenopharyngodon Idella*). *Genomics* 113, 1265–1271. doi:10.1016/j.ygeno.2020.09.043
- Zhou, J., Yue, S., Peng, Q., Wang, L., Wang, Z., and Xue, B. (2020). Metabonomic Responses of Grazing Yak to Different Concentrate

Supplementations in Cold Season. *Animals* 10, 1595. doi:10.3390/ani10091595

Conflict of Interest: The authors declare that the research was conducted in the absence of any commercial or financial relationships that could be construed as a potential conflict of interest.

Publisher's Note: All claims expressed in this article are solely those of the authors and do not necessarily represent those of their affiliated organizations, or those of the publisher, the editors and the reviewers. Any product that may be evaluated in

this article, or claim that may be made by its manufacturer, is not guaranteed or endorsed by the publisher.

Copyright © 2022 Zheng, Du, Zhang, Liang, Ahmad, Shen, Salekdeh and Ding. This is an open-access article distributed under the terms of the Creative Commons Attribution License (CC BY). The use, distribution or reproduction in other forums is permitted, provided the original author(s) and the copyright owner(s) are credited and that the original publication in this journal is cited, in accordance with accepted academic practice. No use, distribution or reproduction is permitted which does not comply with these terms.

GLOSSARY

ACACB	Acetyl-CoA carboxylase β	GSTK1	Glutathione S-transferase kappa 1
ACACA	Acetyl-CoA carboxylase α	HDL-C	high-density lipoprotein cholesterol
ADF	acid detergent fiber	HSL	Hormone-sensitive fatty lipase
ADFD	acid detergent fiber digestibility	IGF-1	insulin-like growth factor-1
AMPK	adenosine 5'-monophosphate-activated protein kinase	IGF-2	insulin-like growth factor-2
ACSL1	Long-chain Acyl-CoA Synthetases 1	INS	insulin
ACSL6	Long-chain Acyl-CoA Synthetases 6	KEGG	Kyoto Encyclopedia of Genes and Genomes
BW	body weight	LPL	lipoprotein lipaselipoprotein lipase
CH	cholesterol	LPL	lipoprotein lipaselipoprotein lipase
CK	creatine kinase	LDH	Lactate dehydrogenase
CPD	crude protein digestibility	LDL-C	low-density lipoprotein cholesterol
CPT1C	Carnitine palmitoyltransferase 1C	MEI	metabolic energy intake
CP	crude protein	NDFD	neutral detergent fiber digestibility
CM	chylomicrons	NEFAs	nonesterified fatty acids
DNL	<i>de novo</i> lipogenesis	NDF	neutral detergent fiber
DM	the dry matter	MDA	malondialdehyde
DMI	dry matter intake	OLR1	Oxidized low-density lipoprotein receptor 1
DMD	dry matter digestibility	OPLS-DA	Orthogonal partial least-squares discriminant analysis
DEGs	differential expression genes	PCA	principal component analysis
EE	ether extract	PC	Phosphatidylcholine
FASN	fatty acid synthase	QTP	Qinghai-Tibetan Plateau
FAS	Fatty acid synthetase	RIN	RNA Integrity Number
FDR	false discovery rate	SOD	Superoxide dismutase
FABP4	fatty acid binding protein 4	SCD	stearoyl-CoA desaturase
GH	growth hormone	SLC27A2	solute carrier family 27 member 2
GSH-PX	Glutathione peroxidase	TG	triglycerides
GLU	glucose	T-AOC	Bovine total antioxidant capability
GO	Gene Ontology	VIP	variable importance in the projection
GSTM3	Glutathione S-transferases Mu 3	YC	cold season group
		YW	warm season group



Analysis of N⁶-Methyladenosine Methylome in Adenocarcinoma of Esophagogastric Junction

Jia-Bin Huang, Bin-Bin Hu[†], Rong He, Lian He, Chen Zou, Chang-Feng Man and Yu Fan^{*}

Cancer Institute, Affiliated People's Hospital of Jiangsu University, Zhenjiang, China

OPEN ACCESS

Edited by:

A. Rasim Barutcu,
University of Toronto, Canada

Reviewed by:

Kunqi Chen,
Fujian Medical University, China
Zhiqing Li,
Southwest University, China
Jiangbo Wei,
University of Chicago, United States

*Correspondence:

Yu Fan
yuf36@sina.com

[†]These authors have contributed
equally to this work and share first
authorship

Specialty section:

This article was submitted to
RNA,
a section of the journal
Frontiers in Genetics

Received: 08 November 2021

Accepted: 30 December 2021

Published: 24 January 2022

Citation:

Huang J-B, Hu B-B, He R, He L, Zou C,
Man C-F and Fan Y (2022) Analysis of
N⁶-Methyladenosine Methylome in
Adenocarcinoma of
Esophagogastric Junction.
Front. Genet. 12:787800.
doi: 10.3389/fgene.2021.787800

Background: From previous studies, we found that there are more than 100 types of RNA modifications in RNA molecules. m⁶A methylation is the most common. The incidence rate of adenocarcinoma of the esophagogastric junction (AEG) at home and abroad has increased faster than that of stomach cancer at other sites in recent years. Here, we systematically analyze the modification pattern of m⁶A mRNA in adenocarcinoma at the esophagogastric junction.

Methods: m⁶A sequencing, RNA sequencing, and bioinformatics analysis were used to describe the m⁶A modification pattern in adenocarcinoma and normal tissues at the esophagogastric junction.

Results: In AEG samples, a total of 4,775 new m⁶A peaks appeared, and 3,054 peaks disappeared. The unique m⁶A-related genes in AEG are related to cancer-related pathways. There are hypermethylated or hypomethylated m⁶A peaks in AEG in differentially expressed mRNA transcripts.

Conclusion: This study preliminarily constructed the first m⁶A full transcriptome map of human AEG. This has a guiding role in revealing the mechanism of m⁶A-mediated gene expression regulation.

Keywords: epigenomics, adenocarcinoma of esophagogastric junction, m⁶A methylation, diagnosis, treatment

INTRODUCTION

In recent years, more and more research studies are based on epigenetics. Epigenetics is a study of reversible and inheritable phenotypes. This study does not involve changes in nuclear DNA sequences (Ng and Gurdon, 2008). RNA epigenetics includes N¹-methyladenosine (m¹A), N⁶-methyladenosine (m⁶A), 5-methylcytidine (m⁵C), and 7-methylguanosine (m⁷G) (Zhao et al., 2017). Among them, m⁶A, discovered in the 1970s, is the most abundant internal modification of mRNA in

Abbreviations: AEG, adenocarcinoma of esophagogastric junction; ALKBH5, a-ketoglutarate-dependent dioxygenase alkB homolog 5; eIF3, eukaryotic initiation factor 3; FTO, obesity-associated protein; HNRNPA2B1, heterogeneous nuclear ribonucleoprotein A2B1; IGF2BP1/2/3, insulin-like growth factor 2 mRNA binding protein 1/2/3; m⁶A, N⁶-methyladenosine; METTL3, methyltransferase-like 3; METTL14, methyltransferase-like 14; METTL16, methyltransferase like 16; RBM15/15B, RNA binding motif protein 15/15B; WTAP, Wilms tumor suppressor-1-associated protein; YTHDC1, YTH domain-containing 1; YTHDC2, YTH domain-containing 2; YTHDF1, YTH N6-methyladenosine RNA binding protein 1; YTHDF2, YTH N6-methyladenosine RNA binding protein 2; YTHDF3, YTH N6-methyladenosine RNA binding protein 3; ZC3H13, Zinc finger CCCH-type containing 13.

most eukaryotes (Chen and Wong, 2020). It involves almost all stages of the life cycle, including normal and pathological processes, for example, animal development (Frye et al., 2018), gene expression regulation (Roundtree et al., 2017), and human diseases (Hsu et al., 2017). With the discovery of research, the occurrence and development of many diseases are closely related to the changes in m⁶A modification, including tumors (Li J. et al., 2021), obesity (Zhao et al., 2014), infertility (Tang et al., 2018), autoimmune diseases (Zhang Y. et al., 2019), neurological diseases (Wu et al., 2019) and so on. Desrosiers et al. (1974) found that about 0.1–0.4% of adenosine in isolated RNA is modified by m⁶A in Sox. Transcriptome-wide research reveals that m⁶A modifications are enriched in the 3'-untranslated regions (UTRs) near the stop codons of mRNAs and it has a consensus sequence of RRACH (R = G or A; H = A, C, or U) (Dominissini et al., 2012). m⁶A modifications are mainly mediated by “writers,” “erasers” and “reader” proteins (Liu et al., 2014). Writers traditionally include methyltransferase-like 3 and 14 proteins (METTL3 and METTL14) and their cofactors WTAP (Wilms tumor suppressor-1-associated protein) (Ping et al., 2014; Schwartz et al., 2014). METTL3 is a member of the S-adenosine-L-methionine-dependent methyltransferase family, and is the main catalytically active enzyme for m⁶A methylation modification and is highly conserved in eukaryotes (Schöller et al., 2018). METTL14 has no catalytic domain and has no enzymatic activity, but it can form a stable heterodimer complex with METTL3 (Zhang et al., 2020). Therefore, METL3 and METL14 constitute the core and structure of the complex, respectively (Wang et al., 2016). WTAP is a pre-mRNA splicing regulator with independent methylation sites. It is mainly responsible for assisting the targeting of METL3 and METL14 to nuclear sites and can specifically methylate some m⁶A sites (Zheng et al., 2019; Liu S. et al., 2020; Zhang et al., 2021). There are also new research findings, methyltransferase-like protein 16 (methyltransferase like 16, METL16) (Aoyama et al., 2020), CCCH-type zinc finger protein 13 (Zinc finger CCCH-type containing 13, ZC3H13) (Wen et al., 2018), RNA binding motif protein 15/15B (RNA binding motif protein 15/15B, RBM15/15B) (Wang T. et al., 2020) is also a component of the methyltransferase complex and can participate in m⁶A methylation modification. Demethylation is achieved by another enzyme family called demethylases (erasers), mainly including FTO and ALKBH5 (Jia et al., 2011; Zheng et al., 2013). In addition to writers and erasers, m⁶A readers also play an important role in m⁶A methylation (Shi et al., 2019). Readers which can recognize m⁶A modification contain the YT521B homology (YTH) domain (Liu et al., 2018). The YTH domain in human cells, including the YTH domain family (YTHDF1-3), YTH domain-containing 1 (YTHDC1), and YTH domain-containing 2 (YTHDC2), have conserved the m⁶A binding domain (Qin et al., 2021). Recent studies have also reported that eukaryotic initiation factor 3 (eIF3) (Liu T. et al., 2020), heterogenous nuclear ribonucleoprotein A2B1 (heterogenous nuclear ribonucleoprotein A2B1, HNRNPA2B1) (Li K. et al., 2021), insulin-like growth factor 2 messenger ribonucleic acid

Binding protein 1/2/3 (insulin-like growth factor 2 mRNA binding protein 1/2/3, IGF2BP1/2/3) (Huang et al., 2018) can also be used as m⁶A reading protein. However, there are still few studies on the related mechanisms of m⁶A methylation.

Gastrointestinal (GI) cancers are one of the most common malignancies, accounting for more than one-fourth of the newly diagnosed cancers worldwide (more than 4 million new cases per year) (Macha et al., 2014; Zhang S. et al., 2019). Among the GI cancers, the esophagogastric junction, or esophagogastric junction (EGJ), is a special anatomical site with a remarkably high risk of adenocarcinoma (Keeney and Bauer, 2006). The incidence of adenocarcinoma of the esophagogastric junction (AEG) has been increasing both in the West and East (Steevens et al., 2010; Yamashita et al., 2017; Imamura et al., 2019). There has been much debate as to the optimal therapy for AEG, and the debate continues (Kauppila and Lagergren, 2016). Here, we demonstrate the presence of m⁶A modification in adenocarcinoma of esophagogastric junction *via* m⁶A-methylated RNA immunoprecipitation (MeRIP) sequencing (MeRIP-seq), a powerful strategy for transcriptome-wide mapping of RNA modifications in mRNAs (Lin et al., 2018). We report transcriptome m⁶A profiling in adenocarcinoma of esophagogastric junction samples and the tumor-adjacent normal tissues for the first time.

MATERIALS AND METHODS

Tissue Collection

Four pairs of matched adenocarcinoma of the esophagogastric junction and para-cancerous tissue samples were derived from adenocarcinoma of esophagogastric junction patients who underwent radical surgery in Affiliated People's Hospital of Jiangsu University, Zhenjiang from July 2018 to November 2018. Adenocarcinoma of esophagogastric junction tissue was excised from the central part of the tumor; the paired paracancerous tissue was taken from normal tissue that was more than 5 cm from the edge of the tumor and had a negative margin. The collection process for all tissue samples was completed within 30 min after the tumor was isolated. The fresh tissue was cut into tissue pieces of about 5 mm in diameter and quickly placed in a sterilized cryotube and stored in an ultra-low temperature freezer at −80°C.

RNA Preparation

For each group, four biological replicates were selected, of which every two were combined into one. Then, the total RNA of tissue was extracted using TRIzol reagent (Invitrogen Corporation, CA, United States) in accordance with the manufacturer's instructions. The Ribo-Zero rRNA Removal Kit (Illumina, Inc., CA, United States) was used to reduce the ribosomal RNA content of total RNAs. Then, the RNA was chemically fragmented into fragments of about 100 nucleotides in length using fragmentation buffer (Illumina, Inc.).

High-Throughput m⁶A and mRNA Sequencing

Total RNA was harvested from tissue samples and underwent a quality control (QC) process using NanoDrop ND-1000 (Thermo Fisher Scientific, MA, United States). High-throughput m⁶A and mRNA sequencing were performed by Cloudseq Biotech, Inc. (Shanghai, China) according to the published procedure with slight modifications. Briefly, fragmented RNA was incubated with anti-m⁶A polyclonal antibody (Synaptic Systems, 202003, Goettingen, Germany) in IP, immunoprecipitation buffer at 4°C for 2 h (Wang H.-F. et al., 2020). The mixture was then immunoprecipitated by incubation with protein-A beads (Thermo Fisher Scientific) at 4°C for an additional 2 h. Then, bound RNA was eluted from the beads with N⁶-methyladenosine (Berry & Associates, PR3732, Dexter, United States) in IP buffer and then extracted with Trizol reagent (Thermo Fisher Scientific) according to the manufacturer's instruction. Purified RNA was used for RNA-seq library generation with NEBNextR Ultra™ RNA Library Prep Kit (New England Biolabs, MA, United States). Both the input samples without immunoprecipitation and the m⁶A IP samples were subjected to 150 bp paired-end sequencing on Illumina HiSeq sequencer, Illumina, CA, United States.

Sequencing Data Analysis

Paired-end reads were harvested from Illumina HiSeq 4000 sequencer and were quality controlled by Q30. After 3'adapter-trimming and low-quality reads were removed using cutadapt software (v1.9.3) (Kechin et al., 2017), the high-quality clean reads of all libraries were aligned to the reference genome (UCSC HG19) by Hisat2 software (v2.0.4) (Kim et al., 2015). For m⁶A sequencing, methylated sites on RNAs (m⁶A peaks) were identified by MACS software (Zhang et al., 2008). Differentially methylated sites were identified by diffReps (Shen et al., 2013). For mRNA sequencing, raw counts were identified by HTSeq software (v0.9.1) and normalized by edgeR software. Differentially expressed mRNAs were identified by *p*-value and fold change. Gene ontology (Geistlinger et al., 2021) and pathway enrichment analysis (Tian et al., 2005) were performed based on the differentially methylated protein coding genes and differentially expressed mRNAs.

Gene-Specific MeRIP-qPCR Validation

Three genes with differentially methylated sites according to m⁶A-seq were tested by reverse transcription RT-qPCR. A portion of fragmented RNA was saved as the input control. The rested RNA was incubated with anti-m⁶A antibody-coupled beads. The m⁶A-containing RNAs were then immunoprecipitated and eluted from the beads.

The following are the gene-specific qPCR primers:

PLCG2:Forward:AGCTTAACCTTCAACCTGTGTG,
Reverse:AAGATAGCTTTTACGGTTGGGT

TPR:Forward:TGCTTTTGGAGAACTAGAGAACA,
Reverse:TGGCGTTTCAAAATTGGTGC

DVL1:Forward:AGCTGCTTCTGTGTAAATGCT,
Reverse:GTCCCATAAATTAACGCTTTT

TABLE 1 | Sequencing reads.

Sample name	Raw reads	Clean reads
737511T.IP	51,034,044	29,314,686
737789T.IP	50,011,084	11,574,526
738156T.IP	91,721,102	42,114,984
739939T.IP	73,896,158	38,570,024
737511N.IP	67,019,630	31,154,202
737789N.IP	103,480,210	76,461,856
738156N.IP	60,176,662	36,498,028
739939N.IP	101,048,022	54,723,832
737511T.Input	55,202,914	54,242,640
737789T.Input	60,311,666	60,160,794
738156T.Input	54,079,092	53,918,834
739939T.Input	50,681,654	50,594,076
737511N.Input	55,340,698	55,193,614
737789N.Input	55,598,832	55,423,884
738156N.Input	52,120,622	51,107,154
739939N.Input	49,555,862	49,100,868

GAPDH:Forward:GGCCTCCAAGGAGTAAGACC, Reverse: AGGGGAGATTCAGTGTGGTG

Statistical Analysis

Data from three or more independent experiments were presented as the mean ± standard deviation (SD). Statistical analysis was done using SPSS 22.0 and GraphPad Prism 5.0 software. Paired Student t-tests were performed between cancer and adjacent normal samples. One-way analysis of variance was used to access the differences among three or more groups. Differences with *p* < 0.05 were defined as the threshold for significance.

RESULTS

Characterization of m⁶A Methylation in Adenocarcinoma of Esophagogastric Junction

Human AEG tissues versus tumor-adjacent normal tissues from four patients were selected for transcriptome-wide m⁶A-sequencing (m⁶A-seq) and RNA-sequencing (RNA-seq) assays. The original sequencing data IP is 50011084-103480210; Input is 49555862-60311666. After preprocessing of the original data (to remove the connector, to remove low-quality reads, to obtain high-quality clean reads), IP is 11574526-76461856; Input is 49100868-60160794 (Table 1). m⁶A is known to be a relatively abundant mRNA modification (Chen and Wong, 2020). In general, a total of 5,814 m⁶A peaks were identified by model-based analysis of ChIP-seq (MACS) (Nilsen, 2014) in the Ca group, representing transcripts of 4,259 genes. In the tumor-adjacent NC group, 4,093 m⁶A peaks were identified, which correspond with transcripts of 3,174 genes. Among them, 1,039 m⁶A peaks (only ~12% of all peaks in cancer and normal groups) were detected within both adenocarcinomas of esophagogastric junction tissues and normal tissues. The low percentage of overlapping m⁶A peaks within

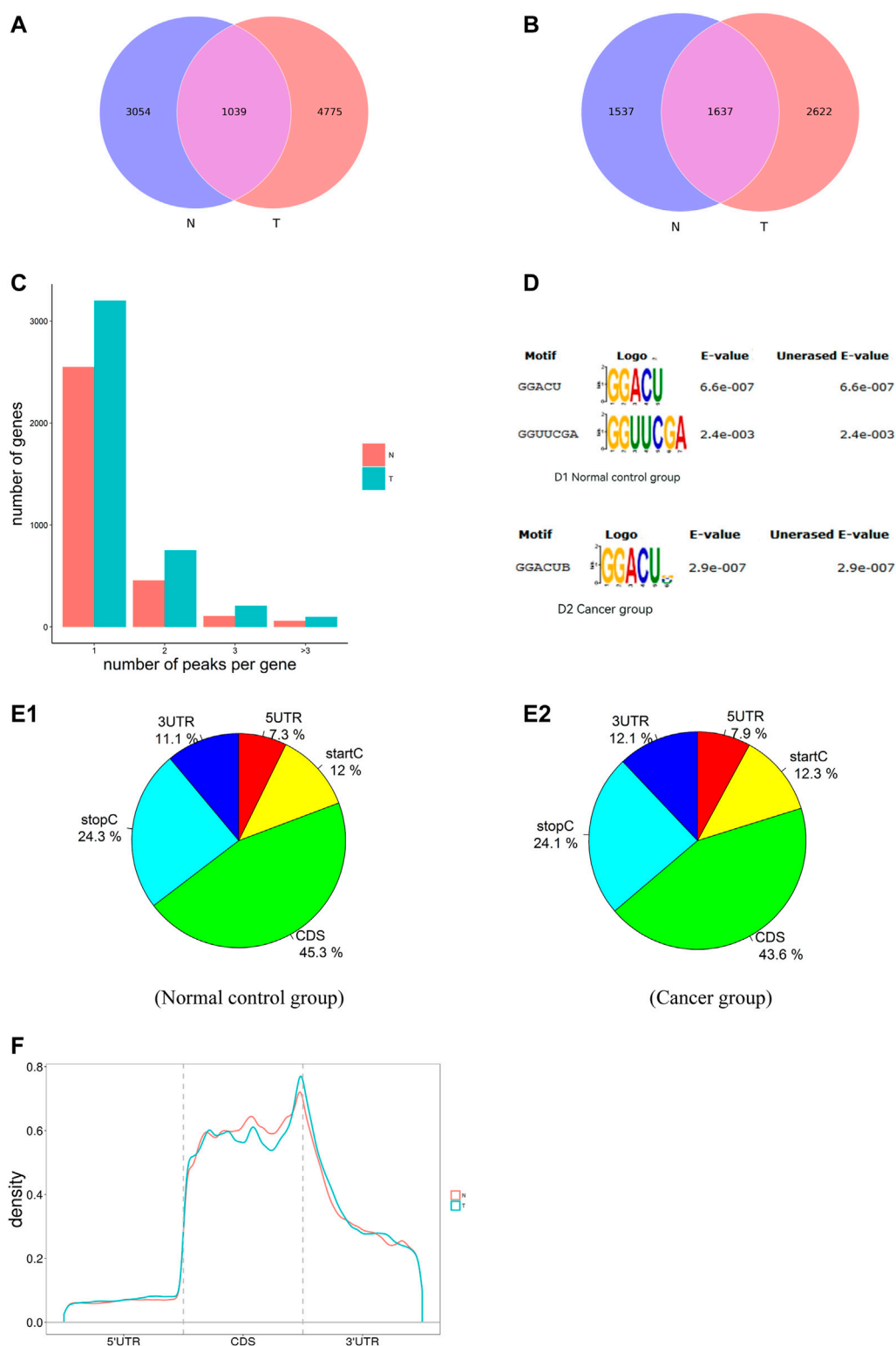


FIGURE 1 | Characteristics of m⁶A methylation in AEG. **(A)** The conserved/specific m⁶A methylation peak. **(B)** The conserved/specific m⁶A methylation genes. **(C)** the distribution of m⁶A-modified peaks per gene. **(D)** The RRACH conserved sequence motif for m⁶A-containing peak regions. **(E)** The percentage of m⁶A methylated peaks in transcripts. Each transcript is divided into five parts: 5'UTRs, CDS, 3'UTRs, start codon, stop codon. **(F)** Accumulation of m⁶A peaks along with transcripts. m⁶A, N⁶-methyladenosine.

mRNAs suggests differences in the m⁶A patterns between two groups (**Figures 1A,B**). By analyzing the distribution of m⁶A-modified peaks per gene, we found the majority of genes had one to three m⁶A modified sites, while a relatively small number of genes contain more (**Figure 1C**).

Motif Analysis of RNA Methylation Region

RNA methylation and demethylation begin with the motif binding of various binding proteins to methylation sites. A motif is essentially a sequence pattern of nucleic acids with biological significance, and these RNA methylation-related enzymes recognize and bind to these motifs, thereby affecting gene expression (Wang et al., 2019). To determine if the m⁶A peaks that we identified contained the m⁶A consensus sequence of RRACH (where R represents purine, A is m⁶A, and H is a non-guanine base). The m⁶A methylomes were further mapped by De reme software. The sequence of the top 300 peaks with the largest enrichment factor of each group (50 bp on each side of the vertex) was taken, and the sequence of these peaks was scanned using De reme to find a meaningful motif sequence. Deme (Bailey, 2011) motif analysis of methylated mRNAs revealed the existence of some motifs containing the consensus sequences (RRACH) of m⁶A modification (**Figure 1D**).

Then, we analyzed the distribution of m⁶A in the whole transcriptome of Ca and NC samples. We determined the distribution of m⁶A reads along with transcripts in the m⁶A-IP and non-IP (input) samples, respectively. Both total and unique m⁶A peaks from the two groups were analyzed. m⁶A peaks were divided into transcription start codon (start c), 5'UTR, coding sequence (CDS), stop codon (stop c) and 3'UTR according to their locations in RNA transcripts. Intriguingly, In general, the m⁶A peaks were enriched in the vicinity of CDS, the stop codon, and the start codon (**Figure 1E**). As shown in **Figure 1E**, about 70% of m⁶A peaks are located in the intergenic region; more than 60% of them are located near the CDS region and stop codon region; while about 30% of m⁶A peaks are located in the 5'UTR, start codon, and 3'UTR region. The distribution trend of the two tissues is highly similar, which indicates that the classical recognition sequence of m⁶A methylation is conserved in human tissues.

To better understand the distribution of m⁶A peaks in the whole mRNA, we divided each m⁶A modified mRNA into three regions: 5'UTR, CDS, and 3'UTR, and calculated the distribution proportion of these three regions. It can be seen from **Figure 1F** that the curve of the whole region of 5'UTR changes very gently until the distribution proportion of m⁶A peaks increases rapidly near the start codon. On the whole, peaks in the CDS area are highly enriched, however, the curve change in the middle of the CDS area is also relatively gentle, which shows that the distribution of the peaks in the middle of CDS is relatively uniform. But there is a peak of m⁶A peaks near

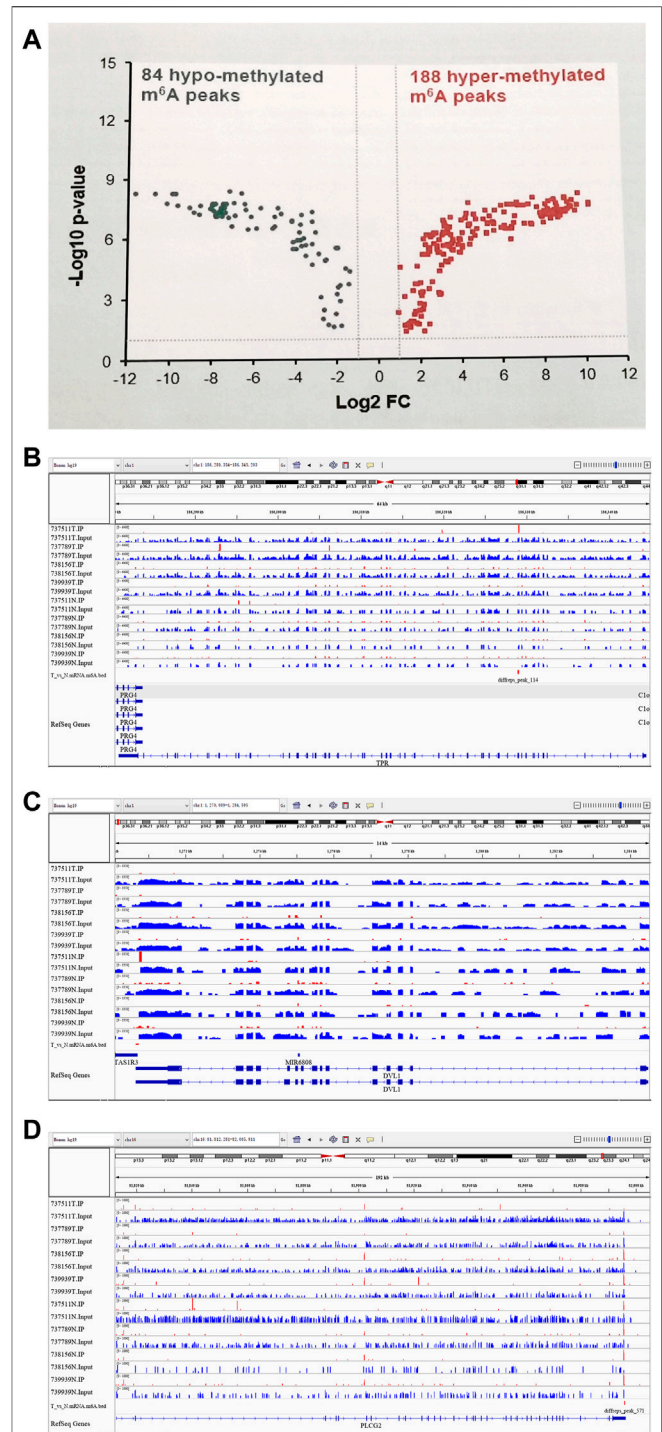


FIGURE 2 | Differentially methylated N⁶-methyladenosine peaks in the tumor and control groups. **(A)** 188 m⁶A hypermethylation sites and 84 m⁶A hypomethylation sites. **(B)** A representative up-methylated gene in the tumor group relative to the control group. **(C,D)** Two representative down-methylated genes in the tumor group relative to the control group.

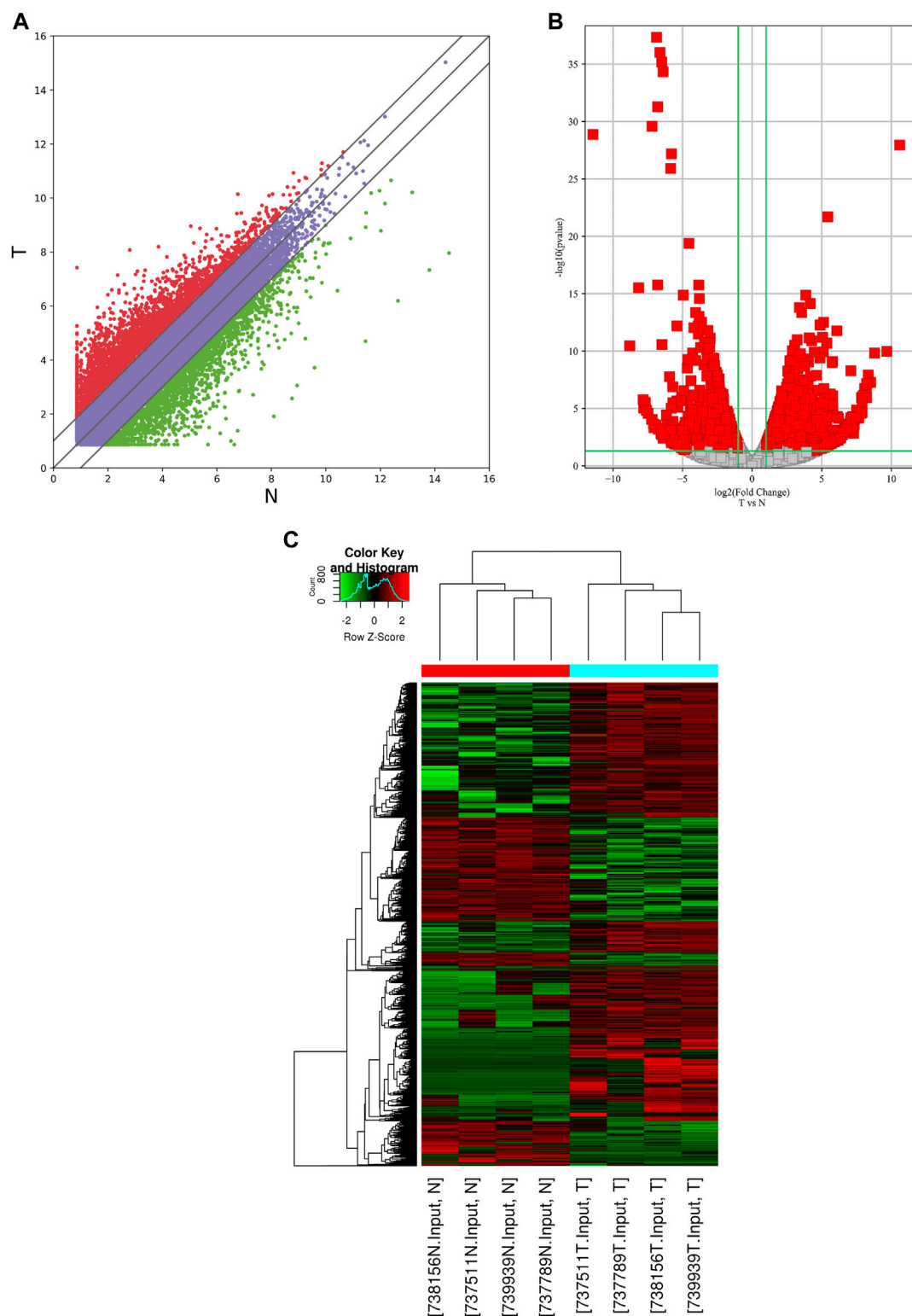


FIGURE 3 | Identification of differentially expressed genes in AEG by RNA-seq. **(A)** the scatter plot of the RNA-seq data. **(B)** Volcano Plot of the RNA-seq data. **(C)** Heat map of RNA-seq data of Ca samples and adjacent normal tissues. Red and Green indicate the upregulation and downregulation of mRNAs, respectively.

TABLE 2 | Hyper-up gene.

Gene name	Pattern	Chromosome	m ⁶ A level change					mRNA level change		
			Peak region	Peak start	Peak end	Fold change	p-value	Strand	Fold change	p-value
MYL12B	Hyper-up	chr18	3'UTR	3278181	3278282	589.5333	4.04E-08	+	2.396340637	0.014228
TRIM69	Hyper-up	chr15	Exonic	45059581	45059960	503.3184	4.62E-08	+	4.361604634	0.01379
TPR	Hyper-up	chr1	Exonic	186000000	186000000	449.3787	4.63E-08	–	2.168355042	0.011414
OLFM4	Hyper-up	chr13	Exonic	53624161	53624380	438.9512	6.89E-08	+	41.40861373	2.09E-11
SNX1	Hyper-up	chr15	3'UTR	64433121	64433400	384.0109	6.36E-08	+	2.273696986	0.020023
FTSJ3	Hyper-up	chr17	3'UTR	61896792	61897000	195.3784	9.49E-09	–	2.83970881	0.000421
THEM6	Hyper-up	chr8	Exonic	144000000	144000000	113.0642	1.61E-08	+	8.357769668	0.000168
DGCR6	Hyper-up	chr22	Exonic	18899052	18899340	105.5676	8.06E-08	+	14.36709026	0.000414
PDAP1	Hyper-up	chr7	Exonic	98997925	98998047	52.41343	0.000000425	–	2.939484153	0.000234
DNAJC21	Hyper-up	chr5	Exonic	34954657	34954960	49.44994	0.000000153	+	2.263359888	0.043718
DIAPH3	Hyper-up	chr13	Exonic	60435387	60435640	42.13218	0.000000179	–	11.87765394	0.005924
ESF1	Hyper-up	chr20	Exonic	13698014	13698161	29.20853	0.000000346	–	10.77001236	0.000268
PHLPP2	Hyper-up	chr16	3'UTR	71681201	71681560	26.70845	0.00000006	–	4.971430367	0.001788
ASPM	Hyper-up	chr1	Exonic	197000000	197000000	21.8376	0.00000021	–	19.67930001	0.00000146
ERCC1	Hyper-up	chr19	Exonic	45981993	45982086	16.93339	0.000000127	–	3.083275918	0.000306
C2orf15	Hyper-up	chr2	Exonic	99766945	99767400	15.76066	0.00000106	+	3.179251174	0.007309
NONO	Hyper-up	chrX	Exonic	70516700	70516897	15.57156	0.00000206	+	2.190048774	0.008746
SMC6	Hyper-up	chr2	Exonic	17899343	17899490	12.53989	0.00000364	–	18.74389666	0.0000171
TPX2	Hyper-up	chr20	Exonic	30380621	30380633	9.823938	0.000000183	+	3.704793164	0.000704
ITGB1	Hyper-up	chr10	Exonic	33218749	33218960	9.433681	0.00000235	–	2.644302086	0.001906
CLCC1	Hyper-up	chr1	Exonic	109000000	109000000	8.576991	0.0000246	–	2.662759259	0.003414
CENPE	Hyper-up	chr4	Exonic	104000000	104000000	7.295365	0.000000566	–	10.56417353	0.007515
CENPF	Hyper-up	chr1	Exonic	215000000	215000000	6.658635	0.000000557	+	4.678360385	0.00000188
ELF1	Hyper-up	chr13	Exonic	41507441	41507760	6.604386	0.000000654	–	2.597993822	0.010944
FEN1	Hyper-up	chr11	3'UTR	61564361	61564714	5.984716	0.000000896	+	9.734534556	0.001119
VRK2	Hyper-up	chr2	Exonic	58373450	58373609	5.662622	0.00000371	+	4.759549413	0.00018
POLE3	Hyper-up	chr9	Exonic	116000000	116000000	5.036067	0.00000204	–	4.962024986	0.000619
SMC3	Hyper-up	chr10	Exonic	112000000	112000000	3.85501	0.000192	+	4.625598352	0.004154
NCL	Hyper-up	chr2	Exonic	232000000	232000000	3.772817	0.0000264	–	2.980307104	0.000137
NCL	Hyper-up	chr2	Exonic	232000000	232000000	3.330097	0.000445	–	2.980307104	0.000137

TABLE 3 | Hyper-down gene.

Gene name	Pattern	Chromosome	m ⁶ A level change					mRNA level change		
			Peak region	Peak start	Peak end	Fold change	p-value	Strand	Fold change	p-value
SERTAD4	Hyper-down	chr1	Exonic	210000000	210000000	913.1	5.73E-09	+	26.69078811	0.006686
UTRN	Hyper-down	chr6	Exonic	145000000	145000000	454.6408	2.88E-08	+	2.596053293	0.001236
MED12L	Hyper-down	chr3	Exonic	151000000	151000000	74.36694	5.11E-08	+	7.028418024	0.036049
FAT4	Hyper-down	chr4	Exonic	126000000	126000000	67.88037	0.000000305	+	3.732908122	0.024065
SPECC1	Hyper-down	chr17	Exonic	20135070	20135144	27.71836	0.000000773	+	2.791750475	0.007659
RTL1	Hyper-down	chr14	Exonic	101000000	101000000	11.87251	8.89E-08	–	4.938866594	0.000164
TBC1D9B	Hyper-down	chr5	Exonic	179000000	179000000	4.061465	0.001852	–	2.012892324	0.027099
F13A1	Hyper-down	chr6	Exonic	6251043	6251162	2.535	0.048738	–	4.559260999	0.04251
OSBPL1A	Hyper-down	chr18	Exonic	21750290	21750417	2.18732	0.0000285	–	3.859703434	0.009948

the stop codon, which indicates that the distribution of m⁶A peaks increases rapidly when the end of CDS is near the stop codon. In the 3'UTR region, m⁶A peaks decrease rapidly from the beginning of the 3'UTR to the 3' ends (Figure 1F).

Differential Methylated Genes Analysis

The abundance of the m⁶A peaks between NC and Ca samples was compared. Among the 1,039 m⁶A peaks detected in both samples, a total of 272 differentially methylated sites were chosen for further study. Among them, there are 188 m⁶A hypermethylation sites and

84 m⁶A hypomethylation sites (Figure 2A). According to the Integrative Genomics Viewer (IGV) software, the hypermethylation gene TPR and hypomethylation genes PLCG2 and DVL1 were displayed (Figures 2B–D).

Identification of Differentially Expressed Genes in AEG by RNA-Seq

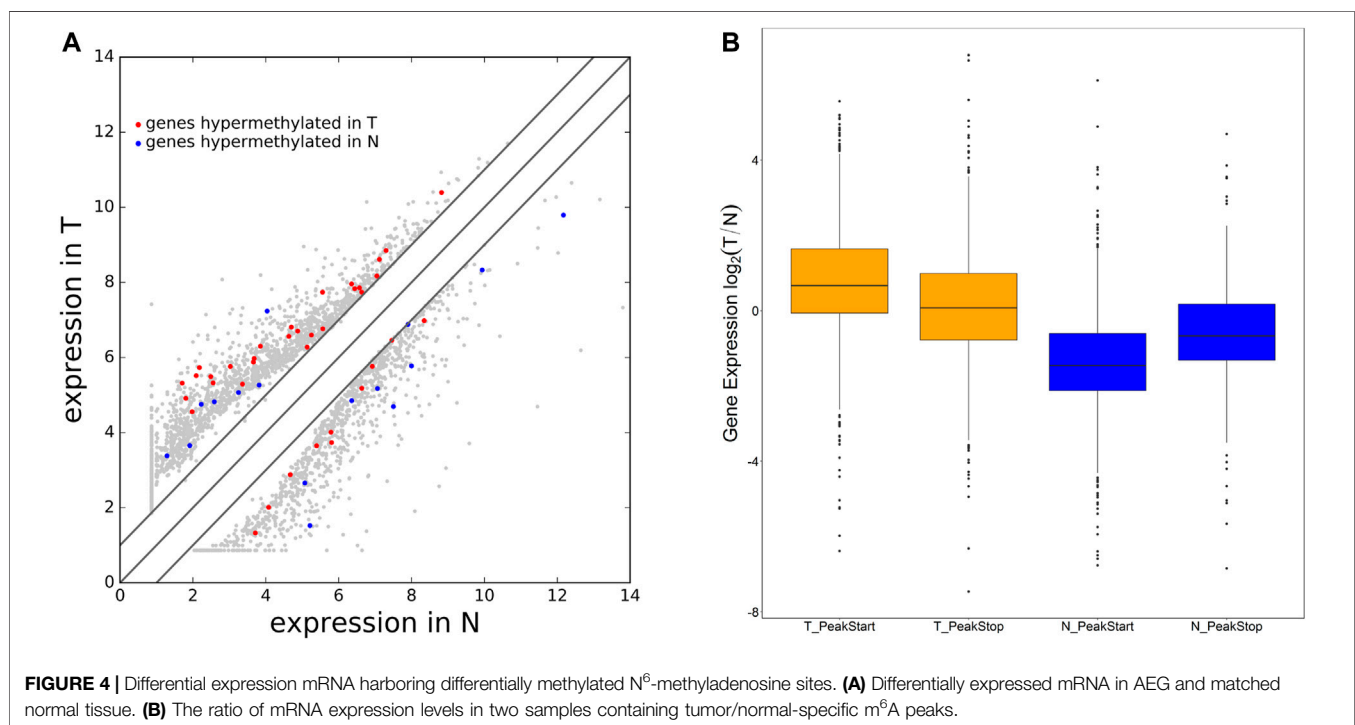
In the RNA-seq dataset (m⁶A-seq input library), we discovered that the global mRNA expression patterns between AEG samples

TABLE 4 | Hypo-up gene.

Gene name	Pattern	Chromosome	m ⁶ A level change					mRNA level change		
			Peak region	Peak start	Peak end	Fold change	p-value	Strand	Fold change	p-value
CENPE	Hypo-up	chr4	Exonic	104000000	104000000	185.5455	2.98E-08	–	7.145663	0.007515
ZNF697	Hypo-up	chr1	Exonic	120000000	120000000	170.5844	0.00000018	–	4.600914	0.031955
RPS27A	Hypo-up	chr2	3'UTR	55462741	55462960	5.496705	0.0000121	+	3.890766	0.048552
MTRNR2L3	Hypo-up	chr20	3'UTR	55933521	55933840	92.85938	4.97E-09	–	6.133057	0.013268
TOP2A	Hypo-up	chr17	Exonic	38551700	38551791	376.6434	6.58E-08	–	34.88758	3.49E-09
ZNF678	Hypo-up	chr1	Exonic	228000000	228000000	8.666667	4.72E-08	+	5.339058	0.020853
ARL5B	Hypo-up	chr10	3'UTR	18964181	18964500	156.4742	4.77E-08	+	5.166949	0.023021

TABLE 5 | Hypo-down gene.

Gene name	Pattern	Chromosome	m ⁶ A level change					mRNA level change		
			Peak region	Peak start	Peak end	Fold change	p-value	Strand	Fold change	p-value
FAM46C	Hypo-down	chr1	Exonic	118000000	118000000	4.347762	0.027232	+	26.56062	0.000000255
C7	Hypo-down	chr5	Exonic	40936439	40936587	217.58	6.58E-08	+	20.4862	0.00000601
ITIH5	Hypo-down	chr10	3'UTR	7601231	7601400	215.1854	5.97E-08	–	10.17475	0.001424
PLCG2	Hypo-down	chr16	3'UTR	81995801	81996000	120.633	1.65E-08	+	6.860429	0.008813
SETBP1	Hypo-down	chr18	Exonic	42533001	42533305	13.46909	4.88E-07	+	13.83856	0.000199
TSC22D3	Hypo-down	chrX	Exonic	107000000	107000000	3.483142	0.001349	–	24.92234	0.000000597
MYH11	Hypo-down	chr16	Exonic	15832421	15832540	15.24643	3.46E-06	–	30.97305	2.62E-08
MYH11	Hypo-down	chr16	Exonic	15831305	15831477	16.42946	3.49E-06	–	30.97305	2.62E-08
JUN	Hypo-down	chr1	Exonic	59247581	59247780	10.93321	2.17E-06	–	15.46234	0.0000842
DVL1	Hypo-down	chr1	Exonic	1270655	1270740	358.0816	2.39E-08	–	5.618537	0.017771
PGC	Hypo-down	chr6	3'UTR	41704448	41704460	141.6648	9.11E-08	–	160.2992	9.73E-37



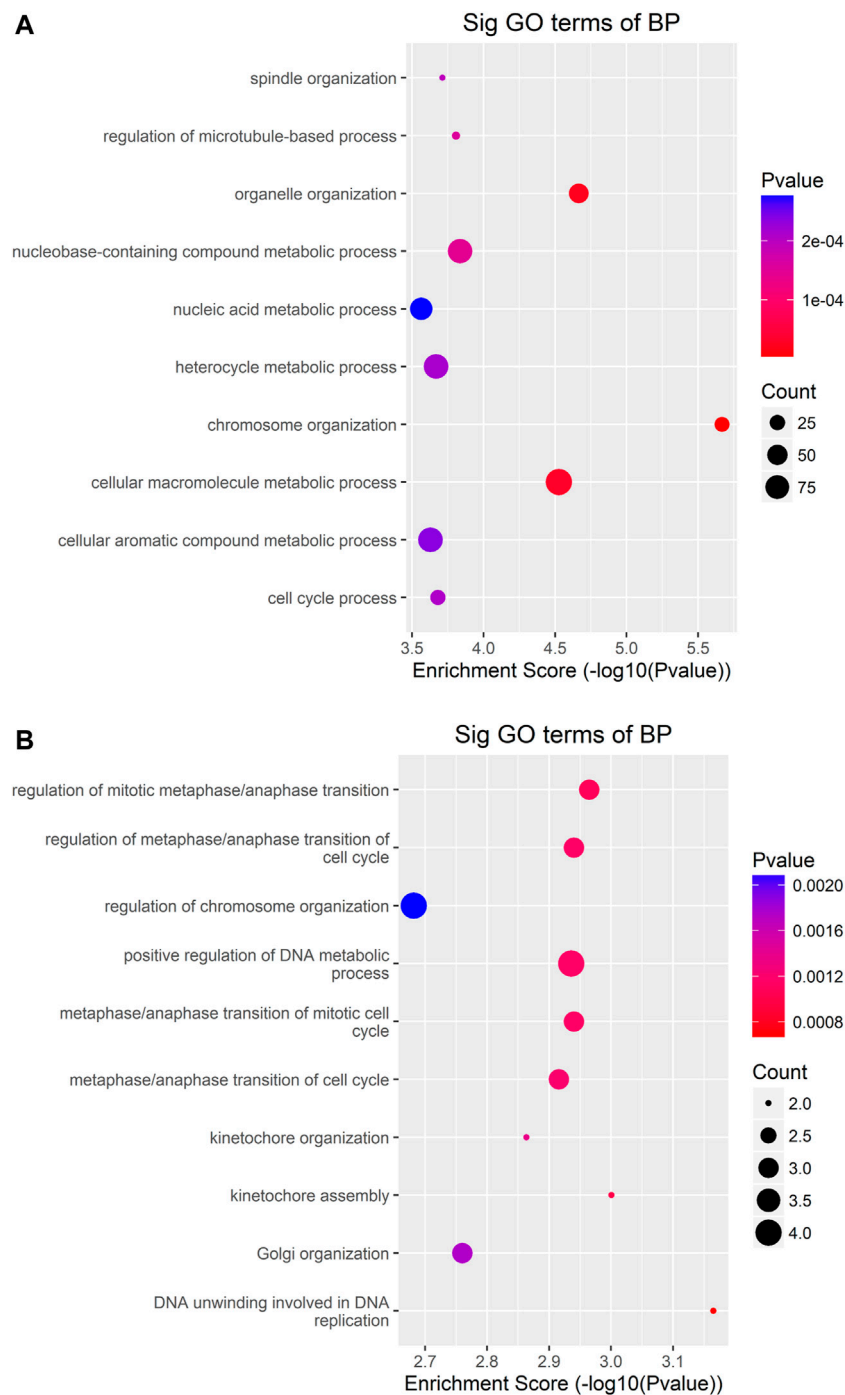


FIGURE 5 | GO-enrichment analysis for differentially methylated mRNAs **(A)** The top ten gene ontology terms of biological processes were significantly enriched for the up-methylated genes. **(B)** The top ten gene ontology terms of biological process significantly enriched for down-methylated genes.

and adjacent normal tissues were significantly different. We calculated gene expression to assign differentially expressed genes (DE genes) of the two tissues. Of the 20,308 mRNAs we have identified, 3,069 were significantly different, while 17,239

were not. Among them, 2,032 is up-expressed and 1,037 is down-expressed (fold change > 2, $p < 0.05$). The volcano Plot, scatter plot, and the hierarchical clustering of the RNA-seq data were shown in **Figures 3A–C**.

Conjoint Analysis of m⁶A-RNA Binding Protein Immunoprecipitation (RIP)-Seq and RNA-Seq Data of AEG and Normal Samples

By cross-analysis of the m⁶A-Seq and RNA-seq data, we studied the relationship between the expression level of the m⁶A modified gene and its mRNA. Using RNA-seq, we found that there were 3,069 differential expression mRNAs, of which 2032 is up-expressed and 1,037 is down-expressed (fold change >2, $p < 0.05$). In 158 hyper-methylated mRNAs detected by m⁶A-Seq, we found thirty targets with upregulated mRNA transcripts (fold change > 2, $p < 0.05$), namely “hyper-up” (Table 2). The expression of 9 hypermethylation mRNA was downregulated (fold change > 2, $p < 0.05$), namely “hyper-down” (Table 3). In the contrast, 7 of 77 genes with hypomethylated m⁶A sites showed upregulated mRNA transcripts (fold change > 2, $p < 0.05$), namely, “hypo-up” (Table 4), and 11 of 77 genes with hypomethylated m⁶A sites showed downregulated mRNA transcripts (fold change > 2, $p < 0.05$), namely, “hypo-down” (Table 5). Notably, the numbers of “hyper-up” and “hypo-down” genes were more than those of “hyper-down” and “hypo-up” genes. To describe the relationship between differential m⁶A modification and its mRNA expression, we plotted a scatter plot. The results show that m⁶A modifications tend to have a positive correlation of mRNA expression in AEG. However, further analysis of the underlying mechanisms is needed (Figure 4A).

We were wondering whether the location of m⁶A peaks in mRNA transcripts was associated with gene expression levels. To further explore how m⁶A modification affects mRNA expression, we divided the gene containing m⁶A sites into PeakStart category (m⁶A peaks around start codon) and PeakStop (m⁶A peaks around stop codon). The results showed that the PeakStart category had higher overall expression levels (Figure 4B, note that the expression ratio of the tumor/normal gene is shown).

Results of Bioinformatics Analysis

To uncover the functions of m⁶A modification in AEG tissues, mRNAs containing DMMSs were selected for GO (gene ontology) enrichment analysis and KEGG pathway analysis. Differently, m⁶A methylation genes are mainly involved in cell DNA metabolism and cell cycle process (Figures 5A,B). Pathway analysis revealed that mRNAs with hypermethylated and hypomethylated m⁶A sites were enriched in many pathways involved in cancer pathogenesis, including Pathways in cancer, Basal cell carcinoma, Wnt signaling pathway, HTLV-I infection, ErbB signaling pathway (Figures 6A,B).

The differentially expressed genes were selected for ingenuity gene ontology and pathway analysis. It revealed that differentially expressed genes were significantly enriched in biological processes involving DNA metabolic process, cell cycle process (Figures 7A,B). Moreover, pathway analysis showed that nucleotide excision repair, cell cycle, and DNA

replication were significantly altered in AEG samples (Figures 8A,B).

The Results of the Preliminary Screening Were Further Verified by mRNA qPCR and MeRIP-qPCR

To further confirm the results of our m⁶A-seq data, we conducted gene-specific MeRIP-qPCR assays for several hypermethylated and hypomethylated genes (TPR, DVL1, and PLCG2). TPR is hypermethylated, but PLCG2, DVL1 are hypomethylated (Table 6 shows the initial detection of methylation of three genes). MeRIP-qPCR results showed that TPR was hypermethylated, while DVL1, PLCG2 were hypomethylated (Figures 9A–C, $p < 0.05$). We observed the same m⁶A-level changes in three out of the three genes (100%), demonstrating the reliability of our transcriptome-wide m⁶A-seq data.

Sequentially, we verified the expression of mRNA by qPCR. We chose PLCG2 as the validation gene. The above results show that the expression of PLCG2 is downregulated, and the fold change is 2.935315743 (Table 7). And after verification by qPCR, the results indicate that PLCG2 is downregulated (Figure 9D, $p < 0.05$). The results of qPCR and MeRIP-qPCR elaborated that the PLCG2 acting as a hypomethylated gene, its expression was down-expressed.

The results of qPCR and MeRIP-qPCR showed that the Melcurve Plots of GAPDH and three mRNAs were single peaks, and the inflection points of each Amplification Plot were obvious, the overall parallelism was good, and the baseline was smooth without rising, indicating that the PCR amplification product specificity, amplification efficiency.

The Results of the Conservation of m⁶A Validated on the ConsRM Online Platform

The recent studies have been proven the m⁶A modification in evolution conservation (Miao et al., 2021; Song et al., 2021), thus, the conservation could be considered in our analysis. Taking PLCG2 as an example, Search for “PLCG2” returns 7 m⁶A sites located on the PLCG2 transcripts on the ConsRM online platform. One of them are highly conserved, among the top 8% most conserved m⁶A sites (Figure 10A). In addition, we can also see that the Gene Region where the most conserved m⁶A site of PLCG2 is located is 3'UTR, which is consistent with our experimental results. Its post-transcriptional regulation involves one RNA binding protein site and two miRNA Targets (Figure 10B).

DISCUSSION

Recent technological advances in high-throughput sequencing in combination with antibody enrichment of modifications have accelerated the detection of distribution and abundance for m⁶A methylation at the transcriptome-wide level (Meyer et al., 2012; Strong et al., 2015). The discovery of m⁶A demethylases indicates that m⁶A methylation of mRNA is a reversible and dynamic process with regulatory functions (Jia et al., 2013; Nilsen, 2014).

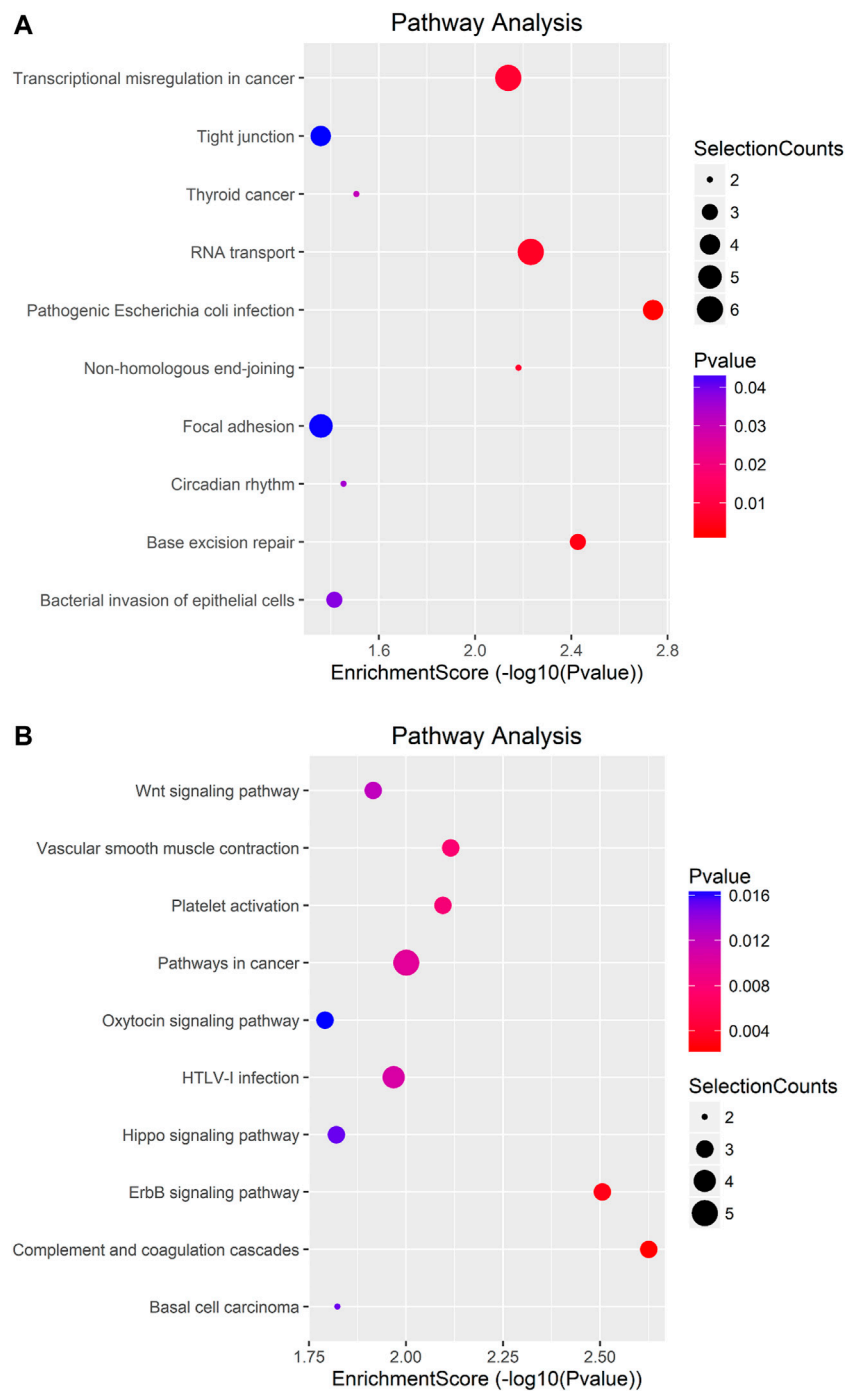


FIGURE 6 | Pathway analysis of mRNAs harboring differentially methylated N⁶-methyladenosine sites. **(A)** Bubble Plot showing the top ten enrichment scores of the significant enrichment pathway for the hyper-methylated genes. **(B)** Bubble Plot showing the top ten enrichment scores of the significant enrichment pathways of the hypo-methylated genes.

In recent years, more and more studies have been conducted on the components of m⁶A writers, erasers, and readers in cancer. Ma et al. (2017) revealed an important role of METTL14 in tumor metastasis and provided a fresh view of m⁶A modification in tumor progression. Zhang J. et al. (2019)

indicated a novel mechanism by which ALKBH5 promotes GC invasion and metastasis by demethylating the lncRNA NEAT1. Tang et al. (2019) found that FTO is essential for the proliferation of pancreatic cancer cells. In our study, we found that the expression level of YTHDF3 was up-

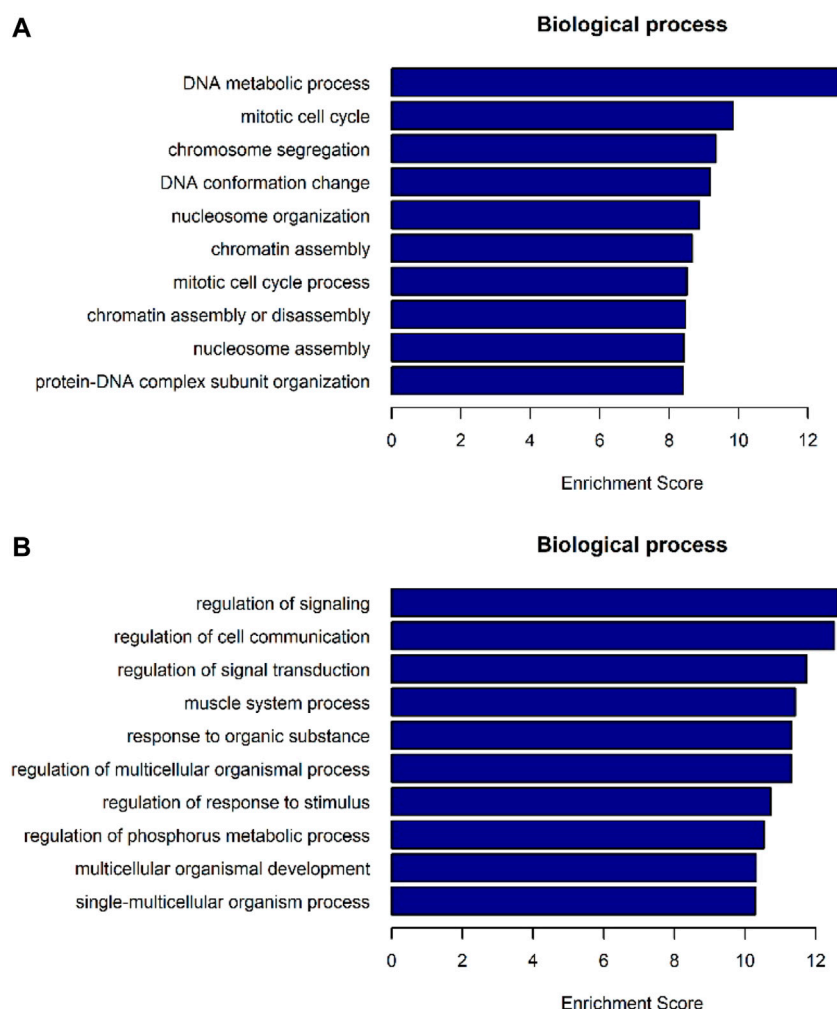


FIGURE 7 | GO-enrichment analysis for differentially expressed mRNAs. **(A)** Top 10 biological processes of mRNA enrichment up-regulated by differences. **(B)** Top 10 biological processes of mRNA enrichment were differentially down-regulated.

regulated ($FC > 2$, $p < 0.05$, **Table 8**), but there was no previous study on the expression level of YTHDF3 in adenocarcinoma of the esophagogastric junction. But limited by the size of our research sample, more research is needed to further explore. But in HCC, Zhou et al. (2019) found that the expression level of YTHDF3 was upregulated.

In this study, we illustrated global m⁶A modification patterns in AEG samples vs. tumor-adjacent normal tissues, analyzing gene expression and cancer-related pathways modulated by abnormal m⁶A RNA modifications. From previous studies, we know that m⁶A modified nucleotides are widely distributed in animal tissues, including the heart, liver, kidney, brain, and lung (Dominissini et al., 2012; Meyer et al., 2012). We figured out that the m⁶A modification pattern in AEG samples was distinct from that of normal controls, with a higher total m⁶A level and 1,721 more m⁶A peaks identified in the Ca group. By analyzing the differently methylated transcripts, cancer-related biological processes and pathways were significantly enriched, indicating

the relationship between abnormal m⁶A modifications and AEG pathogenesis. Such global change of m⁶A modification profiles could result from the abnormal expression of key m⁶A enzymes. Nevertheless, only ~12% of all peaks were detected within both adenocarcinomas of esophagogastric junction tissues and normal tissues. So there are differences between the two kinds of tissues. By analyzing the distribution of m⁶A-modified peaks per gene, we found the majority of genes had one to three m⁶A modified sites, while a relatively small number of genes contain more. Similarly, Chen et al. (2020) found that the majority of genes (6268/8526) had one to three m⁶A modified sites. Using MeRIP-Seq technology, we discovered that the m⁶A peak is abundant near the CDS and the stop codon, followed by the start codon and the 3' UTR. However dominant m⁶A enrichment near stop codons and 3'UTRs is shown in most of mammal mRNA mammal as previously reported (Dominissini et al., 2012), and this m⁶A distributing type may represent the typical m⁶A topological pattern in most of the mature mRNA (Meyer et al., 2012;

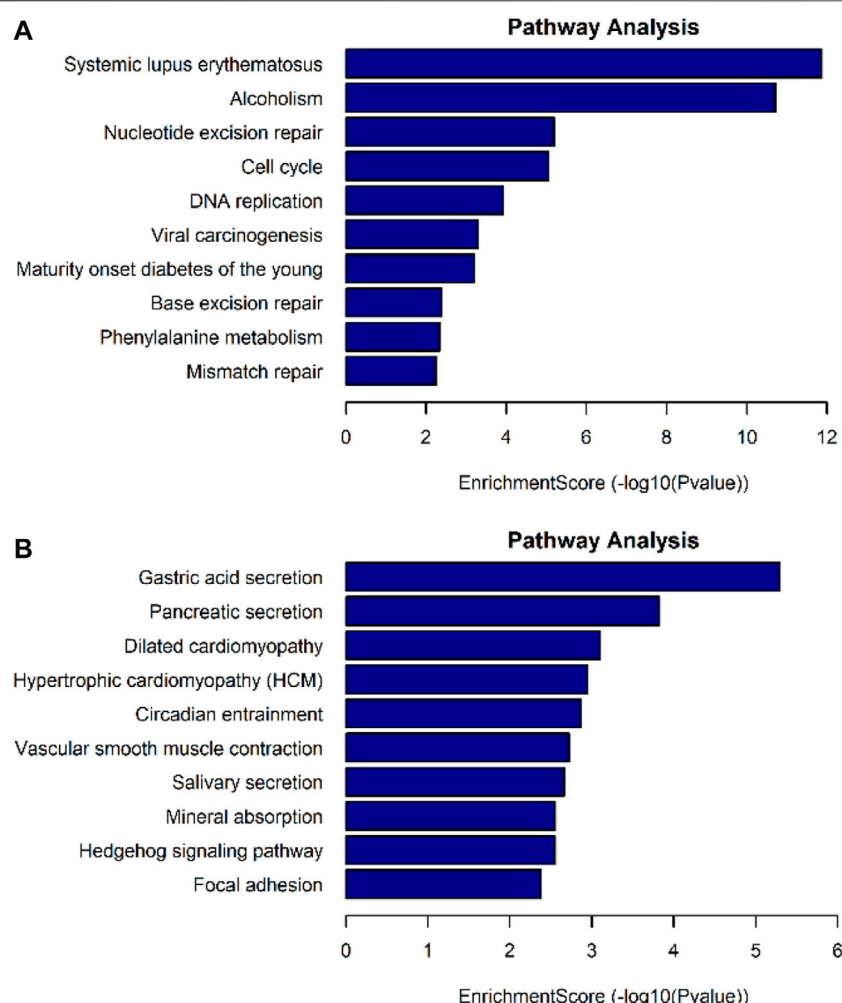


FIGURE 8 | Pathway analysis for differentially expressed mRNAs. **(A)** Up-regulated mRNAs related pathway analysis. **(B)** Down-regulated mRNAs related pathway analysis.

TABLE 6 | Initial detection of methylation of three genes.

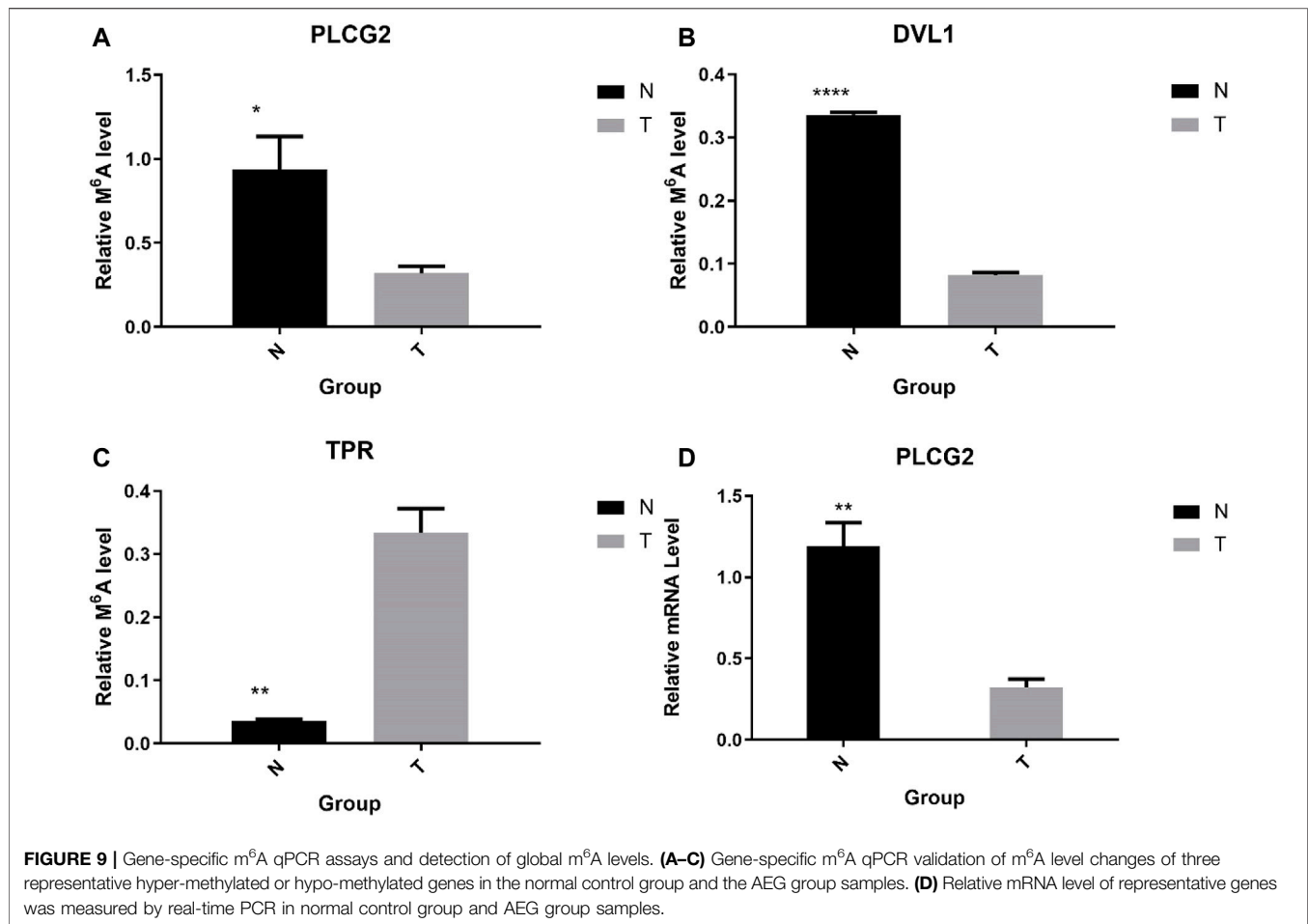
mRNA	Fold change	Methylation level	Chromosome localization
PLCG2	120.633	Down	chr16
TPR	449.3787	Up	chr1
DVL1	358.0816	Down	chr1

Batista et al., 2014). The extensively higher m⁶A signals at the stop codon or 3'UTRs may be responsible for RNA stability, signaling for transport, and translocation (Niu et al., 2013; Wang X. et al., 2014). As recently reported, m⁶A sites in plants are enriched around stop codons within 3'UTRs, start codons, and 5'UTRs (Li et al., 2014; Luo et al., 2014; Wang X. et al., 2014). In order to better understand the distribution of m⁶A peaks in the whole mRNA, we divided each m⁶A modified mRNA into three regions: 5'UTR, CDs and 3'UTR, and calculated the distribution proportion of these three regions. We can conclude that the

distribution of m⁶A peaks in the CDS region is increased and there is a summit in the m⁶A peak near the stop codon of CDS. But in plants, Csepány et al. (1990) found that there was another minor summit of m⁶A peaks at positions near the start codon of CDS both in callus and leaf.

The consensus motif sequence RRACH has previously been shown to be over represented in m⁶A motif regions (Wei and Moss, 1977; Harper et al., 1990) and also further been identified in some high throughput m⁶A RNA sequencing databases (Luo et al., 2014; Wan et al., 2015). Therefore, in our current study, we successfully identified common motifs in the AEG transcriptome. Interestingly, Csepány et al. (1990) failed to find the common RRACH sequence in the m⁶A motif region of rice, but another different motif sequence was enriched by MEME and HOMER.

We additionally analyzed the relationship between methylation genes and their expression levels. Combined analysis of our m⁶A-seq and mRNA-seq data revealed 55

**TABLE 7 |** Expression of PLCG2 obtained by initial screening.

mRNA	Fold change	Expression level	Chromosome localization
PLCG2	2.9534157	Down	chr16

genes in the Ca group, which have differently methylated m⁶A sites along with significant changes of mRNA abundance compared with the NC group (fold change > 2, $p < 0.05$). It indicated that m⁶A modifications tend to have a positive correlation of mRNAs expression in AEG. Similar to our results, Luo et al. (2019) found that compared to hypomethylated genes, the expression of hypermethylated mRNAs tended to be upregulated in the HFD group. But some studies have come to different conclusions (Niu et al., 2013; Schwartz et al., 2014). In addition, we found that the overall expression level of methylated genes near the start codon was higher. Luo et al. (2019) also stated that genes in the PeakStart category possess higher overall expression levels. However, in the study of Luo, the enrichment of m⁶A around the start codon is obvious. Different from the results of Luo, there is no obvious enrichment of m⁶A around the start

codon in our study. Recently, it has been found that the main function of m⁶A is to mediate the degradation of mRNA in mammalian cells (Batista et al., 2014; Wang Y. et al., 2014; Liu et al., 2014).

In combination with various databases and preliminary screening results, we selected three typical mRNAs for further verification. For example, PLCG2 could promote proliferation through inactivating ERK and NF- κ B pathway (Ma et al., 2019), p38 MAPK and JNK MAPK pathways (Chen et al., 2018a), PKC δ -mediated JNK1/2 signaling pathway (Chen et al., 2018b). The TPR contributes to the organization of the nuclear lamina and in cooperation with lamins guards the interphase assembly of nuclear pore complexes (Fišerová et al., 2019). Consistent with the results of the initial screening, TPR was hyper-methylated; DVL1, PLCG2 were hypomethylated. As a hypomethylated gene, the expression of PLCG2 was downregulated. It is further possible to conclude that hypomethylated genes are more prone to low expression. This is similar to the results that m⁶A modifications tend to have a positive correlation of mRNAs expression in AEG. The relationship between gene methylation and gene expression requires further investigation.

ASearch for Gene: **PLCG2**

Show 10 entries

Search:

ConsRM Score	Relative Rank	ID	Position	Gene	Gene Region	Positional Mapping	Tissue Specific Mapping	Supports From Multiple Studies	S
0.6967	8%	Human_m6A_76615	chr16:81991792 +	PLCG2	UTR3	1.0000	0.0000	0.3000	1.0000
0.3521	45%	Human_m6A_165593	chr16:81968128 +	PLCG2	CDS	0.0000	0.0000	0.1000	0.8438
0.0368	86%	Human_m6A_140770	chr16:81995702 +	PLCG2	ncRNA_exonic	0.0000	0.0000	0.1000	0.0000
0.0299	89%	Human_m6A_61151	chr16:81902033 -	PLCG2	intronic	0.0000	0.0000	0.1000	0.0000
0.0283	90%	Human_m6A_61153	chr16:81902057 -	PLCG2	intronic	0.0000	0.0000	0.1000	0.0000
0.0271	91%	Human_m6A_61070	chr16:81902050 +	PLCG2	intronic	0.0000	0.0000	0.1000	0.0000
0.026	92%	Human_m6A_61152	chr16:81902046 -	PLCG2	intronic	0.0000	0.0000	0.1000	0.0000

Showing 1 to 7 of 7 entries

Previous 1 Next

B

ConsRM

Home Database Web Server Help Contact

Conservation degree of human m6A site: [Human_m6A_76615](#)

ConsRM Score	0.6967
Relative Rank	8%
Positional Mapping	1
Tissue-specific Mapping	0
Supports from multiple studies	0.3
Sequence Similarity	1
Machine Learning Model	1
Genome Conservation	0.88

Basic information of human m6A site: [Human_m6A_76615](#)

Site ID	Human_m6A_76615
Position	chr16:81991792 +
Gene	PLCG2
Gene Type	protein_coding
Gene Region	UTR3
Ensembl Gene ID	ENSG00000197943
Human Sequence 11bp	CTTGGACAACT
Corresponding Coordinate In Mouse Transcriptome With m6A Methylation Site	Yes
Predicted RNA Secondary Structure	Stem: Regions of contiguous canonical Watson-Crick base-paired nucleotides.
Supported Studies	m6A-CLIP-seq,28637692,GSE86336,HeLa,Ctrl
Post-transcriptional Regulation Involved	RNA Binding Protein: 1, miRNA Target: 2, Splicing Site: 0
Variants Within Motif Region	Somatic Variant: 0, Germline Variant: 0
JBrowse Genome Browser	JBrowse

The corresponding coordinate in mouse transcriptome: [Mouse_m6A_16546](#)

FIGURE 10 | Results of ConsRM online platform. **(A)** Search for “PLCG2” returns 7 m⁶A sites. **(B)** The detailed conservation metrics and other regulatory information of the most conserved m⁶A site on PLCG2.

TABLE 8 | Expression of m⁶A methylated regulator.

Gene	Chromosome localization	Fold change	Expression level	p value
ZC3H13	chr13	1.732127499	Up	0.051304693
RBM15	chr1	1.263324488	Up	0.557236768
KIAA1429	chr8	1.112162637	Down	0.806428469
METTL3	chr14	1.320213898	Up	0.390769705
METTL14	chr4	1.368793596	Up	0.712905503
WTAP	chr6	1.687160095	Up	0.099719678
FTO	chr16	1.017027554	Up	0.975420319
ALKBH5	chr17	1.493330599	Down	0.349730675
YTHDF1	chr20	1.428774733	Up	0.348060186
YTHDF2	chr1	1.497757976	Up	0.501900856
YTHDF3	chr8	2.79836485	Up	0.049556735
YTHDC1	chr4	1.130674806	Up	0.70423955
YTHDC2	chr5	1.887976428	Down	0.353781994
HNRNPC	chr14	1.911794749	Up	0.138018091

In our study, the human AEG transcriptome modification profile was proposed for the first time and differentially expressed mRNA transcripts were identified through hypermethylation and hypomethylation m⁶A modification. This may help to further study the mechanism of m⁶A-mediated gene expression regulation. It is possible to develop new AEG therapeutic strategies by regulating m⁶A methylation transcripts or m⁶A-related genes. However, this study still has some limitations: 1) the m⁶A-Atlas (Tang et al., 2021) database is currently the human genome database containing the most known modification sites. Our research only selected three typical mRNAs for further verification. In the future, we will further select more novel methylated genes in AEG to compare with methylation data in m⁶A-Atlas, and gradually improve related research. 2) The RMVar (Luo et al., 2021) and RMDisease (Chen et al., 2021) show the potential association between the mutations with m⁶A. In future work, we will further explore the role of m⁶A-related mutations in adenocarcinoma of the esophagogastric junction, look for related mechanisms, and find therapeutic targets Point, provide a theoretical basis for the precision treatment of AEG.

CONCLUSION

This study preliminarily constructed the first m⁶A full transcriptome map of human AEG. This has a guiding role in revealing the mechanism of m⁶A-mediated gene expression regulation.

REFERENCES

- Aoyama, T., Yamashita, S., and Tomita, K. (2020). Mechanistic Insights into m⁶A Modification of U6 snRNA by Human METTL16. *Nucleic Acids Res.* 48 (9), 5157–5168. doi:10.1093/nar/gkaa227
- Bailey, T. L. (2011). DREME: Motif Discovery in Transcription Factor ChIP-Seq Data. *Bioinformatics (Oxford, England)* 27 (12), 1653–1659. doi:10.1093/bioinformatics/btr261
- Batista, P. J., Molinier, B., Wang, J., Qu, K., Zhang, J., Li, L., et al. (2014). m⁶A RNA Modification Controls Cell Fate Transition in Mammalian

DATA AVAILABILITY STATEMENT

The datasets presented in this study can be found in online repositories. The names of the repository/repositories and accession number(s) can be found below: <https://www.ncbi.nlm.nih.gov/geo/GSE189874>.

AUTHOR CONTRIBUTIONS

YF provided direction and guidance throughout the preparation of this manuscript. B-BH and J-BH wrote and edited the manuscript. RH, LH, and C-FM collected and prepared the related articles. CZ reviewed and made significant revisions to the manuscript. All authors read and approved the final manuscript.

FUNDING

Jiangsu Innovative Team Leading Talent Fund (CXTDC2016006, QNRC2016446), Jiangsu 333 Talent Fund (BRA2020016), Jiangsu Provincial Key Research and Development Special Fund (BE2015666), Jiangsu Six High Peak Talent Fund (WSW-205, WSW236), Zhenjiang Key Research and Development Fund (SH2021038), Suqian Science and Technology Support Project Fund (K201907).

- Embryonic Stem Cells. *Cell stem cell* 15 (6), 707–719. doi:10.1016/j.stem.2014.09.019
- Chen, K., Song, B., Tang, Y., Wei, Z., Xu, Q., Su, J., et al. (2021). RMDisease: a Database of Genetic Variants that Affect RNA Modifications, with Implications for Epitranscriptome Pathogenesis. *Nucleic Acids Res.* 49 (D1), D1396–D1404. doi:10.1093/nar/gkaa790
- Chen, M., and Wong, C.-M. (2020). The Emerging Roles of N⁶-Methyladenosine (m⁶A) Deregulation in Liver Carcinogenesis. *Mol. Cancer* 19 (1), 44. doi:10.1186/s12943-020-01172-y
- Chen, X., Lv, Q., Ma, J., and Liu, Y. (2018a). PLCγ2 Promotes Apoptosis while Inhibits Proliferation in Rat Hepatocytes through PKCD/JNK MAPK and

- PKCD/p38 MAPK Signalling. *Cell Prolif* 51 (3), e12437. doi:10.1111/cpr.12437
- Chen, X., Zhu, X., Liu, Y., Lv, Q., and Ma, J. (2018b). Silencing of Phospholipase C Gamma 2 Promotes Proliferation of Rat Hepatocytes *In Vitro*. *J. Cel. Biochem.* 119 (5), 4085–4096. doi:10.1002/jcb.26592
- Chen, Y., Zhou, C., Sun, Y., He, X., and Xue, D. (2020). m6A RNA Modification Modulates Gene Expression and Cancer-Related Pathways in clear Cell Renal Cell Carcinoma. *Epigenomics* 12 (2), 87–99. doi:10.2217/epi-2019-0182
- Csepány, T., Lin, A., Baldick, C. J., and Beemon, K. (1990). Sequence Specificity of mRNA N⁶-Adenosine Methyltransferase. *J. Biol. Chem.* 265 (33), 20117–20122. doi:10.1016/s0021-9258(17)30477-5
- Desrosiers, R., Friderici, K., and Rottman, F. (1974). Identification of Methylated Nucleosides in Messenger RNA from Novikoff Hepatoma Cells. *Proc. Natl. Acad. Sci.* 71 (10), 3971–3975. doi:10.1073/pnas.71.10.3971
- Dominissini, D., Moshitch-Moshkovitz, S., Schwartz, S., Salmon-Divon, M., Ungar, L., Osenberg, S., et al. (2012). Topology of the Human and Mouse m6A RNA Methylomes Revealed by m6A-Seq. *Nature* 485 (7397), 201–206. doi:10.1038/nature11112
- Fišerová, J., Maninová, M., Sieger, T., Uhlířová, J., Šebestová, L., Efenberková, M., et al. (2019). Nuclear Pore Protein TPR Associates with Lamin B1 and Affects Nuclear Lamina Organization and Nuclear Pore Distribution. *Cell. Mol. Life Sci.* 76 (11), 2199–2216. doi:10.1007/s00018-019-03037-0
- Frye, M., Harada, B. T., Behm, M., and He, C. (2018). RNA Modifications Modulate Gene Expression during Development. *Science* 361 (6409), 1346–1349. doi:10.1126/science.aau1646
- Geistlinger, L., Csaba, G., Santarelli, M., Ramos, M., Schiffer, L., Turaga, N., et al. (2021). Toward a Gold Standard for Benchmarking Gene Set Enrichment Analysis. *Brief. Bioinformatics* 22 (1), 545–556. doi:10.1093/bib/bbz158
- Harper, J. E., Miceli, S. M., Roberts, R. J., and Manley, J. L. (1990). Sequence Specificity of the Human mRNA N⁶-Adenosine Methylase *In Vitro*. *Nucl. Acids Res.* 18 (19), 5735–5741. doi:10.1093/nar/18.19.5735
- Hsu, P. J., Shi, H., and He, C. (2017). Epitranscriptomic Influences on Development and Disease. *Genome Biol.* 18 (1), 197. doi:10.1186/s13059-017-1336-6
- Huang, H., Weng, H., Sun, W., Qin, X., Shi, H., Wu, H., et al. (2018). Recognition of RNA N⁶-Methyladenosine by IGF2BP Proteins Enhances mRNA Stability and Translation. *Nat. Cel Biol* 20 (3), 285–295. doi:10.1038/s41556-018-0045-z
- Imamura, Y., Watanabe, M., Toihata, T., Takamatsu, M., Kawachi, H., Haraguchi, I., et al. (2019). Recent Incidence Trend of Surgically Resected Esophagogastric Junction Adenocarcinoma and Microsatellite Instability Status in Japanese Patients. *Digestion* 99 (1), 6–13. doi:10.1159/000494406
- Jia, G., Fu, Y., and He, C. (2013). Reversible RNA Adenosine Methylation in Biological Regulation. *Trends Genet.* 29 (2), 108–115. doi:10.1016/j.tig.2012.11.003
- Jia, G., Fu, Y., Zhao, X., Dai, Q., Zheng, G., Yang, Y., et al. (2011). N⁶-methyladenosine in Nuclear RNA Is a Major Substrate of the Obesity-Associated FTO. *Nat. Chem. Biol.* 7 (12), 885–887. doi:10.1038/nchembio.687
- Kaupilla, J. H., and Lagergren, J. (2016). The Surgical Management of Esophago-Gastric Junctional Cancer. *Surg. Oncol.* 25 (4), 394–400. doi:10.1016/j.suronc.2016.09.004
- Kechin, A., Boyarskikh, U., Kel, A., and Filipenko, M. (2017). cutPrimers: A New Tool for Accurate Cutting of Primers from Reads of Targeted Next Generation Sequencing. *J. Comput. Biol.* 24 (11), 1138–1143. doi:10.1089/cmb.2017.0096
- Keeney, S., and Bauer, T. L. (2006). Epidemiology of Adenocarcinoma of the Esophagogastric junction. *Surg. Oncol. Clin. North America* 15 (4), 687–696. doi:10.1016/j.soc.2006.07.014
- Kim, D., Langmead, B., and Salzberg, S. L. (2015). HISAT: a Fast Spliced Aligner with Low Memory Requirements. *Nat. Methods* 12 (4), 357–360. doi:10.1038/nmeth.3317
- Li, J., Liang, L., Yang, Y., Li, X., and Ma, Y. (2021a). N⁶-methyladenosine as a Biological and Clinical Determinant in Colorectal Cancer: Progression and Future Direction. *Theranostics* 11 (6), 2581–2593. doi:10.7150/thno.52366
- Li, K., Chen, J., Lou, X., Li, Y., Qian, B., Xu, D., et al. (2021b). HNRNP2B1 Affects the Prognosis of Esophageal Cancer by Regulating the miR-17-92 Cluster. *Front. Cel Dev. Biol.* 9, 658642. doi:10.3389/fcell.2021.658642
- Li, Y., Wang, X., Li, C., Hu, S., Yu, J., and Song, S. (2014). Transcriptome-wide N⁶-Methyladenosine Profiling of rice Callus and Leaf Reveals the Presence of Tissue-specific Competitors Involved in Selective mRNA Modification. *RNA Biol.* 11 (9), 1180–1188. doi:10.4161/rna.36281
- Lin, S., Liu, Q., Lelyveld, V. S., Choe, J., Szostak, J. W., and Gregory, R. I. (2018). Mettl1/Wdr4-Mediated m7G tRNA Methylome Is Required for Normal mRNA Translation and Embryonic Stem Cell Self-Renewal and Differentiation. *Mol. Cel.* 71 (2), 244–255. doi:10.1016/j.molcel.2018.06.001
- Liu, J., Yue, Y., Han, D., Wang, X., Fu, Y., Zhang, L., et al. (2014). A METTL3-METTL14 Complex Mediates Mammalian Nuclear RNA N⁶-Adenosine Methylation. *Nat. Chem. Biol.* 10 (2), 93–95. doi:10.1038/nchembio.1432
- Liu, S., Zhuo, L., Wang, J., Zhang, Q., Li, Q., Li, G., et al. (2020a). METTL3 Plays Multiple Functions in Biological Processes. *Am. J. Cancer Res.* 10 (6), 1631–1646.
- Liu, T., Wei, Q., Jin, J., Luo, Q., Liu, Y., Yang, Y., et al. (2020b). The m6A Reader YTHDF1 Promotes Ovarian Cancer Progression via Augmenting EIF3C Translation. *Nucleic Acids Res.* 48 (7), 3816–3831. doi:10.1093/nar/gkaa048
- Liu, Z.-X., Li, L.-M., Sun, H.-L., and Liu, S.-M. (2018). Link between m6A Modification and Cancers. *Front. Bioeng. Biotechnol.* 6, 89. doi:10.3389/fbioe.2018.00089
- Luo, G.-Z., Macqueen, A., Zheng, G., Duan, H., Dore, L. C., Lu, Z., et al. (2014). Unique Features of the m6A Methylome in *Arabidopsis thaliana*. *Nat. Commun.* 5, 5630. doi:10.1038/ncomms6630
- Luo, X., Li, H., Liang, J., Zhao, Q., Xie, Y., Ren, J., et al. (2021). RMVar: an Updated Database of Functional Variants Involved in RNA Modifications. *Nucleic Acids Res.* 49 (D1), D1405–D1412. doi:10.1093/nar/gkaa811
- Luo, Z., Zhang, Z., Tai, L., Zhang, L., Sun, Z., and Zhou, L. (2019). Comprehensive Analysis of Differences of N⁶-Methyladenosine RNA Methylomes between High-Fat-Fed and normal Mouse Livers. *Epigenomics* 11 (11), 1267–1282. doi:10.2217/epi-2019-0009
- Ma, D., Lian, F., and Wang, X. (2019). PLCG2 Promotes Hepatocyte Proliferation *In Vitro* via NF-Kb and ERK Pathway by Targeting Bcl2, Myc and Ccnd1. *Artif. Cell nanomedicine, Biotechnol.* 47 (1), 3786–3792. doi:10.1080/21691401.2019.1669616
- Ma, J. z., Yang, F., Zhou, C. c., Liu, F., Yuan, J. h., Wang, F., et al. (2017). METTL14 Suppresses the Metastatic Potential of Hepatocellular Carcinoma by Modulating N⁶-methyladenosine-dependent Primary MicroRNA Processing. *Hepatology* 65 (2), 529–543. doi:10.1002/hep.28885
- Macha, M., Seshacharyulu, P., Krishn, S., Pai, P., Rachagani, S., Jain, M., et al. (2014). MicroRNAs (miRNAs) as Biomarker(s) for Prognosis and Diagnosis of Gastrointestinal (GI) Cancers. *Curr. Pharm. Des.* 20 (33), 5287–5297. doi:10.2174/1381612820666140128213117
- Meyer, K. D., Saletore, Y., Zumbo, P., Elemento, O., Mason, C. E., and Jaffrey, S. R. (2012). Comprehensive Analysis of mRNA Methylation Reveals Enrichment in 3' UTRs and Near Stop Codons. *Cell* 149 (7), 1635–1646. doi:10.1016/j.cell.2012.05.003
- Miao, Z., Zhang, T., Xie, B., Qi, Y., and Ma, C. (2021). Evolutionary Implications of the RNA N⁶-Methyladenosine Methylome in Plants. *Mol. Biol. Evol.* 2021, msab299. doi:10.1093/molbev/msab299
- Ng, R. K., and Gurdon, J. B. (2008). Epigenetic Inheritance of Cell Differentiation Status. *Cell Cycle* 7 (9), 1173–1177. doi:10.4161/cc.7.9.5791
- Nilsen, T. W. (2014). Internal mRNA Methylation Finally Finds Functions. *Science* 343 (6176), 1207–1208. doi:10.1126/science.1249340
- Niu, Y., Zhao, X., Wu, Y.-S., Li, M.-M., Wang, X.-J., and Yang, Y.-G. (2013). N⁶-methyl-adenosine (m6A) in RNA: an Old Modification with a Novel Epigenetic Function. *Genomics, Proteomics and Bioinformatics* 11 (1), 8–17. doi:10.1016/j.gpb.2012.12.002
- Ping, X.-L., Sun, B.-F., Wang, L., Xiao, W., Yang, X., Wang, W.-J., et al. (2014). Mammalian WTAP Is a Regulatory Subunit of the RNA N⁶-Methyladenosine Methyltransferase. *Cell Res* 24 (2), 177–189. doi:10.1038/cr.2014.3
- Qin, S., Mao, Y., Wang, H., Duan, Y., and Zhao, L. (2021). The Interplay between m6A Modification and Non-coding RNA in Cancer Stemness Modulation: Mechanisms, Signaling Pathways, and Clinical Implications. *Int. J. Biol. Sci.* 17 (11), 2718–2736. doi:10.7150/ijbs.60641
- Roundtree, I. A., Evans, M. E., Pan, T., and He, C. (2017). Dynamic RNA Modifications in Gene Expression Regulation. *Cell* 169 (7), 1187–1200. doi:10.1016/j.cell.2017.05.045
- Schöller, E., Weichmann, F., Treiber, T., Ringle, S., Treiber, N., Flatley, A., et al. (2018). Interactions, Localization, and Phosphorylation of the m6A Generating

- METTL3-METTL14-WTAP Complex. *Rna* 24 (4), 499–512. doi:10.1261/rna.064063.117
- Schwartz, S., Mumbach, M. R., Jovanovic, M., Wang, T., Maciag, K., Bushkin, G. G., et al. (2014). Perturbation of m6A Writers Reveals Two Distinct Classes of mRNA Methylation at Internal and 5' Sites. *Cel Rep*. 8 (1), 284–296. doi:10.1016/j.celrep.2014.05.048
- Shen, L., Shao, N.-Y., Liu, X., Maze, I., Feng, J., and Nestler, E. J. (2013). diffReps: Detecting Differential Chromatin Modification Sites from ChIP-Seq Data with Biological Replicates. *PLoS one* 8 (6), e65598. doi:10.1371/journal.pone.0065598
- Shi, H., Wei, J., and He, C. (2019). Where, when, and How: Context-dependent Functions of RNA Methylation Writers, Readers, and Erasers. *Mol. Cel*. 74 (4), 640–650. doi:10.1016/j.molcel.2019.04.025
- Song, B., Chen, K., Tang, Y., Wei, Z., Su, J., de Magalhães, J. P., et al. (2021). ConsRM: Collection and Large-Scale Prediction of the Evolutionarily Conserved RNA Methylation Sites, with Implications for the Functional Epitranscriptome. *Brief. Bioinformatics* 22 (6). doi:10.1093/bib/bbab088
- Steevens, J., Botterweck, A. A. M., Dirx, M. J. M., Van Den Brandt, P. A., and Schouten, L. J. (2009). Trends in Incidence of Oesophageal and Stomach Cancer Subtypes in Europe. *Eur. J. Gastroenterol. Hepatol*. 22 (6), 1–678. doi:10.1097/MEG.0b013e32832ca091
- Strong, V. E., Wu, A.-w., Selby, L. V., Gonen, M., Hsu, M., Song, K. Y., et al. (2015). Differences in Gastric Cancer Survival between the U.S. And China. *J. Surg. Oncol*. 112 (1), 31–37. doi:10.1002/jso.23940
- Tang, C., Klukovich, R., Peng, H., Wang, Z., Yu, T., Zhang, Y., et al. (2018). ALKBH5-dependent m6A Demethylation Controls Splicing and Stability of Long 3'-UTR mRNAs in Male Germ Cells. *Proc. Natl. Acad. Sci. USA* 115 (2), E325–E333. doi:10.1073/pnas.1717794115
- Tang, X., Liu, S., Chen, D., Zhao, Z., and Zhou, J. (2019). The Role of the Fat Mass and Obesity-associated P-rotein in the P-roliferation of P-ancratic C-ancer C-ells. *Oncol. Lett*. 17 (2), 2473–2478. doi:10.3892/ol.2018.9873
- Tang, Y., Chen, K., Song, B., Ma, J., Wu, X., Xu, Q., et al. (2021). m6A-Atlas: a Comprehensive Knowledgebase for Unraveling the N6-Methyladenosine (m6A) Epitranscriptome. *Nucleic Acids Res*. 49 (D1), D134–D143. doi:10.1093/nar/gkaa692
- Tian, L., Greenberg, S. A., Kong, S. W., Altschuler, J., Kohane, I. S., and Park, P. J. (2005). Discovering Statistically Significant Pathways in Expression Profiling Studies. *Proc. Natl. Acad. Sci*. 102 (38), 13544–13549. doi:10.1073/pnas.0506577102
- Wan, Y., Tang, K., Zhang, D., Xie, S., Zhu, X., Wang, Z., et al. (2015). Transcriptome-wide High-Throughput Deep m6A-Seq Reveals Unique Differential m6A Methylation Patterns between Three Organs in *Arabidopsis thaliana*. *Genome Biol*. 16, 272. doi:10.1186/s13059-015-0839-2
- Wang, H.-F., Kuang, M.-j., Han, S.-j., Wang, A.-b., Qiu, J., Wang, F., et al. (2020a). BMP2 Modified by the m6A Demethylation Enzyme ALKBH5 in the Ossification of the Ligamentum Flavum through the AKT Signaling Pathway. *Calcif Tissue Int*. 106 (5), 486–493. doi:10.1007/s00223-019-00654-6
- Wang, T., Kong, S., Tao, M., and Ju, S. (2020b). The Potential Role of RNA N6-Methyladenosine in Cancer Progression. *Mol. Cancer* 19 (1), 88. doi:10.1186/s12943-020-01204-7
- Wang, X., Feng, J., Xue, Y., Guan, Z., Zhang, D., Liu, Z., et al. (2016). Structural Basis of N6-Adenosine Methylation by the METTL3-METTL14 Complex. *Nature* 534 (7608), 575–578. doi:10.1038/nature18298
- Wang, X., Lu, Z., Gomez, A., Hon, G. C., Yue, Y., Han, D., et al. (2014a). N6-methyladenosine-dependent Regulation of Messenger RNA Stability. *Nature* 505 (7481), 117–120. doi:10.1038/nature12730
- Wang, Y., Li, Y., Toth, J. I., Petroski, M. D., Zhang, Z., and Zhao, J. C. (2014b). N6-methyladenosine Modification Destabilizes Developmental Regulators in Embryonic Stem Cells. *Nat. Cel Biol* 16 (2), 191–198. doi:10.1038/ncb2902
- Wang, Y., Zheng, Y., Guo, D., Zhang, X., Guo, S., Hui, T., et al. (2019). m6A Methylation Analysis of Differentially Expressed Genes in Skin Tissues of Coarse and Fine Type Liaoning Cashmere Goats. *Front. Genet*. 10, 1318. doi:10.3389/fgene.2019.01318
- Wei, C.-M., and Moss, B. (1977). Nucleotide Sequences at the N6-Methyladenosine Sites of HeLa Cell Messenger Ribonucleic Acid. *Biochemistry* 16 (8), 1672–1676. doi:10.1021/bi00627a023
- Wen, J., Lv, R., Ma, H., Shen, H., He, C., Wang, J., et al. (2018). Zc3h13 Regulates Nuclear RNA m6A Methylation and Mouse Embryonic Stem Cell Self-Renewal. *Mol. Cel*. 69 (6), 1028–1038. doi:10.1016/j.molcel.2018.02.015
- Wu, R., Li, A., Sun, B., Sun, J.-G., Zhang, J., Zhang, T., et al. (2019). A Novel m6A Reader Prcc2a Controls Oligodendroglial Specification and Myelination. *Cel Res* 29 (1), 23–41. doi:10.1038/s41422-018-0113-8
- Yamashita, H., Seto, Y., Seto, Y., Sano, T., Makuuchi, H., Ando, N., et al. (2017). Results of a Nation-wide Retrospective Study of Lymphadenectomy for Esophagogastric junction Carcinoma. *Gastric Cancer* 20 (Suppl. 1), 69–83. doi:10.1007/s10120-016-0663-8
- Zhang, J., Guo, S., Piao, H.-y., Wang, Y., Wu, Y., Meng, X.-y., et al. (2019a). ALKBH5 Promotes Invasion and Metastasis of Gastric Cancer by Decreasing Methylation of the lncRNA NEAT1. *J. Physiol. Biochem*. 75 (3), 379–389. doi:10.1007/s13105-019-00690-8
- Zhang, S., Orita, H., and Fukunaga, T. (2019b). Current Surgical Treatment of Esophagogastric junction Adenocarcinoma. *World J. Gastrointest Oncol*. 11 (8), 567–578. doi:10.4251/wjgo.v11.i8.567
- Zhang, W., He, L., Liu, Z., Ren, X., Qi, L., Wan, L., et al. (2020). Multifaceted Functions and Novel Insight into the Regulatory Role of RNA N6-Methyladenosine Modification in Musculoskeletal Disorders. *Front. Cel Dev. Biol*. 8, 870. doi:10.3389/fcell.2020.00870
- Zhang, X., Lu, N., Wang, L., Wang, Y., Li, M., Zhou, Y., et al. (2021). Recent Advances of m6A Methylation Modification in Esophageal Squamous Cell Carcinoma. *Cancer Cel Int* 21 (1), 421. doi:10.1186/s12935-021-02132-2
- Zhang, Y., Liu, T., Meyer, C. A., Eeckhoutte, J., Johnson, D. S., Bernstein, B. E., et al. (2008). Model-based Analysis of ChIP-Seq (MACS). *Genome Biol*. 9 (9), R137. doi:10.1186/gb-2008-9-9-r137
- Zhang, Y., Wang, X., Zhang, X., Wang, J., Ma, Y., Zhang, L., et al. (2019c). RNA-binding Protein YTHDF3 Suppresses Interferon-dependent Antiviral Responses by Promoting FOXO3 Translation. *Proc. Natl. Acad. Sci. USA* 116 (3), 976–981. doi:10.1073/pnas.1812536116
- Zhao, B. S., Roundtree, I. A., and He, C. (2017). Post-transcriptional Gene Regulation by mRNA Modifications. *Nat. Rev. Mol. Cel Biol* 18 (1), 31–42. doi:10.1038/nrm.2016.132
- Zhao, X., Yang, Y., Sun, B.-F., Zhao, Y.-L., and Yang, Y.-G. (2014). FTO and Obesity: Mechanisms of Association. *Curr. Diab Rep*. 14 (5), 486. doi:10.1007/s11892-014-0486-0
- Zheng, G., Dahl, J. A., Niu, Y., Fedorcsak, P., Huang, C.-M., Li, C. J., et al. (2013). ALKBH5 Is a Mammalian RNA Demethylase that Impacts RNA Metabolism and Mouse Fertility. *Mol. Cel*. 49 (1), 18–29. doi:10.1016/j.molcel.2012.10.015
- Zheng, W., Dong, X., Zhao, Y., Wang, S., Jiang, H., Zhang, M., et al. (2019). Multiple Functions and Mechanisms Underlying the Role of METTL3 in Human Cancers. *Front. Oncol*. 9, 1403. doi:10.3389/fonc.2019.01403
- Zhou, Y., Yin, Z., Hou, B., Yu, M., Chen, R., Jin, H., et al. (2019). Expression Profiles and Prognostic Significance of RNA N6-Methyladenosine-Related Genes in Patients with Hepatocellular Carcinoma: Evidence from Independent Datasets. *Cancer Manag. Res*. 11, 3921–3931. doi:10.2147/CMAR.S191565

Conflict of Interest: The authors declare that the research was conducted in the absence of any commercial or financial relationships that could be construed as a potential conflict of interest.

Publisher's Note: All claims expressed in this article are solely those of the authors and do not necessarily represent those of their affiliated organizations, or those of the publisher, the editors, and the reviewers. Any product that may be evaluated in this article, or claim that may be made by its manufacturer, is not guaranteed or endorsed by the publisher.

Copyright © 2022 Huang, Hu, He, He, Zou, Man and Fan. This is an open-access article distributed under the terms of the Creative Commons Attribution License (CC BY). The use, distribution or reproduction in other forums is permitted, provided the original author(s) and the copyright owner(s) are credited and that the original publication in this journal is cited, in accordance with accepted academic practice. No use, distribution or reproduction is permitted which does not comply with these terms.



Global Landscape of m6A Methylation of Differently Expressed Genes in Muscle Tissue of Liaoyu White Cattle and Simmental Cattle

Yunlong Dang^{1,2†}, Qiao Dong^{1,2†}, Bowei Wu^{1,2}, Shuhua Yang^{1,2}, Jiaming Sun^{1,2}, Gengyuan Cui^{1,2}, Weixiang Xu^{1,2}, Meiling Zhao^{1,2}, Yunxuan Zhang^{1,2}, Peng Li^{1,2*} and Lin Li^{1,2*}

¹College of Animal Science and Veterinary Medicine, Shenyang Agricultural University, Shenyang, China, ²Key Laboratory of Ruminant Infectious Disease Prevention and Control (East), Ministry of Agriculture and Rural Affairs, Beijing, China

OPEN ACCESS

Edited by:

Krzysztof Flisikowski,
Technical University of Munich,
Germany

Reviewed by:

Haojie Zhang,
Guangxi University, China
Jiangbo Wei,
University of Chicago, United States

*Correspondence:

Peng Li
Lipeng2018@syau.edu.cn
Lin Li
Lilin619619@syau.edu.cn

[†]These authors have contributed
equally to this work

Specialty section:

This article was submitted to
Epigenomics and Epigenetics,
a section of the journal
Frontiers in Cell and Developmental
Biology

Received: 21 December 2021

Accepted: 22 February 2022

Published: 10 March 2022

Citation:

Dang Y, Dong Q, Wu B, Yang S, Sun J,
Cui G, Xu W, Zhao M, Zhang Y, Li P
and Li L (2022) Global Landscape of
m6A Methylation of Differently
Expressed Genes in Muscle Tissue of
Liaoyu White Cattle and
Simmental Cattle.
Front. Cell Dev. Biol. 10:840513.
doi: 10.3389/fcell.2022.840513

Liaoyu white cattle (LYWC) is a local breed in Liaoning Province, China. It has the advantages of grow quickly, high slaughter rate, high meat quality and strong anti-stress ability. N⁶ methyladenosine (m6A) is a methylation modification of N⁶ position of RNA adenine, which is an important modification mechanism affecting physiological phenomena. In this study, we used the longissimus dorsi muscle of LYWC and SIMC for m6A-seq and RNA-seq high-throughput sequencing, and identified the key genes involved in muscle growth and m6A modification development by bioinformatics analysis. There were 31532 m6A peaks in the whole genome of LYWC and 47217 m6A peaks in the whole genome of SIMC. Compared with Simmental cattle group, LYWC group had 17,351 differentially expressed genes: 10,697 genes were up-regulated, 6,654 genes were down regulated, 620 differentially expressed genes were significant, while 16,731 differentially expressed genes were not significant. Among the 620 significantly differentially expressed genes, 295 genes were up-regulated and 325 genes were down regulated. In order to explore the relationship between m6A and mRNA expression in the muscles of LYWC and SIMC, the combined analysis of MeRIP-seq and RNA-seq revealed that 316 genes were m6A modified with mRNA expression. To identify differentially methylated genes related to muscle growth, four related genes were selected for quantitative verification in LYWC and SIMC. GO enrichment and KEGG analysis showed that the differentially expressed genes modified by m6A are mainly involved in skeletal muscle contraction, steroid biosynthesis process, redox process, PPAR pathway and fatty acid metabolism, and galactose metabolism. These results provide a theoretical basis for further research on the role of m6A in muscle growth and development.

Keywords: m6A methylation, RNA-seq, muscle growth and development, genetic modification, species

INTRODUCTION

To date, more than 150 types of posttranscriptional modifications have been identified in the RNA of all living organisms (Boccalletto et al., 2018). The N⁶-methyladenosine (m6A) modification was discovered in the 1970s and was originally considered to be an abundant nucleotide modification of mRNA in eukaryotic cells (Jia et al., 2013; Yue et al., 2015). Biological functions of m6A modification are mediated

by special binding proteins, including methyltransferases, demethylases, and effectors (Zhang et al., 2019). It is involved in various biological processes, such as lipid production and energy metabolism (Zhao et al., 2014; Wang et al., 2015a). In addition, m6A methylation regulates the splicing, expression, decay and translation of mRNA (Wang et al., 2014; Wang et al., 2015b; Xiao et al., 2016). Until recently, little was known about the specific function and mechanism of m6A. Similar to DNA and histone methylation, m6A methylation is also dynamic and reversible in mammals (Wang et al., 2019). It is modulated by several genes, including methyltransferases (METTL3, METTL4 and WTAP) (Liu et al., 2014; Ping et al., 2014), demethylases (ALKBH5 and FTO), (Jia et al., 2011; Zheng et al., 2013) and reading proteins (YTHDF, eIF3 and HNRNPC) (Cao et al., 2016). m6A modification is co installed by a variety of protein complexes (Roundtree et al., 2017). For example, YTHDF2 binds to m6A in mRNA to degrade target genes, while YTHDF1, YTHDF3 and eIF3 promote the translation of m6A containing transcripts (Wang et al., 2014; Wang et al., 2015a; Meyer et al., 2015). As the transferase of writers, METTL3 is composed of catalytic subunit and many other auxiliary subunits. This protein is very important for embryonic growth and development. Embryos lacking METTL3 show pluripotent degradation and damage (Geula et al., 2015). The distribution of mettl3 varies with the type of cell line. In some cases, the change of cell state will lead to the change of its distribution (Knuckles et al., 2017; Xiang et al., 2017). In the cytoplasm, METTL3 itself recognizes the 3'UTR m6A site on mRNA and promotes the formation of translation loop through the interaction with eif3h, so as to promote the protein translation of transcripts (Shi et al., 2019). METTL3 can be functionally regulated by PTM or its protein interaction. It is reported that METTL14 in human cells is phosphorylated at the residue serine399 site on the protein interface with METTL3, indicating that mettl3 has a regulatory function (Wang et al., 2016; Shi et al., 2019). m6A readers protein contains two kinds: one is a stable and direct protein containing YT521-B homology (YTH) domain, and the other is the common RNA binding domain (RBD) (Shi et al., 2019). Both the YTH domain family 1–3 (YTHDF1–3) and the YTH domain containing 1–2 (YTHDC1–2) in humans are stable and directly exercise the reading function of m6A. YTHDF1 and YTHDF3 translation initiation factors promote the translation of target transcripts in cells, and YTHDC2 mediates mRNA stability and translation and regulates cell development (Hsu et al., 2017). The other uses the common RNA binding domain (RBD), such as K homology (KH) domain, RNA recognition motif (RRM) domain and arginine/glycine rich (RGG) domain to preferentially bind the m6A containing region in RNA and exercise the function of m6A reader by regulating the surrounding RNA protein interaction (Shi et al., 2019). Most studies on m6A modification have focused on humans and mice (Dominissini et al., 2012). The m6A methylation is related to obesity (Wang et al., 2020). FTO was the first m6A mRNA demethylase that was discovered. It mediates DNA and RNA demethylation (Jia et al., 2011). The m6A demethylase FTO plays a key role in regulating postpartum growth and energy consumption. A study reported that AMPK regulates lipid accumulation in skeletal muscle cells by regulating FTO expression and FTO-dependent demethylation of m6A (Wu et al., 2017). Research reports on mouse animal models

TABLE 1 | The primer list.

Gene name	Primer
MYH6-F	5'-ACCCCTACGACTACGCCTTC-3'
MYH6-R	5'-GTCAGCTTGTAGACACCGGC-3'
MYOM2-F	5'-CCGTCCTTCCCAACCCTTAT-3'
MYOM2-R	5'-GCTTGTCGACGTAGTAGCCG-3'
ACTB-F	5'-CTCTTCCAGCCTTCCTTCT-3'
ACTB-R	5'-GGGCAGTGATCTCTTCTGTC-3'
XIRP1-F	5'-CAAACAAGAGGAACCGACAGA-3'
XIRP1-R	5'-GGCATTGGCCATCCTTCT-3'
TNNT1-F	5'-AGAAGTCCGGAAGGGGG-3'
TNNT1-R	5'-ACACGCCAAGGACTCCCA-3'

have shown that FTO plays an important role in the regulation of fat mass, adipogenesis, and body weight (Church et al., 2009; Fischer et al., 2009; Church et al., 2010; Gao et al., 2010; McMurray et al., 2013; Merkestein et al., 2015; Ronkainen et al., 2016).

LYWC are excellent beef cattle based on Charolais, breeding the fourth-generation hybrid herd with Liaoning local cattle as the female parent in Liaoning Province, China. A stable population with 93.75% Charolais pedigree and 6.25% local cattle pedigree was formed. LYWC grow quickly, and the slaughter rate was also higher than that of other beef cattle breeds. Due to the large market demand for beef in China, most farms choose LYWC for its excellent production performance. LYWC has wide adaptability, strong stress resistance, and outstanding cold resistance ability and can withstand a low-temperature environment of -30°C . Although LYWC has a better growth rate and slaughter rate, its rough myofiber always influences beef quality directly compared to Simmental and other beef cattle (Jing et al., 2011; Shuangyong et al., 2011). A large number studies have shown that m6A modification plays an important role in regulating lipid production and energy metabolism, inflammatory mechanisms and tumor formation. Based on the necessary functions of m6A modification in regulating gene expression and involving various biological processes, we speculate that m6A modification is involved in beef cattle muscle growth and development. In this study, we aimed to explore the global landscape of differentially expressed m6A methylation genes in muscle tissue between LYWC and SIMC and provide a theoretical basis for further research on the specific regulatory mechanism of unique meat quality and the optimization and selection of LYWC breeds. However, the effect, mechanism, and function of m6A modification on muscle growth and development still needs further research in the future.

MATERIAL AND METHOD

Sample Collection and Ethics Statement

Three healthy male Liaoyu white cattles and three Simmental cattles were selected for this study and provided the same feed and drinking water during the breeding period. The breeding environment conditions were identical. The average birth

TABLE 2 | Summary of reads quality control.

Sample_	Raw_Reads	Valid_Reads	Valid%	Q20%	Q30%	GC%
LYWC1_IP	75018648	69503364	71.85	98.71	96.25	58.98
LYWC2_IP	63985000	58996716	71.45	98.64	96.03	59.02
LYWC3_IP	73353244	69624344	73.96	98.81	96.37	57.88
SIM1_IP	34991588	32396532	90.24	98.30	95.29	57.62
SIM2_IP	42841030	40364782	91.73	97.87	94.15	58.51
SIM3_IP	50385720	49785152	96.68	98.20	94.82	57.03
LYWC1_input	53535846	52583702	96.52	97.43	92.96	57.89
LYWC2_input	73285174	71862022	96.42	97.35	92.81	57.35
LYWC3_input	42315990	41541788	96.24	97.40	92.95	56.52
SIM1_input	70936986	68695324	89.09	98.18	94.97	58.41
SIM2_input	96166358	95102418	98.52	98.11	94.57	56.15
SIM3_input	66577584	64093630	90.23	97.98	94.45	57.91

TABLE 3 | Summary of reads mapped to the cattle reference genome.

Sample	Valid reads	Mapped reads	Unique mapped reads	Multi mapped reads
LYWC1_IP	69503364	65423613 (94.13%)	53565538 (77.07%)	11858075 (17.06%)
LYWC2_IP	58996716	55968831 (94.87%)	46290788 (78.46%)	9678043 (16.40%)
LYWC3_IP	69624344	66284434 (95.20%)	53585255 (76.96%)	12699179 (18.24%)
LYWC1_input	52583702	50979857 (96.95%)	32727624 (62.24%)	18252233 (34.71%)
LYWC2_input	71862022	69628680 (96.89%)	44600306 (62.06%)	25028374 (34.83%)
LYWC3_input	41541788	40229546 (96.84%)	26453120 (63.68%)	13776426 (33.16%)
SIM1_IP	32396532	30103081 (92.92%)	24045688 (74.22%)	6057393 (18.70%)
SIM2_IP	40364782	36721102 (90.97%)	29120560 (72.14%)	7600542 (18.83%)
SIM3_IP	49785152	45949312 (92.30%)	34638134 (69.58%)	11311178 (22.72%)
SIM1_input	68695324	65225662 (94.95%)	53655224 (78.11%)	11570438 (16.84%)
SIM2_input	95102418	93001053 (97.79%)	63683053 (66.96%)	29318000 (30.83%)
SIM3_input	64093630	60045990 (93.68%)	47919015 (74.76%)	12126975 (18.92%)

weight of LYWC is 40.0 ± 2.0 kg, the average weight at 6 months is 218 ± 5.0 kg, the average weight at 12 months is 366.8 ± 5.0 kg, and the average weight at 24 months is 624.5 ± 5.0 kg. SIMC have an average birth weight of 41 ± 2.0 kg, an average weight of 200 ± 5.0 kg at 6 months, an average weight of 324 ± 5.0 kg at 12 months, and an average weight of 600 ± 5.0 kg at 24 months. They were raised from birth and slaughtered after 24 months.

The longissimus dorsi muscle samples of two breeds of beef cattle were collected after slaughter. A 1 cm^3 muscle sample was taken from the inner side of the spine near the shoulder area. After that, muscle samples were immediately stored in liquid nitrogen. All experimental procedures were approved and performed according to the guidelines of the Laboratory Animal Management Committee of Shenyang Agricultural University.

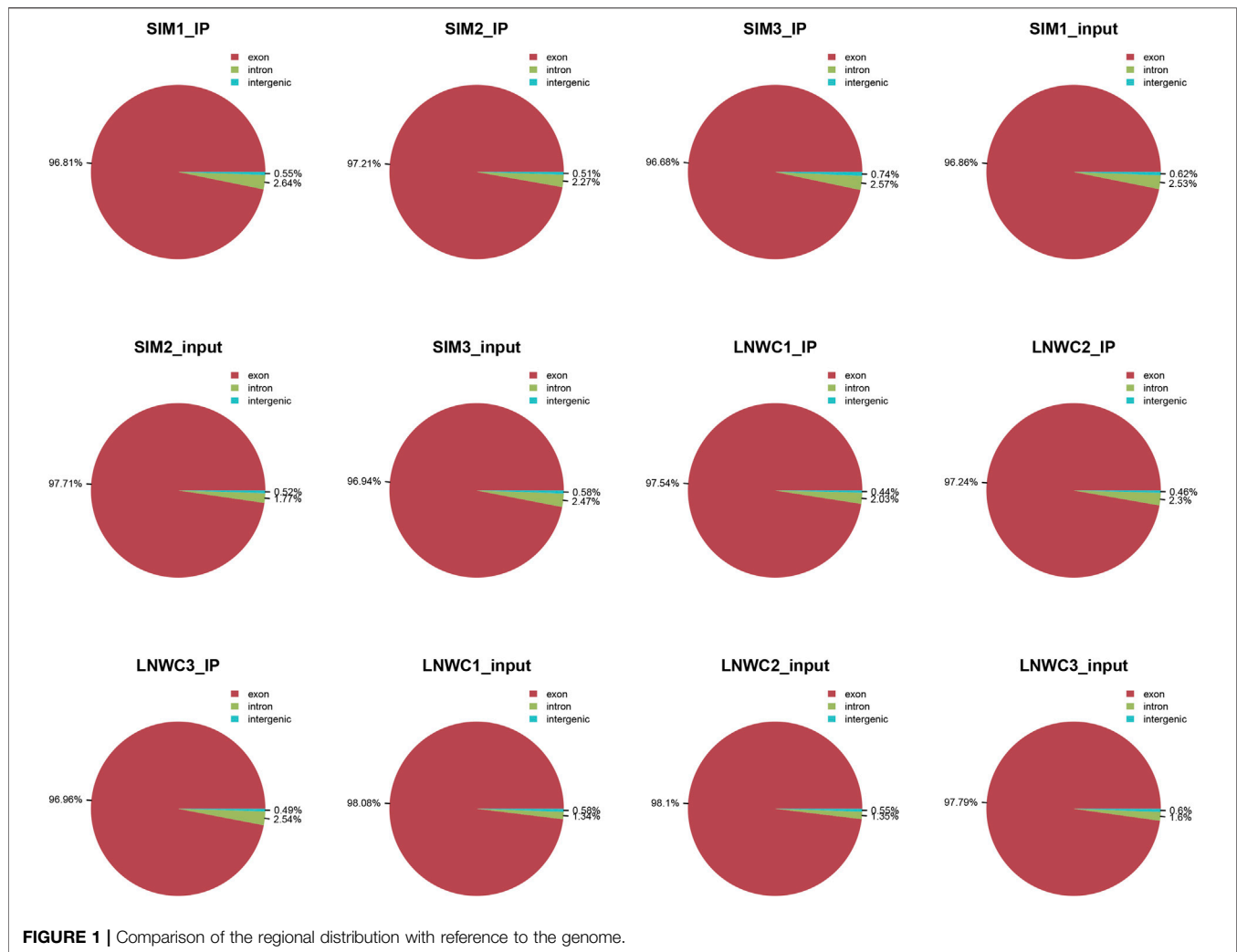
Experimental Procedure

Total RNA was extracted using TRIzol reagent (Invitrogen, CA, United States). The quality and quantity of total RNA were analyzed by Bioanalyzer 2100 and RNA 6000 Nano Labchip kits (Angelon, CA, United States) with value of RIN >7.0 . Oligo-dT magnetic beads were used to enrich total RNA with poly(A) mRNA. Approximately $200 \mu\text{g}$ of total RNA was subjected to isolation of poly(A) mRNA with poly-T oligo-attached magnetic beads (Invitrogen). The lysed RNA fragments were then incubated with m6A-specific antibodies (No. 202003, Synaptic Systems, Germany) in IP

buffer (50 mM Tris-HCl, 750 mM NaCl and 0.5% Igepal CA-630) at 4°C for 2 h with BSA ($0.5 \mu\text{g}/\mu\text{l}$) (1 ml). The mixture was then incubated with protein A beads and eluted with elution buffer ($1\times\text{IP}$ buffer and 6.7 mM m6A). The eluted RNA was precipitated with 75% ethanol. According to the chain-specific library prepared by the dUTP method, the eluted m6A fragment (IP) and the unprocessed input control fragment were converted into the final cDNA library. The average insert size of the paired-end library was 100 ± 50 bp. We performed paired-end 2×150 bp sequencing on the Illumina NovaSeq™ 6000 platform of LC-BIO Biotech Ltd. (Hangzhou, China) according to the protocol recommended by the supplier.

Bioinformatics Analysis Process

First, Cutadapt and local Perl scripts were used to process the data obtained from sequencing to remove low-quality sequences, contaminated sequences, and linker sequences generated by the sequencer to obtain CleanData (Martin, 2011). Fastp (v0.12.6, data quality control doi: 10.1093/bioinformatics/btp616) was used to verify sequence quality, and HISAT2(v2.0.4, alignment reference sequence: doi: 10.1038/nmeth.3317) was used to map the read data to the *Bos taurus* genome of cattle with default parameters (*Bos taurus*_NCBI genome version NA) (USDA ARS) (Kim et al., 2015). The threshold settings of differential peak and differential expression are generally $|\log_2\text{Fc}| \geq 1$ and $P\text{-val} < 0.05$. At the same time, qval/fdr is corrected for P-val. Exome Peak



(v2.13.2, call peak and diff peak: doi: 10.1093/bioinformatics/btt171) read the IP and input data obtained in the experiment (Meng et al., 2014). This program uses bed or bam format files to identify the m6A peak and visualize it in the UCSC genome browser or with IGV software (<http://www.igv.org>). MEME and HOMER were used to discover known motifs and locate the peak of the obtained motifs using a Perl script (diff_peak | $\log_2\text{FC} \geq 1$, $p\text{-value} < 0.05$; call peak $\log_2\text{FC} \geq 1$, $p\text{-value} < 0.05$) (Bailey et al., 2009; Heinz et al., 2010). ChIPseeker analyzes the scanned peak calling and annotates the peak genes (Yu et al., 2015). Then, StringTie (v1.3.4d, assembly quantity: doi: 10.1038/NBT. 3122) was used to perform expression operations on all mRNA in the input database to calculate FPKM ($\text{FPKM} = [\text{total exon fragments}/\text{mapped exon readings (million)} \times \text{exon length (kB)}])$ (Pertea et al., 2015). Using the R language package edgeR (v3.20.9, difference analysis: doi: 10.1093/bioinformatics/btp616), differentially expressed mRNAs with \log_2 (fold change) > 1 or \log_2 (fold change) < -1 and $p\text{-value} < 0.05$ were selected, the reference genome was ARS-UCD1.2 (https://ftp.ncbi.nlm.nih.gov/genomes/all/GCF/002/263/795/GCF_002263795.1_ARS-UCD1.2/) (Robinson et al.

, 2010). The edgeR input file was raw counts, and we used edgeR to analyze the PVAL and qval of the results, calculate fpkm values to measure the expression levels of genes, and compare the fold difference obtained by means of fpkm expression compared to the fold change. Functional enrichment we mapped differential gene functional annotations into different GO term/KEGG pathways by writing our own script, embodying the difference test as a hypergeometric test. The integration of MeRIP-seq and RNA-seq data is related through the annotation of peak, and the qualitative correlation is determined through the up/down of the two parts of regulation. Because exomepeak cannot output the quantification of peak level, it cannot calculate the correlation with the expression.

Real-Time Fluorescence Quantitative PCR

We tested four different genes with m6A methylation modification for qRT-PCR analysis, they are related to muscle growth and development (Kee and Hardeman, 2008; Otten et al., 2012; Flix et al., 2013; Siddique et al., 2016). We validated the methylation-modified differential genes and used

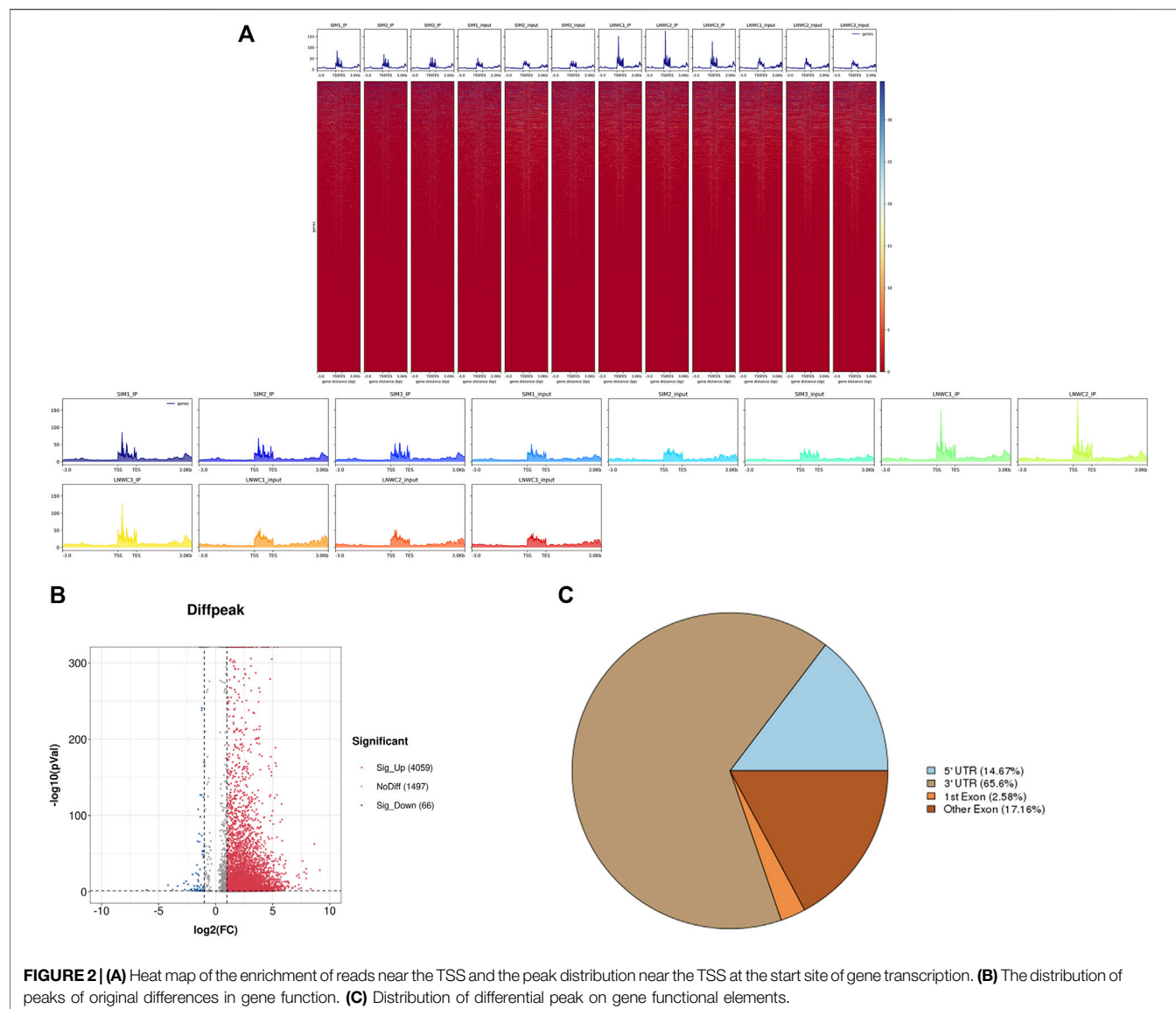


FIGURE 2 | (A) Heat map of the enrichment of reads near the TSS and the peak distribution near the TSS at the start site of gene transcription. **(B)** The distribution of peaks of original differences in gene function. **(C)** Distribution of differential peak on gene functional elements.

a qRT-PCR kit (Takara, Dalian, China) to reverse-transcribe the total RNA extracted from the muscle into cDNA. SYBR Green (Vazyme-Q711, China) was used to perform real-time fluorescent quantitative PCR according to the instructions. The ACTB gene was used as an internal reference gene to standardize the expression level of genes. Three trials were performed on three LYWC and three SIM muscle samples. Primer 5 was used to design four pairs of primers, the primer list is shown in **Table 1**. All primers span the end of the gene. The relative expression of differentially expressed genes was calculated by the $2^{-\Delta\Delta C_t}$ method. The data are expressed as the mean \pm standard error (sample number $n = 3$). The t -test in SPSS statistical software (version 22.0, Chicago, IL, United States) was used to perform the statistical analyses in the two groups, and the difference was significant when $p < 0.05$.

RESULTS AND ANALYSIS

Sequence Statistics and Quality Control

First, the raw data generated by sequencing needed to be preprocessed. Cutadapt filtered out unqualified sequences and removed reads with an adaptor, low quality, and unsure base information. The original sequencing volume, effective sequencing volume, Q20, Q30, and GC content were counted, and appropriate evaluation was conducted. Effective data (Clean Data) was prepared for analysis. In the MeRIP-seq library, we obtained two sets of muscle sample data reads. Three biological replicates were performed in each group, and the effective reading data were as follows: LYWC group: 75018648, 63985000 and 73353244; SIM group: 34991588, 42841030 and 50385720. The percentages of valid data (Clean Data) in the two

TABLE 4 | The top 20 differentially expressed m6A peaks.

Gene name	Fold change	Regulation	Chromosome	Peak region	Peak start	Peak end	p-value
GLUL	560.28	Up	16	5' UTR	63478467	63478646	9.99E-288
LOC112445778	398.93	Up	Un	Exon	987	1142	1.6E-82
BRICD5	321.80	Up	25	3' UTR	1740015	1740254	1E-221
WASF2	245.57	Up	2	Exon	125880669	125880759	0.000000000025
SNRPA	243.88	Up	18	3' UTR	50032385	50032564	0.0000000000000001
PTGDS	242.19	Up	11	3' UTR	106024413	106024969	1.6E-87
COPZ1	215.27	Up	5	5' UTR	25742023	25742113	3.2E-32
JSP.1	195.36	Up	23	Exon	28666476	28666821	1E-24
PPP1R3B	179.77	Up	27	5' UTR	25190141	25190261	0.00059
PAFAH1B1	160.90	Up	19	5' UTR	23512920	23513159	6.3E-27
TYW5	0.02	Down	2	3' UTR	88497265	88497444	0.000026
TACC1	0.06	Down	27	Exon	33995126	33998354	0.00000046
MTSS1	0.07	Down	14	Exon	15550578	15550728	0.00000023
MAML1	0.10	Down	7	Exon	1553848	1553937	0.000087
ARHGAP21	0.15	Down	13	Exon	25465042	25465341	0.0000000000000032
RTF1	0.15	Down	18	Exon	36887325	36887415	0.0000074
ATXN1L	0.17	Down	18	Exon	39240553	39240912	0.0000000000000005
ANKRD11	0.19	Down	18	Exon	14335439	14335618	0.000000013
EVI5L	0.22	Down	7	5' UTR	16608242	16608302	0.000000000002
MASP1	0.22	Down	1	3' UTR	80048359	80048508	0.0000000087

groups of data were 71.85, 71.45, and 73.96% in the LYWC group and 90.24, 91.73, and 96.68% in the SIM group, respectively. In the RNA-seq library, we obtained two sets of muscle sample data reads, each of which was subjected to three biological replicates: the effective read data were as follows: LYWC group: 53535846, 73285174, and 42315990; SIM group: 70936986, 96166358 and 66577584. The percentages of valid data in the two groups of data were 96.52, 96.42, and 96.24% in the LYWC group and 89.09, 98.52, and 90.23% in the SIM group, respectively (**Table 2**). In **Table 2**, the proportion of Q20% bases with a quality value ≥ 20 (sequencing error rate is less than 0.01) and the proportion of Q30% bases with a quality value ≥ 30 (the sequencing error rate is less than 0.001) are shown.

Map Data to Genome

We used HISAT2 for reference genome comparison of the preprocessed valid data and mapped reads to the *Bos taurus* cattle (*Bos taurus*_NCBI, version NA) genome with default parameters. By comparing the obtained reads with the reference genome sequence, we can perform detailed statistics on the data obtained by sequencing and its distribution in the genome. In the m6A-seq library, the IP samples of the longissimus dorsi muscle of beef cattle are LYWC_IP and SIM_IP, and we performed three replicates for each set of samples. The LYWC_IP effective data mapping read rates were 94.13, 94.87, and 95.20%; the SIM_IP effective data mapping read rates were 92.92, 90.97, and 92.30%. In the RNA-seq library, the longissimus dorsi samples of beef cattle are LYWC_input and SIM_input, and we performed three replicates for each set of samples. The effective data mapping read rates of LYWC_input are 96.95, 96.89, and 96.84%, respectively; the effective data mapping read rates of SIM_input are 94.95, 97.79, and 93.68%, respectively. Unique mapped reads are shown in **Table 3**. According to the regional

distribution information of the reference genome, it can be defined as alignment to three parts of exon (exon), intron (intron) and intergenic (intergenic region). In general, the percentage of the sequence alignment to the exon region should be the highest. The results of this experiment showed that the IP samples of Liaoyu white cattle accounted for 97.54, 97.24 and 96.96% in the exon region; the ratios of the input samples were 98.08, 98.10 and 97.79%, respectively. The IP samples of Simmental cattle accounted for 96.81, 97.21 and 96.68% in the exon region; the ratios of the input samples were 96.86, 97.71 and 96.94%, and the results are shown in **Figure 1**.

Identification of m6A Modification Sites and Analysis of Differentially Methylated Genes

Use peak-calling software, the R language toolkit exomePeak, was used to scan the m6A peak in the entire genetic dataset. Based on the identification of the IP and input libraries, biological information such as the position and length of the peak in the gene can be obtained. The call peak portion we choose $P\text{-val} < 0.05$, and the diff peak and diff expression portions generally choose $|\log_2 \text{fc}| \geq 1$ and $P\text{-val} < 0.05$. We counted and combined all the samples and the degree of enrichment of the reads near the gene transcription start site (TSS). The peaks that could be combined near the TSS are represented in the form of a heat map, as shown in **Figure 2A**. ChIP seeker software was used to annotate the different peaks and perform GO and KEGG enrichment analyses. In general, the default $p < 0.05$ was the filter condition of the peak. Compared with Simmental cattle group, we screened 5631 difference peaks in Liaoyu white cattle group, of which 4,059 m6A peaks were significantly up-regulated and 66 m6A peaks were significantly down regulated, as shown in **Figure 2B**. The distribution of m6A










Rank	Motif	p-value
1		1e-158
2		1e-20
3		1e-19
4		1e-18
5		1e-16
6		1e-15
7		1e-14
8		1e-13
9 *		1e-11

FIGURE 3 | Sequence showing the motifs with significant differences in muscle samples at the m6A peak.

peak in transcripts was analyzed. Analysis of the distribution of m6Apeak in the transcript was performed. We divided the transcript into four parts: 5'-UTR, 3'-UTR, first exon and other exons. It was used to analyze the distribution of different peaks in the original gene function, as shown in **Figure 2C**. As shown in **Table 4**, the m6A modification was

mainly enriched in the 3'-UTR, and we report the top 20 differences m6Apeak. Difference factor <1 indicates hypomethylation, and difference factor >1 indicates hypermethylation.

Motif Analysis

As a dynamic modification phenomenon, RNA methylation is mainly accomplished by the combined action of multiple methylases and methylation binding site motifs. A motif is a nucleotide sequence pattern with biological significance, and the sequence has a high degree of conservation. The methylases involved in the process of RNA methylation recognize the motifs in the gene to generate methylation and regulate gene expression. The motif software MEME was used to search for more credible motifs in the peak area and obtain information about the width, E-value, and location of each motif. We performed motif prediction on each set of samples, and the results are shown in **Figure 3**. A motif structure that is reported commonly in RNA modifications are RRACH (where R = A or G, H = A, C or U).

Whole Gene Analysis and Differential Gene Analysis

The expression level of genes is mainly measured by RPKM (reads per kilobase of exon model per million mapped reads) or FPKM (fragments per kilobase of exon model per million mapped reads) to measure the abundance value of gene expression. In our research, we chose FPKM to report the expression abundance values of different samples of known genes. Compared with Simmental cattle, Liao yu white cattle detected 17,351 differentially expressed genes, 620 genes were significantly different and 16,731 genes were not significantly different ($|\log_2fc| \geq 1$ and $p < 0.05$). Among the differentially expressed genes, 10,697 genes were upregulated and 6,654 genes were downregulated. Among the 620 significantly differentially expressed genes, 295 were up-regulated and 325 were down regulated. **Table 5** shows the top 20 differentially expressed genes we screened. Among the top 20 differentially expressed genes, there are 10 up-regulated genes and 10 down-regulated genes. We used **Figures 4A,B** to show the gene expression and expression density. We plotted the overall distribution statistics of differentially expressed genes, as shown in **Figure 4C**. **Figure 4D** shows the gene heat map between LYWC and SIM samples.

Joint Analysis of Differentially Expressed Genes and Differentially Expressed Genes

In the entire transcriptome sequencing, we found that there were upregulated and downregulated genes. In the MeRIP-seq sequencing results, according to the changes in abundance, we found that the methylation of the gene itself was upregulated and downregulated. Therefore, we combined the correlation analysis of the two sequencing results to compare and analyze the transcription level and methylation level. In the

TABLE 5 | The top 20 differentially expressed genes.

Gene name	Fold change	Regulation	Locus	Strand	p-value
ZIC4	408.70	Up	Chr1:120900467-120920588	+	0.0000893270205096843
ZIC1	154.75	Up	Chr1:120896651-120900435	–	6.48985151731775E–07
KCNQ2	121.11	Up	Chr24:614160-636366	–	0.00333415305292261
HOXC5	100.57	Up	Chr5:25998379-25999826	–	0.0000215125233082445
LOC101905242	96.40	Up	Chr1:42016839-42017535	+	2.6240518996526E–08
LOC104972118	65.46	Up	Chr4:70745406-70752937	–	0.00252204598175991
HOXC4	53.97	Up	Chr5:25977635-25994974	–	0.00209569391674476
EMX2	53.11	Up	Chr26:37830529-37837034	+	0.0144795011020604
ABI2	51.26	Up	Chr2:91544895-91646688	+	0.0142005975927657
COL23A1	50.83	Up	Chr7:39317415-39719111	–	0.00151425556715255
LOC112445780	0.0019054052765261	Down	Chr1:1379-3188	–	8.00798384058217E–11
PITX1	0.00192374812736059	Down	Chr7:46474414-46480622	–	2.15915187958383E–21
LOC112445782	0.00526541615536884	Down	Chr1:37307-41037	–	8.49182655839351E–08
HOXC10	0.00878243398141918	Down	Chr5:26042721-26047450	–	7.56247125923241E–25
COL22A1	0.0106909776847475	Down	Chr14:4095051-4319199	+	0.00608209941205491
LOC101905017	0.013655843197307	Down	Chr11:100029843-100030458	–	0.0111876548271218
COMP	0.0150500815850192	Down	Chr7:4422721-4430541	+	0.00230163465282101
BOLA	0.0199056647166198	Down	Chr23:27943375-27950488	+	0.000265837339817353
LYL1	0.0201706382454435	Down	Chr7:12473687-12479882	+	0.000260783474606451
OTUD1	0.0208958121373525	Down	Chr13:24387754-24390638	+	2.18756401110904E–11

samples of the LYWC group, 13,624 genes have been modified by m6A, and in the samples of the SIMC group, 24,522 genes have been modified by m6A. We found that among the differentially expressed genes, 620 genes were significantly expressed. Based on this, we screened 316 genes with significant differential expression and m6A methylation modification. The result is shown in **Figure 5**. Since this experiment mainly explored the regulation of muscle growth and development, we screened four candidate genes related to muscle cell growth and development, as shown in **Table 6**. The m6A regulation of these genes was upregulated, while gene regulation was downregulated. At the same time, the difference between the two sets of samples were significant.

GO Analysis and KEGG Pathway Analysis of Differentially Expressed m6A Methylation Genes

To deeply study the significance of m6A modification in physiological and biochemical processes, we conducted GO (<http://www.geneontology.org/>) and KEGG (<http://www.kegg.jp/>) analyses of the different peaks of m6A. The peaks selected were enriched with 898 GO items and 162 pathways. **Figure 6A** shows the top 25 items in biological processes, the top 15 items in cell components, and the top 10 items in molecular functions. GO analysis (**Figure 6B**) showed that differentially methylated genes significantly enriched fibers in fat granule tissue, skeletal muscle contraction, and muscle contraction. KEGG pathway analysis (**Figure 6C**) showed that differentially methylated genes were related to the p53 signaling pathway and PPAR pathway. At the same time, they are also involved in biological processes such as galactose metabolism, fatty acid metabolism, adipocytokine pathway, nitrogen metabolism, arginine synthesis, etc.

Verification of Differentially Expressed Genes

To study the function of gene m6A modification and determine the key genes that regulate muscle growth and development in beef cattle muscle cells, We used qRT-PCR for experimental verification. RNA-seq results showed that among the screened differential genes, the expression of Liaoyu white cattle group was lower than that of Simmental cattle group. The qRT-PCR results also confirmed that the m6A-modified gene is indeed present in the Liaoyu white cattle muscle. The trends of these genes are consistent with the RNA-seq results (**Figure 7**).

DISCUSSION

The modification of m6A is involved in many physiological processes, such as: Mediates mRNA output and synthesis, affects cell maturation, lipogenesis, maintains embryonic development stability, affects cell circadian rhythm, regulates stem cell differentiation, maintains Tregs stability, participates in inflammatory response, apoptosis, muscle production, cell Physiological and biochemical processes such as division. At the same time, the modification of RNA methylation is a dynamic change (Jia et al., 2011) (Zheng et al., 2013) (Feng et al., 2018). m6A RNA modification is dynamically regulated by methyltransferases (writers) and demethylases (erasers). Since m6A bases cannot be directly detected by sequencing, the dissection of the m6A landscape is hindered; they do not change the base pairing properties and cannot be distinguished from conventional bases by reverse transcription (Brocard et al., 2017). Recently, new methods based on m6A immunoprecipitation or modified selective RNA chemistry methods to isolate modified RNA fragments coupled with high-throughput sequencing, namely,

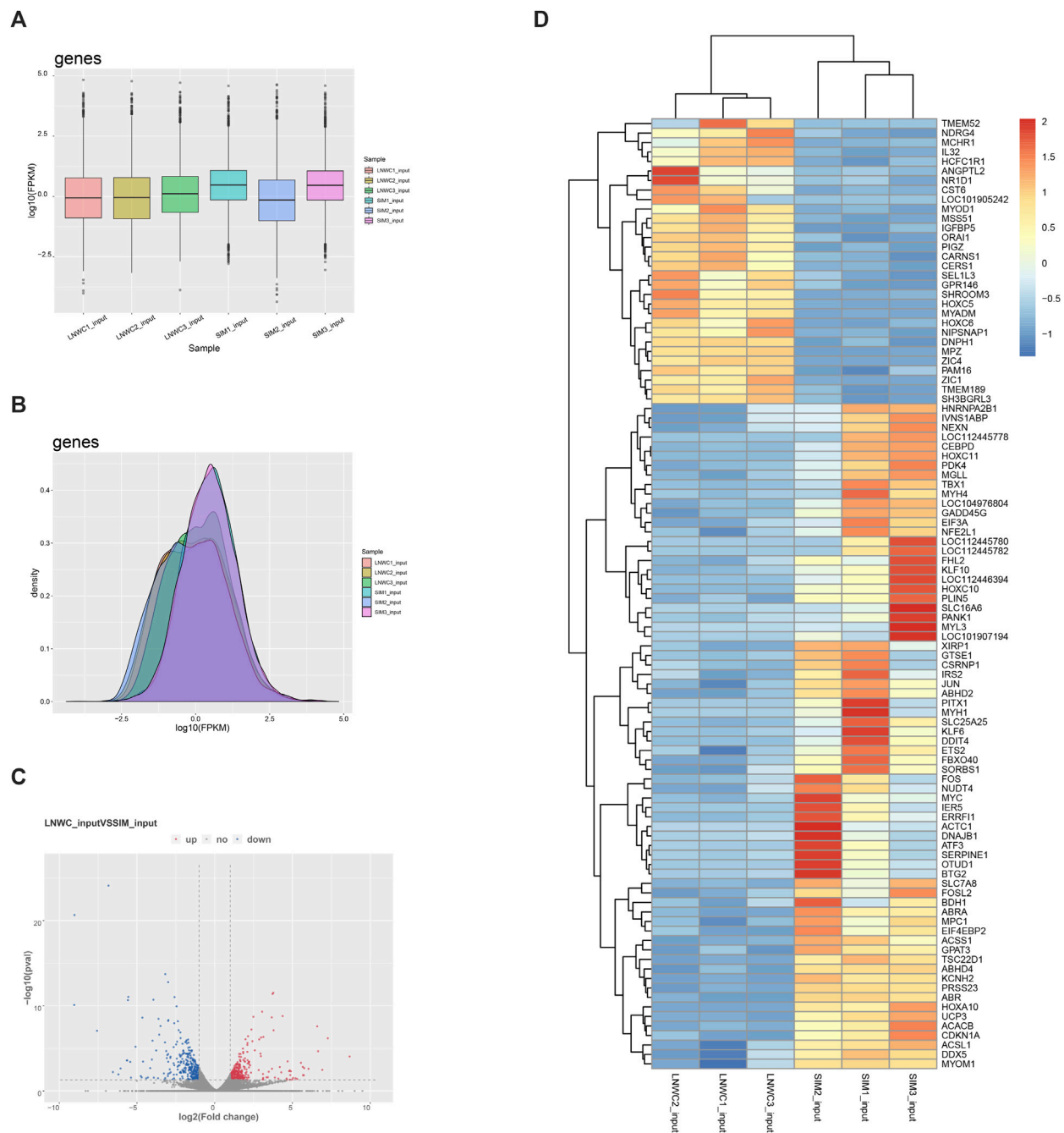
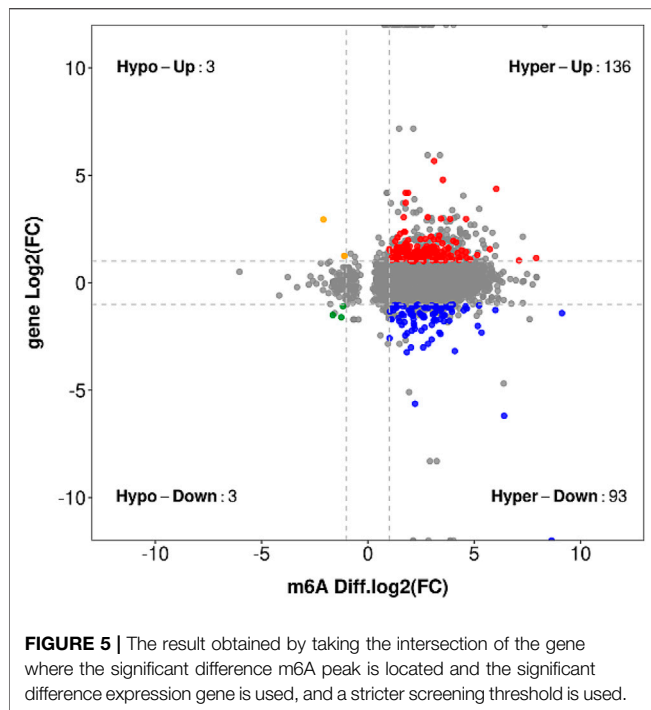


FIGURE 4 | (A) Gene expression cassette diagram. **(B)** Gene expression density diagram. **(C)** Differential gene expression volcano diagram. In the figure, log₂ of the fold change is the horizontal coordinate, and -log₁₀ (*p*-value) is used as the vertical coordinate. The horizontal coordinate represents the gene expression in different samples; the vertical coordinate represents the significant difference in gene expression. Among them, red represents upregulated significantly differentially expressed genes, blue represents downregulated significantly differentially expressed genes, and gray represents nonsignificantly differentially expressed genes. **(D)** LYWC and SIMC gene heat map. Using zscore standardization, the expression levels of genes in different samples can be compared horizontally. From blue to red, the expression amount of genes ranges from low to high.

m6A-seq and MeRIP-seq, have identified thousands of hundred-nucleotide fragments containing modifications in the transcriptomes of mammalian cells (Dominissini et al.,

2012; Meyer et al., 2012). Modification of m6A has been successively discovered in many animals, plants, bacteria and other microorganisms.



Based on numerous research reports, it is found that the majority of cows mammary gland and lymphocytes undergo m6A modification phenomenon (Burtseva et al., 1979; Horowitz et al., 1984; Wu et al., 2021). However, there are still few reports on beef cattle. We speculate that m6A is involved in the muscle growth and development process of beef cattle. Our data show that there are a large number of methylation modifications during muscle growth and development. It may have an important effect on the types of muscle fibers, the maturation of muscle cells, and the changes in muscle structure.

Through laser-induced microdamage of zebrafish muscles combined with cell repair, it was found that the XIRP1 gene is abundant in skeletal muscle and involved in cell repair, cells and new myofibrils, and the repair of damage does not involve cell proliferation (Otten et al., 2012). Troponin T (TNNT1) exists as a group of homologous proteins in the striated muscle of vertebrates and invertebrates. Mutations in the TNNT1 gene can cause rod-shaped myopathy. From animal model experiments, it was found that lack of TNNT1 reduced the content of slow fibers, accompanied by type II fiber hypertrophic growth and increased muscle fatigue (Feng et al., 2009; Wei et al., 2014). Myosin 2 (MYOM2) is the main component of the myofibril M-band of the sarcomere and the central gene in the interaction of sarcomere genes (Auxerre-Plantie et al., 2020). Research by Auxerre-Plantie found that loss of function and moderate knockdown of this gene can lead to myocardial expansion, and severe knockdown can lead to increased sarcomeric myosin (Auxerre-Plantie et al., 2020). Research by Andrei found that in hypothyroid rats, MYOM2 expression increased 3.4 times. Through small-molecule interference of RNA with MYOM2, it was found that the contraction speed of cardiomyocytes were severely reduced

(Rozanski et al., 2013). Myosin heavy chain 6 (MYH6) is widely found mainly in the heart and smooth muscle. This gene is mainly expressed in type I fibers. The presence or absence of MYH6 and its family gene MYH7 determines the slow or fast-twitch phenotype of skeletal muscle (Stuart et al., 2016).

Based on GO enrichment and KEGG pathway analysis, we speculate that m6A modification in genes has potentially important functions and may play a vital role in certain pathways are involved in cell growth and development. Peroxisome proliferator-activated receptors (PPARs) are nuclear hormone receptors activated by fatty acids and their derivatives. They are ligand-activated receptors in the nuclear hormone receptor family. Three subtypes have been found in different species, which control many intracellular metabolic processes. The subtypes include PPAR α (also known as NR1C1). PPAR α participates in the liver and skeletal muscle through regulation and expression of lipid metabolism genes. PPAR β/δ participates in lipid oxidation and cell proliferation. PPAR γ promotes the differentiation of adipocytes to enhance blood glucose uptake. PPAR transcriptional activity can be regulated by nongene crosstalk with phosphatases and kinases, including ERK1/2, p38-MAPK, PKA, PKC, AMPK and GSK3. At the same time, nuclear receptor coactivator (coactivator) and PPAR-RXR act synergistically and complement and stabilize the active transcription complex, which can regulate lipid metabolism and fat formation, maintain metabolic homeostasis and the expression of inflammation genes, and induce anticancer effects in a variety of human tumors.

The m6A regulation level of the differentially expressed genes screened in this study was negatively correlated with the transcription level. The RNA-seq results showed that the differential gene expression in LYWC was lower than that in SIM. The results of qRT-PCR showed that the differentially expressed genes for m6A methylation were all present in the muscle tissue of beef cattle. Therefore, this indicates that m6A modification not only participates in the process of muscle growth and development but may also regulate mRNA degradation.

Skeletal muscle development is a complex biological process. The regulatory role of myogenic regulatory factors and the study of apparent modifications, including DNA methylation and histone modification, in the regulation of skeletal muscle development have given us a preliminary understanding of the regulatory network of skeletal muscle development. Based on the involvement of m6A in the regulation of mouse brain development, fat formation, and other tissue development processes, we speculate that m6A is also involved in the regulation of skeletal muscle development (Zhao et al., 2014; Ma et al., 2018; Wang et al., 2018). Studies have shown that the regulation of METTL3 gene expression and regulation of m6A levels in myoblasts affect the differentiation process of myocytes and the expression of key regulatory genes (Kudou et al., 2017; Chen et al., 2019). This shows that m6A is involved in the regulation of muscle cell differentiation. During the development of animal embryos and the growth and development of brain tissue after birth, neural stem cells are required for differentiation and self-

TABLE 6 | M6A -modified candidate genes related to muscle cell growth and development.

Gene name	Gene ID	M6A regulation	Gene regulation	FPKM.LYWC_input			FPKM.SIM_input		
				LYWC1	LYWC2	LYWC3	SIM1	SIM2	SIM3
TNNT1	282095	up	Down	6852.32	4722.65	7863.95	14067.95	12547.06	20219.39
MYOM2	524077	up	Down	603.17	446.51	330.98	990.94	1472.69	395.06
XIRP1	509670	up	Down	235.30	353.27	241.41	1260.87	1205.70	609.67
MYH6	100296004	up	Down	156.23	115.56	364.75	508.30	365.54	564.40

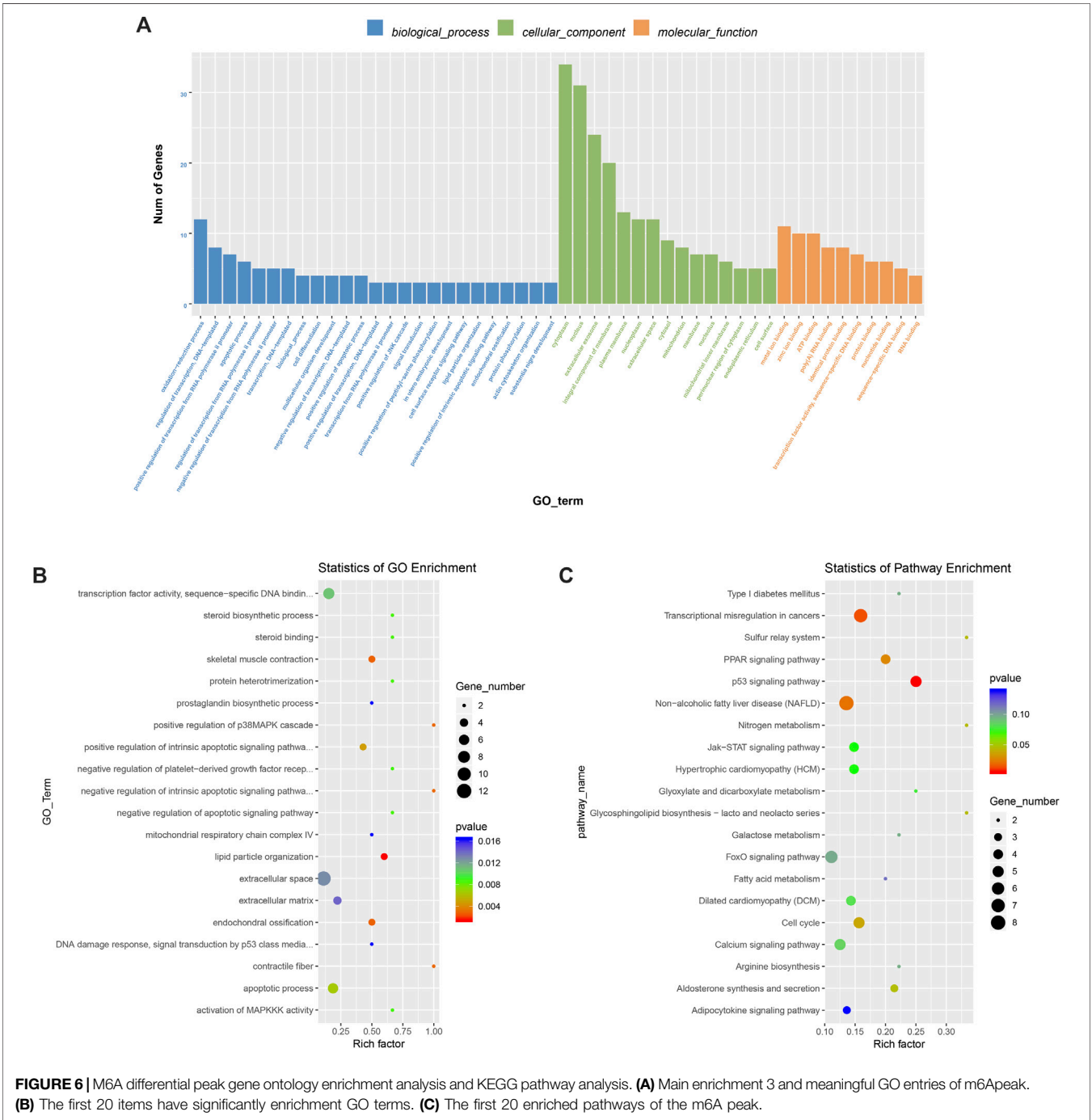


FIGURE 6 | M6A differential peak gene ontology enrichment analysis and KEGG pathway analysis. **(A)** Main enrichment 3 and meaningful GO entries of m6Apeak. **(B)** The first 20 items have significantly enrichment GO terms. **(C)** The first 20 enriched pathways of the m6A peak.

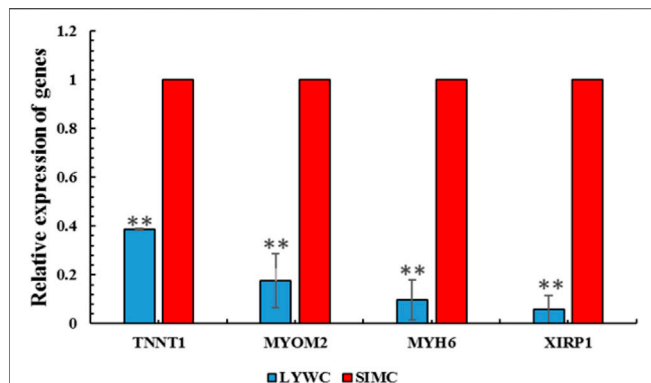


FIGURE 7 | QPCR results of four different m6A-modified genes in LYWC and SIMC.

renewal. Studies have shown that knocking out METTL14 in mouse embryos will interrupt the cycle of radial glial cells in the nerves, which will eventually lead to a decrease in the thickness of the cerebral cortex and even death after birth. Overexpression and specific knockout of the FTO and METTL3 genes in pig adipocytes revealed that FTO expression levels are negatively correlated with m6A levels and positively correlated with adipogenesis, while METTL3 expression levels are positively correlated with m6A levels and negatively correlated with adipogenesis (Wang et al., 2015b). Mice lacking FTO function experience increased energy expenditure, growth retardation, lean body size after birth and deformity (Boissel et al., 2009). Through transcriptome sequencing of the muscle tissues of three different breeds of wild boar, Landrace pig and Rongchang pig, a complete transcriptome map of m6A was drawn. It was found that m6A is widely distributed in muscle tissue, and m6A is mainly enriched in related gene stop codons, 3'UTRs, and protein coding-regions. In addition, data show that there is a clear m6A peak around the stop codon of the cAMP response element-binding protein CREB and zinc finger protein ZNF-related genes, indicating that m6A is enriched here. CREB was first discovered as a transcriptional regulator of cell metabolism that regulates the cAMP response. It is an important gene regulating somatostatin. ZNF has also been considered one of the most important eukaryotic transcription factors and plays an important role in gene regulation.

In conclusion, this study analyzed m6A methylation modification in the muscle tissue of Liaoyu white cattle and Simmental cattle. Based on our experimental results, we

speculate that m6A modification plays an important role in muscle growth and development. This study shows that TNNT1, XIRP1, MYOM2, and MYH6 are likely to play a key role in muscle growth and muscle differentiation. In addition, the data obtained through high-throughput sequencing provide a theoretical basis for further exploring the function of m6A modification on muscle growth and development. At the same time, the regulatory mechanism of m6A modification in muscle still needs to be studied in depth in the future.

DATA AVAILABILITY STATEMENT

The datasets presented in this study can be found in online repositories. The names of the repository/repositories and accession number(s) can be found below: NCBI [accession: PRJNA778440].

ETHICS STATEMENT

The animal study was reviewed and approved by Laboratory Animal Management Committee of Shenyang Agricultural University.

AUTHOR CONTRIBUTIONS

PL and LL conceived and designed the study. YD and QD performed the main experiments. BW, JS, GC, and WX Sample collection. MZ, YZ, and SY performed data analysis. YD, QD, PL, and LL drafted and revised the manuscript. All authors contributed to the article and approved the submitted version.

FUNDING

This research was funded by the National Natural Science Foundation of China (grants No. 31872538) and Scientific Research Funding Project of Liaoning Province (No. 2021JH1/10400033), Education Department of Liaoning Province (No. LSNFW201901, LSNJC202012). Liaoning Provincial joint fund for innovation capability improvement (2021-NLTS-11-05).

REFERENCES

- Auxerre-Plantie, E., Nielsen, T., Grunert, M., Olejniczak, O., Perrot, A., Özcelik, C., et al. (2020). Identification of MYOM2 as a Candidate Gene in Hypertrophic Cardiomyopathy and Tetralogy of Fallot and its Functional Evaluation in the *Drosophila* Heart. *Dis. Model. Mech.* 13, dmm045377. doi:10.1242/dmm.045377
- Bailey, T. L., Boden, M., Buske, F. A., Frith, M., Grant, C. E., Clementi, L., et al. (2009). MEME SUITE: Tools for Motif Discovery and Searching. *Nucleic Acids Res.* 37, W202. doi:10.1093/nar/gkp335
- Boccaletto, P., Machnicka, M. A., Purta, E., Piątkowski, P., Bagiński, B., Wirecki, T. K., et al. (2018). MODOMICS: a Database of RNA Modification Pathways. 2017 Update. *Nucleic Acids Res.* 46 (D1), D303–D307. doi:10.1093/nar/gkx1030
- Boissel, S., Reish, O., Proulx, K., Kawagoe-Takaki, H., Sedgwick, B., Yeo, G. S. H., et al. (2009). Loss-of-function Mutation in the Dioxygenase-Encoding FTO Gene Causes Severe Growth Retardation and Multiple Malformations. *Am. J. Hum. Genet.* 85 (1), 106–111. doi:10.1016/j.ajhg.2009.06.002
- Brocard, M., Ruggieri, A., and Locker, N. (2017). m6A RNA Methylation, a New Hallmark in Virus-Host Interactions. *J. Gen. Virol.* 98 (9), 2207–2214. doi:10.1099/jgv.0.000910

- Burtseva, N. N., Azizov, Iu. M., and Vaniushin, B. F. (1979). Tissue Specificity of the Decrease of Cattle Lymphocyte DNA Methylation during Chronic Lymphoid Leukemia. *Biokhimiia* 44 (7), 1296–1302.
- Cao, G., Li, H.-B., Yin, Z., and Flavell, R. A. (2016). Recent Advances in Dynamic m6A RNA Modification. *Open Biol.* 6 (4), 160003. doi:10.1098/rsob.160003
- Chen, J. N., Chen, Y., Wei, Y. Y., Raza, M. A., Zou, Q., Xi, X. Y., et al. (2019). Regulation of m6A RNA Methylation and its Effect on Myogenic Differentiation in Murine Myoblasts. *Mol. Biol. (Mosk)* 53 (3), 436–445. doi:10.1134/S0026898419030042
- Church, C., Lee, S., Bagg, E. A. L., McTaggart, J. S., Deacon, R., Gerken, T., et al. (2009). A Mouse Model for the Metabolic Effects of the Human Fat Mass and Obesity Associated FTO Gene. *Plos Genet.* 5 (8), e1000599. doi:10.1371/journal.pgen.1000599
- Church, C., Moir, L., McMurray, F., Girard, C., Banks, G. T., Teboul, L., et al. (2010). Overexpression of Fto Leads to Increased Food Intake and Results in Obesity. *Nat. Genet.* 42 (12), 1086–1092. doi:10.1038/ng.713
- Dominissini, D., Moshitch-Moshkovitz, S., Schwartz, S., Salmon-Divon, M., Ungar, L., Osenberg, S., et al. (2012). Topology of the Human and Mouse m6A RNA Methylomes Revealed by m6A-Seq. *Nature* 485 (7397), 201–206. doi:10.1038/nature11112
- Feng, H.-Z., Wei, B., and Jin, J.-P. (2009). Deletion of a Genomic Segment Containing the Cardiac Troponin I Gene Knocks Down Expression of the Slow Troponin T Gene and Impairs Fatigue Tolerance of Diaphragm Muscle. *J. Biol. Chem.* 284 (46), 31798–31806. doi:10.1074/jbc.M109.020826
- Feng, Z., Li, Q., Meng, R., Yi, B., and Xu, Q. (2018). METTL3 Regulates Alternative Splicing of MyD88 upon the Lipopolysaccharide-induced Inflammatory Response in Human Dental Pulp Cells. *J. Cell Mol Med* 22 (5), 2558–2568. doi:10.1111/jcmm.13491
- Fischer, J., Koch, L., Emmerling, C., Vierkotten, J., Peters, T., Brüning, J. C., et al. (2009). Inactivation of the Fto Gene Protects from Obesity. *Nature* 458 (7240), 894–898. doi:10.1038/nature07848
- Flix, B., de la Torre, C., Castillo, J., Casal, C., Illa, I., and Gallardo, E. (2013). Dysferlin Interacts with Calsequestrin-1, Myomesin-2 and Dynein in Human Skeletal Muscle. *Int. J. Biochem. Cell Biol.* 45 (8), 1927–1938. doi:10.1016/j.biocel.2013.06.007
- Gao, X., Shin, Y.-H., Li, M., Wang, F., Tong, Q., and Zhang, P. (2010). The Fat Mass and Obesity Associated Gene FTO Functions in the Brain to Regulate Postnatal Growth in Mice. *PLoS One* 5 (11), e14005. doi:10.1371/journal.pone.0014005
- Geula, S., Moshitch-Moshkovitz, S., Dominissini, D., Mansour, A. A., Kol, N., Salmon-Divon, M., et al. (2015). m6A mRNA Methylation Facilitates Resolution of Naïve Pluripotency toward Differentiation. *Science* 347 (6225), 1002–1006. doi:10.1126/science.1261417
- Heinz, S., Benner, C., Spann, N., Bertolino, E., Lin, Y. C., Laslo, P., et al. (2010). Simple Combinations of Lineage-Determining Transcription Factors Prime Cis-Regulatory Elements Required for Macrophage and B Cell Identities - ScienceDirect. *Mol. Cell* 38 (4), 576–589. doi:10.1016/j.molcel.2010.05.004
- Horowitz, S., Horowitz, A., Nilsen, T. W., Munns, T. W., and Rottman, F. M. (1984). Mapping of N6-Methyladenosine Residues in Bovine Prolactin mRNA. *Proc. Natl. Acad. Sci.* 81 (18), 5667–5671. doi:10.1073/pnas.81.18.5667
- Hsu, P. J., Zhu, Y., Ma, H., Guo, Y., Shi, X., Liu, Y., et al. (2017). Ythdc2 Is an N6-Methyladenosine Binding Protein that Regulates Mammalian Spermatogenesis. *Cell Res* 27 (9), 1115–1127. doi:10.1038/cr.2017.99
- Jia, G., Fu, Y., and He, C. (2013). Reversible RNA Adenosine Methylation in Biological Regulation. *Trends Genet.* 29 (2), 108–115. doi:10.1016/j.tig.2012.11.003
- Jia, G., Fu, Y., Zhao, X., Dai, Q., Zheng, G., Yang, Y., et al. (2011). N6-methyladenosine in Nuclear RNA Is a Major Substrate of the Obesity-Associated FTO. *Nat. Chem. Biol.* 7 (12), 885–887. doi:10.1038/nchembio.687
- Jing, L., Huaiye, L., and Maobin, Q. (2011). A Contrast Experimental Report about slaughter Performance of Liaoyu White Cattle and 5 Varieties (Hybrid) Cattle. *Mod. Anim. Husbandry Vet.* (2), 30–33. doi:10.3969/j.issn.1672-9692.2011.02.011
- Kee, A. J., and Hardeman, E. C. (2008). Tropomyosins in Skeletal Muscle Diseases. *Adv. Exp. Med. Biol.* 644, 143–157. doi:10.1007/978-0-387-85766-4_12
- Kim, D., Langmead, B., and Salzberg, S. L. (2015). HISAT: A Fast Spliced Aligner with Low Memory Requirements. *Nat. Methods* 12 (4), 357–360. doi:10.1038/nmeth.3317
- Knuckles, P., Carl, S. H., Musheev, M., Niehrs, C., Wenger, A., and Bühler, M. (2017). RNA Fate Determination through Cotranscriptional Adenosine Methylation and Microprocessor Binding. *Nat. Struct. Mol. Biol.* 24 (7), 561–569. doi:10.1038/nsmb.3419
- Kudou, K., Komatsu, T., Nogami, J., Maehara, K., Harada, A., Saeki, H., et al. (2017). The Requirement of Mettl3-Promoted MyoD mRNA Maintenance in Proliferative Myoblasts for Skeletal Muscle Differentiation. *Open Biol.* 7 (9), 170119. doi:10.1098/rsob.170119
- Liu, J., Yue, Y., Han, D., Wang, X., Fu, Y., Zhang, L., et al. (2014). A METTL3-METTL14 Complex Mediates Mammalian Nuclear RNA N6-Adenosine Methylation. *Nat. Chem. Biol.* 10 (2), 93–95. doi:10.1038/nchembio.1432
- Ma, C., Chang, M., Lv, H., Zhang, Z.-W., Zhang, W., He, X., et al. (2018). RNA m6A Methylation Participates in Regulation of Postnatal Development of the Mouse Cerebellum. *Genome Biol.* 19 (1), 68. doi:10.1186/s13059-018-1435-z
- Martin, M. (2011). Cutadapt Removes Adapter Sequences from High-Throughput Sequencing Reads. *Embnet J.* 17 (1). doi:10.14806/ej.17.1.200
- McMurray, F., Church, C. D., Larder, R., Nicholson, G., Wells, S., Teboul, L., et al. (2013). Adult Onset Global Loss of the Fto Gene Alters Body Composition and Metabolism in the Mouse. *Plos Genet.* 9 (1), e1003166. doi:10.1371/journal.pgen.1003166
- Meng, J., Lu, Z., Liu, H., Zhang, L., Zhang, S., Chen, Y., et al. (2014). A Protocol for RNA Methylation Differential Analysis with MeRIP-Seq Data and exomePeak R/Bioconductor Package. *Methods A Companion Methods Enzymol.* 69, 274. doi:10.1016/j.ymeth.2014.06.008
- Merkestein, M., Laber, S., McMurray, F., Andrew, D., Sachse, G., Sanderson, J., et al. (2015). FTO Influences Adipogenesis by Regulating Mitotic Clonal Expansion. *Nat. Commun.* 6, 6792. doi:10.1038/ncomms7792
- Meyer, K. D., Patil, D. P., Zhou, J., Zinoviev, A., Skabkin, M. A., Elemento, O., et al. (2015). 5' UTR m6A Promotes Cap-independent Translation. *Cell* 163 (4), 999–1010. doi:10.1016/j.cell.2015.10.012
- Meyer, K. D., Saletore, Y., Zumbo, P., Elemento, O., Mason, C. E., and Jaffrey, S. R. (2012). Comprehensive Analysis of mRNA Methylation Reveals Enrichment in 3' UTRs and Near Stop Codons. *Cell* 149 (7), 1635–1646. doi:10.1016/j.cell.2012.05.003
- Otten, C., van der Ven, P. F., Lewrenz, I., Paul, S., Steinhagen, A., Busch-Nentwich, E., et al. (2012). Xirp Proteins Mark Injured Skeletal Muscle in Zebrafish. *PLoS One* 7 (2), e31041. doi:10.1371/journal.pone.0031041
- Peretea, M., Peretea, G. M., Antonescu, C. M., Chang, T.-C., Mendell, J. T., and Salzberg, S. L. (2015). StringTie Enables Improved Reconstruction of a Transcriptome from RNA-Seq Reads. *Nat. Biotechnol.* 33 (3), 290–295. doi:10.1038/nbt.3122
- Ping, X.-L., Sun, B.-F., Wang, L., Xiao, W., Yang, X., Wang, W.-J., et al. (2014). Mammalian WTAP Is a Regulatory Subunit of the RNA N6-Methyladenosine Methyltransferase. *Cell Res* 24 (2), 177–189. doi:10.1038/cr.2014.3
- Robinson, M. D., McCarthy, D. J., and Smyth, G. K. (2010). edgeR: a Bioconductor Package for Differential Expression Analysis of Digital Gene Expression Data. *Bioinformatics* 26, 139. doi:10.1093/bioinformatics/btp616
- Ronkainen, J., Mondini, E., Cinti, F., Cinti, S., Sebér, S., Savolainen, M. J., et al. (2016). Fto-Deficiency Affects the Gene and MicroRNA Expression Involved in Brown Adipogenesis and Browning of White Adipose Tissue in Mice. *Int. J. Mol. Sci.* 17 (11). doi:10.3390/ijms17111851
- Roundtree, I. A., Evans, M. E., Pan, T., and He, C. (2017). Dynamic RNA Modifications in Gene Expression Regulation. *Cell* 169 (7), 1187–1200. doi:10.1016/j.cell.2017.05.045
- Rozanski, A., Takano, A. P. C., Kato, P. N., Soares, A. G., Lellis-Santos, C., Campos, J. C., et al. (2013). M-protein Is Down-Regulated in Cardiac Hypertrophy Driven by Thyroid Hormone in Rats. *Mol. Endocrinol.* 27 (12), 2055–2065. doi:10.1210/me.2013-1018
- Shi, H., Wei, J., and He, C. (2019). Where, when, and How: Context-dependent Functions of RNA Methylation Writers, Readers, and Erasers. *Mol. Cell* 74 (4), 640–650. doi:10.1016/j.molcel.2019.04.025
- Shuangyong, J., Huaiye, L., and Maobin, Q. (2011). A Contrast Experimental Report about Beef Quality of Liaoyu White Cattle and 5 Varieties (Hybrid) Cattle. *Mod. J. Anim. Husbandry Vet. Med* 2011 (3), 22–25. doi:10.3969/j.issn.1672-9692.2011.03.009
- Siddique, B. S., Kinoshita, S., Wongkarangkana, C., Asakawa, S., and Watabe, S. (2016). Evolution and Distribution of Teleost myomiRNAs: Functionally

- Diversified myomiRs in Teleosts. *Mar. Biotechnol.* 18 (3), 436–447. doi:10.1007/s10126-016-9705-9
- Stuart, C. A., Stone, W. L., Howell, M. E. A., Brannon, M. F., Hall, H. K., Gibson, A. L., et al. (2016). Myosin Content of Individual Human Muscle Fibers Isolated by Laser Capture Microdissection. *Am. J. Physiology-Cell Physiol.* 310 (5), C381–C389. doi:10.1152/ajpcell.00317.2015
- Wang, C.-X., Cui, G.-S., Liu, X., Xu, K., Wang, M., Zhang, X.-X., et al. (2018). METTL3-mediated m6A Modification Is Required for Cerebellar Development. *Plos Biol.* 16 (6), e2004880. doi:10.1371/journal.pbio.2004880
- Wang, J.-y., Chen, L.-j., and Qiang, P. (2020). The Potential Role of N6-Methyladenosine (m6A) Demethylase Fat Mass and Obesity-Associated Gene (FTO) in Human Cancers. *Ott* 13, 12845–12856. doi:10.2147/ott.s283417
- Wang, X., Feng, J., Xue, Y., Guan, Z., Zhang, D., Liu, Z., et al. (2016). Structural Basis of N6-Adenosine Methylation by the METTL3-METTL14 Complex. *Nature* 534 (7608), 575–578. doi:10.1038/nature18298
- Wang, X., Lu, Z., Gomez, A., Hon, G. C., Yue, Y., Han, D., et al. (2014). N6-methyladenosine-dependent Regulation of Messenger RNA Stability. *Nature* 505 (7481), 117–120. doi:10.1038/nature12730
- Wang, X., Zhao, B. S., Roundtree, I. A., Lu, Z., Han, D., Ma, H., et al. (2015). N6-methyladenosine Modulates Messenger RNA Translation Efficiency. *Cell* 161 (6), 1388–1399. doi:10.1016/j.cell.2015.05.014
- Wang, X., Zhu, L., Chen, J., and Wang, Y. (2015). mRNA m6A Methylation Downregulates Adipogenesis in Porcine Adipocytes. *Biochem. Biophysical Res. Commun.* 459 (2), 201–207. doi:10.1016/j.bbrc.2015.02.048
- Wang, Y., Zheng, Y., Guo, D., Zhang, X., Guo, S., Hui, T., et al. (2019). m6A Methylation Analysis of Differentially Expressed Genes in Skin Tissues of Coarse and Fine Type Liaoning Cashmere Goats. *Front. Genet.* 10, 1318. doi:10.3389/fgene.2019.01318
- Wei, B., Lu, Y., and Jin, J.-P. (2014). Deficiency of Slow Skeletal Muscle Troponin T Causes Atrophy of Type I Slow Fibres and Decreases Tolerance to Fatigue. *J. Physiol.* 592 (6), 1367–1380. doi:10.1113/jphysiol.2013.268177
- Wu, K., Jia, S., Zhang, J., Zhang, C., Wang, S., Rajput, S. A., et al. (2021). Transcriptomics and Flow Cytometry Reveals the Cytotoxicity of Aflatoxin B1 and Aflatoxin M1 in Bovine Mammary Epithelial Cells. *Ecotoxicology Environ. Saf.* 209, 111823. doi:10.1016/j.ecoenv.2020.111823
- Wu, W., Feng, J., Jiang, D., Zhou, X., Jiang, Q., Cai, M., et al. (2017). AMPK Regulates Lipid Accumulation in Skeletal Muscle Cells through FTO-dependent Demethylation of N6-Methyladenosine. *Sci. Rep.* 7, 41606. doi:10.1038/srep41606
- Xiang, Y., Laurent, B., Hsu, C.-H., Nachtergaele, S., Lu, Z., Sheng, W., et al. (2017). RNA m6A Methylation Regulates the Ultraviolet-Induced DNA Damage Response. *Nature* 543 (7646), 573–576. doi:10.1038/nature21671
- Xiao, W., Adhikari, S., Dahal, U., Chen, Y.-S., Hao, Y.-J., Sun, B.-F., et al. (2016). Nuclear M6A Reader YTHDC1 Regulates mRNA Splicing. *Mol. Cell* 61 (4), 507–519. doi:10.1016/j.molcel.2016.01.012
- Yu, G., Wang, L. G., and He, Q. Y. (2015). ChIPseeker: an R/Bioconductor Package for ChIP Peak Annotation, Comparison and Visualization. *Bioinformatics* 31 (14), 2382–2383. doi:10.1093/bioinformatics/btv145
- Yue, Y., Liu, J., and He, C. (2015). RNA N6-Methyladenosine Methylation in post-transcriptional Gene Expression Regulation. *Genes Dev.* 29 (13), 1343–1355. doi:10.1101/gad.262766.115
- Zhang, C., Fu, J., and Zhou, Y. (2019). A Review in Research Progress Concerning m6A Methylation and Immunoregulation. *Front. Immunol.* 10, 922. doi:10.3389/fimmu.2019.00922
- Zhao, X., Yang, Y., Sun, B.-F., Shi, Y., Yang, X., Xiao, W., et al. (2014). FTO-dependent Demethylation of N6-Methyladenosine Regulates mRNA Splicing and Is Required for Adipogenesis. *Cell Res* 24 (12), 1403–1419. doi:10.1038/cr.2014.151
- Zheng, G., Dahl, J. A., Niu, Y., Fedorcsak, P., Huang, C.-M., Li, C. J., et al. (2013). ALKBH5 Is a Mammalian RNA Demethylase that Impacts RNA Metabolism and Mouse Fertility. *Mol. Cell* 49 (1), 18–29. doi:10.1016/j.molcel.2012.10.015

Conflict of Interest: The authors declare that the research was conducted in the absence of any commercial or financial relationships that could be construed as a potential conflict of interest.

Publisher's Note: All claims expressed in this article are solely those of the authors and do not necessarily represent those of their affiliated organizations, or those of the publisher, the editors and the reviewers. Any product that may be evaluated in this article, or claim that may be made by its manufacturer, is not guaranteed or endorsed by the publisher.

Copyright © 2022 Dang, Dong, Wu, Yang, Sun, Cui, Xu, Zhao, Zhang, Li and Li. This is an open-access article distributed under the terms of the Creative Commons Attribution License (CC BY). The use, distribution or reproduction in other forums is permitted, provided the original author(s) and the copyright owner(s) are credited and that the original publication in this journal is cited, in accordance with accepted academic practice. No use, distribution or reproduction is permitted which does not comply with these terms.

Advantages of publishing in Frontiers



OPEN ACCESS

Articles are free to read
for greatest visibility
and readership



FAST PUBLICATION

Around 90 days
from submission
to decision



HIGH QUALITY PEER-REVIEW

Rigorous, collaborative,
and constructive
peer-review



TRANSPARENT PEER-REVIEW

Editors and reviewers
acknowledged by name
on published articles

Frontiers

Avenue du Tribunal-Fédéral 34
1005 Lausanne | Switzerland

Visit us: www.frontiersin.org

Contact us: frontiersin.org/about/contact



REPRODUCIBILITY OF RESEARCH

Support open data
and methods to enhance
research reproducibility



DIGITAL PUBLISHING

Articles designed
for optimal readership
across devices



FOLLOW US

@frontiersin



IMPACT METRICS

Advanced article metrics
track visibility across
digital media



EXTENSIVE PROMOTION

Marketing
and promotion
of impactful research



LOOP RESEARCH NETWORK

Our network
increases your
article's readership